DAN ZHANG

KINETOSTATIC ANALYSIS AND OPTIMIZATION OF PARALLEL AND HYBRID ARCHITECTURES FOR MACHINE TOOLS

Thèse

présentée

à la Faculté des études supérieures

de l'Université Laval

pour l'obtention

du grade de Philosophiae Doctor (Ph.D.)

Département de génie mécanique

FACULTÉ DES SCIENCES ET DE GÉNIE

UNIVERSITÉ LAVAL

QUÉBEC

APRIL 2000

Short Abstract

The kinetostatic analysis and optimization of parallel and hybrid architectures for machine tools are conducted in this thesis.

First, a topological representation of all possible architectures which can provide 5 degrees of freedom between the tool and the workpiece is developed. The most promising kinematic structures are automatically generated based on the Chebychev-Grübler-Kutzbach criterion and some other design criteria.

Then, a generic stiffness model for fully-parallel mechanisms with various types of actuator stiffnesses is established and verified by examples of planar parallel mechanisms in a CAD system. In particular, several new types of spatial parallel kinematic mechanisms with prismatic/revolute actuators whose degree of freedom is dependent on a constraining passive leg connecting the base and the platform are introduced. A general kinetostatic model is established with the consideration of the characteristics of joints and links flexibilities. The model is used to demonstrate that flexible links have significant effects on the stiffness and accuracy of parallel kinematic machines. Examples for 3-dof, 4-dof, 5-dof, 6-dof and the Tricept machine tool families are given in detail to illustrate the results. Stiffness mappings are shown and design guidelines for parallel kinematic machines are concluded.

Finally, the optimization of system parameters in achieving a better system stiffness is performed. This includes the development of a more explicit representation of an

objective function in the optimization model. The genetic algorithm is employed to solve this optimization problem. As a result, a significant improvement of the system stiffness is achieved.

Dan Zhang

Clément M. Gosselin

Résumé court

Cette thèse porte sur l'analyse cinéto-statique et l'optimisation d'architectures parallèles et hybrides pouvant être utilisées comme machines-outils.

Premièrement, une représentation topologique de toutes les architectures pouvant produire 5 degrés de liberté entre l'outil et la pièce à usiner est developpée. Les structures cinématiques les plus prometteuses sont automatiquement générées d'après le critère de Tchebychev-Grübler-Kutzbach et d'autres critères de conception.

Ensuite, un modèle général pour la rigidité, pouvant être utilisé pour les mécanismes pleinement parallèles avec des rigidités variables aux actionneurs, est présenté et vérifié dans un logiciel de CAO sur des mécanismes parallèles plans. En particulier, plusieurs nouveaux types de mécanismes parallèles spatiaux avec actionneurs prismatiques et rotoïdes, et pour lesquels les degrés de liberté sont dépendants d'une patte passive contraignante reliant la base et la plate-forme, sont proposés. Un modèle cinéto-statique général est présenté en prenant en considération les caractéristiques des articulations et la flexibilité des membrures. Le modèle est utilisé pour démontrer que la flexibilité des membrures a un effet significatif sur la rigidité et la précision des mécanismes parallèles. Des exemples sur des mécanismes à 3-ddl, 4-ddl, 5-ddl, 6-ddl et sur les machines-outils de type *Tricept* sont présentés en détails pour illustrer les résultats obtenus. Les courbes de rigidité sont montrées et des lignes directrices sont proposées pour la conception de mécanismes parallèles.

Finalement, une optimisation est effectuée afin d'obtenir une meilleur rigidité du système. Ceci inclut une représentation plus explicite de la fonction objective dans le modèle d'optimisation. Un algorithme génétique est employé pour résoudre le problème d'optimisation. Les résultats démontrent des améliorations significatives de la rigidité du système après l'optimisation.

Dan Zhang

Clément M. Gosselin

Abstract

Research and development of various parallel mechanism applications in engineering are now being performed more and more actively in every industrial field. Parallel Kinematic Machines (hereafter called PKMs) development is considered a key technology of robot applications in manufacturing industries in the future.

Nevertheless, most of the existing work regarding parallel kinematic machines was built upon the concept of traditional "Gough-Stewart" mechanism type. This suggests that most of the parallel mechanisms developed have six degrees of freedom. However, in many applications such as low-cost flight simulation and axisymmetric machining, five degrees of freedom are required at most. Hence, there is a need to study parallel mechanisms with less than six degrees of freedom.

The study described in this thesis is concerned with developing mechanisms with less than 6-dof. In the thesis, a family of new alternative mechanical architectures which could be used for machine tools with parallel or hybrid architecture is investigated. The kinematic analysis, stiffness analysis, the kinetostatic modeling, optimization, design of these mechanism systems and their rigidity and precision analysis are also presented.

Firstly, a topological representation of different combinations of kinematic structures is developed using a graph based approach, and the possible architectures that will provide 5 degrees of freedom between the tool and the workpiece are generated. The detailed list of possible topologies is obtained and the most promising architectures

are screened out based on the design criteria.

Stiffness analysis of parallel mechanisms is addressed and a generic stiffness model for fully-parallel mechanism with various types of actuator stiffnesses is established. Lumped models for the joints and links are introduced. Equations for the computation of the equivalent virtual joint stiffnesses are derived. With the generic stiffness model, examples are given for planar 2-dof mechanisms with revolute actuators and planar 3-dof mechanisms with prismatic actuators. The stiffness mappings are implemented as a visualization tool. An alternative verification for the correctness of the generic stiffness model is conducted using Pro/Engineer software package.

Next, a family of new types of spatial parallel mechanisms with prismatic actuators and revolute actuators whose degree of freedom is dependent on a constraining passive leg connecting the base and the platform is proposed. A general kinetostatic model is established for the analysis of the structural rigidity and accuracy of this family of mechanisms. The geometric models of this family of mechanisms are introduced. A general lumped kinetostatic model is proposed in order to account for joint and link compliances. These new methods and models are also applicable to any other type of parallel mechanism for their rigidity and precision analysis. Moreover, they can be used for parallel mechanism design and optimization. The inverse kinematics and global velocity equations are given for both rigid-link mechanisms and flexible-link mechanisms. With the kinetostatic model, design guidelines are summarized for different kinds of mechanisms, and their stiffness mappings are obtained. One can then determine which regions of the workspace will satisfy the stiffness criteria from the stiffness maps.

Additionally, kinetostatic analysis for 6-dof fully-parallel mechanisms are presented in the thesis. A new method based on the theorem of velocity compatibility is applied to establish the kinetostatic model of this type of mechanism. Examples of 3-leg and 6-leg spatial fully-parallel mechanisms with revolute actuators and 6-leg spatial fully-parallel mechanism with prismatic actuators are given, respectively, to study the effects of the joint and link flexibility.

Finally, optimization criteria are proposed. A novel optimization technique called genetic algorithms (GAs) is applied. The rationale for using this method together with

the determination of the parameters and the objective function are addressed and justified. The detailed analysis of the kinetostatics of the parallel mechanisms conducted in previous chapters is used to specify and optimize their geometry and properties. The implementation and optimum results for all kinds of mechanisms discussed in the thesis are given. The final results show that the optimization can yield a remarkable improvement of the kinetostatic properties.

Dan Zhang   Clément M. Gosselin

Résumé

La recherche et le développement sur les mécanismes parallèles produit de plus en plus d'activités en industrie. Le développement des machines cinématiques parallèles (appelées ici PKMs) est maintenant considéré comme une solution technologique d'avenir pour les entreprises manufacturières utilisant des procédés robotisés.

Cependant, la plupart des travaux qui ont été effectués dans le domaine des machines cinématiques parallèles l'ont été suivant le concept traditionnel de la plate-forme de "Gough-Stewart". Ceci explique donc pourquoi la plupart des mécanismes parallèles développés ont six degrés de liberté (ddl). Cependant, dans plusieurs applications, comme les simulateurs de vol bas de gamme et les machines-outils à outil axisymétrique, un maximum de cinq degrés de liberté (ddl) est nécessaire. Ainsi, un besoin réel existe pour l'utilisation de mécanismes parallèles performants avec moins de six degrés de liberté (ddl).

L'étude décrite dans cette thèse porte donc sur le développement de mécanismes avec moins de 6-ddl. Une famille d'architectures mécaniques alternatives pouvant être utilisée comme machines-outils, et construite à partir d'architectures parallèles ou hydrides, est étudiée. Les divers points abordés comprennent l'analyse cinématique, l'analyse des rigidités, les modèles cinéto-statiques, l'optimisation, la conception de ces systèmes mécaniques et leurs rigidités ainsi que l'analyse de la précision.

Premièrement, une représentation topologique des différentes combinaisons de structures cinématiques est présentée utilisant une approche graphique. Les différentes architectures pouvant produire 5 degrés de liberté entre l'outil et la pièce à usiner sont alors générées. Une liste détaillée des différentes topologies possibles est obtenue et les architectures les plus prometteuses sont retenues.

L'analyse de la rigidité des mécanismes parallèles est par la suite expliquée et un modèle général pour la rigidité, pouvant être utilisé pour les mécanismes pleinement parallèles avec des rigidités variables aux actionneurs, est présentée. Aussi, des modèles à paramètres localisés pour les articulations et les membrures sont introduits. Les équations permettant le calcul de la rigidité des articulations virtuelles équivalentes sont ensuite dérivées. Avec le modèle général de rigidité, des exemples sont donnés pour des mécanismes plans à 2-ddl avec actionneurs rotoïdes et pour des mécanismes plans à 3-ddl avec actionneurs prismatiques. Les courbes de rigidité sont utilisées dans ces cas comme outil de visualisation. Une vérification est également faite avec le logiciel *Pro/Engineer* pour vérifier le modèle général de rigidité.

Par la suite, une nouvelle famille de mécanismes parallèles spatiaux avec actionneurs prismatiques et rotoïdes, et pour lesquels les degrés de liberté sont dépendants d'une patte passive contraignante reliant la base et la plate-forme, est proposée. Un modèle cinéto-statique général est présenté pour l'analyse de la rigidité et l'analyse de la précision structurelle de cette famille de mécanismes. Les modèles géométriques sont alors introduits. Un modèle général cinéto-statique à paramètres localisés est présenté afin de prendre en considération la flexibilité des articulations et des membrures. A noter que ces nouvelles méthodes et nouveaux modèles peuvent également être utilisés pour n'importe quel type de mécanismes parallèles pour ses analyses de rigidité et de précision. De plus, ils peuvent aussi être utilisés pour la conception et l'optimisation de mécanismes parallèles. Le modèle géométrique inverse et les équations de vitesse sont données à la fois pour des mécanismes à membrures rigides et à membrures flexibles. Avec le modèle cinéto-statique, des lignes directrices pour la conception sont résumées pour différents types de mécanismes, et leurs courbes de rigidité sont obtenues. On peut donc déterminer quelles régions de l'espace de travail vont rencontrer les critères de rigidité d'après les courbes de rigidité.

De plus, l'analyse cinéto-statique des mécanismes parallèles à 6-ddl est présentée

dans cette thèse. Une nouvelle méthode basée sur le théorème de compatibilité des vitesses est appliquée pour établir le modèle cinéto-statique de ce type de mécanisme. Des exemples de mécanismes parallèles avec 3 et 6 pattes avec actionneurs rotoïdes et 6 pattes avec actionneurs prismatiques sont donnés pour montrer l'effet de la flexibilité des actionneurs et des membrures.

Finalement, des critères d'optimisation sont proposés. Une nouvelle technique d'optimisation appelée algorithme génétique (GAs) est appliquée. Les raisons qui justifient l'utilisation de cette méthode, de même que la façon de déterminer la fonction objective et les différents paramètres sont discutées. L'analyse cinéto-statique détaillée des mécanismes parallèles réalisée dans les chapitres précédents est utilisée pour spécifier et analyser leur geométrie et leurs propriétés. Les calculs et les résultats optimums pour tous les types de mécanismes présentés dans la thèse sont donnés. Les résultats finaux démontrent que l'optimisation peut conduire à des améliorations significatives des propriétés cinéto-statiques.

Dan Zhang   Clément M. Gosselin

Foreword

This thesis describes my major work in the Laboratory of Robotics of the Department of Mechanical Engineering of Laval University, Québec, Canada, during 1997 – 2000.

First and foremost, I would like to thank my supervisor, Professor Clément M. Gosselin, for his invaluable supervision, full support and critical review of the manuscript. Through his direction, I have broadened my theoretical background, and had an opportunity to view my work from a new perspective. He has helped me so much, and I have all reasons to say: without his ideas and continuous encouragements, this work would never have been possible.

Thanks also go to Professor Marc J. Richard for his preview of my thesis and many helpful comments. I am grateful to Professor Alain Curodeau and Professor Chris Zhang of the University Saskatchewan for their contributions as my Ph.D. defense committee members and their academic advice.

I would like to thank all the colleagues in the Robotics Laboratory for their help and cooperation. I would, in particular, like to express my special thanks to Boris Mayer St-Onge for his enthusiastic help and kindness in using laboratory facilities and assisting me in many aspects, he also helped me to translate the abstract of my thesis into French. Many thanks to Jiegao Wang for all his kind help offered since the date I arrived in Québec City. I am thankful to Thierry Laliberté and Gabriel Coté for the CAD models of the mechanisms, and Ilian A. Bonev for the helpful discussions on my

thesis.

I would also like to thank Professor Roger Boudreau of Moncton University and Dr. Jeffrey A. Joines of North Carolina State University for their advice in Genetic Algorithms issues.

I am deeply indebted to my parents who inspired the thirst for knowledge in me and made sure that I got the education I wanted.

I am also greatly indebted to my wife Junmei Guo for her patience and understanding during the past three years as well as her time spent and effort made in assisting me to complete my thesis. I am much obliged to my daughter, Mengjia Zhang, with whom, I could not afford to spend much time in the evenings and during weekends.

Contents

List of Tables

xxiii

List of Figures

Chapter 1

Introduction

This thesis describes the establishment of a **Kinetostatic Model** and its application to machine tool design. Several **new types of parallel mechanisms** whose degree of freedom is dependent on a constraining passive leg are proposed. To formulate the subject of the study, Section 1.1 answers the following questions:

- What is the **Kinetostatic Model** about?

- Why is it needed?

- What are the **new architectures of parallel mechanisms** proposed here? and

- Why are such types of mechanism proposed?

To highlight the significance of the study and derive the main philosophy behind this thesis work, Section 1.2 presents a literature review regarding the current research and

development of parallel kinematic machines, including stiffness analysis. Section 1.3 describes the key issues which will be discussed in this thesis. Section 1.4 presents the main philosophy behind the thesis work. Finally, Section 1.5 provides a brief introduction to the subsequent chapters and their relationships.

1.1   The Subject of the Study

The analysis of the positioning and orientation (pose) error of the platform in the presence of manufacturing tolerances, joint clearances and leg flexibility, also known as sensitivity analysis (Gregorio and Parenti-Castelli 1999), has not received much attention in the recent literature. However, these errors could not be neglected in practice, since it has been shown that if the mechanism flexibility is considered, the performances may become very poor and the main feature of the mechanism is lost. Additionally, considering the above errors may lead to singular mechanism configurations which must be avoided during motion, the subject of which cannot be studied by the mobility analysis of the rigid legged mechanism model (Gregorio and Parenti-Castelli 1999). As it will be derived in Chapter 3, the Cartesian stiffness matrix $\mathbf{K}_C$ for rigid spatial parallel mechanisms can be expressed as

$$\mathbf{K}_C = \mathbf{J}^T \mathbf{K}_J \mathbf{J} \tag{1.1}$$

where $\mathbf{K}_J$ is the joint stiffness matrix of a parallel mechanism, $\mathbf{K}_J = diag[k_1, \ldots, k_n]$, k_i is a scalar representing the joint stiffness of each actuator, which is modeled as linear spring, and $\mathbf{J}$ is the Jacobian matrix of the mechanism. If

$$det[\mathbf{J}^T \mathbf{K}_J \mathbf{J}] = 0 \tag{1.2}$$

then singular configurations appear. Anyhow, this can be avoided by adjusting the actuated joint variable or architecture design parameters. Since it will be shown in Chapters 4, 5 and 6, link flexibilities have significant effects on the Jacobian matrix. Eq. (1.2) has implied that even if there is no singular configuration in the rigid case, it is still possible that the singular configuration can appear in a flexible case. Hence, it is of paramount necessity to take link flexibilities into account. A kinetostatic model is therefore established for the study of flexible parallel mechanisms. The model is a

stiffness/compliance model in which both link and joint compliances are considered and the relationship between mechanism global stiffness and link flexibilities is derived.

Among most of the existing applications of parallel mechanisms for machine tool design, only five or less than five degrees of freedom are required because of the ax-isymmetric machining (tool revolves around its own axis). Therefore, research and development of parallel mechanisms with less than 6-dof is necessary. In this thesis, we will propose several new types of parallel mechanisms with fewer than six degrees of freedom. They are a series of n-dof parallel mechanisms which consist of n identical actuated legs with six degrees of freedom and one passive leg with n degrees of freedom connecting the platform to the base. The degree of freedom of the manipulator is dependent on the passive leg's degree of freedom. One can improve the rigidity of this type of mechanism through the optimization of the link rigidities to reach the maximal global stiffness and precision. Moreover, this series of mechanisms have the character-istics of reconfigurability and modularity since they have identical actuated legs, thus, the entire mechanism essentially consists of repeated parts, offering price benefits for manufacturing, assembling and purchasing.

The **subject** of the present study in particular is to develop theories, methods and a series of prototypes used for parallel kinematic machine tool design. The implementa-tion in the present study is focused on stiffness mappings, the design guidelines and the optimization of the machine tools, i.e. the parallel kinematic mechanisms in particular. It is also envisaged that the kinetostatic model can be used for the optimum design to increase the stiffness and accuracy of machine tools. Eventually, the accessibility and usability of the model in industrial design practices could tremendously improve the characteristics of parallel machine tools.

1.2   Literature Review

Because of the recent trend towards high-speed machining (HSM), there is a demand to develop machines with high dynamic performance, i.e. there is a demand for stiff constructions with little moving mass. Parallel mechanisms have been targeted for the design and development of applications for real-world industrial problems. In situations

where the need for accuracy and high stiffness is crucial, parallel mechanisms present themselves as feasible alternatives to their serial counterparts. They have the potential to be more accurate and repeatable than serial mechanisms in part due to the fact that their position errors do not accumulate, thus the total position error rarely exceeds the error caused by a single leg of the mechanism.

Parallel mechanisms generally comprise two platforms which are connected by joints or legs acting in-parallel. The most common configuration comprises six legs, and the legs are linear actuators such as hydraulic cylinders, or in the case of a passive mechanism that could be spring loaded. One of the platforms is defined as the "movable platform", which has six degrees of freedom relative to the other platform, which is the "base". With six degrees of freedom, the movable platform is capable of moving in three linear directions and three angular directions independently or in any combination. One such platform known as the "Gough-Stewart" platform was introduced by Gough (1956) as a tire testing machine and then by Stewart (1965) for use in an aircraft simulator. Over the past decades, parallel mechanisms have received more and more attention from researchers and industries. They have been continually developed and refined by many researchers, e.g., Hunt, Kohli, Bailey, etc. They can be found in several practical applications, such as aircraft simulators (Stewart 1965; Pouliot *et al.* 1998; Advani 1998), adjustable articulated trusses (Reinholz and Gokhale 1987), mining machines (Arai *et al.* 1991), pointing devices (Gosselin and Hamel 1994) and micro-positioning devices (Physik-Instrumente 1997). More recently, they have been used in the development of high precision machine tools (Boër *et al.* 1999; Lauffer *et al.* 1996; Bailey 1994; Hollingum 1997) by several companies such as Giddings & Lewis, Ingersoll, Hexel, Geodetic, Toyoda, and others. The Hexapod machine tool (Bailey 1994; Hollingum 1997; Pritschow and Wurst 1997; Aronson 1997; Matar 1997) is one of the successful applications.

Research and development in new alternative mechanical architectures for machine tools can generally be divided into two categories. One studies the most suitable components for machine tools. This includes the development of independent joints with various specifications and links as well as rapid interfaces between joints and links. The other is aimed at providing a theoretical analysis (including kinetostatic analysis, dynamic analysis and optimization) system for the formulation of a suitable

configuration through a combination of all those possibilities (both in architectures and degree of freedom). In the second category, less work has been done. Our proposed investigation is therefore in the second category, especially focusing on kinetostatic analysis and optimization of parallel and hybrid architectures for machine tools. Of particular significance to new generation machine tools is the fact that there has been a growing demand for increasing stiffness, speed, precision and working volume; the proposed investigation is conducive to the application of robots to modern machine tool design.

1.2.1   Parallel Mechanism Based Machine Tools

Hexapod machine tool, as one kind of parallel kinematic machines, has been widely studied and developed by researchers. Matar (1997) defines a "Hexapod" as a geometric structure where a hexagon provides the points on a frame for six struts which are then collected into pairs to form a triangle, whose position in free space can be uniquely described by the struts length.

The parallel kinematic mechanism offers higher stiffness, lower moving mass, higher acceleration, potential higher accuracy, reduced installation requirements, and mechanical simplicity relative to existing conventional machine tools (Boër *et al.* 1999; Warnecke *et al.* 1998; Rehsteiner *et al.* 1999). By virtue of these attributes, the parallel kinematic mechanism offers the potential to change the current manufacturing paradigm. It has the potential to be a highly modular, highly reconfigurable and high precision machine. Other potential advantages include high dexterity, the requirement for simpler and fewer fixtures, multi-mode manufacturing capability, and a small foot print. A comparison between the Hexapod machine tools and the conventional machine tools is given in Table 1.1 by Giddings & Lewis. It shows that the Hexapod machine tool has improved machine tools substantially in terms of precision (about 7 times), rigidity (about 5 times), and speed (about 4 times) (Xi and Mechefske 2000).

So far, there are several companies and institutes involved in research and development of this kind of machine tool. Aronson (1997) summarized the four major companies, and they are Giddings & Lewis, Ingersoll Milling Machine Co., Hexel Corporation and Geodetic Technology International Ltd. Giddings & Lewis did some of the early

Table 1.1: Comparison of Hexapod machine tools and conventional machine tools (conducted by Giddings & Lewis Inc.)

Machine Tool	Hexapod	Convention	Improvement
Precision	4/1000"	30/1000"	7times
Rigidity	1M lb/in	0.2M lb/in	5times
Speed	2598 in/min	650 in/min	4times

pioneering effort on the Variax, the Giddings & Lewis hexapod machine. Moreover, the industrial interest is continually growing (Owen 1999).

Figure 1.1 represents a parallel mechanism module from Ingersoll Milling Machine Co. (Lauffer *et al.* 1996), it consists of a fixed upper dome platform and a moving lower platform, connected by six struts, which are precision ballscrews. On the upper platform the six struts are driven by motor driven ballnuts. These alter the position and attitude of the lower platform by extending or retracting the struts. The ballscrews join the lower platform at three points, with two struts sharing a ball-and-socket joint. Various head attachments can be incorporated to suit a variety of applications. Each individual axis (leg drive) is independent from the others and comes with a personality file containing information such as error mapping (e.g. lead pitch variation), mounting offsets, physical performance and thermal expansion characteristics.

There are some other institutes and industries doing research and development work in this area. They are, NEOS Robotics (Tricept series), Toyoda Machine Works (HexaM Machine), ITIA-CNR (ACROBAT), Seoul National University (ECLIPSE), Sandia Hexapod Testbed, Swiss Federal Institute of Technology (Hexaglide), Materials Engineering Division (MMED) from Lawrence Livermore National Laboratory (LLNL) (Octahedral Hexapod), SMARTCUTS (Simultaneous MAchining through Real Time Control of Universal Tooling System) (modular 3-DOF parallel link mechanism), LME Hexapod machine (Hexapod software model), University of Stuttgart (modular parallel mechanism design) and others.

Moreover, there are also many publications concerning the research and development of parallel kinematic machines. Heisel (1999) presents the precision requirements for parallel kinematic machine tools design. Wang *et al.* (1997) discuss the design
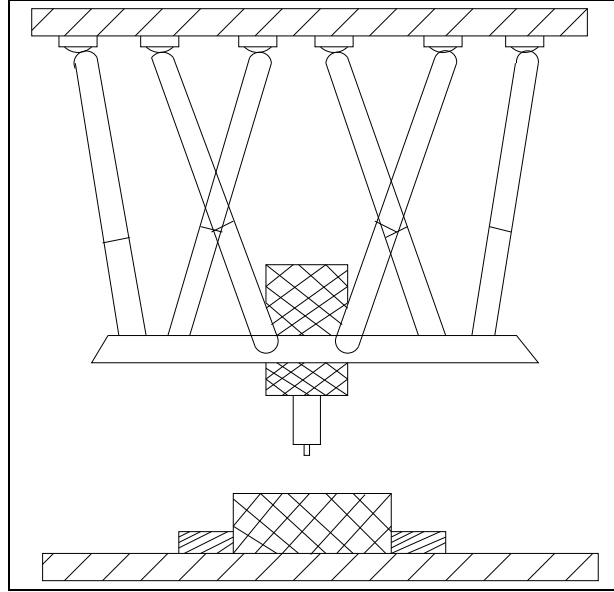
Figure 1.1: Schematic of a six-axis Hexapod machining center.

and kinematics of parallel mechanisms for manufacturing. Pritschow and Wurst (1997) describe a systematic design procedure that allows the evaluation of the technological feasibility of hexapods, and the parallel kinematic machines (PKMs) types that are currently being investigated by European researchers are presented in (Pritschow 1999). Wavering (1999) introduces the history of PKMs research at the NIST Manufacturing Engineering laboratory, the current research areas and the potential directions for future work. Abbasi *et al.* (1997) address a parametric design methodology for a special 6-6 parallel platform for contour milling. Warnecke *et al.* (1998) present the analysis, designs and variants of parallel-structure based machine tools, different design variants are compared with regard to the load of the structures and the singularities. Gopalakrishnan and Kota (1998) study various parallel manipulator configurations and the possibility of their integration under the evaluation of reconfigurable machining systems. The modular concepts for PKMs are proposed in the paper, similarly to (Wurst 1999). An approach to Parallel Kinematic Machines design integrating tools for machine configuration, synthesis and analysis is presented in (Molinari-Tosatti *et al.* 1997). Fassi *et al.* (1999) present an approach to the development of a computer aided configuration tool for parallel kinematic machines. The goal of this tool is to enable a quick comparison between different machine structures. Bianchi *et al.* (2000) propose a virtual prototyping environment for PKMs analysis to ease the industrial adoption

of PKMs by availability of methodologies and integrated tools able to analyze PKMs of any architecture in a short period of time, providing the key data needed to design the machine. Weck *et al.* (1999) discuss the substantial features of PKMs with special focus on structurally caused problems in design, control and calibration and takes Ingersoll Octahedral Hexapod and the Dyna-M concept as examples for possible solutions. Some industrial applications are reported in the literature. For instance, Honegger *et al.* (1997) present the adaptive control of the Hexaglide. Ryu *et al.* (1999) present the "Eclipse" machine tool designed for rapid machining with their research of kinematic analysis. Powell *et al.* (1999) focus on the Giddings & Lewis Variax Hexapod machine tool by presenting different metal cutting tests and analyzing the machine tools performances. Tönshoff *et al.* (1999) present the structure and characteristics of the hybrid manipulator "Georg V" at Hannover University. Pierrot and Shibukawa (1999) report the patented machine tools "HEXA" and "HexaM" at Toyoda Machine Works Ltd. Rey and Clavel (1999) display the "Delta" parallel robot, and some others.

In summary, all the existing parallel kinematic machines can be classified as follows:

1. From the viewpoint of the frame, two approaches to (PKMs) frame design exist. Ingersoll Milling Machine Co. (in conjunction with National Institute of Standards and Technology, NIST) (Figure 1.1), Hexel Corporation, and Geodetic Technology International Ltd. all use a separate frame that suspends the hexapod, while Giddings & Lewis connected the spindle platform directly to the table platform (Figure 1.2), thus avoiding thermal distortion and improving stiffness.

2. From the viewpoint of the structure, a new design called the Triax — not technically a hexapod — has been investigated by Giddings & Lewis. It will operate in only three axes. In contrast to the Hexapod machine from Ingersoll or Giddings & Lewis, The Institute for Control Technology of Machine Tools and Construction Units (ISW) of the University of Stuttgart has developed a Hexapod (Pritschow and Wurst 1997) whose motion is generated by linear movement of the base points of fixed length links and not by changing the leg length (Figure 1.3). The Hexaglide (Honegger *et al.* 1997) (Figure 1.4) from Swiss Federal Institute of Technology also falls into this type.

3. From the viewpoint of workspace volume, the Hexaglide (Honegger *et al.* 1997)
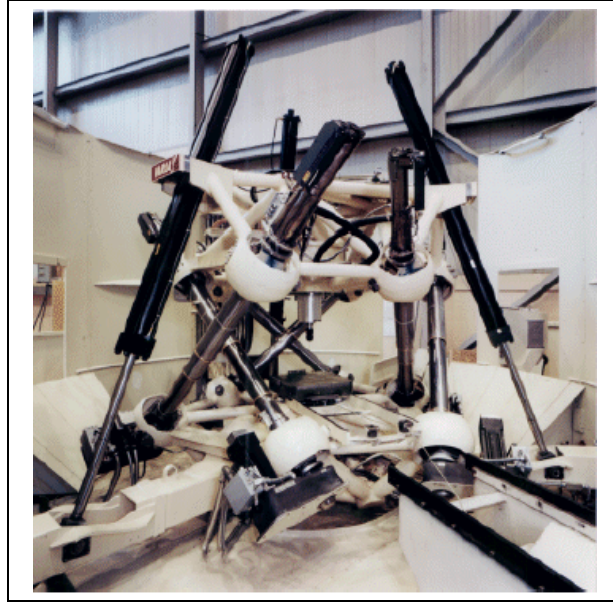
Figure 1.2: The Variax Hexacenter (Figure from Giddings & Lewis).

(Figure 1.4) from the Swiss Federal Institute of Technology differs from the Hexapod by the fact that the joints are placed on parallel guideways. Thus, instead of changing the total length of the legs, they have the possibility to make the guideways longer in order to extend the workspace of the machine in one direction. All other dimensions stay unaffected. This makes the Hexaglide an ideal mechanism for the machining of long parts. The Hexaglide is also easier to build and to measure than the Hexapod.

4. From the viewpoint of actuated joints, there are three types of parallel kinematic machines:

   - Prismatic actuated machines with variable leg lengths and fixed joints (e.g. Ingersoll, Neos Robotics),

   - Linear Motion (LM) actuated machines with fixed leg lengths and base joints movable on linear guideways (e.g. HexaM, ECLIPSE, Hexaglide, Triaglide, Linapod),

   - Revolute actuated machines with fixed leg lengths (e.g. Delta, Hexa),

5. From the viewpoint of research methodology, there are OKP (One-of-a-Kind Production) design methodology (e.g. Tricept, HexaM) which is suitable for those
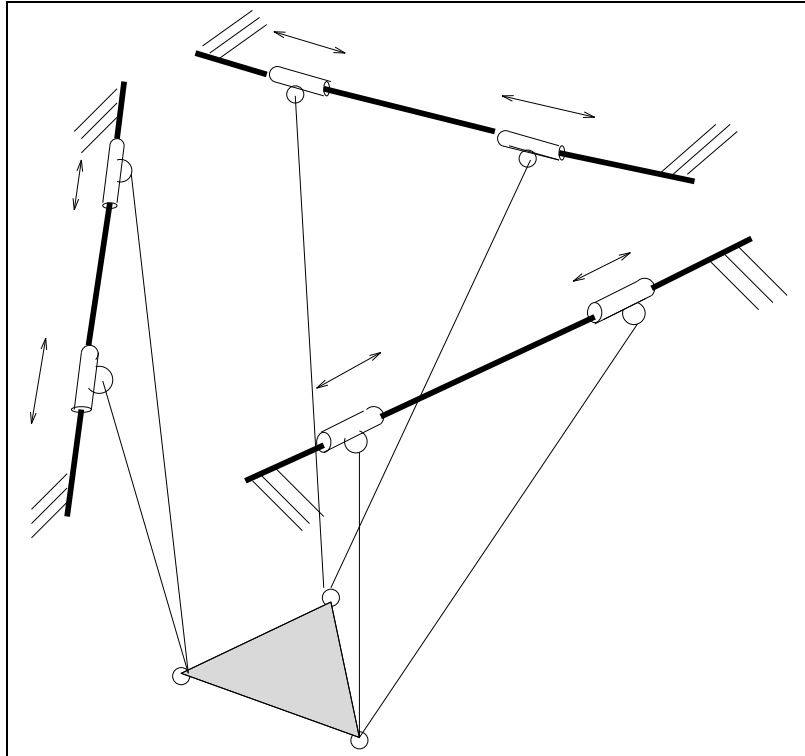
Figure 1.3: Kinematic structure of the 6-dof machine tools.

industrial companies, and systematic design of Hexapods using modular robot methodology (e.g. Linapod). Modular robot concepts and techniques have been of interest in the robotics field since the 1980s (Cohen 1992; Chen 1994), since selecting an industrial robot that will best suit the needs of a forecast set of tasks can be a difficult and costly exercise. This problem can be alleviated by using a modular robot (system) that consists of standard units such as joints and links, which can be efficiently configured into the most suitable leg geometry for these tasks. From this point of view, modular robots introduce a new dimension to flexible automation in terms of hardware flexibility, compared to conventional industrial robots.

Figure 1.5 shows some of the possible configurations of parallel kinematic mechanisms that can be found primarily in (Merlet 1997). The patented machine tools in Figure 1.5(a) "Hexa" (Uchiyama 1994) and (b) "Rotary Hexapod" (Chi 1999) are revolute actuated ones while (c) 6-dof parallel mechanism (Alizade and Tagiyev 1994) and (d) "Eclipse" (Ryu *et al.* 1999) are the combination of revolute and prismatic actuated
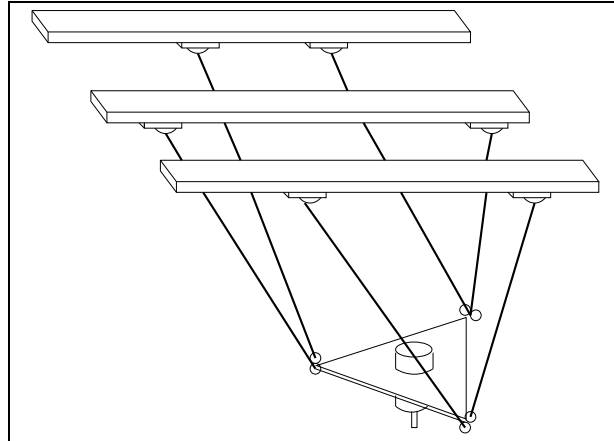
Figure 1.4: Kinematic structure of the Hexaglide

mechanisms. Figure 1.5(e) 6-dof "minimanipulator" (Tahmasebi and Tsai 1994) uses 2 prismatic actuators with fixed leg lengths and Figure 1.5(f) (Behi 1988) displays the combination of a linear driven base point and variable strut lengths.

Philosophically, most of the work above was built upon the concept of the traditional "Gough-Stewart" mechanism type. This suggests that most parallel mechanisms have six degrees of freedom. A question left open in previous work is: The vast majority of the machining is done with less than 6-dof, so why should we pay for six? In this thesis, we will focus our attention on 5-dof or less than 5-dof parallel mechanisms (Figure 1.6), since machining consists in orienting an axisymmetric body (the tool), which requires only five degrees of freedom.

In this thesis, we propose a series of n-dof parallel mechanisms which consist of n identical actuated legs with six degrees of freedom and one passive leg with n degrees of freedom connecting the platform and the base. The degree of freedom of the mechanism is dependent on the passive leg's degree of freedom. One can improve the rigidity of this type of mechanism through optimization of the link rigidities to reach the maximal global stiffness and precision.

1.2.2   Parallel Mechanisms Stiffness and Compliance Analysis

For the issues of stiffness and precision of parallel mechanisms, there also exists significant work. Although parallel mechanisms are inherently very stiff, elastic deformations
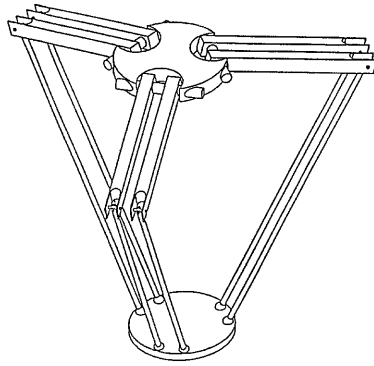
(a) The "Hexa" robot (Uchiyama 1994).
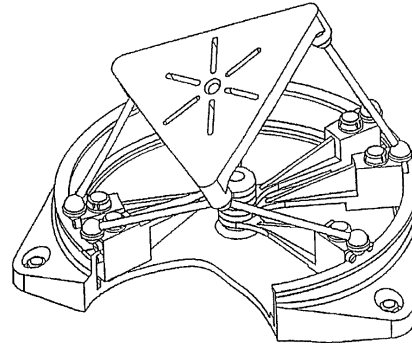
(b) The "Rotary Hexapod" by Hexel (Chi 1999).
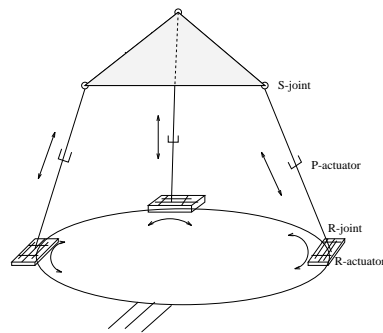
(c) Circular movement of the base point.
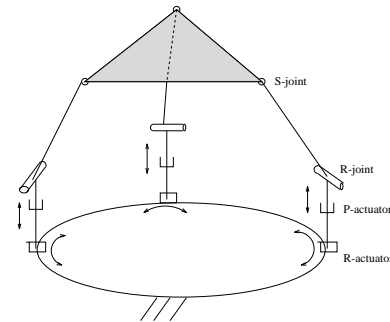
(d) "Eclipse" from SNU.
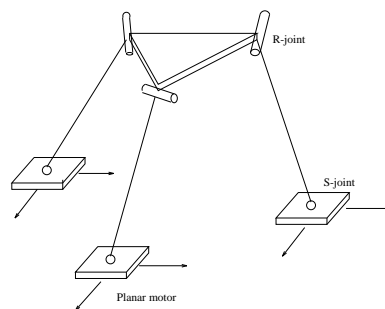
(e) 6-dof "minimanipulator".
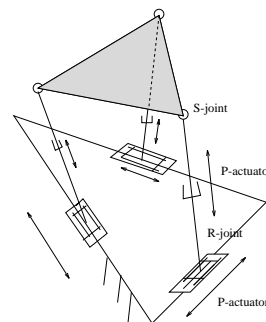
(f) Combination of linear driven base point and variable strut length.

Figure 1.5: Selected parallel kinematic mechanisms.
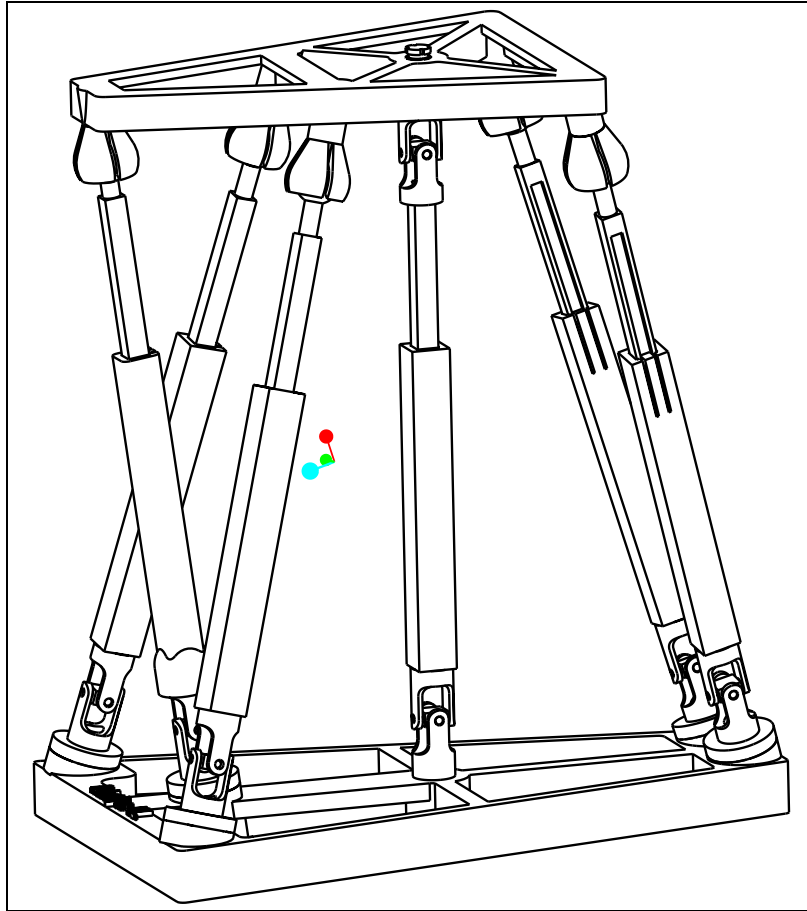
Figure 1.6: CAD model of the 5-dof parallel mechanism (Figure by Gabriel Coté).

may still occur under large payloads. In the real world, what the standard of a rigid body is has been studied by many researchers. Two main limitations of a rigid body are noted: i) the accuracy of the rigid body parameters with respect to the real values, and ii) the validity of the rigid body assumption. Several authors have proposed methods for the calibration of the rigid body parameters (Everett and Hsu 1989; Hayati *et al.* 1988; Hsu and Everett 1985; Stone 1987). On the other hand, other researchers have incorporated the structural flexibilities in the geometric model of the mechanism (Chen and Chao 1986; Judd and Knasinski 1990; Whitney *et al.* 1986). Still others have focused on dynamic semi-flexible models in a control oriented perspective (Chang and Hamilton 1991a; Chang and Hamilton 1991b; Jonker 1990). Experimental results have been reported to justify the efforts committed to the development of representative semi-flexible models. The gain in absolute precision obtained from rigid body geometric calibrations has been said to be of the order of 75% to 80% (Caenen and Angue

1990; Judd and Knasinski 1990). An additional 16% increase in absolute precision was obtained by Caenen and Angue (1990) when the calibration of current industrial robots incorporated flexibilities.

Incremental flexible models have also been proposed. In these models, gross motion is described with the Denavit-Hartenberg convention (Denavit and Hartenberg 1955), while, for example, additional homogeneous transformations express local corrections, defined with the help of small displacement theory (Tang and Wang 1987). Moreover, joint variables are sometimes expanded to compensate for joint flexibilities. Meghdari (1991) worked on a model similar to Tang and Wang (1987) but which included only vertical bending. A single beam is associated with the mechanism: individual joints are thus regarded as non-rigid components of that beam. Caenen and Angue (1990) enhanced a model first developed by Hsu and Everett (1985). In this model, three springs are added to each of joint and the three orientation parameters per link are amended in order to compensate for the effects of gravity. Cléroux *et al.* (1995) presented a semi-flexible static model. The term semi-flexible is used to denote the fact that a first order approximation is used in the description of the orientation changes induced by the beam deformation, but she took the whole structure as the objective and it brought difficulties in parameter calibrations. Some others (Fattah *et al.* 1994) have addressed the flexibilities in parallel robotic mechanisms. But none of them use the theory of lumped flexibilities to calibrate the stiffness of the mechanism. This theory will be employed in this thesis.

Stiffness is a very important factor in many applications including machine tool design, since it affects the precision of machining. Induced vibration is explicitly linked to machine tool stiffness. For a metal cutting machine tool, high stiffness allows higher machining speeds and feeds while providing the desired precision, surface finish and tool life (Huber 1993), thus reduce vibration (such as chatter). Therefore, to build and study a general stiffness model of parallel mechanisms is very important for machine tool design.

From the viewpoint of mechanics, the stiffness is the measurement of the ability of a body or structure to resist deformation due to the action of external forces. The stiffness of a parallel mechanism at a given point of its workspace can be characterized by its stiffness matrix. This matrix relates the forces and torques applied at the gripper link in

Cartesian space to the corresponding linear and angular Cartesian displacements. The stiffness matrix of a mechanism is generally defined as the transformation which relates the generalized force (force and torque) applied to the end-effector and its resulting displacement (translation and orientation) (Asada and Slotine 1986). This matrix can be obtained using kinematic and static equations. Gosselin (1990) developed stiffness maps for a Stewart Platform for specified directions of perturbation.

Two main methods have been used to establish mechanism stiffness models. The first one is called matrix structural analysis (Martin 1966; Wang 1966), which models structures as a combination of elements and nodes. The stiffness matrix depends on the nature of the elements in the structure. Clinton *et al.* (1997) used this method to derive the stiffness matrix for each of the elements in the structure model and assemble them into a system-wide stiffness matrix. In their study, the mechanism stiffness model relies on truss elements. They also used experimental stiffness measurements to estimate the system parameters, the average error between the results calculated based on the model and the experimental results was around 9.0%. The second method relies on the calculation of the parallel mechanism's Jacobian matrix (Gosselin 1990; El-Khasawneh and Ferreira 1999; Kerr 1989; Tahmasebi 1993). Among others, El-Khasawneh and Ferreira (1999) addressed the problem of finding the minimum and maximum stiffnesses and the directions for a mechanism in a given posture. In addition, the computation of stiffness in an arbitrary direction is also discussed in their paper. Furthermore, they used Finite Element Analysis model to demonstrate the correctness of their model. The fact that the minimum stiffness is experienced in the direction of the eigenvector that corresponds to the minimum eigenvalue of a stiffness matrix of the mechanism is shown in their paper. A corresponding result is obtained for the maximum stiffness of the mechanism. On the other hand, they used the eigenvalues of the system stiffness matrix to represent the principal stiffness in different directions. Since the units of the different entries of the matrix are not uniform, the dimensions of the eigenvalues of the stiffness include both force/length and force-length. Hence, the eigenvalue problem for stiffness is dimensionally inconsistent and does not make sense physically. Tahmasebi (1993) also used the eigenvalues to determine the stiffness of mechanisms. He improved the matrix condition and defined a dimensionally-uniform generalized force applied to the platform and used it in connection with the definitions of the previous Jacobian matrix to obtain a dimensionally-uniform stiffness matrix. Because all the aforementioned

work relies on the eigenvalues, compound stiffnesses are obtained which are difficult to interpret physically. Gosselin (1990) uses the diagonal elements of the stiffness matrix as the stiffness. These elements represent the pure stiffnesses in each direction, they reflect the stiffness of machine tools more clearly and directly. Hence, this method is adopted in this thesis.

1.3 The Objectives and Scope of the Study

Conventional machine tools are usually based on a serial structure. There are as many degrees of the freedom as required, and the axes are arranged in series. This leads to a single kinematic chain. The axes are usually arranged according to the Cartesian axes, which means there is a X, Y, and Z axis and rotational axes if needed. These machines are easy to operate because each axis directly controls one Cartesian degree of freedom and there is no coupling between the axes.

A parallel kinematic machine promises to increase stiffness, higher speed and acceleration due to reduced moving mass, reduced production and installation costs. Research in this kind of architectures for machine tools has been growing since the 1980s (Bailey 1994; Kempfer 1994; Hollingum 1997; Aronson 1997). Although a number of new devices were patented, none seems to take the structure flexibility into account. While the joints and links have become commercially available, the study for the most promising architecture for machine tools through kinetostatic analysis, dynamics and optimization is still a challenge. The proposed investigation plans to meet this challenge. The **aim** of this thesis work is to investigate new alternative mechanical architectures which could be used in the design of a machine tool with parallel or hybrid architecture. To reach this aim, the **objectives** are set as follows:

1. *Development of a topological representation and generation of all possible architectures that will provide 5 degrees of freedom between the tool and the workpiece.* The topological representation serves to develop a database for conceptual design to obtain the most promising kinematic architectures for 5-dof or fewer than 5-dof machine tools. The key consideration in achieving this objective are (i) both the tool and the workpiece can be actuated independently and 5 dofs are

required for manufacturing tasks, (ii) the possible combinations of 5 dofs are: (5,0), (4,1) and (3,2), and (iii) for each of these combinations, the kinematic chains involved may lead to several possibilities (serial, parallel or hybrid) and additionally, redundancy may be an option. At the end of this study, a detailed list of possible topologies will be obtained and the most promising architectures will be highlighted.

2. *Development of geometric design model.* The key task is for the topologies selected in the previous study, to define geometric parameters and investigate the geometric design. The geometric design must take into account the actuation issues, the working volume, and mechanical interferences. The selected designs will be modeled using *Pro-Engineer* which will facilitate this step. Again, all possibilities of configurations will be investigated.

3. *Development of a general model of the stiffness of the mechanisms screened out from the list of some promising configurations.* Using a formulation based on lumped flexibilities, write a general model of the stiffness of the concerned mechanisms. Using this model, all concerned mechanisms will be analyzed for their stiffness and accuracy at the tool, which is the most important property of the mechanism. In the lumped model, links and actuators will be replaced by springs whose stiffness will represent the stiffness of the link or the actuator. This will allow to obtain a relatively simple kinetostatic model and with which all mechanisms will be analyzed.

4. *Kinetostatic modeling and optimization.* Using the kinetostatic model developed in the preceding step, optimize the most promising architectures for stiffness (accuracy) based on constraints associated with size and geometry.

The **product** of the proposed investigation now becomes obvious: build the kinetostatic model, optimize the most promising architectures for stiffness (accuracy). Although the proposed investigation is aimed at the most promising 5-dof or fewer than 5-dof machine tools architectures for accuracy, those issues addressed in the four objectives are fundamental. Therefore the results of the work can provide a framework for facilitating a further study of parallel mechanisms for machine tools such as parameter calibration, simulation and control program generation.

1.4   The Main Philosophy behind the Thesis Work

Taking the discussion of the preceding three sections as input we shall set up some philosophies or strategies behind this thesis work and summarize them as follows:

1. *Learn from Chebychev-Grübler-Kutzbach criterion*

   The degree of freedom (or Mobility) of a kinematic chain can be defined as the minimum number of independent variables necessary to specify the location of all links in the chain relative to a reference link. A preliminary evaluation of the mobility of a kinematic chain can be found from the Chebychev-Grübler-Kutzbach formula. It will be employed to enumerate all the possibilities of kinematic chains and finally the most promising kinematic architectures in this thesis.

2. *Place emphasis on kinetostatic analysis*

   We can describe the term "Kinetostatic Analysis" as such: Given the mechanism motion, calculate the unknown internal joint forces and external input forces or torques. Kinetostatic analysis includes two analyzes in this thesis work:

   - kinematic solutions to provide the mechanism motion;
   - stiffness solutions to relate the forces and torques to the motion;

3. *Learn from Principle of Kinematic/Static Duality*

   Since a duality exists between the kinematics and statics of mechanisms, therefore, the statics of mechanisms can be taken as a transition between their kinematics and dynamics. Kinematic/static duality can be derived by considering the power input to and output from a system which can neither store nor dissipate energy, namely, a system in which kinetic energy, strain energy, friction and damping are all absent and where gravitational forces are considered as external forces applied to the system. In this case, the principle of conservation of energy allows us to conclude that the power input to the system is equal to the power output from the system. This principle will be used to establish the kinetostatic model.

4. *Learn from the theory of lumped flexibilities*

In the analysis of every engineering problem, the system under scrutiny must be represented by a physical model. It is often permissible to represent a *continuous* or *distributed-parameter system* (in which the mass and spring elements are continuously spreaded over a space) by a *discrete* or *lumped-parameter model* (in which the mass and spring are concentrated at certain points in a space).

In this thesis work, we will represent the motions as the sum of large motions and small motions, and build a lumped model where joints and actuators will be replaced by springs whose stiffness will represent the stiffness of the link or the actuator. We assume that springs are located in specified localized places, and then the flexible links can be considered as equivalent to rigid ones. Therefore, the large motions will be the equivalent to rigid link motions but not identical to the actual rigid link motion. The small motions are both small rigid body motions and body deformations, i.e., the deviations of the flexible link manipulator relative to the equivalent rigid links, and the small motions can be replaced by lumped springs in our case.

5. *Learn from Genetic Algorithms*

Genetic algorithms have been shown to solve linear and nonlinear problems by exploring all regions of state space and exponentially exploiting promising areas through mutation, crossover, and selection operations applied to individuals in the population (Michalewicz 1994).

The architectures being studied, contain many geometric and behavior parameters and complicated matrix computations. In order to optimize the structure to reach the optimal stiffness, it is very difficult to write out the analytical expressions for each stiffness element. Moreover, for traditional optimization methods, only a few geometric parameters (Gosselin and Guillot 1991) could be handled due to the lack of convergence of the optimization algorithm when used with more complex problems. Therefore, genetic algorithms are the best candidate and will be used for such optimization problems.

1.5   The Organization of the Thesis

Chapter 2 presents the topological study of the kinematic structure. Some concepts underlying kinematic structure development will be addressed, such as the Chebychev-Grübler-Kutzbach criterion — a basic theory for kinematic chain degree-of-freedom distribution and criteria for better and practical kinematic structures of machine tools. All the possible kinematic structures which can be used for 5-dof or fewer than 5-dof machine tool design will be enumerated based upon these concepts. Finally, the detailed list of possible topologies has been obtained and the most promising architectures are pointed out under the design criteria. These most promising architectures will be analyzed and optimized in Chapters 4, 5, 6 and 7.

Chapter 3 introduces the lumped flexibility model for joints and links. A general stiffness model for fully-parallel mechanisms is established. Implementation of the models for planar 2-dof and planar 3-dof parallel mechanisms are given. Furthermore, the correctness of the stiffness model is verified with Pro/Engineer.

Chapter 4 and Chapter 5 present several new types of n-DOF parallel mechanisms with one passive constraining leg. The geometric configuration of these new types of mechanisms is introduced first, followed by the kinematic analysis for this type of mechanisms. This includes the solution of the inverse kinematic problem, Jacobian matrices and global velocity equations, in which structures with rigid-link and flexible-link are discussed, respectively. The general kinetostatic model is then established with consideration of the characteristics of lumped joints and links model. The arguments to develop this model are illustrated. Implementation of the model is discussed as well. Examples for this type of mechanisms with 3-dof, 4-dof, and 5-dof are given. Stiffness mappings are illustrated in these chapters.

There are four purposes for the implementations in Chapters 4 and 5:

- to demonstrate the idea that flexible links have significant effects on parallel kinematic machines' stiffness and accuracy. These effects cannot be neglected in machine tool design.

- to provide the designers with a powerful tool to obtain the design guidelines easily.

- to demonstrate that the kinetostatic model can be easily extended to any other kind of parallel kinematic machines.

- to verify the correctness of the theories, methods, and the kinetostatic model.

Chapter 4 discusses the mechanisms with prismatic actuators, while Chapter 5 discusses the mechanisms with revolute actuators. In particular, Chapter 4 also presents a commercial parallel kinematic machine called "Tricept" and its kinetostatic analysis.

Chapter 6 describes the kinetostatic analysis and general stiffness model for spatial six-degree-of-freedom mechanisms. Cases of 3-leg and 6-leg fully-parallel mechanisms with revolute actuators and 6-leg fully-parallel mechanism with prismatic actuators are given, respectively. In this chapter, an alternative method is used to establish the kinetostatic model. It is based on the theorem of velocity compatibility (Angeles 1997). The general purpose of the discussion in this chapter is to further provide some verifications of the theories, viewpoints, and approaches developed in the preceding chapters in an alternative method and predicate the perspective of kinetostatic models.

Chapter 7 addresses the implementation of optimization techniques. The optimum design of parallel kinematic mechanisms is based on global stiffness improvement related to geometric and behavior parameters. The genetic algorithms theory is first briefly introduced, then the determination of parameters and the objective function establishment are addressed as well. The detailed analysis of the kinetostatics of the parallel manipulators conducted in previous chapters are used to define and optimize their geometric sizes and properties. Finally, the implementation and optimal results for all kinds of mechanisms discussed in this thesis are given. Results show that the global stiffnesses of the mechanisms are significantly increased after optimization. Machine tool designers can obtain the desired stiffness easily by adjusting the geometric dimensions and properties.

Chapter 8 brings together the most important conclusions and observations of the study and suggests the work to be done in the future.

Chapter 2

Mechanism Kinematic Structure

2.1 Introduction

One of the objectives of this thesis work is to find the most promising kinematic struc-
tures which can be used for machine tool design. Hence, some well-known principles
are applied to investigate all the possibilities of structure in detail. A mechanism is
defined as a kinematic chain with one of its components (link or joint) connected to the
frame. A kinematic chain consists of a set of links, coupled by joints (cylindrical, pla-
nar, screw, prismatic, revolute, spherical, and Hooke) between adjacent links. In this
chapter, a topological study of different combinations of kinematic chain structures will
be performed using a graph representation approach. The number of links and joints for
the desired system and their interconnections, neglecting geometric details (link length
and link shape), are described. The possible architectures that will provide 5 degrees

of freedom between the tool and the workpiece are generated. In Section 2.2, the basic concept of the graph representation of a kinematic structure is addressed. Then, a topological study of the kinematic structures is described in Section 2.3. First, the Chebychev-Grübler-Kutzbach criterion is introduced. Second, requirements for possible kinematic structures are set up. Finally, the structural representation of kinematic chains and architectures with consideration of serial, parallel and hybrid cases is illustrated. A remark on the role of redundancy is also given. Section 2.4 discusses the reason for choosing parallel and hybrid mechanisms for PKMs. In Section 2.5, the most promising architectures are established by specifying the design criteria of the desired kinematic structures. A summary with discussion of related work is presented in Section 2.6.

2.2 Graph Representation of Kinematic Structures

A kinematic chain can be described as a set of rigid bodies attached to each other by kinematic pairs, resulting in a mechanical network containing joints and links (Gosselin 1988). A kinematic structure represents the kinematic chain without considering the detailed geometric, kinematic, and functional properties. The range of kinematic structures given particular constraints on the number and type of joints and links can be examined exhaustively. This range represents a set of logical possibilities for design of a particular type of mechanism. This set is a framework in which designs are to be realized.

In this thesis, a systematic method of enumerating all the possible kinematic chains — kinematic architectures — is needed to meet the required degrees of freedom, i.e. 3-dof, 4-dof, and 5-dof. There were several methods reported in the literature. Hunt (1978) used the theory of screw systems to enumerate parallel mechanisms exhaustively. Earl and Rooney (1983) proposed a network approach which enables consideration of two or more structures into another one. In this thesis, we will use a graph representation.

Graph theory is a field of applied mathematics (Harary 1969), which provides a useful abstraction for the analysis and classification of the topology of kinematic chains,

and it offers a systematic way of representing the topology of complex kinematic chains. The graph of a kinematic chain consists of a diagram where each link is represented by a point and each joint by a line. Thus, the graph representation of a kinematic chain will take the form of a collection of points connected by lines. The graph representation of kinematic chains has been used by, among others, Baker (1992), Gosselin (1988), Tsai and Lee (1989), Zhang (1994), Zhang and Li (1999).

2.3 Topological Study

Since both the tool and the workpiece can be actuated independently and that 5 dofs are required for manufacturing tasks, the possible combinations of 5 dofs are: (5,0), (4,1) and (3,2). For each of these combinations, the kinematic chains involved may lead to several possibilities (serial, parallel or hybrid) and additionally, redundancy may be of an option. The followings are the details for this enumeration process.

2.3.1 Chebychev-Grübler-Kutzbach Criterion

The degree of freedom (or mobility) of a kinematic chain (Hunt 1978) can be defined as the minimum number of independent variables necessary to specify the location of all links in the chain relative to a reference link. The choice of the reference link does not affect the resulting mobility. A preliminary evaluation of the mobility of a kinematic chain can be found from the Chebychev-Grübler-Kutzbach formula.

$$l = d(n - g - 1) + \sum_{i=1}^{g} f_i \tag{2.1}$$

with

l: the degree of freedom of the kinematic chain;

d: the degree of freedom of each unconstrained individual body (6 for the spatial case, 3 for the planar case) (Hunt 1983);

n: the number of rigid bodies or links in the chain;

g: the number of joints; and

f_i: the number of degrees of freedom allowed by the ith joint;

2.3.2 Possible Architectures with Five Degrees of Freedom between the Tool and the Workpiece

2.3.2.1 Serial Mechanisms

Serial mechanisms have been extensively studied in terms of their design, kinematic and dynamic modeling, and control by many researchers. When properly designed, the serial structure has the benefit of possessing a large workspace volume in comparison to the physical size of the mechanism.

Since serial mechanisms only have one open kinematic chain, this means that the serial mechanisms only have one possibility in architecture.

The serial mechanisms have many drawbacks. Due to the serial nature of actuation and transmission, related masses must be mounted distal to the base of the mechanism leading to a small ratio of payload over machine mass, poor dynamic performance in terms of acceleration capability, and poor system stiffness presented at the end-effector. Since a lower axis has to carry both the loads (in all directions) and the weights of all its upper axes, dynamic behaviors of the lower axes will be poor, especially to machine tools which carry high loads. In addition, the serial structure leads to joint errors being additive, and combined with the inherent low system stiffness, this leads to poor accuracy at the end-effector. Thus, the drawbacks in their structures limit the performance.

2.3.2.2 Parallel Mechanisms

Among the three possibilities (serial, parallel and hybrid), the parallel mechanisms are the basic and the most important ones in building all the possible architectures, because of the disadvantages of the serial mechanisms. The hybrid mechanisms will be built through the combination of parallel mechanisms.

The possibility of parallel mechanisms will be investigated for the combinations of dofs in (5,0), (4,1) and (3,2). The workpiece can be fixed (0-dof), or move along one

axis (1-dof) or move along the X and Y axes (2-dof) or rotate about one or two axes. Hence, one will consider the possibilities of parallel mechanisms with 5-dof, 4-dof, 3-dof and 2-dof; besides, the case with 6-dof is taken as an option with redundancy. The detail is shown as follows.

1. DOF distributions for each leg

   For a given parallel platform, we can always make the following assumptions:

   number of known bodies = 2 (platform and base),

   number of parallel legs = L, and

   degree of freedom of the ith leg = f_{l_i},

   then one can rewrite eq. (2.1) as

   $$
   \begin{aligned}
   l &= 6[2 + \sum_{i=1}^{L}(f_{l_i} - 1) - \sum_{i=1}^{L} f_{l_i} - 1] + \sum_{i=1}^{g} f_i \\
   &= 6 - 6L + \sum_{i=1}^{g} f_i
   \end{aligned}
   \tag{2.2}
   $$

   From this equation, it is apparent that there exist thousands of possibilities for 5-dof or less than 5-dof cases. Hence, some constraints introduced and are specified as follows:

   - from the viewpoint of fully-parallel mechanism, the maximum number of parallel legs are kept equal to the degree of freedom of the mechanism, thus to guarantee the possibility of installing one actuator in each leg, one has

     $$L \leq l \tag{2.3}$$

   - although two-leg spatial parallel mechanisms are of little direct use independently, they are useful to constructing "Hybrid" mechanisms, the minimum number of the leg is given by

     $$L \geq 2 \tag{2.4}$$

   Based on the constraints represented by eqs. (2.3) and (2.4), and one can enumerate the possible dofs distributions as in Table 2.1. It is noted that these are the basic combinations for different architectures, and one can remove or add legs which have 6-dof for symmetric purpose in any of the basic structures at ease.

Table 2.1: The possible degree-of-freedom distribution for each leg.

Degree of freedom	Number of legs	f_{l_1}	f_{l_2}	f_{l_3}	f_{l_4}	f_{l_5}	f_{l_6}
l = 2	L = 2	2	6				
		3	5				
		4	4				
l = 3	L = 2	3	6				
		4	5				
	L = 3	3	6	6			
		4	5	6			
		5	5	5			
l = 4	L = 2	4	6				
		5	5				
	L = 3	4	6	6			
		5	5	6			
	L = 4	4	6	6	6		
		5	5	6	6		
l = 5	L = 2	5	6				
	L = 3	5	6	6			
	L = 4	5	6	6	6		
	L = 5	5	6	6	6	6	
l = 6	L = 2	6	6				
	L = 3	6	6	6			
	L = 4	6	6	6	6		
	L = 5	6	6	6	6	6	
	L = 6	6	6	6	6	6	6

2. Possible Structures

The variables for combining different kinds of architectures are mainly decided by (i) leg length; (ii) position of the base points; or (iii) both the leg length and position of the base points.

(a) Possible legs

Based on the required DOF distributions for each leg, one can find different kinds of legs to meet the requirement through the combination of different joints such as spherical joint (with 3-dof), Hooke joint (with 2-dof), revolute joint (with 1-dof) and prismatic joint (with 1-dof). One can combine them to meet the dof requirements for each leg shown in Table 2.2, where

S: spherical joint;

R: revolute joint;

H: Hooke joint; and

P: prismatic joint;

Table 2.3 shows all the possible legs with a different degree-of-freedom.

(b) Vertex structures

From the literature related to the Stewart platform, various architectures have been developed or proposed for the platform mechanisms, such as 3-6, 4-4, 4-5, and 4-6 (the numbers of vertices in the mobile and base plates) platforms (Chen and Song 1992; Fichter 1986; Griffis and Duffy 1989; Lin *et al.* 1994; Zhang and Song 1992). Since two spherical joints can be combined to one concentric spherical joint, one can obtain two types of vertices for parallel mechanisms as shown in Figure 2.1.
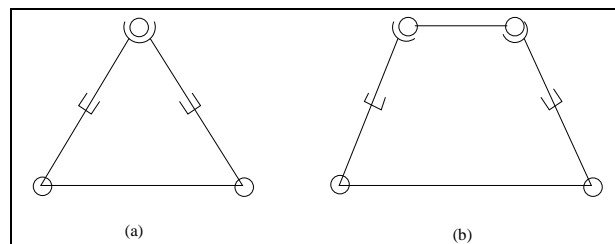
Figure 2.1: Two types of vertex structures.

Table 2.2: Possible joint combinations for different degrees of freedom.

Number of possibilities	DOFs = 2	DOFs = 3	DOFs = 4	DOFs = 5	DOFs = 6
1	2R	1R2P	1S1P	1S2R	2S
2	2P	2R1P	1S1R	1S2P	1S1H1P
3	1R1P	3R	1R3P	1S1R1P	1S1H1R
4	1H	3P	2R2P	1S1H	1S3R
5		1H1R	3R1P	1H3R	1S3P
6		1H1P	4R	1H2R1P	1S2R1P
7		1S	4P	1H1R2P	1S1R2P
8			1H2R	1H3P	1H4R
9			1H2P	5R	1H3R1P
10			1H1R1P	4R1P	1H2R2P
11				3R2P	1H1R3P
12				2R3P	1H4P
13				1R4P	6R
14				5P	5R1P
15					4R2P
16					3R3P
17					2R4P
18					1R5P
19					6P

Based on these two vertex structures, various types of parallel mechanism structures can be obtained through different arrangements of the joints on the base and mobile platforms.

(c) Platform structures

Once the type of vertex structure is decided, one can obtain the platform structure according to the number of vertices.

3. Possible architectures for parallel mechanisms

Based on the above analysis, one can assemble all the possible architectures as

Table 2.3: Possible leg types with different degrees of freedom.

Possible numbers	DOFs = 2	DOFs = 3	DOFs = 4	DOFs = 5	DOFs = 6
1	2R	1S	2R1H	1H2R1P	1S2R1P
2	1R1P	2R1P	1H1R1P	2H1R	1S1H1P
3	1H	1R2P	1S1P	2H1P	1S1H1R
4		3R	1S1R	1S1R1P[1]	1S1R1P
5		3P	2R2P	1S2R[1]	1S1H1P
6		1H1R	1R3P	1S2P	2S
7		1H1P	3R1P	1H3P	1S3P
8			4R	1H1R2P	1S3R
9			4P	1H3R	1H2R2P
10			1H2P	4R1P	1H3R1P
11				5R	1H4R
12				5P	6R
13				1R4P	6P
14				3R2P	1H4P
15				2R3P	3R3P
16					1H1R3P
17					5R1P
18					1R5P
19					2R4P
20					4R2P
Total possibilities	3	7	10	15	20

shown in Figure 2.2 to Figure 2.5.
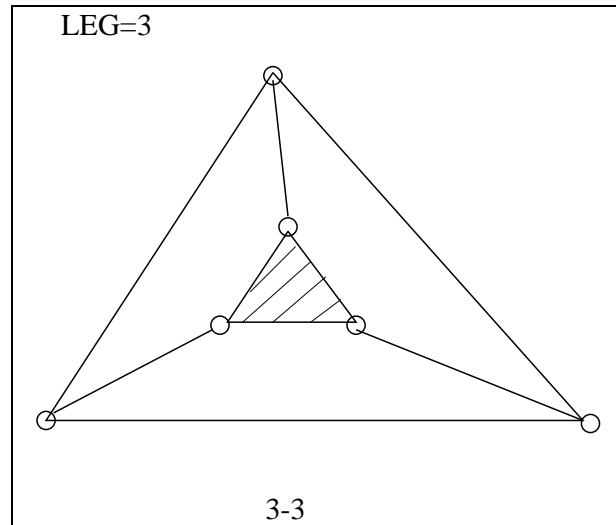
Figure 2.2: Possible architectures for parallel mechanisms with 3 legs.

4. The most promising architectures

As listed in Table 2.1 and Table 2.2, although we have already given constraints to DOF distributions for each leg, there are still lots of possible combinations for parallel mechanisms which meet the machine tool's DOF requirement, *e.g.*, for DOFs = 3, from Table 2.1, there are 3 possible combinations of legs with degree-of-freedom of 3, 4, 5, and 6. Meanwhile, from Table 2.2, there are 7, 10, 14, and 19 possible combinations for legs with dofs of 3, 4, 5, and 6, thus we still have many architectures through the permutation and combination. In order to find the most promising architectures, the criteria for selection of joints and legs are given as follows

(a) Proper number and type of DOFs

In order to ensure the required motions (i.e., 5-dof between the tool and the workpiece) in Table 2.4, the DOFs distribution numbers and the type of motions for each leg should be properly arranged. Each leg can be facilitated with spherical, prismatic, Hooke and revolute joints.

(b) Simplicity and practicability

The legs used in machine tools must be simple and practical. For the sake of the simplicity and dexterity of mechanism, we prefer to use 'spherical'
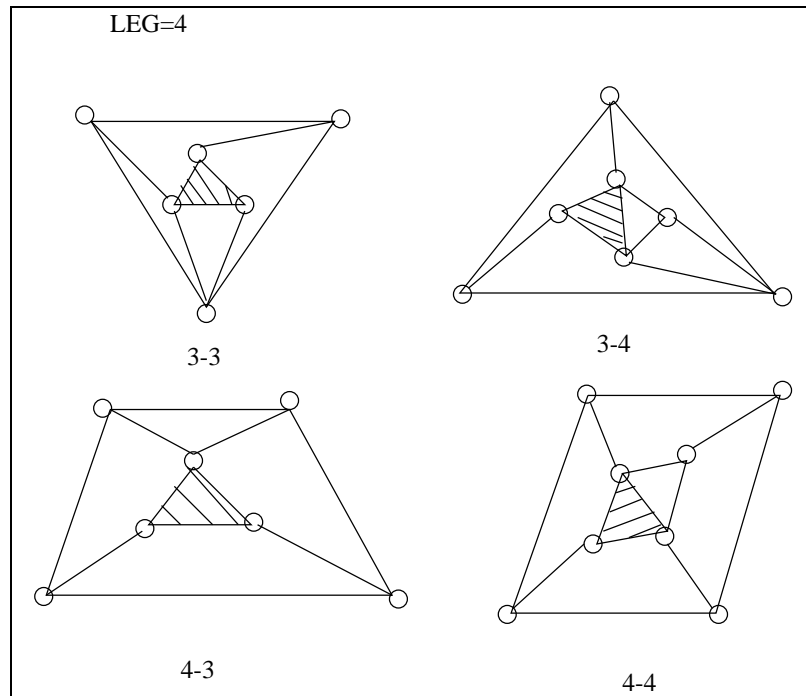
Figure 2.3: Possible architectures for parallel mechanisms with 4 legs.

pairs as the joints between link and platform for those legs with more than 3 dofs. Since the serially connected revolute joints easily lead to 'Singularity' and the 'manufacturability' is difficult, so we abandon to use of more than 2 revolute joints connected in series.

(c) Elimination of passive prismatic joints

Because it is difficult to control passive prismatic joints, in order to avoid the existence of passive prismatic joints, we specify

$$\text{Number of actuators} \geq \text{Number of prismatic joints} \qquad (2.5)$$

meanwhile, as we desire to put the actuators at the base of each link, therefore at most one prismatic joint can be used for each leg.

(d) Elimination of the rotation around the Z axis

Since the rotation around the Z axis is not needed, we can introduce a n-dof passive leg into the mechanism to reach the desired motion. "Spherical joint" on the movable platform will be replaced by "Hooke joint" + "Prismatic joint" or "Hooke joint" + "Revolute joint" so as to constrain the rotation around the Z axis. The passive constraining leg will be put in the center
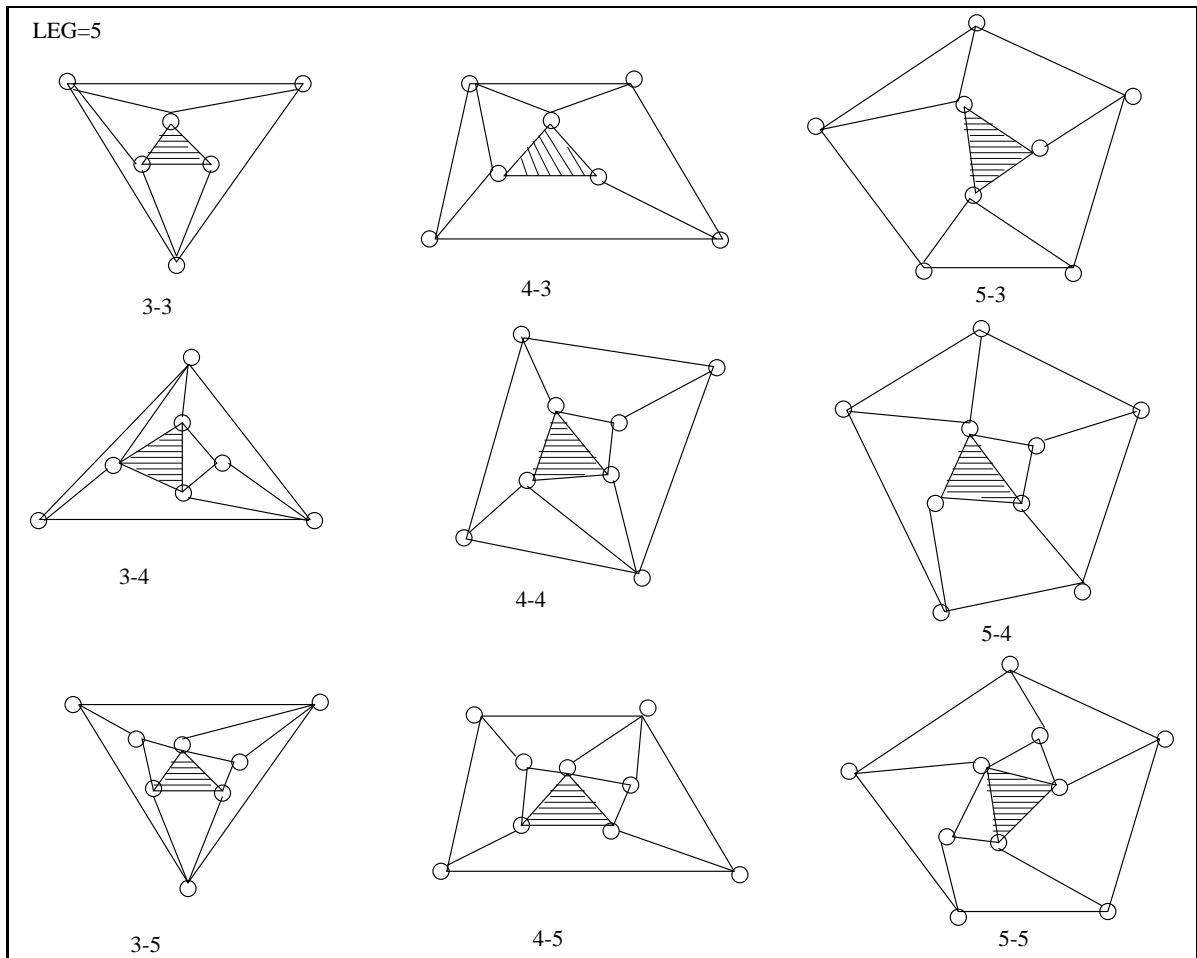
Figure 2.4: Possible architectures for parallel mechanisms with 5 legs.

of the platform to minimize the torque and force. Since the external loads on the platform will induce a bending and/or torsion in the passive leg, its mechanical design is a very important issue which can be addressed using the kinetostatic model later. In this case, the actuators are put in each of the identical legs and leave the special one (different DOFs) as the passive link since its structure in design size is larger than the other legs to sustain the large wrench.

(e) Structure of the mechanisms

The study is based on fully-parallel mechanisms, but one can add legs (with 6-dof) to keep the structure symmetric. For the shape of the platforms, one should avoid the use of regular polygon, since it may lead to singularity.
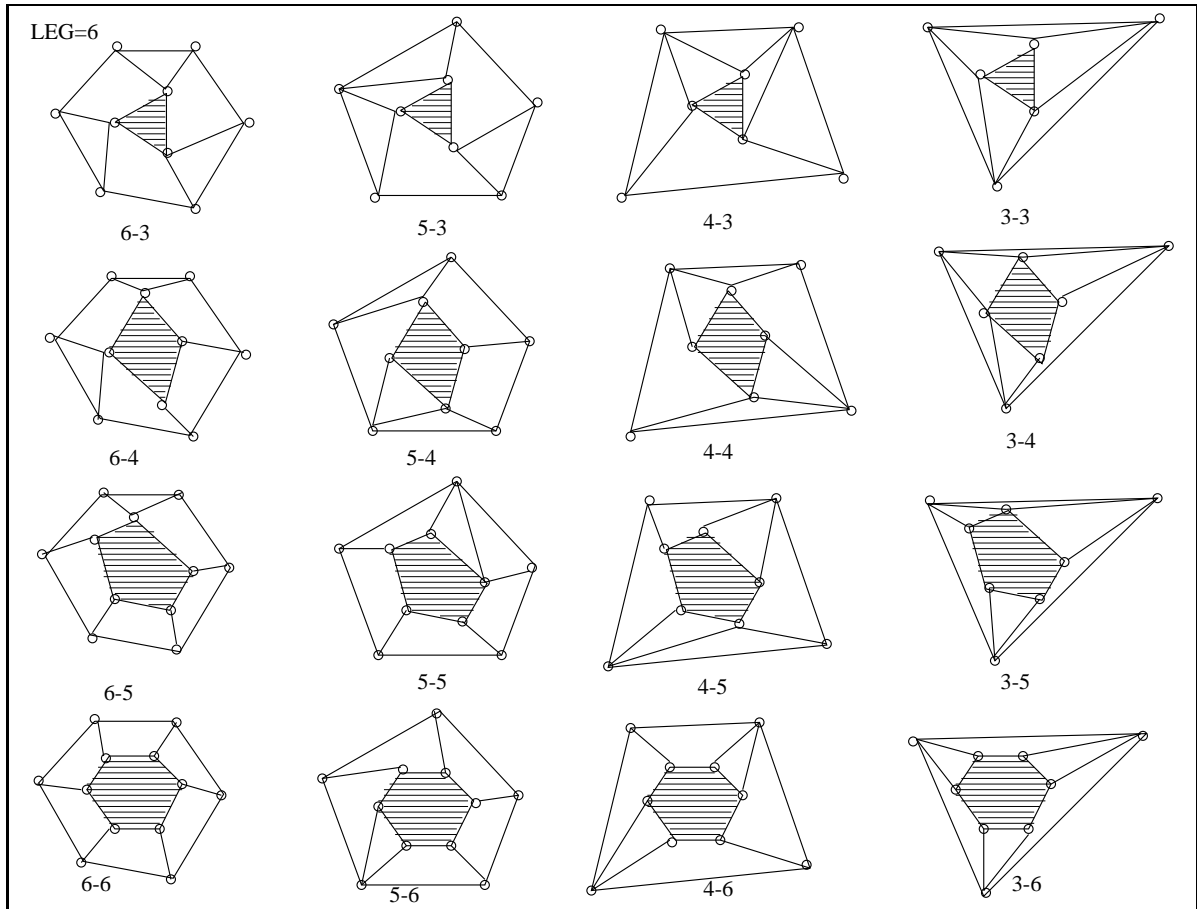
Figure 2.5: Possible architectures for parallel mechanisms with 6 legs.

Based on the discussion above, we eliminate some of the impractical joint combinations and obtain the prospective ones as shown in Table 2.5

Through the combinations of the possibilities, we obtain the number of the most promising possible architectures shown in Table 2.6. When $L = l$, we obtain a fully-parallel mechanism.

2.3.2.3 Hybrid Mechanisms

A hybrid (serial-parallel) mechanism is a combination of serial and parallel mechanisms. It comprises two parallel actuated mechanisms connected in series, one of them is the upper stage, the other is the lower stage, and the moving platform of the lower stage is the base platform of the upper stage. This special structure results in a mechanism

Table 2.4: The possible motion distributions for required 5-dof between the tool and the workpiece.

DOFs (machine tools)	Motion of workpiece	Motion of machine tool
l = 3	X, Y: translation	Z: translation, X, Y: rotation
	X, Y: rotation	X, Y, Z: translation
	combination of R & T	X, Y, Z: combination of R & T
l = 4	X (or Y) translation	X, (or Y), Z: translation; X, Y: rotation
	X, (or Y): rotation	X, Y, Z: translation; X, (or Y): rotation
	combination of R & T	X, Y, Z: combination of R & T
l = 5	fixed	X, Y, Z: translation; X, Y: rotation

Table 2.5: Possible leg types with different degrees of freedom.

Possible numbers	DOFs = 2	DOFs = 3	DOFs = 4	DOFs = 5	DOFs = 6
1	2R	1S	2R1H	1H2R1P	1S2R1P
2	1R1P	2R1P	1H1R1P	2H1R	1S1H1P
3	1H			2H1P	1S1H1R
4				1S1R1P[1]	
5				1S2R[1]	
6				1S1H[1]	
Total possibilities	3	2	2	6	3

with the attributes of both. It provides a balance between exclusively serial and parallel mechanisms and better dexterity. It can even improve the ratio of workspace to architecture size and the accuracy.

In order to meet the required 5-dof motion, 2-dof and 3-dof parallel mechanisms are chosen to construct the "Hybrid" mechanisms. Since the upper stage is connected with the end-effector, and it requires high stiffness, so a 3-dof parallel mechanism is considered as the upper stage while a 2-dof parallel stage is taken as the lower stage.

For a 2-dof parallel mechanism — the lower stage of hybrid mechanism — both

---

[1]they are only suitable for those with identical legs, e.g., 3-DOF mechanism

Table 2.6: The possible architectures.

Degree of freedom	Number of legs	f_{l_1}	f_{l_2}	f_{l_3}	f_{l_4}	f_{l_5}	f_{l_6}	Possible architectures	Possible architectures with identical dof structure	$L = l$
$l = 2$	L = 2	2	6					9	9	9
		3	5					12	12	12
		4	4					3	2	2
$l = 3$	L = 2	3	6					6	6	
		4	5					12	12	
	L = 3	3	6	6				12	6	6
		4	5	6				36	36	36
		5	5	5				56	6	6
$l = 4$	L = 2	4	6					6	6	
		5	5					6	3	
	L = 3	4	6	6				12	6	
		5	5	6				18	9	
	L = 4	4	6	6	6			20	6	6
		5	5	6	6			36	9	9
$l = 5$	L = 2	5	6					9	9	
	L = 3	5	6	6				18	9	
	L = 4	5	6	6	6			30	9	
	L = 5	5	6	6	6	6		45	9	9
$l = 6$	L = 2	6	6					9	3	
	L = 3	6	6	6				10	3	
	L = 4	6	6	6	6			15	3	
	L = 5	6	6	6	6	6		21	3	
	L = 6	6	6	6	6	6	6	28	3	3
Total								429	179	98

planar and spatial parallel mechanisms can be considered. Referring to eq. (2.2), for planar mechanisms $(d = 3)$, then one has

$$
\begin{aligned}
l &= 3[2 + \sum_{i=1}^{L}(f_{l_i} - 1) - \sum_{i=1}^{L} f_{l_i} - 1] + \sum_{i=1}^{g} f_i \\
&= 3 - 3L + \sum_{i=1}^{g} f_i
\end{aligned}
\tag{2.6}
$$

Therefore, the possible DOFs distribution for planar mechanisms can be found in Table 2.7.

Table 2.7: The possible degree-of-freedom distribution for planar mechanisms.

Degree of freedom	number of legs	f_{l_1}	f_{l_2}	f_{l_3}
l = 2	L = 2	2	3	
l = 3	L = 3	3	3	3
		2	3	4

The hybrid motions (5-dof) can be arranged as follows:

- upper stage: X, Y axes rotation, Z axis translation; lower stage: X, Y axes translation

  One can realize this motion through either the combination of 3SPR as upper stage and 'Linear motion components' (LM) as the lower stage (special case) or the combination of 3SPR as upper stage and 3RRR planar parallel mechanism as the lower stage.

- upper stage: X, Y axes translation, Z axis translation; lower stage: X, Y axes rotation

  One can realize this motion through the combination of 3SRR as upper stage and 2-dof spherical parallel mechanism as the lower stage. Because of the complexity in manufacturing spherical parallel mechanisms, low stiffness, low precision, and small workspace, we discard spherical parallel mechanisms in our research.

The "Hybrid" mechanisms can also be implemented in an alternative way, i.e. using positioning head (wrist) for machine tools design, this will be described in the next section.

2.3.3　Redundancy

The main purpose of adopting redundancy is to improve reliability and dexterity. In order to make the parallel kinematic machines capable of arbitrarily positioning and orienting the end-effector in a three-dimensional workspace, redundancy factor may be considered. In this thesis, only 3-dof, 4-dof, 5-dof and 6-dof spatial parallel mechanisms are discussed. Generally, all these types of mechanisms are used for base platform, one can select a positioning head (wrist) with 1-dof, 2-dof, or 3-dof in conjunction with the base platform. This constructs a hybrid mechanism and it will lead to some redundant cases.

2.4　Rationale for Using Parallel and Hybrid Architectures for Machine Tools

Because the serial structure has many drawbacks — as described in Section 2.3.2.1 — it cannot meet the requirements of machine tools. Whereas parallel mechanisms have remarkable advantages over serial mechanisms, such as high precision, high load capacity, high rigidity and high speed. Parallel mechanisms have received a great attention as alternative structures for robot mechanisms. They do not have the problem of accumulation of actuator errors — while this is the case for serial mechanisms — therefore they can be positioned very precisely. Moreover, the end-effector is supported by more than one link, hence, parallel mechanisms possess high load capacity and high rigidity. Since the actuator can be put on the base parts, so movable parts can be lightened remarkably, thus giving rise to high speed characteristics.

Meanwhile, a hybrid (serial-parallel) mechanism has the advantages of both types. Therefore, the parallel and hybrid architectures have a potential to achieve some better performance and are selected as the objectives for machine tool design.

2.5 The Most Promising Architectures

In the following discussions, more constraints that take into account heuristic rules to lead to a set of more practical configurations are discussed.

- For the case with $l = L = 2$ and $f_{l_1} = f_{l_2} = 4$, the resultant motion is a complex motion, as the lower stage of the "Hybrid one", it is difficulty to control the motion, hence this case is eliminated;

- According to the "Symmetry criteria" (Gosselin and Angeles 1988), although we cannot obtain the complete symmetry, we can require structures as symmetric as possible, thus the cases with $l = L = 3$ and $f_{l_1} = 4$, $f_{l_2} = 5$, $f_{l_3} = 6$ are discarded;

- For the case with $l = L = 6$, the leg structures $1S2R1P$ and $1S1H1P$ have the same function, so the case $1S2R1P$ is eliminated;

- In order to keep all the structures consistent, we have

  - For the case with $l = L = 3$ and $f_{l_1} = 3, f_{l_2} = f_{l_3} = 6$, we add one more 6-dof leg – $f_{l_4} = 6$, and let the leg ($f_{l_1} = 3$) be located in the center and act as a passive constraining leg;

  - For the case with $l = L = 4$ and $f_{l_1} = 4, f_{l_2} = f_{l_3} = f_{l_4} = 6$, we add one more 6-dof leg – $f_{l_5} = 6$, and let the leg ($f_{l_1} = 4$) be located in the center and act as a passive constraining leg;

  - For the case with $l = L = 5$ and $f_{l_1} = 5, f_{l_2} = f_{l_3} = f_{l_4} = f_{l_5} = 6$, we add one more 6-dof leg – $f_{l_6} = 6$, and let the leg ($f_{l_1} = 5$) be located in the center and act as a passive constraining leg;

- For the leg of type $1S$, it is seldom used in our structures, so it is discarded;

- For the leg with 5-dof, the case $1H2R1P$ restricts the 2 rotations around Z and X or Y, so this case is eliminated;

- For the leg with 5-dof, the case $1S1H$ restricts the translation along Z;

- For the leg with 3-dof, the case $2R1P$ cannot meet the required motions for 3-dof mechanisms, i.e. one translation, 2 rotations, it should be replaced by $1H1P$ and

is put in the center of the platform, leaving the other 3 legs with 6-dof located at the vertices to meet the desired motions;

Besides the above criteria, some other factors are also important for machine tool design, such as the cost, workspace, static properties and payload capacity, mechanical error, etc. One should take these factors into account too.

After rearrangement of Tables 2.5 and 2.6, the most promising architectures and possible leg types with different degrees of freedom are obtained in Tables 2.8 and 2.9. In this thesis, the cases of 6-dof fully-parallel mechanisms and 3-dof, 4-dof and 5-dof mechanisms with one passive constraining leg will be discussed. They are listed in Table 2.10.

2.6   Conclusions

The kinematic structures used for 5-dof or less than 5-dof machine tools design with their underlying design principles have been made more explicit through the discussion and enumeration in this chapter. From the results obtained, it can be seen that both the tool and the workpiece can be actuated independently and that 5-dof is required for manufacturing tasks, the possible combinations of degree-of-freedom are: (5,0), (4,1) and (3,2). Moreover, for each of these combinations, the kinematic chains involved lead to several possibilities (serial, parallel or hybrid) and additionally, redundancy is taken as an option. Finally, a detailed list of possible topologies has been obtained and the most promising architectures are pointed out under the design criteria. These most promising architectures will be analyzed and optimized in Chapters 4, 5, 6 and 7, respectively.

Table 2.8: The most promising architectures.

Degree of freedom	Number of legs	f_{l_1}	f_{l_2}	f_{l_3}	f_{l_4}	f_{l_5}	f_{l_6}	Possible architectures	Possible architectures with identical dof structure	$L = l$
$l = 2$	L = 2	2	6					9	9	6
		3	5					12	12	2
$l = 3$	L = 2	3	6					6	6	
		4	5					12	12	
	L = 3	3	6	6				12	6	2
		5	5	5				56	6	4
$l = 4$	L = 2	4	6					6	6	
		5	5					6	3	
	L = 3	4	6	6				12	6	
		5	5	6				18	9	
	L = 4	4	6	6	6			20	6	4
		5	5	6	6			36	9	4
$l = 5$	L = 2	5	6					9	9	
	L = 3	5	6	6				18	9	
	L = 4	5	6	6	6			30	9	
	L = 5	5	6	6	6	6		45	9	4
$l = 6$	L = 2	6	6					9	3	
	L = 3	6	6	6				10	3	
	L = 4	6	6	6	6			15	3	
	L = 5	6	6	6	6	6		21	3	
	L = 6	6	6	6	6	6	6	28	3	2
Total								390	141	28

Table 2.9: The most promising leg types and parameter numbers with different degrees of freedom.

No.	DOFs = 2		DOFs = 3		DOFs = 4		DOFs = 5		DOFs = 6	
	S	P	S	P	S	P	S	P	S	P
1	2R	2	1H1P	2	2R1H	3	1S1R1P[1]	3	1S1H1R	3
2	1R1P	2			1H1R1P	2	1S2R[1]	3	1S1H1P	3
3	1H	1					2H1R	3		
4							2H1P	2		
S = kinematic structure of the leg, P = number of the parameters.										

Table 2.10: The most promising architectures with one passive constraining leg.

Degree of freedom	Number of legs	f_{l_1}	f_{l_2}	f_{l_3}	f_{l_4}	f_{l_5}	f_{l_6}	passive leg architecture	actuated leg architectures	Cases
$l = 3$	L = 4	3	6	6	6			1H1P	1S1H1R	2
									1S1H1P	
$l = 4$	L = 5	4	6	6	6	6		2R1H	1S1H1R	4
								1H1R1P	1S1H1P	
$l = 5$	L = 6	5	6	6	6	6	6	2H1R	1S1H1R	4
								2H1P	1S1H1P	
$l = 6$	L = 6	6	6	6	6	6	6		1S1H1R	2
									1S1H1P	
Total										12

Chapter 3

Stiffness Analysis of Planar Parallel Mechanisms

3.1 Introduction

PKMs with their unique characteristics of high stiffness (their actuators bear no moment loads but act in a simple tension or compression) and high speeds and feeds (high stiffness allows higher machining speeds and feeds while providing the desired precision, surface finish, and tool life), combined with versatile contouring capabilities have made parallel mechanisms the best candidates for the machine tool industry to advance machining performance. It is noted that the stiffness is the most important factor in machine tool design since it affects the precision of machining. Therefore, to build and study a general stiffness model is a very important task for machine tool design. In this

chapter, we will build a general stiffness model through the approach of kinematic and static equations. The objective of this model is to provide an understanding of how the stiffness of the mechanism changes as a function of its position and as a function of the characteristics of its components. This can be accomplished using stiffness mapping.

In what follows, a general stiffness model for fully-parallel mechanisms with various actuator stiffnesses is first established. The lumped models for the joints and links are then introduced. According to these models, the compliance of the links can be replaced by virtual compliant joints and rigid links. Then, equations allowing the computation of the equivalent virtual joint stiffnesses are derived. They are applied to planar 2-dof mechanisms with revolute actuators and planar 3-dof mechanisms with prismatic actuators. The stiffness mappings are implemented as a visualization tool. Finally, the correctness of the developed general stiffness model is validated by the software Pro/Engineer.

3.2 General Stiffness Model for Fully-Parallel Mechanisms

As introduced in Section 1.2.2, there are two methods to build mechanism stiffness models. Among them, the method which relies on the calculation of the parallel mechanism's Jacobian matrix is adopted in this thesis.

It will be shown that the stiffness of a parallel mechanism is dependent on the joint's stiffness, the leg's structure and material, the platform and base stiffness, the geometry of the structure, the topology of the structure and the end-effector position and orientation.

Since stiffness is the force corresponding to coordinate i required to produce a unit *displacement* of coordinate j, the stiffness of a parallel mechanism at a given point of its workspace can be characterized by its stiffness matrix. This matrix relates the forces and torques applied at the gripper link in Cartesian space to the corresponding linear and angular Cartesian displacements. It can be obtained using kinematic and static equations. The parallel mechanisms considered here are such that the velocity

relationship can be written as in eq. (3.1),

$$\dot{\boldsymbol{\theta}} = \mathbf{J}\dot{\mathbf{x}} \tag{3.1}$$

where $\dot{\boldsymbol{\theta}}$ is the vector of joint rates, and $\dot{\mathbf{x}}$ is the vector of Cartesian rates — a six-dimensional twist vector containing the velocity of a point on the platform and its angular velocity. Matrix $\mathbf{J}$ is usually termed Jacobian matrix, and it is the mapping from the Cartesian velocity vector to the joint velocity vector. From eq. (3.1), one can conclude that

$$\delta\boldsymbol{\theta} = \mathbf{J}\delta\mathbf{x} \tag{3.2}$$

where $\delta\boldsymbol{\theta}$ and $\delta\mathbf{x}$ represent joint and Cartesian infinitesimal displacements, respectively. Then, one can get the stiffness of this mechanism using the principle of kinematic/static duality. The forces and moments applied at the gripper under static conditions are related to the forces or moments required at the actuators to maintain the equilibrium by the transpose of the Jacobian matrix $\mathbf{J}$. This is also true for parallel mechanism (Merlet 1987), and one can then write

$$\mathbf{F} = \mathbf{J}^T\mathbf{f} \tag{3.3}$$

where $\mathbf{f}$ is the vector of actuator forces or torques, and $\mathbf{F}$ is the generalized vector of Cartesian forces and torques at the gripper link, which is also called the wrench acting at this link (Yoshikawa 1984; Asada and Granito 1985). The actuator forces and displacements can be related by Hooke's law, one has

$$\mathbf{f} = \mathbf{K}_J\delta\boldsymbol{\theta} \tag{3.4}$$

with $\mathbf{K}_J = diag[k_1, \ldots, k_n]$, where each of the actuators in the parallel mechanism is modeled as an elastic component, $\mathbf{K}_J$ is the joint stiffness matrix of the parallel mechanism, k_i is a scalar representing the joint stiffness of each actuator, which is modeled as linear spring, and the ith component of vector $\mathbf{f}$, noted f_i is the force or torque acting at the ith actuator. Substituting eq. (3.2) into eq. (3.4), one obtains

$$\mathbf{f} = \mathbf{K}_J\mathbf{J}\delta\mathbf{x} \tag{3.5}$$

Then, substituting eq. (3.5) into eq. (3.3), yields

$$\mathbf{F} = \mathbf{J}^T\mathbf{K}_J\mathbf{J}\delta\mathbf{x} \tag{3.6}$$

Hence, $\mathbf{K}_C$, the stiffness matrix of the mechanism in the Cartesian space is then given by the following expression

$$\mathbf{K}_C = \mathbf{J}^T \mathbf{K}_J \mathbf{J} \tag{3.7}$$

Particularly, in the case for which all the actuators have the same stiffnesses, i.e., $k_1 = k_2 = \ldots = k_n$, then eq. (3.7) will be reduced to

$$\mathbf{K} = k\mathbf{J}^T\mathbf{J} \tag{3.8}$$

which is the equation given in (Gosselin 1990).

The stiffness matrix is a positive semidefinite symmetric matrix whose eigenvalues represent the coefficients of stiffness in the principal directions, which are given by the eigenvectors. These directions are in fact represented by twist vectors, i.e., generalized velocity vectors. Moreover, the square root of the ratio of the smallest eigenvalue to the largest one gives the reciprocal of the condition number κ of the Jacobian matrix (Klein and Blaho 1987), which is a measure of the dexterity of the mechanism (Gosselin 1988). It can be written as

$$\frac{1}{\kappa} = \sqrt{\frac{\lambda_{min}}{\lambda_{max}}} \tag{3.9}$$

where λ_{min} and λ_{max} are the smallest and largest eigenvalues of the stiffness matrix, respectively.

From eq. (3.7), it is clear that if the Jacobian matrix of a mechanism $\mathbf{J}$ is singular, then obviously, the stiffness matrix of the mechanism, $\mathbf{J}^T\mathbf{K}_J\mathbf{J}$ is also singular, thus the mechanism loses stiffness, there is no precision also for the mechanism. Hence, one can study the precision of machine tools through their stiffness model, and then find the most suitable designs.

3.3 Lumped Models for Joint and Link Compliances

The flexibilities included in the model can be classified in two types (Cléroux and Gosselin 1996): i) the flexibilities at the joints and ii) the flexibilities of the links. Hence, the complete lumped model should include the following three sub-models,

- the *Denavit-Hartenberg model* which defines the nominal geometry of each of the

kinematic chains of the mechanism, the kinematics described by the Denavit-Hartenberg matrix are straightforward and systematic for mechanisms with rigid links. They are also effective for mechanisms with flexible links;

- *a lumped joint model* which is defined in Tables 3.1 and 4.1;

- *an equivalent beam model* at each link which accounts for the deformations of the link caused by the external forces and torques;

3.3.1   Lumped Models for Joint Compliances

In order to simplify the model of the stiffness, link stiffnesses will be lumped into local compliant elements (spring) located at the joints. This is justified by the fact that no dynamics is included in the model (it is purely kinematic) and that limited numerical accuracy is acceptable. Indeed, the objective of this study is to obtain engineering values for the stiffness and to determine which areas of the workspace lead to better stiffness properties.
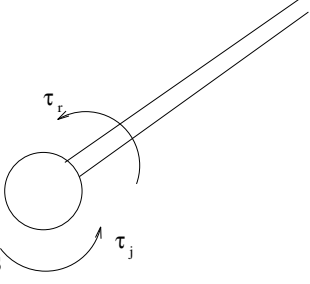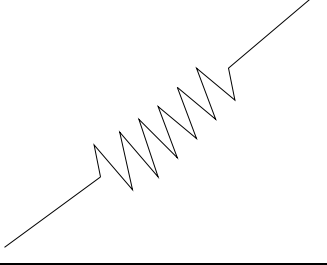
Physically, the bending deformation in joints is presented in different ways. In the planar case, the unactuated revolute joint does not induce any bending whereas in the spatial case, a bending is presented in a direction perpendicular to the joint. Hence, it is necessary to establish a lumped joint model for each possible case. In the lumped joint model, deformations caused by link flexibility can be considered as virtual joints fixed at this point; the details are given in (Gosselin and Zhang 1999) and Table 3.1.

3.3.2   Lumped Models for Link Compliances

3.3.2.1   Deformation Induced by Wrench

A linear beam is shown in Figure 3.1, where F the external force, E the elastic modulus, L the length of the beam, and I the section moment of inertia of the beam. In a lumped model, the flexible beam will be replaced by a rigid beam mounted on a pivot plus a torsional spring located at the joint, as illustrated in Figure 3.1b. The objective is to determine the equivalent torsional spring stiffness that will produce the same tip

Table 3.1: Lumped joint models for planar system.

joint type	if actuated, the equivalent model	if unactuated, the equivalent model
revolute	2 torsional springs	no bending
prismatic	actuated spring	uncertainty

deflection as that of the beam under the load F. As it can be seen on the figure, the lumped model will lead to a different orientation of the tip of the beam. However, assuming that the deformation is small, angle θ will also be small, thus the difference in orientation between the original beam and the equivalent link can be neglected. Moreover, since in the mechanisms considered here, the legs are attached to the platform with spherical joints, there is not any moment presented at the spherical joint, hence, the end link orientation of the beam is irrelevant. Let δ be the deflection of the beam. Based on the Castiliano's theorem (Timoshenko and Gere 1972), one can build an

(a) Flexible beam.   (b) Virtual rigid beam.
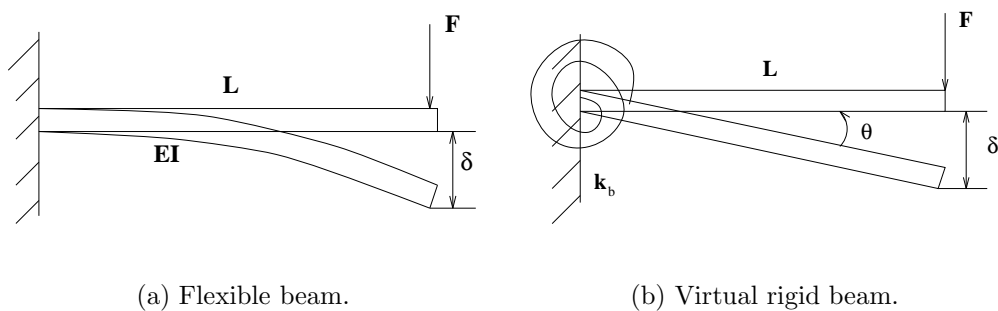
Figure 3.1: Link deformation induced by wrench.

equivalent rigid beam model based solely on the deflection of the free end. With a force F applied at the free end of the beam, the resulting deformation can be written as (see Figure 3.1a)

$$\delta = \frac{FL^3}{3EI} \qquad (3.10)$$

and assuming small deformations, the corresponding rotational deformation of an equivalent rigid beam with a torsional spring would be

$$\theta \simeq \frac{\delta}{L} \qquad (3.11)$$

Let the deflection in both cases (Figure 3.1a and Figure 3.1b) be the same. Substituting eq. (3.10) into eq. (3.11), yields

$$\theta = \frac{FL^2}{3EI} \qquad (3.12)$$

where

δ is the flexible beam's deflection at the free end,

θ is the rigid beam's rotation around the joint,

Since the flexible beam model can be lumped into a torsional spring with equivalent stiffness k_b at the shoulder joint (Figure 3.1b), based on the principle of work and energy, one has

$$\frac{1}{2}F\delta = \frac{1}{2}k_b(\theta)^2 \qquad (3.13)$$

where k_b is the lumped stiffness of the flexible beam. Substituting eq. (3.11) to eq. (3.13), one obtains

$$FL\theta = k_b\theta^2 \qquad (3.14)$$

or

$$k_b = \frac{FL}{\theta} \qquad (3.15)$$

substituting eq. (3.12) into eq. (3.15), one obtains the equivalent stiffness for the flexible beam as

$$k_b = \frac{3EI}{L} \qquad (3.16)$$

(a) Circular cylinder. (b) Rectangular parallelepiped.
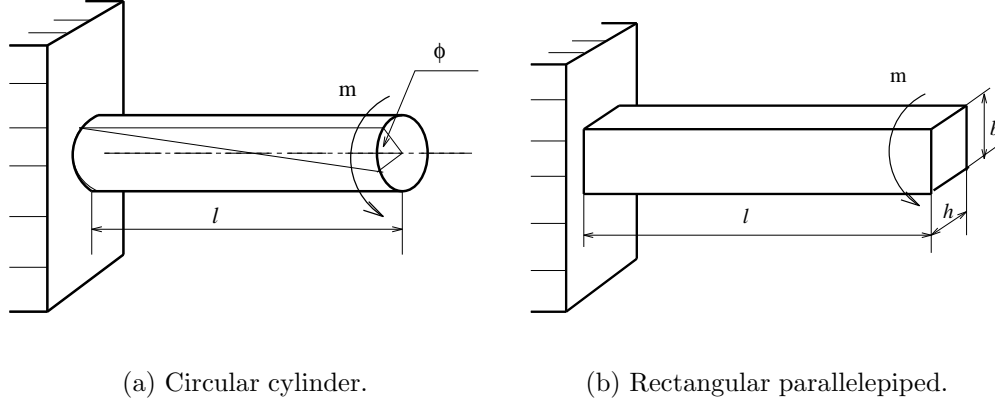
Figure 3.2: Link deformation induced by twist.

3.3.2.2 Deformation Induced by Twist

Here the lumped stiffness expression for a single flexible beam undergoing twisting is addressed. A linear beam is shown in Figure 3.2, where m (Nm) the external torque, G (N/m^2) the shear elastic modulus, l (m) the length of the beam, and I (m^4) the section moment of inertia of the beam. Similarly to the preceding section, the flexible beam is replaced by a rigid beam mounted at the end plus a torsional spring located at the end. The objective is to determine the equivalent torsional spring stiffness that will produce the same tip deflection as that of the beam under the load m. Assuming that the deformation is small, angle ϕ will also be small, then, with a twist m applied at the free end of the beam, the resulting deformation can be written as

$$\Delta\phi = \frac{ml}{GI}, \quad \text{for Circular cylinder} \tag{3.17}$$

$$\Delta\phi = \frac{ml}{G\beta h^3 b}, \quad \text{for Rectangular parallelepiped} \tag{3.18}$$

where

b is the height of the flexible beam,

h is the width of the flexible beam,

β is a coefficient related to b and h.

Since one has

$$m = k_t \Delta\phi \tag{3.19}$$

hence one can obtain the lumped stiffness k_t of the beam as

$$k_t = \frac{GI}{l}, \quad \text{for Circular cylinder} \tag{3.20}$$

$$k_t = \frac{G\beta h^3 b}{l}, \quad \text{for Rectangular parallelepiped} \tag{3.21}$$

3.4 Stiffness Analysis of a Planar 2-dof Parallel Mechanism with Revolute Actuators

As shown in Figure 3.3, we take the case of revolute type into account. A planar 2-dof mechanism can be used to position a point on the plane and the Cartesian coordinates associated with this mechanism are the position coordinates of one point of the platform, noted (x, y). Vector $\boldsymbol{\theta}$ represents the actuated joint coordinates of the planar parallel mechanism and is defined as $\boldsymbol{\theta} = [\theta_1, \theta_2, \ldots, \theta_n]^T$, where n is the number of degrees of freedom of the mechanism studied, and the only actuated joints are those directly connected to the fixed link (Gosselin and Wang 1997; Gosselin and Angeles 1990; Sefrioui and Gosselin 1993).
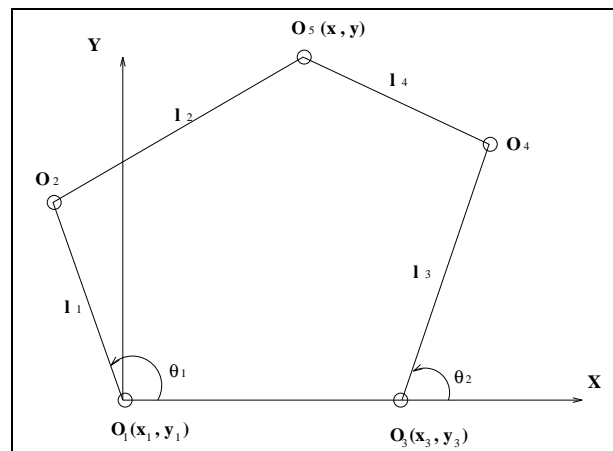
Figure 3.3: A planar 2-dof parallel mechanism with revolute actuators.

3.4.1 The Jacobian Matrix

As illustrated in Figure 3.3, a two-degree-of-freedom planar parallel mechanism is constructed by four movable links and five revolute joints (noted as O_1 to O_5). The two

links — whose length are l_1 and l_3 — are the input links. They are assumed to be flexible beams, and points O_1 and O_3 are the only actuated joints in this planar 2-dof parallel mechanism. The lengths of the other two links are denoted as l_2 and l_4, respectively. Point $O_5(x, y)$ is the point to be positioned by the mechanism. The origin of the fixed Cartesian coordinate system is located on joint O_1. (x_1, y_1) and (x_3, y_3) are the coordinates of points O_1 and O_3, respectively, and one has $x_1 = y_1 = y_3 = 0$.

At points O_2 and O_4, one has

$$x_2 = l_1 \cos \theta_1 + x_1 \tag{3.22}$$

$$y_2 = l_1 \sin \theta_1 + y_1 \tag{3.23}$$

$$x_4 = l_3 \cos \theta_2 + x_3 \tag{3.24}$$

$$y_4 = l_3 \sin \theta_2 + y_3 \tag{3.25}$$

From this figure, one obtains

$$l_2^2 = (x - x_2)^2 + (y - y_2)^2 \tag{3.26}$$

$$l_4^2 = (x - x_4)^2 + (y - y_4)^2 \tag{3.27}$$

Substituting eqs. (3.22) – (3.25) into eqs. (3.26) – (3.27), one gets

$$l_2^2 = (x - l_1 \cos \theta_1)^2 + (y - l_1 \sin \theta_1)^2 \tag{3.28}$$

$$l_4^2 = (x - (l_3 \cos \theta_2 + x_3))^2 + (y - l_3 \sin \theta_2)^2 \tag{3.29}$$

The kinematic relationship can be obtained as follows

$$\mathbf{F}(\boldsymbol{\theta}, \mathbf{p}) = \begin{bmatrix} (x - l_1 \cos \theta_1)^2 + (y - l_1 \sin \theta_1)^2 - l_2^2 \\ (x - (l_3 \cos \theta_2 + x_3))^2 + (y - l_3 \sin \theta_2)^2 - l_4^2 \end{bmatrix} = 0 \tag{3.30}$$

Let

$$\dot{\boldsymbol{\theta}} = \begin{bmatrix} \dot{\theta}_1 \\ \dot{\theta}_2 \end{bmatrix}, \quad \dot{\mathbf{p}} = \begin{bmatrix} \dot{x} \\ \dot{y} \end{bmatrix} \tag{3.31}$$

One can obtain the Jacobian matrices of the parallel mechanism as

$$\mathbf{A} = \frac{\partial \mathbf{F}}{\partial \mathbf{p}}, \quad \mathbf{B} = \frac{\partial \mathbf{F}}{\partial \boldsymbol{\theta}} \tag{3.32}$$

In particular, the Jacobian matrices of this planar 2-dof parallel mechanism are as follows:

$$\mathbf{A} = \begin{bmatrix} (x - l_1 \cos \theta_1) & (y - l_1 \sin \theta_1) \\ (x - l_3 \cos \theta_2 - x_3) & (y - l_3 \sin \theta_2) \end{bmatrix} \tag{3.33}$$

$$\mathbf{B} = \begin{bmatrix} (x\sin\theta_1 - y\cos\theta_1)l_1 & 0 \\ 0 & [(x-x_3)\sin\theta_2 - y\cos\theta_2]l_3 \end{bmatrix} \tag{3.34}$$

The velocity equations can be written as $\mathbf{A}\dot{\mathbf{p}} + \mathbf{B}\dot{\boldsymbol{\theta}} = 0$, and

$$\mathbf{J} = -\mathbf{B}^{-1}\mathbf{A} = \begin{bmatrix} a_1/d_1 & b_1/d_1 \\ a_2/d_2 & b_2/d_2 \end{bmatrix} \tag{3.35}$$

with

$$a_1 = x - l_1\cos\theta_1 \tag{3.36}$$

$$a_2 = x - l_3\cos\theta_2 - x_3 \tag{3.37}$$

$$b_1 = y - l_1\sin\theta_1 \tag{3.38}$$

$$b_2 = y - l_3\sin\theta_2 \tag{3.39}$$

$$d_1 = -(x\sin\theta_1 - y\cos\theta_1)l_1 \tag{3.40}$$

$$d_2 = -[(x-x_3)\sin\theta_2 - y\cos\theta_2]l_3 \tag{3.41}$$

3.4.2   Inverse Kinematics

In order to compute the Jacobian matrix of eq. (3.35), one has to know the joint angles of Figure 3.3 first. Therefore, it is necessary to calculate the inverse kinematics of this planar 2-dof parallel mechanism to determine the joint angles for any given end-effector position and orientation. Unlike many serial mechanisms, the calculation of the inverse kinematics of a parallel mechanism is generally straightforward.

From eq. (3.28), one obtains

$$2l_1x\cos\theta_1 + 2l_1y\sin\theta_1 = x^2 + y^2 + L_1^2 - L_2^2 \tag{3.42}$$

therefore, one can obtain θ_1 as follow

$$\sin\theta_1 = \frac{BC + K_1A\sqrt{A^2 + B^2 - C^2}}{A^2 + B^2} \tag{3.43}$$

$$\cos\theta_1 = \frac{AC - K_1B\sqrt{A^2 + B^2 - C^2}}{A^2 + B^2} \tag{3.44}$$

where

$$A = 2l_1x \tag{3.45}$$

$$B = 2l_1 y \tag{3.46}$$

$$C = x^2 + y^2 + L_1^2 - L_2^2 \tag{3.47}$$

$$K_1 = \pm 1 \tag{3.48}$$

and K_1 is the branch index, which can be used to distinguish the four branches of the inverse kinematic problem. In the same way, from eq. (3.29), one obtains

$$2l_3(x - x_3)\cos\theta_2 + 2l_3 y \sin\theta_2 = (x - x_3)^2 + y^2 + l_3^2 - l_4^2 \tag{3.49}$$

hence one obtains the joint angle θ_2 as

$$\sin\theta_2 = \frac{BC + K_2 A\sqrt{A^2 + B^2 - C^2}}{A^2 + B^2} \tag{3.50}$$

$$\cos\theta_2 = \frac{AC - K_2 B\sqrt{A^2 + B^2 - C^2}}{A^2 + B^2} \tag{3.51}$$

where

$$A = 2l_3(x - x_3) \tag{3.52}$$

$$B = 2l_3 y \tag{3.53}$$

$$C = (x - x_3)^2 + y^2 + l_3^2 - l_4^2 \tag{3.54}$$

$$K_2 = \pm 1 \tag{3.55}$$

again, K_2 is the branch index.

3.4.3 Kinetostatic Model

Assume the actuator stiffnesses of O_1 and O_3 are k_1 and k_1', respectively, and the lumped stiffness for beam $O_1 O_2$ and $O_3 O_4$ are k_b and k_b'. Then the compound stiffness at points O_1 and O_3 are written as

$$k = \frac{k_1 k_b}{k_1 + k_b} \tag{3.56}$$

$$k' = \frac{k_1' k_b'}{k_1' + k_b'} \tag{3.57}$$

where

k, k' are the total stiffnesses at the active joint,

k_1, k_1' are the actuator stiffnesses,

k_b, k_b' are the lumped stiffnesses as indicated in eq. (3.16),

One can find the kinetostatic model for this planar 2-dof parallel mechanism by using eq. (3.7), i.e.,

$$\mathbf{K}_C = \mathbf{J}^T \mathbf{K}_J \mathbf{J} \tag{3.58}$$

where

$\mathbf{K}_J$ is the joint stiffness matrix of the parallel mechanism,

$\mathbf{J}$ is the Jacobian matrix of this planar 2-dof parallel mechanism.

3.4.4 Stiffness Mapping

The analysis described above is now used to obtain the stiffness maps for this planar two-degree-of-freedom parallel mechanism. The maps are drawn on a section of the workspace of the variation of the end-effector's position.

A program has been written with the software Matlab. Given the values of $l_1 = l_4 = 0.5$ m, $l_2 = 0.6$ m, $l_3 = 0.8$ m and $O_1O_3 = 0.7$ m. The contour graph can be shown in Figure 3.4

(a) Stiffness in X axis   (b) Stiffness in Y axis
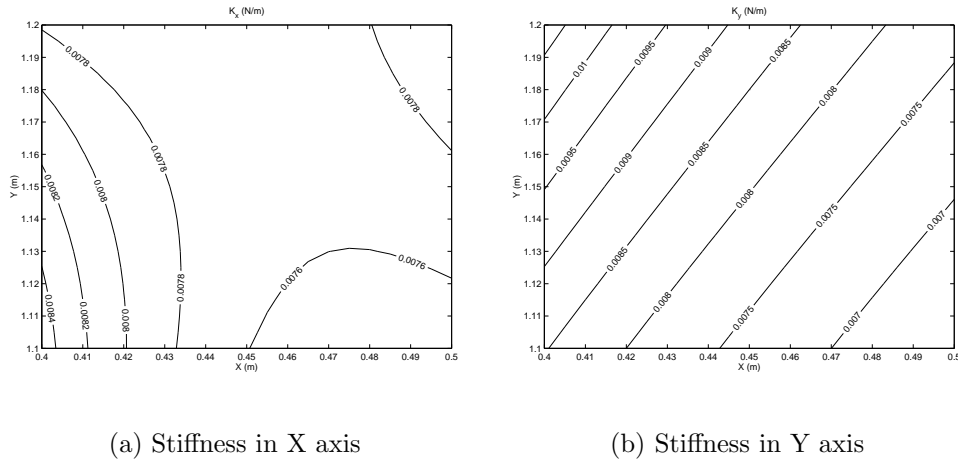
Figure 3.4: Stiffness contour graph for a planar 2-dof parallel mechanism with revolute actuators.

3.5 Stiffness Analysis of a Planar 3-dof Parallel Mechanism with Prismatic Actuators

A symmetric mechanism identical to the one studied in (Gosselin 1988) and (Gosselin and Angeles 1988) is now analyzed with the procedure described above. The characteristics of this mechanism are as follows: Points A_i, $i = 1, 2, 3$ and points B_i, $i = 1, 2, 3$ (Figure 3.5) are, respectively, located on the vertices of an equilateral triangle and that the minimum and maximum lengths of each of the legs are the same. The mechanism is therefore completely symmetric. The dimensions and the stiffness of each leg are given in Table 3.2.

Table 3.2: Geometric properties of symmetric planar parallel mechanism (all length units in mm and stiffness units in N/m).

i	x_{ai}	y_{ai}	x_{bi}	y_{bi}	k_i
1	-1/2	$-\sqrt{3}/6$	-1/12	$-\sqrt{3}/36$	1000
2	1/2	$-\sqrt{3}/6$	1/12	$-\sqrt{3}/36$	1500
3	0	$\sqrt{3}/3$	0	$\sqrt{3}/18$	700
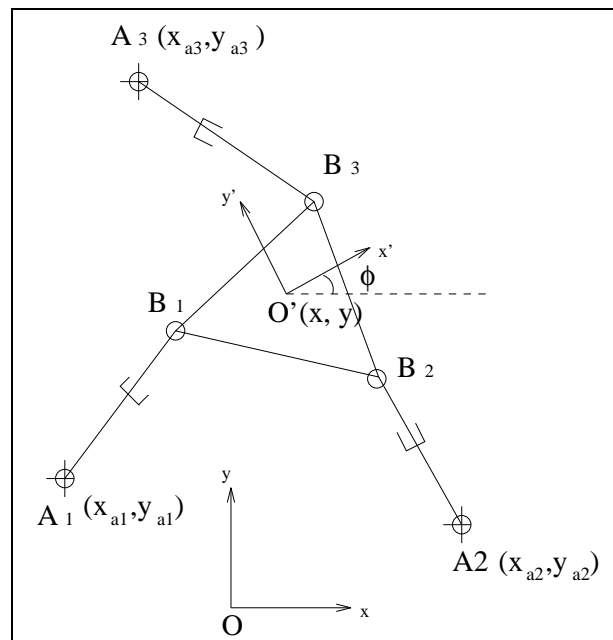
Figure 3.5: A planar 3-dof parallel mechanism with prismatic actuators.

3.5.1 Stiffness Model

Since one has

$$x_i = x - L\cos\phi_i - x_{ai}, \quad i = 1, 2, 3 \tag{3.59}$$

$$y_i = y - L\sin\phi_i - y_{ai}, \quad i = 1, 2, 3 \tag{3.60}$$

$$p_i = \sqrt{x_i^2 + y_i^2}, \quad i = 1, 2, 3 \tag{3.61}$$

where L is the length of the gripper, and p_i is the length of the leg, The Jacobian matrix is given by Gosselin (1988) as follows

$$\mathbf{J} = \begin{bmatrix} a_1/p_1 & b_1/p_1 & c_1/p_1 \\ a_2/p_2 & b_2/p_2 & c_2/p_2 \\ a_3/p_3 & b_3/p_3 & c_3/p_3 \end{bmatrix} \tag{3.62}$$

with

$$a_i = x - x_{ai} - L\cos\phi_i \tag{3.63}$$

$$b_i = y - y_{ai} - L\sin\phi_i \tag{3.64}$$

$$c_i = (x - x_{ai})L\sin\phi_i - (y - y_{ai})L\cos\phi_i \tag{3.65}$$

Hence, according to eq. (3.7), one can find the stiffness model for this planar 3-dof parallel mechanism.

3.5.2 Stiffness Mapping

The above model is now used to obtain the stiffness maps for this planar three-degree-of-freedom parallel mechanism. Given the values shown in Table 3.2, one can obtain the stiffness contour and mesh graphs in x, y, and ϕ shown in Figures 3.6 – 3.9.

One can find from the stiffness map that the symmetric mechanism is in a singular configuration when positioned at the center of the workspace. Also, from such stiffness maps, one can determine which regions of the workspace will satisfy some stiffness criteria. From the mesh graphs, one can view the stiffness distribution more intuitively.

(a) Stiffness in X axis   (b) Stiffness in Y axis   (c) Stiffness in ϕ

Figure 3.6: Stiffness mesh graphs for a planar 3-dof parallel mechanism with prismatic actuators ($\phi = 0$).

(a) Stiffness in X axis   (b) Stiffness in Y axis   (c) Stiffness in ϕ

Figure 3.7: Stiffness contour graphs for a planar 3-dof parallel mechanism with prismatic actuators ($\phi = 0$).

3.6   Verification of the General Stiffness Model

A model (Figure 3.10) for this planar 3-dof parallel mechanism has been built using the software Pro/Engineer to simulate the physical structure on Pro/Motion.

With the geometric properties given in Table 3.3 and the center of the triangle located at $(75, 65)$, after applying the forces and torque $F_x = 100\ N, F_y = 100\ N, \tau = 60\ Nm$ at the center of the triangle, the three legs deform. One obtains the deformation of the center using Pro/Motion as $\Delta x = 0.09697\ mm$, $\Delta y = 0.14959\ mm$, $\Delta \phi = -0.0020$. Meanwhile, the results obtained from the equations developed in the previous section are $\Delta x = 0.0962\ mm$, $\Delta y = 0.1548\ mm$, $\Delta \phi = -0.0020$. This shows that the results from Pro/Motion and the kinetostatic model are very close to each other.

(a) Stiffness in X axis   (b) Stiffness in Y axis   (c) Stiffness in ϕ

Figure 3.8: Stiffness mesh graphs for a planar 3-dof parallel mechanism with prismatic actuators ($\phi = \pi/2$).

(a) Stiffness in X axis   (b) Stiffness in Y axis   (c) Stiffness in ϕ
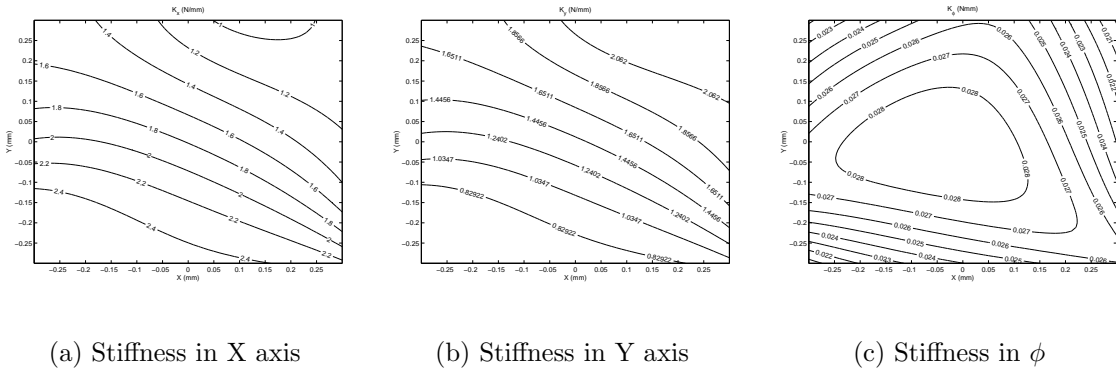
Figure 3.9: Stiffness contour graphs for a planar 3-dof parallel mechanism with prismatic actuators ($\phi = \pi/2$).

3.7   Conclusions

A general stiffness model for fully-parallel mechanisms with different actuator stiffnesses has been presented in this chapter. It has been shown that this general stiffness model can be used to evaluate the stiffness properties of parallel mechanisms. Examples have been given to illustrate how this model is used. Meanwhile, the lumped models for joints and links are proposed. They can be applied to establish kinetostatic models for both 2-dof and 3-dof mechanisms which are also mentioned in this chapter. Finally, the reliability of the stiffness model has been demonstrated using the computer program Pro/Engineer.
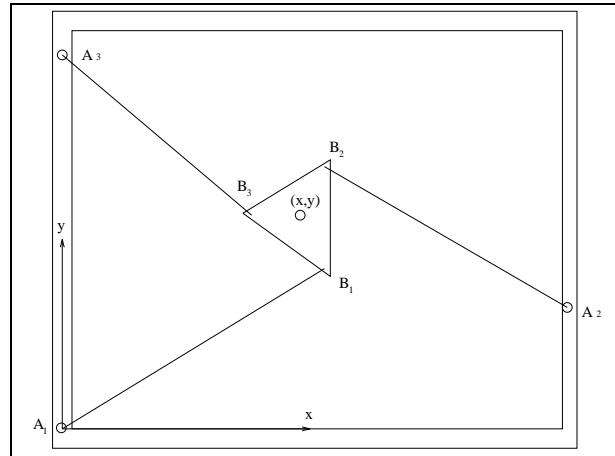
Figure 3.10: Validation model of the planar 3-dof parallel mechanism in Pro/Motion.

Table 3.3: Geometric properties of planar parallel mechanism (all units in mm).

i	x_{ai}	y_{ai}	x_{bi}	y_{bi}	k_i
1	0	0	84.547	48.464	400
2	150	49	84.547	81.536	400
3	0	130	55.91	65	400

Chapter 4

Kinetostatic Analysis of Spatial n-DOF Parallel Mechanisms with a Passive Constraining Leg and n Identical Legs with Prismatic Actuators

4.1   Introduction

This chapter introduces several new types of parallel mechanisms with prismatic actuators whose degree of freedom is dependent on a constraining passive leg connecting

the base and the platform. The mechanisms introduced in this chapter are a series of n-dof parallel mechanisms which consist of n identical actuated legs with six degrees of freedom and one passive leg with n degrees of freedom connecting the platform and the base. This series of mechanisms has the characteristics of reproduction since they have identical actuated legs, thus, the entire mechanism essentially consists of repeated parts, offering price benefits for manufacturing, assembling, and maintenance.

A simple method for the stiffness analysis of spatial parallel mechanisms is presented using a lumped parameter model. Although it is essentially general, the method is specifically applied to spatial parallel mechanisms. A general kinetostatic model is established for the analysis of the structural rigidity and accuracy of this family of mechanisms. One can improve the rigidity of this type of mechanism through optimization of the link rigidities and geometric dimensions to reach the maximized global stiffness and precision. In what follows, the geometric model of this class of mechanisms is first introduced. The virtual joint concepts are employed to account for the compliance of the links. A general kinetostatic model of the family of parallel mechanisms is then established and analyzed using the lumped-parameter model. Equations allowing the computation of the equivalent joint stiffnesses are developed. Additionally, the inverse kinematics and velocity equations are given for both rigid-link and flexible-link mechanisms. Finally, examples for 3-dof, 4-dof, 5-dof and the Tricept machine tool families are given in detail to illustrate the results. Some discussions are given to account for the effect of the variation of structure parameters including material properties on the system behavior, and the behavior *vs* structural parameters. Stiffness/Compliance mappings are obtained as a visualization tool to aid in the use of the kinetostatic model. The design and control of this families of parallel mechanisms for a better stiffness can be performed based on the stiffness/compliance maps.

4.2 General Kinetostatic Model for Spatial $n-$DOF Mechanisms with a Passive Constraining Leg and Prismatic Actuators

4.2.1 Geometric Modeling

An example of parallel mechanisms belonging to the family of mechanisms studied in this chapter is shown in Figures 4.1 and 4.2. It is a 5-dof parallel mechanism with prismatic actuators. This mechanism consists of six kinematic chains, including five variable length legs with identical topology and one passive leg which connects the fixed base to the moving platform. In this 5-dof parallel mechanism, the kinematic chains associated with the five identical legs consist, from base to platform, of a fixed Hooke joint, a moving link, an actuated prismatic joint, a second moving link and a spherical joint attached to the platform. The sixth chain (central leg) connecting the base center to the platform is a passive constraining leg and has an architecture different from the other chains. It consists of a revolute joint attached to the base, a moving link, a Hooke joint, a second moving link and another Hooke joint attached to the platform. This last leg is used to constrain the motion of the platform to only five degrees of freedom. This mechanism could be built using only five legs, i.e., by removing one of the five identical legs and actuating the first joint of the passive constraining leg. However, the uniformity of the actuation would be lost.

Similarly, families of 3-dof and 4-dof parallel mechanisms can be built using three or four identical legs with six degrees of freedom and one passive constraining leg with three or four degrees of freedom, respectively, and they will also be discussed in this chapter. The aim of using the passive leg is to limit the degrees of freedom to the desired ones. Since the external loads on the platform will induce bending and/or torsion in the passive leg, its mechanical design is a very important issue which can be addressed using the kinetostatic model proposed here. It should be noted, however, that the final geometry and mechanical design of the passive leg may be significantly different from the generic representation given in Figure 4.1.
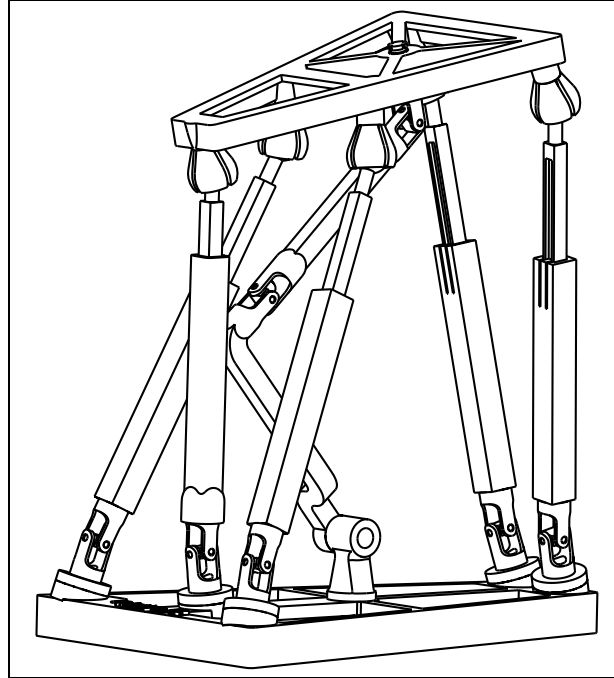
Figure 4.1: CAD model of the spatial 5-dof parallel mechanism with prismatic actuators (Figure by Gabriel Coté).

4.2.2   Lumped Models for Joint and Link Compliances

Similarly to the discussion in Section 3.3.1, the lumped joint compliance model for spatial systems is discussed in this section. In this framework, link bending stiffnesses are replaced by equivalent torsional springs located at virtual joints, as illustrated in Table 4.1. Actuator stiffnesses are also included and modeled as torsional or linear springs for revolute and prismatic actuators, respectively.

4.2.3   Inverse Kinematics

Since the platform of the mechanism has n degrees of freedom, only n of the six Cartesian coordinates of the platform are independent. For the 5-dof mechanism of Figure 4.1, the independent coordinates have been chosen for convenience as $(x, y, z, \theta_i, \theta_j)$, where x, y, z are the position coordinates of a reference point on the platform and (θ_i, θ_j) are the joint angles of the Hooke joint attached to the platform. Other coordinates may be chosen.
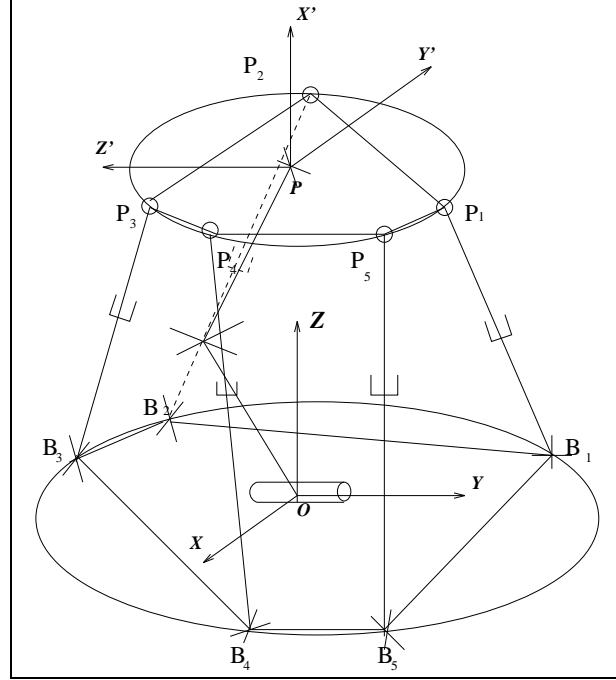
Figure 4.2: Schematic representation of the spatial 5-dof parallel mechanism with prismatic actuators.
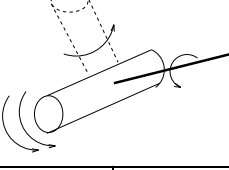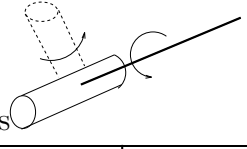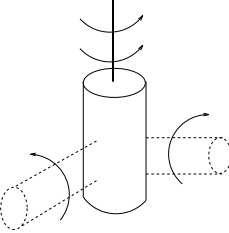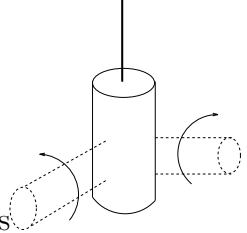
Assume that the centers of the joints located on the base and on the platform are located on circles with radii R_b and R_p, respectively. A fixed reference frame $O - xyz$ is attached to the base of the mechanism and a moving coordinate frame $P - x'y'z'$ is attached to the platform. In Figure 4.2, the points of attachment of the actuated legs to the base are represented with B_i and the points of attachment of all legs to the platform are represented by P_i, with $i = 1, \ldots, n$. Point P is the reference point on the platform and its position coordinates are $P(x, y, z)$.

The Cartesian coordinates of the platform are given by the position of point P with respect to the fixed frame, and the orientation of the platform (orientation of frame $P - x'y'z'$ with respect to the fixed frame), represented by matrix $\mathbf{Q}$.

If the coordinates of the point P_i in the moving reference frame are represented with (x'_i, y'_i, z'_i) and the coordinates of the point B_i in the fixed frame are represented by vector $\mathbf{b}_i$, then for $i = 1, \ldots, n$, one has

$$
\mathbf{p}_i = \begin{bmatrix} x_i \\ y_i \\ z_i \end{bmatrix}, \quad \mathbf{r}'_i = \begin{bmatrix} x'_i \\ y'_i \\ z'_i \end{bmatrix}, \quad \mathbf{p} = \begin{bmatrix} x \\ y \\ z \end{bmatrix}, \quad \mathbf{b}_i = \begin{bmatrix} b_{ix} \\ b_{iy} \\ b_{iz} \end{bmatrix} \tag{4.1}
$$

Table 4.1: Lumped joint compliance models for spatial system.

joint type	if actuated, the equivalent model	if unactuated, the equivalent model
spherical	N/A	no transformation
Hooke	N/A	no transformation
revolute	4 torsional springs	2 torsional springs
	4 torsional springs	2 torsional springs

where $\mathbf{p}_i$ is the position vector of point P_i expressed in the fixed coordinate frame whose coordinates are defined as (x_i, y_i, z_i), $\mathbf{r}'_i$ is the position vector of point P_i expressed in the moving coordinate frame, and $\mathbf{p}$ is the position vector of point P expressed in the fixed frame as defined above, and the angles between the points of attachment and the Cartesian X axis along the circle are given by $\boldsymbol{\theta}_{bi}$ (base) and $\boldsymbol{\theta}_{pi}$ (platform).

$$\boldsymbol{\theta}_{bi} = \begin{bmatrix} \theta_{b1} \\ \vdots \\ \theta_{bn} \end{bmatrix}, \quad \boldsymbol{\theta}_{pi} = \begin{bmatrix} \theta_{p1} \\ \vdots \\ \theta_{pn} \end{bmatrix} \tag{4.2}$$

One can then write

$$\mathbf{p}_i = \mathbf{p} + \mathbf{Q}\mathbf{r}'_i \tag{4.3}$$

where the rotation matrix can be written as a function of the n joint angles of the $(n+1)$th leg. This matrix is written as

$$\mathbf{Q} = \mathbf{Q}_0\mathbf{Q}_1 \ldots \mathbf{Q}_n, \quad n = 3,\ 4,\ \text{or } 5 \tag{4.4}$$

where $\mathbf{Q}_0$ is the rotation matrix from the fixed reference frame to the first frame (fixed) of the passive constraining leg.

In order to solve the inverse kinematic problem, one must first consider the passive constraining leg as a serial n-dof mechanism whose n Cartesian coordinates are known, which is a well known problem (Angeles 1997; Hong *et al.* 1997; Kohli and Osvatic 1993; Lee and Kim 1993; Lee and Reinholtz 1996; Manocha and Canny 1992). Once the solution to the inverse kinematics of this n-dof serial mechanism is found, the complete pose (position and orientation) of the platform can be determined using the direct kinematic equations for this serial mechanism.

Subtracting vector $\mathbf{b}_i$ from both sides of eq. (4.3), one obtains

$$\mathbf{p}_i - \mathbf{b}_i = \mathbf{p} + \mathbf{Q}\mathbf{r}'_i - \mathbf{b}_i, \quad i = 1, \ldots, n, \quad n = 3, 4, \text{ or } 5 \tag{4.5}$$

Then, taking the Euclidean norm on both sides of eq. (4.5), one has

$$\| \mathbf{p}_i - \mathbf{b}_i \| = \| \mathbf{p} + \mathbf{Q}\mathbf{r}'_i - \mathbf{b}_i \| = \rho_i, \quad i = 1, \ldots, n, \quad n = 3, 4, \text{ or } 5 \tag{4.6}$$

where ρ_i is the length of the ith leg, i.e., the value of the ith joint coordinate. The solution of the inverse kinematic problem for the n-dof platform is therefore completed and can be written as

$$\rho_i^2 = (\mathbf{p}_i - \mathbf{b}_i)^T(\mathbf{p}_i - \mathbf{b}_i), \quad i = 1, \ldots, n, \quad n = 3, 4, \text{ or } 5 \tag{4.7}$$

4.2.4 Jacobian Matrices

4.2.4.1 Rigid Model

Each of the kinematic chains connecting the base to the platform can be taken as a serial mechanism, and a Hooke joint can be replaced by two orthogonal revolute joints in the present study.

A line L_i is associated with the axis of the ith revolute joint, and a positive direction along this line is defined arbitrarily through a unit vector $\mathbf{e}_i$. Thus, a rotation of the ith link with respect to the $(i-1)$th link is totally defined by the geometry of the link, i.e., by the DH parameters a_i, b_i, and α_i, plus $\mathbf{e}_i$ and its associated joint variable θ_i (Angeles 1997). Then, one has, according to the DH notation

$$[\mathbf{Q}_i]_i = \begin{bmatrix} \cos\theta_i & -\cos\alpha_i \sin\theta_i & \sin\alpha_i \sin\theta_i \\ \sin\theta_i & \cos\alpha_i \cos\theta_i & -\sin\alpha_i \cos\theta_i \\ 0 & \sin\alpha_i & \cos\alpha_i \end{bmatrix}, \quad [\mathbf{a}_i]_i = \begin{bmatrix} a_i \cos\theta_i \\ a_i \sin\theta_i \\ b_i \end{bmatrix} \tag{4.8}$$

$\mathbf{Q}_i$ and $\mathbf{a}_i$ denote, respectively, the matrix rotating the frame attached to the ith link (F_i) into an orientation coincident with that of the $(i + 1)$th body (F_{i+1}), and the vector joining the origin of F_i with that of F_{i+1} directed from the former to the latter. According to the DH notation, one has

$$[\mathbf{e}_i]_i = \begin{bmatrix} 0 \\ 0 \\ 1 \end{bmatrix}, \quad i = 1, \dots, n \tag{4.9}$$

The parallel mechanisms studied here comprise two main components, namely, the constraining leg — which can be thought of as a serial mechanism — and the actuated legs acting in parallel.

Considering the constraining leg, one can write

$$\mathbf{J}_{n+1}\dot{\boldsymbol{\theta}}_{n+1} = \mathbf{t}, \quad n = 3, 4, \text{ or } 5 \tag{4.10}$$

where $\mathbf{t} = \begin{bmatrix} \boldsymbol{\omega}^T & \dot{\mathbf{p}}^T \end{bmatrix}^T$ is the twist of the platform, with $\boldsymbol{\omega}$ the angular velocity of the platform and

$$\dot{\boldsymbol{\theta}}_{n+1} = \begin{bmatrix} \dot{\theta}_{n+1,1} & \cdots & \dot{\theta}_{n+1,n} \end{bmatrix}^T, \quad n = 3, 4, \text{ or } 5 \tag{4.11}$$

is the joint velocity vector associated with the constraining leg. Matrix $\mathbf{J}_{n+1}$ is the Jacobian matrix of the constraining leg considered as a serial n-dof mechanism, which can be expressed as (Angeles 1997)

$$\mathbf{J}_{n+1} = \begin{bmatrix} \mathbf{e}_{n+1,1} & \cdots & \mathbf{e}_{n+1,n} \\ \mathbf{e}_{n+1,1} \times \mathbf{r}_{n+1,1} & \cdots & \mathbf{e}_{n+1,n} \times \mathbf{r}_{n+1,n} \end{bmatrix}, \quad n = 3, 4, \text{ or } 5 \tag{4.12}$$

where $\mathbf{r}_i$ is the vector connecting the origin of frame F_i to the origin of the platform frame. It is important to note that if the ith pair is a revolute joint, then the ith column of $\mathbf{J}_{n+1}$, noted $\mathbf{j}_i$, can be written as

$$\mathbf{j}_i = \begin{bmatrix} \mathbf{e}_i \\ \mathbf{e}_i \times \mathbf{r}_i \end{bmatrix} \tag{4.13}$$

On the other hand, if the ith pair is a prismatic joint, then the $(i - 1)$th and the ith links have the same angular velocity, for a prismatic joint does not allow any relative rotation, then the ith column of $\mathbf{J}_{n+1}$ changes to

$$\mathbf{j}_i = \begin{bmatrix} \mathbf{0} \\ \mathbf{e}_i \end{bmatrix} \tag{4.14}$$

4.2.4.2 Compliant Model

If the compliance of the links and joints is included, $(6 - n)$ virtual joints are then added in order to account for the compliance of the links (Gosselin and Zhang 1999). Hence, the Jacobian matrix of the constraining leg becomes

$$\mathbf{J}'_{n+1} \dot{\boldsymbol{\theta}}'_{n+1} = \mathbf{t}, \quad n = 3, 4, \text{ or } 5 \tag{4.15}$$

where

$$\dot{\boldsymbol{\theta}}'_{n+1} = \begin{bmatrix} \dot{\theta}_{n+1,1} & \cdots & \dot{\theta}_{n+1,6} \end{bmatrix}^T, \quad n = 3, 4, \text{ or } 5 \tag{4.16}$$

and the Jacobian matrix of the passive constraining leg of the mechanism $\mathbf{J}'_{n+1}$ can be expressed as

$$\mathbf{J}'_{n+1} = \begin{bmatrix} \mathbf{e}_{n+1,1} & \cdots & \mathbf{e}_{n+1,6} \\ \mathbf{e}_{n+1,1} \times \mathbf{r}_{n+1,1} & \cdots & \mathbf{e}_{n+1,6} \times \mathbf{r}_{n+1,6} \end{bmatrix}, \quad n = 3, 4, \text{ or } 5 \tag{4.17}$$

4.2.5 Global Velocity Equation

Now considering the parallel component of the mechanism, the parallel Jacobian matrix can be obtained by differentiating eq. (4.7) with respect to time, one obtains

$$\rho_i \dot{\rho}_i = (\mathbf{p}_i - \mathbf{b}_i)^T \dot{\mathbf{p}}_i, \quad i = 1, \ldots, n \tag{4.18}$$

Since one has

$$\dot{\mathbf{Q}} = \boldsymbol{\Omega} \mathbf{Q} \tag{4.19}$$

with

$$\boldsymbol{\Omega} = \mathbf{1} \times \boldsymbol{\omega} = \begin{bmatrix} 0 & -\omega_3 & \omega_2 \\ \omega_3 & 0 & -\omega_1 \\ -\omega_2 & \omega_1 & 0 \end{bmatrix} \tag{4.20}$$

differentiating eq. (4.3), one obtains

$$\dot{\mathbf{p}}_i = \dot{\mathbf{p}} + \dot{\mathbf{Q}} \mathbf{r}'_i \tag{4.21}$$

Then, for $n = 3, 4, \text{ or } 5$, eq. (4.18) can be rewritten as

$$\rho_i \dot{\rho}_i = (\mathbf{p}_i - \mathbf{b}_i)^T (\dot{\mathbf{p}} + \dot{\mathbf{Q}} \mathbf{r}'_i)$$

$$
\begin{aligned}
&= (\mathbf{p}_i - \mathbf{b}_i)^T(\dot{\mathbf{p}} + \mathbf{\Omega}\mathbf{Q}\mathbf{r}'_i) \\
&= (\mathbf{p}_i - \mathbf{b}_i)^T\dot{\mathbf{p}} + (\mathbf{p}_i - \mathbf{b}_i)^T\mathbf{\Omega}\mathbf{Q}\mathbf{r}'_i \\
&= (\mathbf{p}_i - \mathbf{b}_i)^T\dot{\mathbf{p}} + (\mathbf{p}_i - \mathbf{b}_i)^T[\boldsymbol{\omega} \times (\mathbf{Q}\mathbf{r}'_i)] \\
&= (\mathbf{p}_i - \mathbf{b}_i)^T\dot{\mathbf{p}} + [(\mathbf{Q}\mathbf{r}'_i) \times (\mathbf{p}_i - \mathbf{b}_i)]^T\boldsymbol{\omega}, \quad i = 1, \ldots, n
\end{aligned}
\tag{4.22}
$$

Hence, one can write the velocity equation as

$$
\mathbf{A}\mathbf{t} = \mathbf{B}\dot{\boldsymbol{\rho}}
\tag{4.23}
$$

where vector $\dot{\boldsymbol{\rho}}$ is defined as

$$
\dot{\boldsymbol{\rho}} = \begin{bmatrix} \dot{\rho}_1 & \dot{\rho}_2 & \cdots & \dot{\rho}_n \end{bmatrix}^T
\tag{4.24}
$$

and

$$
\mathbf{A} = \begin{bmatrix} \mathbf{m}_1^T \\ \mathbf{m}_2^T \\ \vdots \\ \mathbf{m}_n^T \end{bmatrix}, \quad \mathbf{B} = diag[\rho_1, \rho_2, \ldots, \rho_n]
\tag{4.25}
$$

where $\mathbf{m}_i$ is a vector with 6 components, which can be expressed as

$$
\mathbf{m}_i = \begin{bmatrix} (\mathbf{Q}\mathbf{r}'_i) \times (\mathbf{p}_i - \mathbf{b}_i) \\ (\mathbf{p}_i - \mathbf{b}_i) \end{bmatrix}
\tag{4.26}
$$

Hence, eq. (4.10) or (4.15) relates the twist of the platform to the joint velocities of the passive constraining leg through the serial Jacobian matrix $\mathbf{J}_{n+1}$ or $\mathbf{J}'_{n+1}$ while eq. (4.23) relates the twist of the platform to the actuator velocities through parallel Jacobian matrices $\mathbf{A}$ and $\mathbf{B}$. It should be pointed out that the dimensions of matrix $\mathbf{J}_{n+1}$ will be $(6 \times n)$, matrix $\mathbf{J}'_{n+1}$ will be (6×6), matrix $\mathbf{A}$ will be $(n \times 6)$ and matrix $\mathbf{B}$ will be $(n \times n)$. The derivation of the relationship between Cartesian velocities and joint rates is thereby completed.

4.2.6   Kinetostatic Model for the Mechanism with Rigid Links

In this section, the velocity equations derived in the previous section will be used to obtain the kinetostatic model for the mechanism with rigid links.

According to the principle of virtual work, one has

$$\boldsymbol{\tau}^T \dot{\boldsymbol{\rho}} = \mathbf{w}^T \mathbf{t} \tag{4.27}$$

where $\boldsymbol{\tau}$ is the vector of actuator forces applied at each actuated joint and $\mathbf{w}$ is the wrench (torque and force) applied to the platform and where it is assumed that no gravitational forces act on any of the intermediate links. In practice, gravitational forces may often be neglected in machine tool applications.

One has $\mathbf{w} = \begin{bmatrix} \mathbf{n}^T & \mathbf{f}^T \end{bmatrix}^T$ where $\mathbf{n}$ and $\mathbf{f}$ are respectively the external torque and force applied to the platform.

Rearranging eq. (4.23) and substituting it into eq. (4.27), one obtains

$$\boldsymbol{\tau}^T \mathbf{B}^{-1} \mathbf{A} \mathbf{t} = \mathbf{w}^T \mathbf{t} \tag{4.28}$$

Now, substituting eq. (4.10) into eq. (4.28), one has

$$\boldsymbol{\tau}^T \mathbf{B}^{-1} \mathbf{A} \mathbf{J}_{n+1} \dot{\boldsymbol{\theta}}_{n+1} = \mathbf{w}^T \mathbf{J}_{n+1} \dot{\boldsymbol{\theta}}_{n+1} \tag{4.29}$$

The latter equation must be satisfied for arbitrary values of $\dot{\boldsymbol{\theta}}_{n+1}$ and hence one can write

$$(\mathbf{A} \mathbf{J}_{n+1})^T \mathbf{B}^{-T} \boldsymbol{\tau} = \mathbf{J}_{n+1}{}^T \mathbf{w} \tag{4.30}$$

The latter equation relates the actuator forces to the Cartesian wrench, $\mathbf{w}$, applied at the end-effector in static mode. Since all links are assumed rigid, the compliance of the mechanism will be induced solely by the compliance of the actuators. An actuator compliance matrix $\mathbf{C}$ is therefore defined as

$$\mathbf{C} \boldsymbol{\tau} = \Delta \boldsymbol{\rho} \tag{4.31}$$

where $\boldsymbol{\tau}$ is the vector of actuated joint forces and $\Delta \boldsymbol{\rho}$ is the induced joint displacement. Matrix $\mathbf{C}$ is a $(n \times n)$ diagonal matrix whose ith diagonal entry is the compliance of the ith actuator.

Now, eq. (4.30) can be rewritten as

$$\boldsymbol{\tau} = \mathbf{B}^T (\mathbf{A} \mathbf{J}_{n+1})^{-T} \mathbf{J}_{n+1}{}^T \mathbf{w} \tag{4.32}$$

The substitution of eq. (4.32) into eq. (4.31) then leads to

$$\Delta \boldsymbol{\rho} = \mathbf{C} \mathbf{B}^T (\mathbf{A} \mathbf{J}_{n+1})^{-T} \mathbf{J}_{n+1}{}^T \mathbf{w} \tag{4.33}$$

Moreover, for a small displacement vector $\Delta\boldsymbol{\rho}$, eq. (4.23) can be written as

$$\Delta\boldsymbol{\rho} \simeq \mathbf{B}^{-1}\mathbf{A}\Delta\mathbf{c} \qquad (4.34)$$

where $\Delta\mathbf{c}$ is a vector of small Cartesian displacement and rotation defined as

$$\Delta\mathbf{c} = \left[\begin{array}{cc} \Delta\mathbf{p}^T & \Delta\boldsymbol{\alpha}^T \end{array}\right]^T \qquad (4.35)$$

in which $\Delta\boldsymbol{\alpha}$, the change of orientation, is defined from eqs. (4.19) and (4.20) as

$$\Delta\boldsymbol{\alpha} = vect(\Delta\mathbf{Q}\mathbf{Q}^T) \qquad (4.36)$$

where $\Delta\mathbf{Q}$ is the variation of the rotation matrix and $vect(\cdot)$ is the vector linear invariant of its matrix argument.

Similarly, eq. (4.10) can also be written , for small displacements, as

$$\mathbf{J}_{n+1}\Delta\boldsymbol{\theta}_{n+1} \simeq \Delta\mathbf{c} \qquad (4.37)$$

where $\Delta\boldsymbol{\theta}_{n+1}$ is a vector of small variations of the joint coordinates of the constraining leg.

Substituting eq. (4.34) into eq. (4.33), one obtains

$$\mathbf{B}^{-1}\mathbf{A}\Delta\mathbf{c} = \mathbf{C}\mathbf{B}^T(\mathbf{A}\mathbf{J}_{n+1})^{-T}\mathbf{J}_{n+1}^T\mathbf{w} \qquad (4.38)$$

Premultiplying both sides of eq. (4.38) by $\mathbf{B}$, and substituting eq. (4.37) into eq. (4.38), one obtains,

$$\mathbf{A}\mathbf{J}_{n+1}\Delta\boldsymbol{\theta}_{n+1} = \mathbf{B}\mathbf{C}\mathbf{B}^T(\mathbf{A}\mathbf{J}_{n+1})^{-T}\mathbf{J}_{n+1}^T\mathbf{w} \qquad (4.39)$$

Then, premultiplying both sides of eq. (4.39) by $(\mathbf{A}\mathbf{J}_{n+1})^{-1}$, one obtains,

$$\Delta\boldsymbol{\theta}_{n+1} = (\mathbf{A}\mathbf{J}_{n+1})^{-1}\mathbf{B}\mathbf{C}\mathbf{B}^T(\mathbf{A}\mathbf{J}_{n+1})^{-T}\mathbf{J}_{n+1}^T\mathbf{w} \qquad (4.40)$$

and finally, premultiplying both sides of eq. (4.40) by $\mathbf{J}_{n+1}$, one obtains,

$$\Delta\mathbf{c} = \mathbf{J}_{n+1}(\mathbf{A}\mathbf{J}_{n+1})^{-1}\mathbf{B}\mathbf{C}\mathbf{B}^T(\mathbf{A}\mathbf{J}_{n+1})^{-T}\mathbf{J}_{n+1}^T\mathbf{w} \qquad (4.41)$$

Hence, one obtains the Cartesian compliance matrix as

$$\mathbf{C}_c = \mathbf{J}_{n+1}(\mathbf{A}\mathbf{J}_{n+1})^{-1}\mathbf{B}\mathbf{C}\mathbf{B}^T(\mathbf{A}\mathbf{J}_{n+1})^{-T}\mathbf{J}_{n+1}^T \qquad (4.42)$$

with

$$\Delta \mathbf{c} = \mathbf{C}_c \mathbf{w} \tag{4.43}$$

where $\mathbf{C}_c$ is a symmetric positive semi-definite (6×6) matrix, as expected.

It is noted that, in nonsingular configurations, the rank of $\mathbf{B}$, $\mathbf{C}$ and $\mathbf{J}_{n+1}$ is n, and hence the rank of $\mathbf{C}_c$ will be n, where $n = 3$, 4, or 5, depending on the degree of freedom of the mechanism. Hence, the nullspace of matrix $\mathbf{C}_c$ will not be empty and there will exist a set of vectors $\mathbf{w}$ that will induce no Cartesian displacement $\Delta \mathbf{c}$. This corresponds to the wrenches that are supported by the constraining leg, which is considered infinitely rigid. These wrenches are orthogonal complements of the allowable twists at the platform. Hence, matrix $\mathbf{C}_c$ cannot be inverted and this is why it was more convenient to use compliance matrices rather than stiffness matrices in the above derivation.

In the next section, the kinetostatic model will be developed for the case in which the flexibility of the links is considered. In this case, stiffness matrices will be used.

4.2.7 Kinetostatic Model for the Mechanism with Flexible Links

According to the principle of virtual work, one can write

$$\mathbf{w}^T \mathbf{t} = \boldsymbol{\tau}_{n+1}^T \dot{\boldsymbol{\theta}}'_{n+1} + \boldsymbol{\tau}^T \dot{\boldsymbol{\rho}} \tag{4.44}$$

where $\boldsymbol{\tau}$ is the vector of actuator forces and $\dot{\boldsymbol{\rho}}$ is the vector of actuator velocities (actuated legs), and $\boldsymbol{\tau}_{n+1}$ is the vector of joint torques in the constraining leg. This vector is defined as follows, where $\mathbf{K}_{n+1}$ is the stiffness matrix of the constraining leg,

$$\boldsymbol{\tau}_{n+1} = \mathbf{K}_{n+1} \Delta \boldsymbol{\theta}'_{n+1} \tag{4.45}$$

Matrix $\mathbf{K}_{n+1}$ is a diagonal (6×6) matrix in which the ith diagonal entry is zero if it is associated with a real joint while it is equal to k_i if it is associated with a virtual joint, where k_i is the stiffness of the virtual spring located at the ith joint. The stiffness of the virtual springs is determined using the structural properties of the flexible links as shown in Chapter 3.

From eqs. (4.15) and (4.23), eq. (4.44) can be rewritten as

$$\mathbf{w}^T \mathbf{t} = \boldsymbol{\tau}_{n+1}^T (\mathbf{J}'_{n+1})^{-1} \mathbf{t} + \boldsymbol{\tau}^T \mathbf{B}^{-1} \mathbf{A} \mathbf{t} \tag{4.46}$$

Since this equation is valid for any value of $\mathbf{t}$, one can write

$$\mathbf{w} = (\mathbf{J}'_{n+1})^{-T} \boldsymbol{\tau}_{n+1} + \mathbf{A}^T \mathbf{B}^{-T} \boldsymbol{\tau} \tag{4.47}$$

which can be rewritten as

$$\mathbf{w} = (\mathbf{J}'_{n+1})^{-T} \mathbf{K}_{n+1} \Delta\boldsymbol{\theta}'_{n+1} + \mathbf{A}^T \mathbf{B}^{-T} \mathbf{K}_J \Delta\boldsymbol{\rho} \tag{4.48}$$

where $\mathbf{K}_J$ is a $(n \times n)$ diagonal joint stiffness matrix for the actuated joints.

Using the kinematic equations, one can then write:

$$\mathbf{w} = (\mathbf{J}'_{n+1})^{-T} \mathbf{K}_{n+1} (\mathbf{J}'_{n+1})^{-1} \Delta\mathbf{c} + \mathbf{A}^T \mathbf{B}^{-T} \mathbf{K}_J \mathbf{B}^{-1} \mathbf{A} \Delta\mathbf{c} \tag{4.49}$$

which is in the form

$$\mathbf{w} = \mathbf{K} \Delta\mathbf{c} \tag{4.50}$$

where $\mathbf{K}$ is the Cartesian stiffness matrix, which is equal to

$$\mathbf{K} = [(\mathbf{J}'_{n+1})^{-T} \mathbf{K}_{n+1} (\mathbf{J}'_{n+1})^{-1} + \mathbf{A}^T \mathbf{B}^{-T} \mathbf{K}_J \mathbf{B}^{-1} \mathbf{A}] \tag{4.51}$$

Matrix $\mathbf{K}$ is a symmetric (6×6) positive semi-definite matrix, as expected. However, in this case, matrix $\mathbf{K}$ will be of full rank in non-singular configurations. Indeed, the sum of the two terms in eq. (4.51) will span the complete space of constraint wrenches.

In the next sections, the kinetostatic models derived above will be applied to different families of parallel mechanisms.

4.3 Spatial Three-Degree-of-Freedom Mechanisms with Prismatic Actuators

4.3.1 Geometric Modeling

As represented in Figures 4.3, 4.4 and 4.5, the spatial three-degree-of-freedom mechanism consists of four kinematic chains, including three variable length legs with identical

topology and one passive constraining leg, connecting the fixed base to a moving platform. In this 3-dof parallel mechanism, the kinematic chains associated with the three identical legs consist — from base to platform — of a fixed Hooke joint, a moving link, an actuated prismatic joint, a moving link and a spherical joint attached to the platform. The fourth chain connecting the base center to the platform center is a passive constraining leg and has a different architecture from the other three identical chains. It consists of a prismatic joint attached to the base, a moving link and a Hooke joint attached to the platform. This last leg is used to constrain the motion of the platform to only three degrees of freedom.

The lumped compliance model described in Section 4.2.2 will be used to establish a simple kinetostatic model for this mechanism.
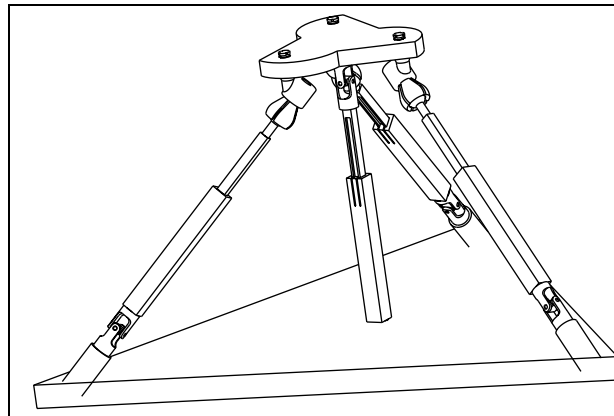
Figure 4.3: CAD model of the spatial 3-dof parallel mechanism with prismatic actuators (Figure by Gabriel Coté).

4.3.2   Inverse Kinematics

In this 3-dof mechanism, only three of the six Cartesian coordinates of the platform are independent. In the present study, the independent coordinates have been chosen for convenience as $(z, \theta_{42}, \theta_{43})$, where θ_{42}, θ_{43} are the joint angles of the Hooke joint attached to the platform and z is the height of the platform.
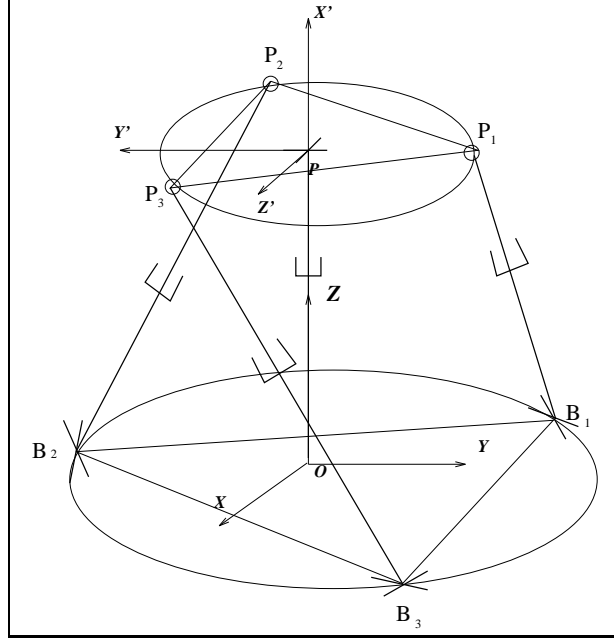
Figure 4.4: Schematic representation of the spatial 3-dof parallel mechanism with prismatic actuators.

According to eqs. (4.1), (4.2) and Figure 4.5, for $i = 1, 2, 3$, one has

$$\mathbf{r}_i' = \begin{bmatrix} 0 \\ -R_p \sin \theta_{pi} \\ R_p \cos \theta_{pi} \end{bmatrix}, \quad \mathbf{b}_i = \begin{bmatrix} R_b \cos \theta_{bi} \\ R_b \sin \theta_{bi} \\ 0 \end{bmatrix} \tag{4.52}$$

$$\boldsymbol{\theta}_{bi} = \begin{bmatrix} \theta_{b1} \\ \theta_{b2} \\ \theta_{b3} \end{bmatrix} = \begin{bmatrix} \pi/3 \\ \pi \\ -\pi/3 \end{bmatrix}, \quad \boldsymbol{\theta}_{pi} = \begin{bmatrix} \theta_{p1} \\ \theta_{p2} \\ \theta_{p3} \end{bmatrix} = \begin{bmatrix} 0 \\ 2\pi/3 \\ -2\pi/3 \end{bmatrix} \tag{4.53}$$

based on eqs. (4.3) – (4.7), the inverse kinematic problem for the 3-dof platform can finally be written as

$$\rho_i^2 = (\mathbf{p}_i - \mathbf{b}_i)^T (\mathbf{p}_i - \mathbf{b}_i), \quad i = 1, 2, 3 \tag{4.54}$$

4.3.3 Jacobian Matrices

4.3.3.1 Rigid Model

From Figure 4.6, one can obtain the Denavit-Hartenberg parameters given in Table 4.2.
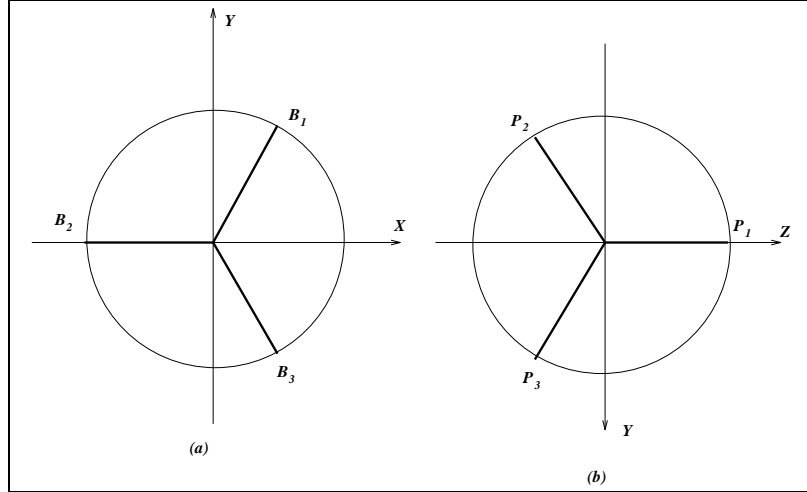
Figure 4.5: Position of the attachment points: (a)on the base, (b)on the platform.
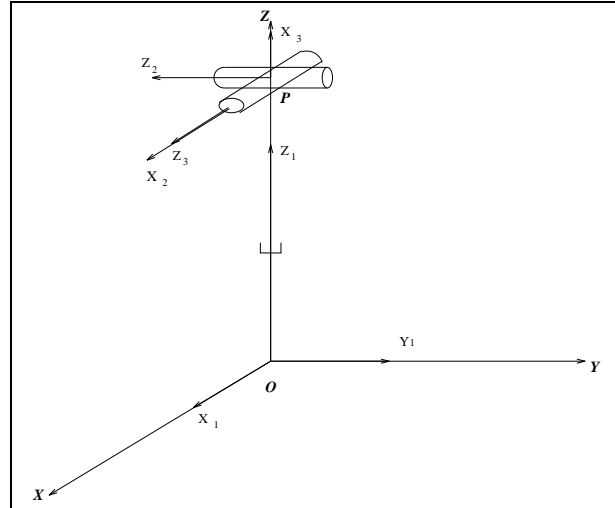
Figure 4.6: The passive constraining leg with rigid links.

A transformation for each local coordinate is required, we take the Cartesian coordinate frame as frame $\mathbf{0}$, and define $\alpha_0 = 0, \theta_0 = 0$, then one has

$$\mathbf{Q}_{40} = \mathbf{1} \tag{4.55}$$

where $\mathbf{Q}_{40}$ is the rotation matrix from the fixed reference frame to the first frame of the passive constraining leg. Premutiplying eq. (4.55) in each equation by $\mathbf{e}_{4j}$ and $\mathbf{r}_{4j}$, then one obtains

$$\mathbf{e}_{41} = \mathbf{Q}_{40}\mathbf{e}_{40} \tag{4.56}$$

$$\mathbf{e}_{42} = \mathbf{Q}_{40}\mathbf{Q}_{41}\mathbf{e}_{40} \tag{4.57}$$

Table 4.2: The DH parameters for the passive constraining leg with rigid links.

i	a_i	b_i	α_i	θ_i
0	0	0	0	0
1	0	Z	90°	0
2	0	0	90°	θ_{42}
3	0	0	0	θ_{43}

$$\mathbf{e}_{43} = \mathbf{Q}_{40}\mathbf{Q}_{41}\mathbf{Q}_{42}\mathbf{e}_{40} \tag{4.58}$$

and the position vectors can be expressed as follows

$$\mathbf{r}_{41} = \mathbf{Q}_{40}\mathbf{a}_{41} + \mathbf{Q}_{40}\mathbf{Q}_{41}\mathbf{a}_{42} + \mathbf{Q}_{40}\mathbf{Q}_{41}\mathbf{Q}_{42}\mathbf{a}_{43} \tag{4.59}$$

$$\mathbf{r}_{42} = \mathbf{Q}_{40}\mathbf{Q}_{41}\mathbf{a}_{42} + \mathbf{Q}_{40}\mathbf{Q}_{41}\mathbf{Q}_{42}\mathbf{a}_{43} \tag{4.60}$$

$$\mathbf{r}_{43} = \mathbf{Q}_{40}\mathbf{Q}_{41}\mathbf{Q}_{42}\mathbf{a}_{43} \tag{4.61}$$

For the fourth kinematic chain, one has the velocity equation

$$\mathbf{J}_4\dot{\boldsymbol{\theta}}_4 = \mathbf{t} \tag{4.62}$$

where

$$\dot{\boldsymbol{\theta}}_4 = \begin{bmatrix} \dot{\rho} & \dot{\theta}_{42} & \dot{\theta}_{43} \end{bmatrix}^T \tag{4.63}$$

and the Jacobian matrix of the passive constraining leg of the mechanism $\mathbf{J}_4$ can be expressed as

$$\mathbf{J}_4 = \begin{bmatrix} \mathbf{0} & \mathbf{e}_{42} & \mathbf{e}_{43} \\ \mathbf{e}_{41} & \mathbf{e}_{42} \times \mathbf{r}_{42} & \mathbf{e}_{43} \times \mathbf{r}_{43} \end{bmatrix} \tag{4.64}$$

4.3.3.2 Compliant Model

In this section, the equations for all the three identical legs are the same as in the rigid model, we only need to study the passive constraining leg with virtual joint.

From Figure 4.7, one can obtain the Denavit-Hartenberg parameters as in Table 4.3. For the passive constraining leg, we have the velocity equation using the same method as for the rigid links.

$$\mathbf{J}'_4\dot{\boldsymbol{\theta}}'_4 = \mathbf{t} \tag{4.65}$$
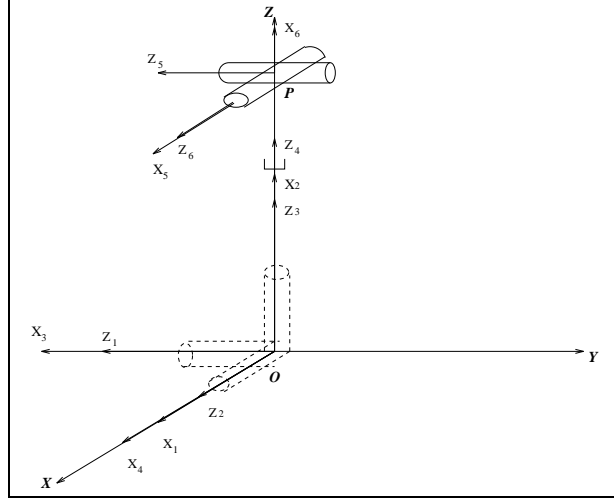
Figure 4.7: The passive constraining leg with flexible links.

Table 4.3: The DH parameters for the passive constraining leg with flexible links.

i	a_i	b_i	α_i	θ_i
0	0	0	$90°$	0
1	0	0	$90°$	θ_{41}
2	0	0	$90°$	θ_{42}
3	0	0	0	θ_{43}
4	0	Z	$90°$	θ_{44}
5	0	0	$90°$	θ_{45}
6	0	0	0	θ_{46}

where

$$\dot{\boldsymbol{\theta}}'_4 = \begin{bmatrix} \dot{\theta}_{41} & \dot{\theta}_{42} & \dot{\theta}_{43} & \dot{\rho}_{44} & \dot{\theta}_{45} & \dot{\theta}_{46} \end{bmatrix}^T \qquad (4.66)$$

$$\mathbf{J}'_4 = \begin{bmatrix} \mathbf{e}_{41} & \mathbf{e}_{42} & \mathbf{e}_{43} & 0 & \mathbf{e}_{45} & \mathbf{e}_{46} \\ \mathbf{e}_{41} \times \mathbf{r}_{41} & \mathbf{e}_{42} \times \mathbf{r}_{42} & \mathbf{e}_{43} \times \mathbf{r}_{43} & \mathbf{e}_{44} & \mathbf{e}_{45} \times \mathbf{r}_{45} & \mathbf{e}_{46} \times \mathbf{r}_{46} \end{bmatrix} \qquad (4.67)$$

After considering the parallel component of the mechanism, the relationship between Cartesian velocities and joint rates can be obtained by eqs. (4.18) to (4.23).

4.3.4 Kinetostatic Models

In this section, the velocity equation derived in the previous section is used to obtain the kinetostatic model for the mechanism with rigid links. The compliance matrix for the rigid model can be written as

$$\mathbf{C}_c = \mathbf{J}_4(\mathbf{A}\mathbf{J}_4)^{-1}\mathbf{B}\mathbf{C}\mathbf{B}^T(\mathbf{A}\mathbf{J}_4)^{-T}\mathbf{J}_4^T \tag{4.68}$$

where $\mathbf{C} = diag[c_1, c_2, c_3]$, with c_1, c_2 and c_3 the compliance of the actuators and $\mathbf{J}_4$ is the Jacobian matrix of the constraining leg in this 3-dof case. Matrices $\mathbf{A}$ and $\mathbf{B}$ are the Jacobian matrices of the structure without the passive constraining leg.

Similarly, the stiffness matrix for the mechanism with flexible links can be written as

$$\mathbf{K} = [(\mathbf{J}_4')^{-T}\mathbf{K}_4(\mathbf{J}_4')^{-1} + \mathbf{A}^T\mathbf{B}^{-T}\mathbf{K}_J\mathbf{B}^{-1}\mathbf{A}] \tag{4.69}$$

with

$$\mathbf{K}_4 = diag[k_{41}, k_{42}, k_{43}, 0, 0, 0] \tag{4.70}$$

where k_{41}, k_{42} and k_{43} are the stiffnesses of the virtual joints introduced to account for the flexibility of the links in the constraining leg. The architecture of the constraining leg including the virtual joints is represented in Figure 4.7, and $\mathbf{J}_4'$ is the Jacobian matrix of the constraining leg in this 3-dof case, while $\mathbf{A}$ and $\mathbf{B}$ are the Jacobian matrices of the structure without the constraining leg.

4.3.5 Implementation

4.3.5.1 Stiffness Evolution and Compliance Comparison

We implemented the above model for both the flexible case and the rigid case. A program has been written with the software Mathematica, the stiffness trends are obtained in each direction with the variation of links stiffness (i.e, the link's flexibility). Figure 4.8 shows that with the improvement of link stiffness, the mechanism's stiffness with flexible link is becoming a constant, this means that we can assume the flexible mechanism to be rigid only if the link stiffness reaches a certain high value. It also verifies the correctness of the kinetostatic model. The comparison between the mech-

(a) Stiffness in θ_z

(b) Stiffness in x
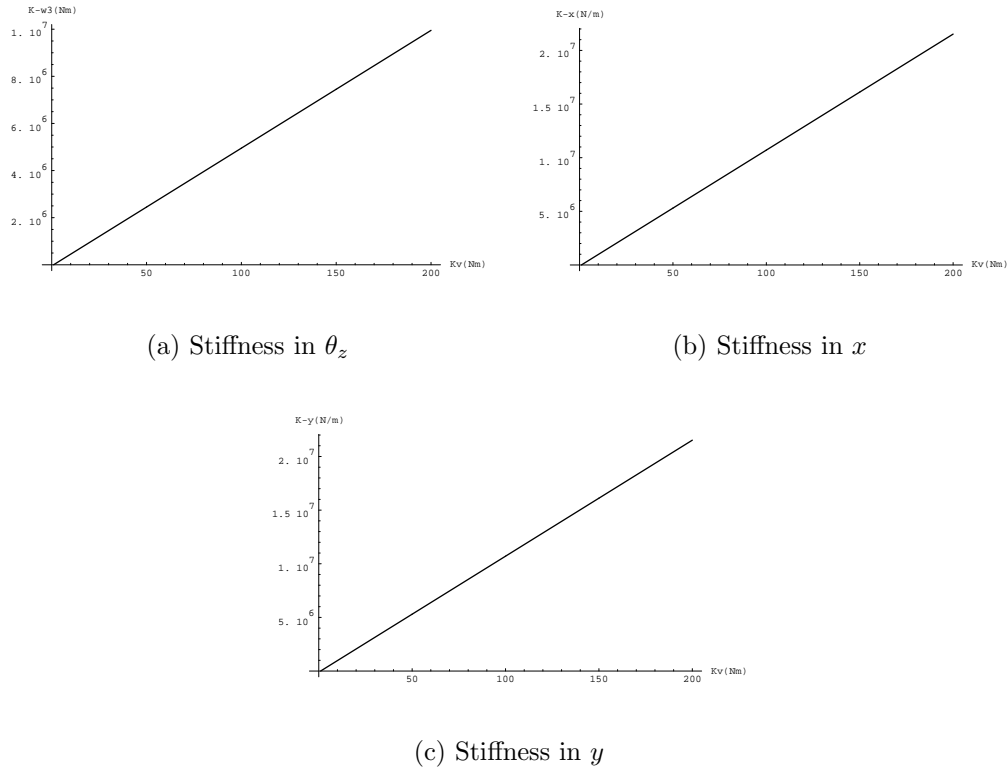
(c) Stiffness in y

Figure 4.8: Evolution of the stiffness as a function of the passive link's lumped stiffness in θ_z, x, y directions (all the other directions are constants).

anism with rigid links (without virtual joints) and the mechanism with flexible links (with virtual joints) is given in Table 4.4 (compliances have slightly variations in the θ_x, θ_y and Z directions although the stiffnesses in these directions are constant, this is because of the inverse operation of stiffness matrix to compliance matrix.). The Cartesian compliance in each of the directions is given for a reference configuration of the mechanism, for progressively increasing values of the link stiffnesses. From Table 4.4, one can find that with the improvement of the link stiffness, the mechanism's compliance is very close to that of mechanism with rigid link, this gives an alternative proof of the above conclusion.

4.3.5.2 Compliance Mappings

The analysis described above is now used to obtain the compliance mappings. They are drawn on a section of the workspace of the platform.

Table 4.4: Comparison of the mechanism compliance between the mechanism with rigid links and the mechanism with flexible links.

K_a	$K_{passive}$	$\kappa_{\theta_x} = \kappa_{\theta_y}$	κ_{θ_z}	$\kappa_x = \kappa_y$	κ_z
1000	1000	0.192784	10^{-3}	4.624×10^{-4}	3.4569×10^{-4}
1000	$10K_a$	0.192509	10^{-4}	4.624×10^{-5}	3.4567×10^{-4}
1000	$10^2 K_a$	0.192081	10^{-5}	4.624×10^{-6}	3.4566×10^{-4}
1000	$10^3 K_a$	0.192038	10^{-6}	4.624×10^{-7}	3.4566×10^{-4}
1000	$10^4 K_a$	0.192034	10^{-7}	4.624×10^{-8}	3.4566×10^{-4}
1000	$10^5 K_a$	0.192034	10^{-8}	4.624×10^{-9}	3.4566×10^{-4}
1000	$10^6 K_a$	0.192034.	10^{-9}	4.624×10^{-10}	3.4566×10^{-4}
1000	$10^7 K_a$	0.192034	10^{-10}	4.624×10^{-11}	3.4566×10^{-4}
1000	rigid	0.192034	0.0	0.0	3.4566×10^{-4}

Visualization tools to aid in the use of such expressions have been developed. A computer program has been written with software Mathematica. After giving the initial values above, then the contour maps can be obtained as shown in Figure 4.9. From such plots one can determine which regions of the workspace will satisfy some compliance criteria.

In Figures 4.9(a) and 4.9(b), the torsional compliances in θ_x and θ_y are shown, the compliances are symmetric. In Figure 4.9(f) the stiffness in z is higher near the center of the workspace, which is the best position for supporting vertical loads. This is due to the architecture chosen, which aims at supporting heavy objects in an environment where the gravity is acting along the negative direction of z axis. All these are in accordance with what would be intuitively expected.

4.3.6 Design Guidelines

Based on the above model, an example is now given to illustrate the effect of flexible links (virtual joints) on the parallel mechanism. Referring to Figure 4.4, the parameters used in this example are given as

$$\theta_{b1} = \pi/3, \theta_{b2} = \pi, \theta_{b3} = -\pi/3,$$

(a) Compliance in θ_x (1/Nm)

(b) Compliance in θ_y (1/Nm)

(c) Compliance in θ_z (1/Nm)

(d) Compliance in z (m/N)
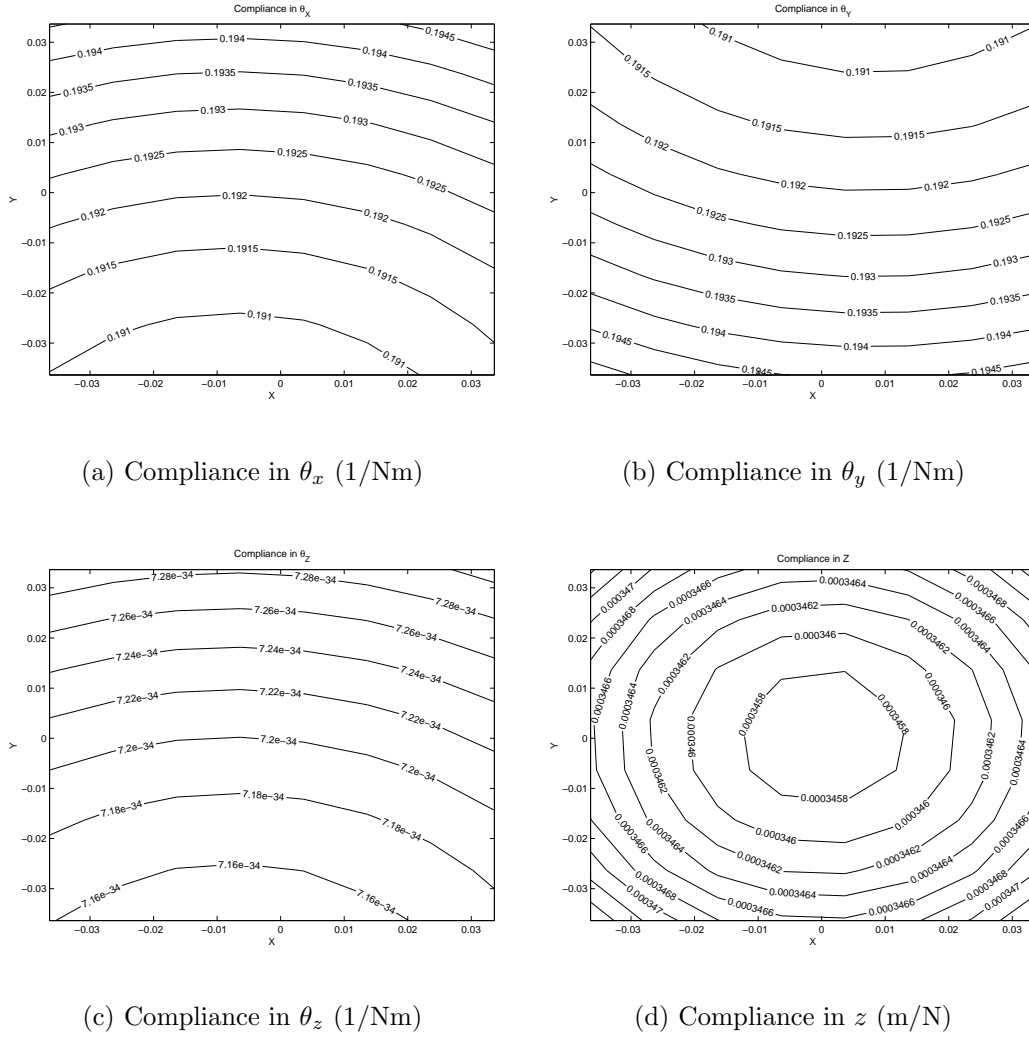
Figure 4.9: Compliance mappings of the spatial 3-dof parallel mechanism with prismatic actuators (all length units in m).

$$\theta_{p1} = 0, \theta_{p2} = 2\pi/3, \theta_{p3} = -2\pi/3,$$

$$R_p = 6 \ cm, R_b = 15 \ cm,$$

$$k_{i1} = 1000 \ N/m, \quad i = 1, \ldots, 3$$

where k_{i1} is the actuator stiffness.

$$x \in [-3, 3] \ cm, y \in [-3, 3] \ cm, z = 68 \ cm,$$

$$\theta_{42} = \pi/2, \theta_{43} = 0,$$

For the configuration specified as

$$x = 0, y = 0, z = 68 \ cm,$$

$$\theta_{42} = \pi/2, \theta_{43} = 0,$$

one can find the global stiffnesses in all directions as a function of the actuator stiffness and link stiffness (actuated and passive constraining leg), they are

$$K_{\theta_x} = 0.00520742 K_a \tag{4.71}$$

$$K_{\theta_y} = 0.00520742 K_a \tag{4.72}$$

$$K_{\theta_z} = 0.000380083 K_a + K_{43} \tag{4.73}$$

$$K_x = 0.0534932 K_a + 2.16263 K_{41} \tag{4.74}$$

$$K_y = 0.0534932 K_a + 2.16263 K_{42} \tag{4.75}$$

$$K_z = 2.89301 K_a \tag{4.76}$$

where K_a represents the actuator stiffness, K_{41}, K_{42} and K_{43} represent the lumped stiffnesses of the passive leg in X, Y and Z directions caused by the link bending and torsion (flexibility).

Based on the results of the preceding section and the expression of eqs. (4.71) – (4.76), the following design guidelines can be established as the reference for the design of such mechanisms. The common design guidelines for this series of mechanisms will be given in Section 4.7.

1. The stiffnesses K_{θ_x}, K_{θ_y} and K_z are in direct proportion to the actuator stiffness and have no relationship with the rigidity of passive constraining leg.

2. K_{41} and K_{42}, i.e., the passive leg's bending stiffness along the X and Y axes, play the same function of limiting the movement of the platform along the X and Y. K_{43}, i.e., the passive constraining leg's torsional stiffness around the Z axis, plays the function of limiting the rotation of the platform around the Z axis.

3. From the equations above, one can find that the stiffness along the Z axis is the largest one among all the directions, and K_{θ_y} is equal to K_{θ_x} because of the structure's symmetrical configuration.

4. From Figure 4.8 and Table 4.4, we can also see that K_{θ_z}, K_x and K_y are becoming infinite while the flexible links are becoming more rigid, it corresponds to the motions prevented by the passive constraining leg.

We also find the following facts about the mechanism after performing some tests and varying the parameters of the mechanism.

1. For a certain platform size, the larger the link length, the larger the global stiffness values in all directions.

2. For a given link length, the smaller the platform size, the smaller the torsional stiffness values around the X and Y axes, and the larger the stiffness values along the Z axis.

4.4 Spatial Four-Degree-of-Freedom Mechanisms with Prismatic Actuators

4.4.1 Geometric Modeling

Figures 4.10 and 4.11 represent a 4-dof parallel mechanism's CAD model and its schematic representation, the joint distribution both on the base and on the platform is shown in Figure 4.12. This mechanism consists of five kinematic chains, including four 6-dof variable length links with identical topology — as in the previous mechanism — and one passive constraining link, connecting the fixed base to a moving platform. The fifth chain connecting the base center to the platform center consists of a revolute joint attached to the base, a moving link, a revolute joint, a second moving link and a Hooke joint attached to the platform. This last leg is used to constrain the motion of the platform to only four degrees of freedom.

4.4.2 Inverse Kinematics

There are four independent Cartesian coordinates of the platform. In the current study, the independent coordinates have been chosen for convenience as $(x, z, \theta_{53}, \theta_{54})$, where θ_{53}, θ_{54} are the joint angles of the Hooke joint attached to the platform. For $i = 1, \ldots, 4$,
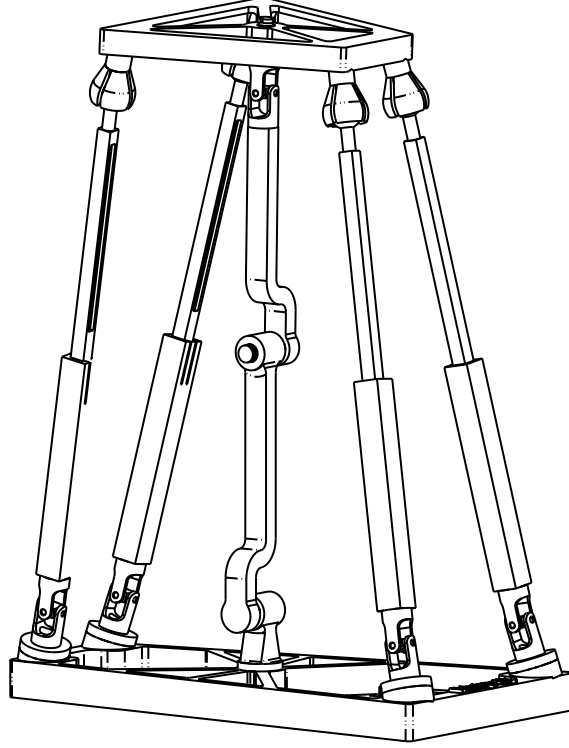
Figure 4.10: CAD model of the spatial 4-dof parallel mechanism with prismatic actuators (Figure by Gabriel Coté).

one has

$$
\mathbf{r}'_i = \begin{bmatrix} 0 \\ -R_p \sin \theta_{pi} \\ R_p \cos \theta_{pi} \end{bmatrix}, \quad
\mathbf{b}_i = \begin{bmatrix} R_b \cos \theta_{bi} \\ R_b \sin \theta_{bi} \\ 0 \end{bmatrix}
\tag{4.77}
$$

$$
\boldsymbol{\theta}_{bi} = \begin{bmatrix} \theta_{b1} \\ \theta_{b2} \\ \theta_{b3} \\ \theta_{b4} \end{bmatrix} = \begin{bmatrix} \alpha \\ \pi - \beta \\ \pi + \beta \\ -\alpha \end{bmatrix}, \quad
\boldsymbol{\theta}_{pi} = \begin{bmatrix} \theta_{p1} \\ \theta_{p2} \\ \theta_{p3} \\ \theta_{p4} \end{bmatrix} = \begin{bmatrix} \beta \\ \pi - \alpha \\ \pi + \alpha \\ -\beta \end{bmatrix}
\tag{4.78}
$$

according to eqs. (4.3) − (4.7), the inverse kinematic problem for the 4-dof platform can finally be written as

$$
\rho_i^2 = (\mathbf{p}_i - \mathbf{b}_i)^T (\mathbf{p}_i - \mathbf{b}_i), \quad i = 1, \dots, 4
\tag{4.79}
$$
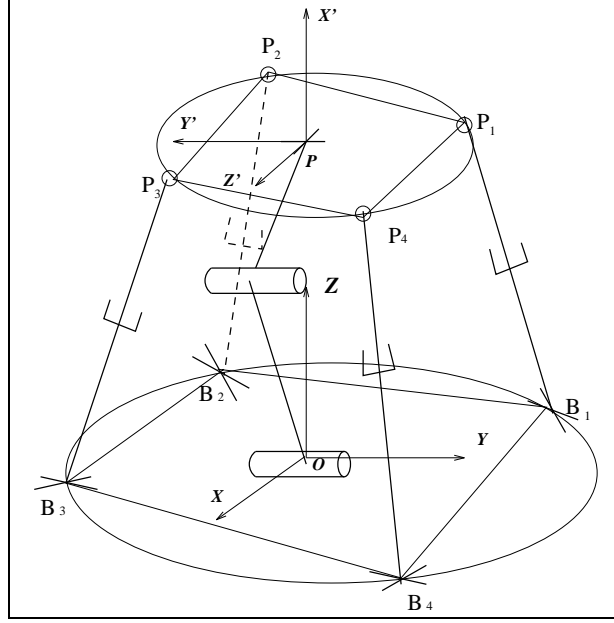
Figure 4.11: Schematic representation of the spatial 4-dof parallel mechanism with prismatic actuators.

4.4.3 Jacobian Matrices

4.4.3.1 Rigid Model

Table 4.5: The DH parameters for the passive constraining leg with rigid links.

i	a_i	b_i	α_i	θ_i
0	0	0	$90°$	0
1	l_{51}	0	0	θ_{51}
2	l_{52}	0	0	θ_{52}
3	0	0	$90°$	θ_{53}
4	0	0	0	θ_{54}

From Figure 4.13, one can obtain the Denavit-Hartenberg parameters given in Table 4.5. A procedure similar to the previous mechanism is then completed to compute vectors $\mathbf{e}_{5i}$ and $\mathbf{r}_{5i}$, for $i = 1, \ldots, 4$. For the fifth kinematic chain (passive constraining leg), one finally has the velocity equation

$$\mathbf{J}_5 \dot{\boldsymbol{\theta}}_5 = \mathbf{t} \tag{4.80}$$
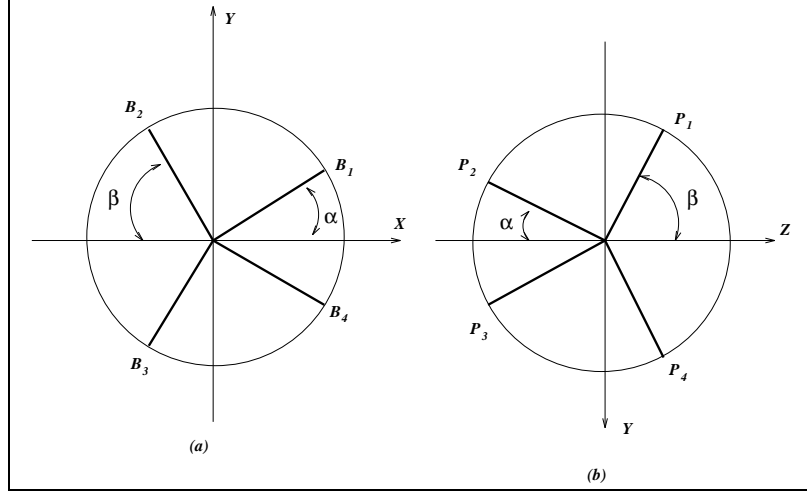
Figure 4.12: Position of the attachment points: (a)on the base, (b)on the platform.

where

$$\dot{\boldsymbol{\theta}}_5 = \begin{bmatrix} \dot{\theta}_{51} & \dot{\theta}_{52} & \dot{\theta}_{53} & \dot{\theta}_{54} \end{bmatrix}^T \tag{4.81}$$

and the Jacobian matrix of the passive constraining leg $\mathbf{J}_5$ can be expressed as

$$\mathbf{J}_5 = \begin{bmatrix} \mathbf{e}_{51} & \mathbf{e}_{52} & \mathbf{e}_{53} & \mathbf{e}_{54} \\ \mathbf{e}_{51} \times \mathbf{r}_{51} & \mathbf{e}_{52} \times \mathbf{r}_{52} & \mathbf{e}_{53} \times \mathbf{r}_{53} & \mathbf{e}_{54} \times \mathbf{r}_{54} \end{bmatrix} \tag{4.82}$$

4.4.3.2 Compliant Model

Here, the equations for all the four identical legs are the same as in the rigid model. Figure 4.14 illustrates the configuration of the passive constraining leg with flexible links. θ_{51} and θ_{53} can be obtained with the method described in Appendix B.1.

From Figure 4.14, the Denavit-Hartenberg parameters can be obtained as in Table 4.6, then, the velocity equation can be written as

$$\mathbf{J}'_5 \dot{\boldsymbol{\theta}}'_5 = \mathbf{t} \tag{4.83}$$

where

$$\dot{\boldsymbol{\theta}}'_5 = \begin{bmatrix} \dot{\theta}_{51} & \dot{\theta}_{52} & \dot{\theta}_{53} & \dot{\theta}_{54} & \dot{\theta}_{55} & \dot{\theta}_{56} \end{bmatrix}^T \tag{4.84}$$

$$\mathbf{J}'_5 = \begin{bmatrix} \mathbf{e}_{51} & \mathbf{e}_{52} & \mathbf{e}_{53} & \mathbf{e}_{54} & \mathbf{e}_{55} & \mathbf{e}_{56} \\ \mathbf{e}_{51} \times \mathbf{r}_{51} & \mathbf{e}_{52} \times \mathbf{r}_{52} & \mathbf{e}_{53} \times \mathbf{r}_{53} & \mathbf{e}_{54} \times \mathbf{r}_{54} & \mathbf{e}_{55} \times \mathbf{r}_{55} & \mathbf{e}_{56} \times \mathbf{r}_{56} \end{bmatrix} \tag{4.85}$$
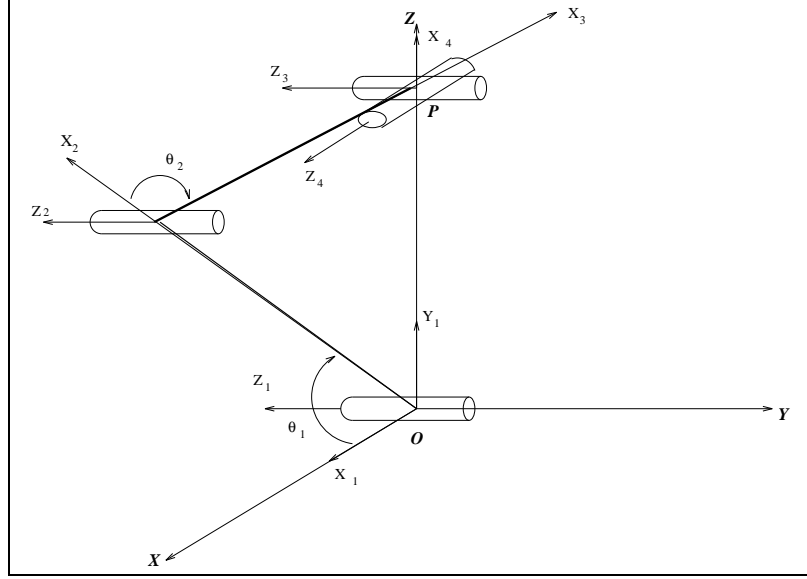
Figure 4.13: The passive constraining leg with rigid links.

Considering the parallel component of the mechanism, the relationship between Cartesian velocities and joint rates can be obtained by eqs. (4.18) to (4.23).

4.4.4 Kinetostatic Models

For the mechanism illustrated in Figure 4.10, the compliance matrix for the mechanism with rigid links can be written as

$$\mathbf{C}_c = \mathbf{J}_5(\mathbf{A}\mathbf{J}_5)^{-1}\mathbf{B}\mathbf{C}\mathbf{B}^T(\mathbf{A}\mathbf{J}_5)^{-T}\mathbf{J}_5^T \tag{4.86}$$

where

$$\mathbf{C} = diag[c_1, c_2, c_3, c_4] \tag{4.87}$$

with c_i is the compliance of the ith actuator, and $\mathbf{J}_5$ is the Jacobian matrix of the rigid constraining leg in this 4-dof case. Matrices $\mathbf{A}$ and $\mathbf{B}$ are the Jacobian matrices of the structure without the constraining leg.

Similarly, the stiffness matrix for the mechanism with flexible links can be written as

$$\mathbf{K} = [(\mathbf{J}_5')^{-T}\mathbf{K}_5(\mathbf{J}_5')^{-1} + \mathbf{A}^T\mathbf{B}^{-T}\mathbf{K}_J\mathbf{B}^{-1}\mathbf{A}] \tag{4.88}$$

where

$$\mathbf{K}_5 = diag[0, k_{52}, 0, k_{54}, 0, 0] \tag{4.89}$$
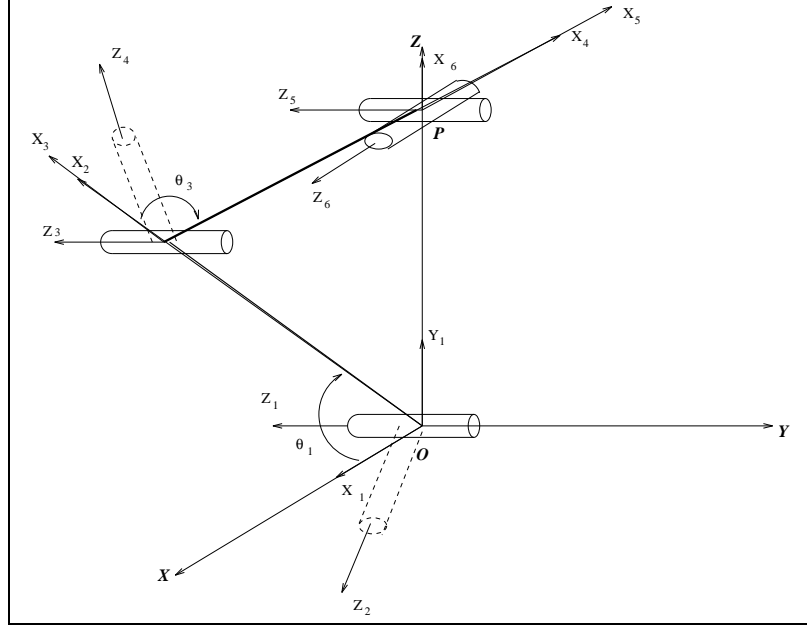
Figure 4.14: The passive constraining leg with flexible links.

with k_{52} and k_{54} are the stiffnesses of the virtual joints. Matrix $\mathbf{J}'_5$ is the Jacobian matrix of the compliant constraining leg in this 4-dof case, while $\mathbf{A}$ and $\mathbf{B}$ are the Jacobian matrices of the structure without the constraining leg.

4.4.5   Implementation

4.4.5.1   Stiffness Evolution and Compliance Comparison

The model developed above has been implemented — for both the flexible case and the rigid case — using the software Mathematica. A reference configuration is given below to illustrate the effect of flexible links on the parallel mechanism.

$$\alpha = 30°, \beta = 60°, R_p = 12 \ cm, R_b = 22 \ cm,$$
$$k_{i1} = 1000 \ N/m, \quad i = 1, \ldots, 4$$

where k_{i1} is the actuator stiffness, and the Cartesian coordinates are given by

$$x \in [-4, 4] \ cm, y \in [-4, 4] \ cm, z = 68 \ cm,$$
$$\theta_{53} = -\pi/3, \theta_{54} = 2\pi/3,$$

Table 4.6: The DH parameters for the passive constraining leg with flexible links.

i	a_i	b_i	α_i	θ_i
0	0	0	$90°$	0
1	0	0	$90°$	θ_{51}
2	l_{51}	0	$-90°$	θ_{52}
3	0	0	$90°$	θ_{53}
4	l_{52}	0	$-90°$	θ_{54}
5	0	0	$90°$	θ_{55}
6	0	0	0	θ_{56}
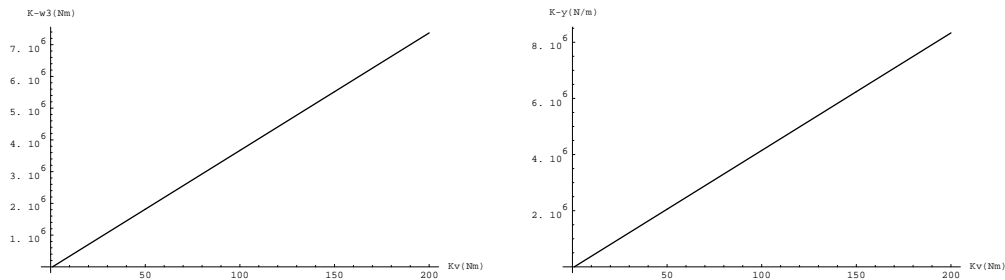
(a) Stiffness in θ_z

(b) Stiffness in y

Figure 4.15: Evolution of the stiffness as a function of the passive link's lumped stiffness in θ_z and y directions (all the other directions are constants).

The compliance comparison between the mechanism with rigid links (without virtual joints) and the mechanism with flexible links (with virtual joints) is given in Table 4.7. Figure 4.15 shows the stiffness trends obtained in each direction with the variation of links stiffness (i.e, the link's flexibility). The passive constraining leg's lumped stiffness effects on the mechanism's stiffness. Again, the effect of the link flexibility is clearly demonstrated.

4.4.5.2 Compliance Mappings

The analysis described above is now used to obtain the compliance mappings for this mechanism. Figure 4.16 shows the compliance maps which are drawn on a section of

Table 4.7: Comparison of the mechanism compliance between the mechanism with rigid links and the mechanism with flexible links.

$K_{actuator}$	$K_{passive}$	κ_{θ_x}	κ_{θ_y}	κ_{θ_z}	κ_x	κ_y	κ_z
1000	1000	0.52371	1.41939	1.5×10^{-3}	0.915208	5.78×10^{-4}	0.0111974
1000	$10^1 K_a$	0.523128	1.41007	1.5×10^{-4}	0.912371	5.78×10^{-5}	0.0111751
1000	$10^2 K_a$	0.51707	1.40514	1.5×10^{-5}	0.909087	5.78×10^{-6}	0.0111429
1000	$10^3 K_a$	0.516464	1.40464	1.5×10^{-6}	0.908758	5.78×10^{-7}	0.0111396
1000	$10^4 K_a$	0.516404	1.4046	1.5×10^{-7}	0.908726	5.78×10^{-8}	0.0111393
1000	$10^5 K_a$	0.516398	1.40459	1.5×10^{-8}	0.908722	5.78×10^{-9}	0.0111393
1000	$10^6 K_a$	0.516397	1.40459	1.5×10^{-9}	0.908722	5.78×10^{-10}	0.0111393
1000	$10^7 K_a$	0.516397	1.40459	1.5×10^{-10}	0.908722	5.78×10^{-11}	0.0111393
1000	rigid	0.516397	1.40459	0.0	0.908722	0.0	0.0111393

the workspace of the platform. From such plots one can determine which regions of the workspace will satisfy some compliance criteria.

From Figure 4.15 and Table 4.7, one can see that K_{θ_z} and K_y are becoming infinite while the flexible links are becoming more rigid. It corresponds to the motions prevented by the passive constraining leg. K_{θ_x} is also large enough because of the structure of the passive constraining leg. The stiffness in Z is higher near the center of the workspace, which is the best position for supporting vertical loads along the Z axis. All these observations are in accordance with what would be intuitively expected.

4.4.6   Design Guidelines

For instance, for the configuration specified as

$$x = 0, y = 0, z = 68 \ cm,$$
$$\theta_{53} = -\pi/3, \theta_{54} = 2\pi/3,$$

the global stiffnesses expression becomes

$$K_{\theta_x} \quad = \quad 0.00850551 K_a \tag{4.90}$$
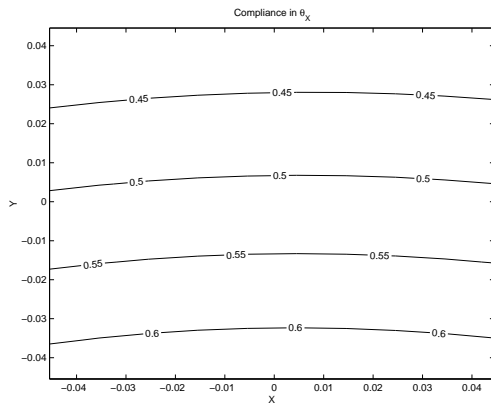
(a) Compliance in θ_x (1/Nm)
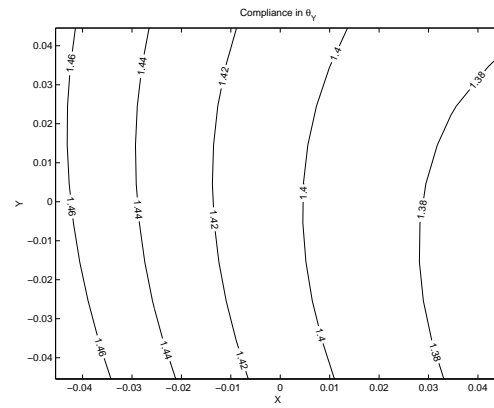
(b) Compliance in θ_y (1/Nm)
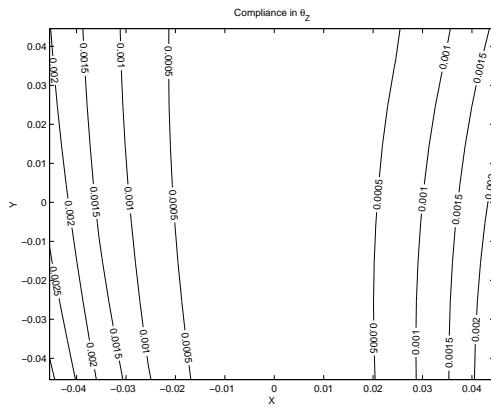
(c) Compliance in θ_z (1/Nm)
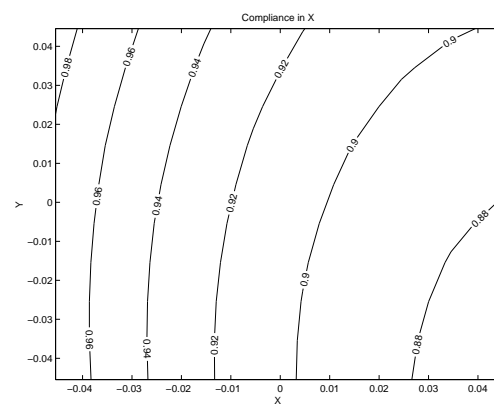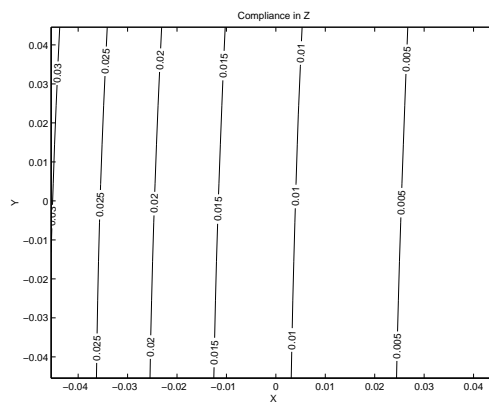
(d) Compliance in x (m/N)

(e) Compliance in z (m/N)

Figure 4.16: Compliance mappings of the spatial 4-dof parallel mechanism with prismatic actuators (all length units in m).

$$K_{\theta_y} = 0.0262118 K_a \tag{4.91}$$

$$K_{\theta_z} = 0.00324089 K_a + 0.592593 K_{52} + 0.148148 K_{54} \tag{4.92}$$

$$K_x = 0.0704587 K_a \tag{4.93}$$

$$K_y = 0.301223 K_a + 0.961169 K_{52} + 0.961169 K_{54} \tag{4.94}$$

$$K_z = 3.62832 K_a \tag{4.95}$$

where K_a represents the actuator stiffness, K_{52} and K_{54} represent the first and second (from bottom to platform) link's lumped stiffnesses of the passive constraining leg.

Based on the results above, apart from the common design guidelines given in Section 4.7, the following design guidelines can be established and as reference for designing such mechanisms:

1. The stiffnesses K_{θ_x}, K_{θ_y}, K_x and K_z are in direct proportion to actuator stiffness and have no relationship with the rigidity of passive constraining leg's.

2. If $K_{52} \neq K_{54}$, i.e., the passive constraining leg's first link (from bottom to platform) is not as rigid as the second link, then the first link's rigidity is more important than the second link's for limiting the platform's degrees of freedom, this can be observed from the coefficients of K_{52} and K_{54} in eqs. (4.92) and (4.94).

3. From the equations, one can find that the stiffness along the Z axis is the largest one among all the directions, and K_{θ_y} is larger than K_{θ_x}.

We also found the following facts about the mechanism after performing some tests and varying the parameters of the mechanism.

1. For a certain platform size, the larger the link length, the smaller the global stiffnesses.

2. For a given link length, the larger the platform size (within a certain range), the larger the torsional stiffnesses around the X and Y axes, and the smaller the stiffnesses along the X and Z axes.

4.5 Spatial Five-Degree-of-Freedom Mechanisms with Prismatic Actuators

4.5.1 Geometric Modeling

A 5-dof parallel mechanism's CAD model, schematic representation and joint distribution both on the base and on the platform are shown in Figures 4.1, 4.2 and 4.17, respectively. A lumped compliance model should be established in order to obtain a simple kinetostatic model, as it has been discussed in Section 4.2.2.
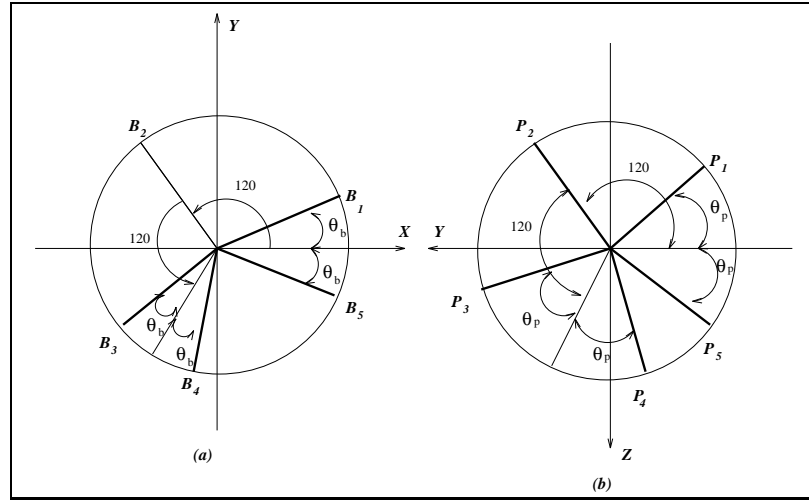
Figure 4.17: Position of the attachment points: (a)on the base, (b)on the platform.

4.5.2 Inverse Kinematics

As described in Section 4.2.3, for $i = 1, \ldots, 5$, one has

$$
\mathbf{r}_i' = \begin{bmatrix} 0 \\ -R_p \cos \theta_{pi} \\ -R_p \sin \theta_{pi} \end{bmatrix}, \quad \mathbf{b}_i = \begin{bmatrix} R_b \cos \theta_{bi} \\ R_b \sin \theta_{bi} \\ 0 \end{bmatrix} \tag{4.96}
$$

$$\boldsymbol{\theta}_{bi} = \begin{bmatrix} \theta_{b1} \\ \theta_{b2} \\ \theta_{b3} \\ \theta_{b4} \\ \theta_{b5} \end{bmatrix} = \begin{bmatrix} \theta_b \\ 2\pi/3 \\ 4\pi/3 - \theta_b \\ 4\pi/3 + \theta_b \\ -\theta_b \end{bmatrix}, \quad \boldsymbol{\theta}_{pi} = \begin{bmatrix} \theta_{p1} \\ \theta_{p2} \\ \theta_{p3} \\ \theta_{p4} \\ \theta_{p5} \end{bmatrix} = \begin{bmatrix} \pi/3 - \theta_p \\ \pi/3 + \theta_p \\ \pi \\ 5\pi/3 - \theta_p \\ 5\pi/3 + \theta_p \end{bmatrix} \tag{4.97}$$

the inverse kinematic problem for the 5-dof platform can finally be written as

$$\rho_i^2 = (\mathbf{p}_i - \mathbf{b}_i)^T (\mathbf{p}_i - \mathbf{b}_i), \quad i = 1, \ldots, 5 \tag{4.98}$$

4.5.3 Jacobian Matrices

4.5.3.1 Rigid Model
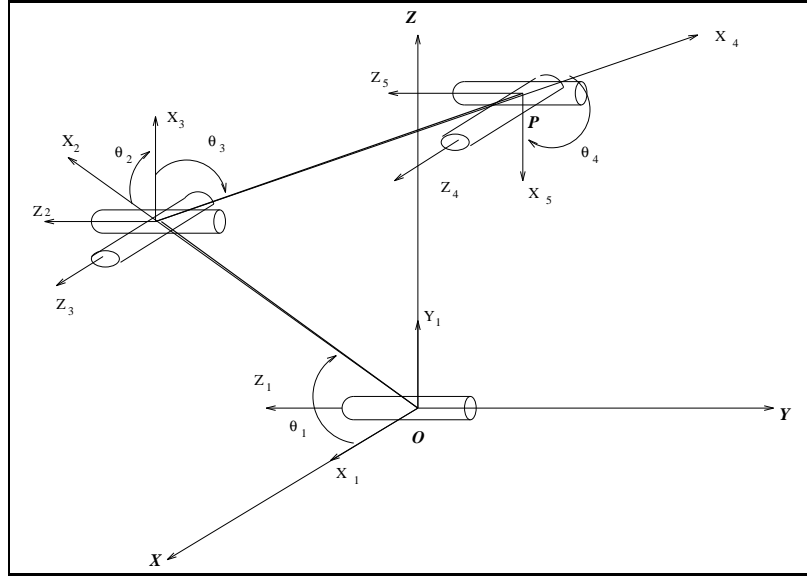
Figure 4.18: The passive constraining leg with rigid links.

From Figure 4.18, one can obtain the Denavit-Hartenberg parameters of the passive leg as in Table 4.8. We take the Cartesian coordinate frame as frame **0**, and define $\alpha_0 = 90°$, $\theta_0 = 0°$, then one obtains

$$\mathbf{Q}_{60} = \begin{bmatrix} 1 & 0 & 0 \\ 0 & 0 & -1 \\ 0 & 1 & 0 \end{bmatrix} \tag{4.99}$$

Table 4.8: The DH parameters for the passive constraining leg with rigid links.

i	a_i	b_i	α_i	θ_i
0	0	0	90°	0
1	l_{61}	0	0	θ_{61}
2	0	0	90°	θ_{62}
3	l_{62}	0	0	θ_{63}
4	0	0	90°	θ_{64}
5	0	0	0	θ_{65}

The expressions for vectors $\mathbf{e}_{6i}$ and $\mathbf{r}_{6i}$ are then obtained following the procedure given above.

For the passive constraining leg, one then has the velocity equation as

$$\mathbf{J}_6\dot{\boldsymbol{\theta}}_6 = \mathbf{t} \tag{4.100}$$

where

$$\dot{\boldsymbol{\theta}}_6 = \begin{bmatrix} \dot{\theta}_{61} & \dot{\theta}_{62} & \dot{\theta}_{63} & \dot{\theta}_{64} & \dot{\theta}_{65} \end{bmatrix}^T \tag{4.101}$$

and the Jacobian matrix of the passive constraining leg $\mathbf{J}_6$ can be expressed as

$$\mathbf{J}_6 = \begin{bmatrix} \mathbf{e}_{61} & \mathbf{e}_{62} & \mathbf{e}_{63} & \mathbf{e}_{64} & \mathbf{e}_{65} \\ \mathbf{e}_{61} \times \mathbf{r}_{61} & \mathbf{e}_{62} \times \mathbf{r}_{62} & \mathbf{e}_{63} \times \mathbf{r}_{63} & \mathbf{e}_{64} \times \mathbf{r}_{64} & \mathbf{e}_{65} \times \mathbf{r}_{65} \end{bmatrix} \tag{4.102}$$

4.5.3.2 Compliant Model

In this section, the equations for the five identical legs are the same as in the rigid model, only the passive constraining leg with virtual joint is needed to study in this analysis.

Figure 4.19 illustrates the configuration of the passive constraining leg with virtual joint Z_2. Angle θ_{61} is the same as in the rigid case, $\theta_{62} = 0$, and θ_{63} and θ_{64} have the same angles as θ_{62} and θ_{63}, respectively in the rigid case, therefore, we can find them easily as described in the section with the rigid link model.

Figure 4.19: The passive constraining leg with flexible links.

From Figure 4.19, one can obtain the Denavit-Hartenberg parameters of the passive leg as in Table 4.9, then the velocity equation of the sixth kinematic chain (central leg) can be obtained as follows

$$\mathbf{J}'_6\dot{\boldsymbol{\theta}}'_6 = \mathbf{t} \tag{4.103}$$

where

$$\dot{\boldsymbol{\theta}}'_6 = \begin{bmatrix} \dot{\theta}_{61} & \dot{\theta}_{62} & \dot{\theta}_{63} & \dot{\theta}_{64} & \dot{\theta}_{65} & \dot{\theta}_{66} \end{bmatrix}^T \tag{4.104}$$

$$\mathbf{J}'_6 = \begin{bmatrix} \mathbf{e}_{61} & \mathbf{e}_{62} & \mathbf{e}_{63} & \mathbf{e}_{64} & \mathbf{e}_{65} & \mathbf{e}_{66} \\ \mathbf{e}_{61} \times \mathbf{r}_{61} & \mathbf{e}_{62} \times \mathbf{r}_{62} & \mathbf{e}_{63} \times \mathbf{r}_{63} & \mathbf{e}_{64} \times \mathbf{r}_{64} & \mathbf{e}_{65} \times \mathbf{r}_{65} & \mathbf{e}_{66} \times \mathbf{r}_{66} \end{bmatrix} \tag{4.105}$$

The global velocity equation can then be obtained by exploiting eqs. (4.18) to (4.23).

4.5.4 Kinetostatic Models

This mechanism is illustrated in Figure 4.1, the compliance matrix for the mechanism with rigid links can be written as

$$\mathbf{C}_c = \mathbf{J}_6(\mathbf{A}\mathbf{J}_6)^{-1}\mathbf{B}\mathbf{C}\mathbf{B}^T(\mathbf{A}\mathbf{J}_6)^{-T}\mathbf{J}_6^T \tag{4.106}$$

with

$$\mathbf{C} = diag[c_1, c_2, c_3, c_4, c_5] \tag{4.107}$$

Table 4.9: The DH parameters for the passive constraining leg with flexible links.

i	a_i	b_i	α_i	θ_i
0	0	0	$90°$	0
1	0	0	$90°$	θ_{61}
2	l_{61}	0	$-90°$	θ_{62}
3	0	0	$90°$	θ_{63}
4	l_{62}	0	0	θ_{64}
5	0	0	$90°$	θ_{65}
6	0	0	0	θ_{66}

where c_i is the compliance of the ith actuator, and $\mathbf{J}_6$ is the Jacobian matrix of the rigid constraining leg in this 5-dof case. Matrices $\mathbf{A}$ and $\mathbf{B}$ are the Jacobian matrices of the structure without the passive constraining leg.

Similarly, the stiffness matrix for the mechanism with flexible links can be written as

$$\mathbf{K} = [(\mathbf{J}_6')^{-T}\mathbf{K}_6(\mathbf{J}_6')^{-1} + \mathbf{A}^T\mathbf{B}^{-T}\mathbf{K}_J\mathbf{B}^{-1}\mathbf{A}] \tag{4.108}$$

with

$$\mathbf{K}_6 = diag[0, k_{62}, 0, 0, 0, 0] \tag{4.109}$$

where k_{62} is the stiffness of the virtual joint and $\mathbf{J}_6'$ is the Jacobian matrix of the compliant passive constraining leg in this 5-dof case, while $\mathbf{A}$ and $\mathbf{B}$ are the Jacobian matrices of the structure without the passive constraining leg.

4.5.5 Implementation

4.5.5.1 Stiffness Evolution and Compliance Comparison

The model developed above has been implemented for both the flexible case and the rigid case. A program has been written using the software Mathematica.

The comparison between the mechanism with rigid links (without virtual joints) and the mechanism with flexible links (with virtual joints) is given in Table 4.10. Figure 4.20

(a) Stiffness in θ_x　　　　　　　(b) Stiffness in θ_z
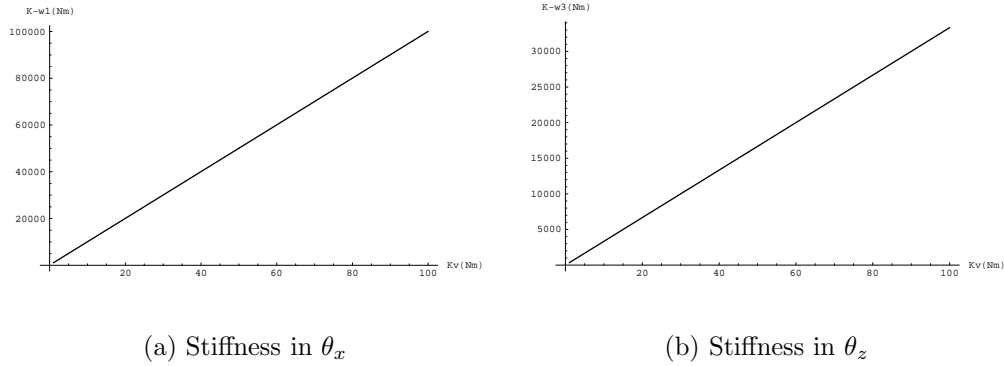
Figure 4.20: Evolution of the stiffness as a function of the passive link's lumped stiffness in θ_x and θ_z directions (all the other directions are constants).

shows the variation of the stiffness for this type of mechanism. The results are similar to those obtained in previous cases.

Table 4.10: Comparison of the mechanism compliance between the mechanism with rigid links and the mechanism with flexible links.

K_a	$K_{passive}$	κ_{θ_x}	κ_{θ_y}	κ_{θ_z}	κ_x	κ_y	κ_z
1000	1000	0.0862844	0.0980888	0.261173	0.0735117	0.0303542	0.000255386
1000	$10^1 K_a$	0.0862729	0.098054	0.259051	0.0734333	0.0303281	0.000255386
1000	$10^2 K_a$	0.0862717	0.0980506	0.258838	0.0734254	0.0303255	0.000255386
1000	$10^3 K_a$	0.0862716	0.0980502	0.258817	0.0734246	0.0303252	0.000255386
1000	$10^4 K_a$	0.0862716	0.0980502	0.258815	0.0734245	0.0303252	0.000255386
1000	$10^5 K_a$	0.0862716	0.0980502	0.258815	0.0734245	0.0303252	0.000255386
1000	rigid	0.0862716	0.0980502	0.258815	0.0734245	0.0303252	0.000255386

4.5.5.2 Compliance Mappings

The kinetostatic model is now used to obtain the compliance mappings for the spatial five-degree-of-freedom parallel mechanisms. The maps are drawn on square areas of the variation of the end-effector's position as shown in Figure 4.21. From the plots one can determine which regions of the workspace will satisfy some compliance criteria.

From Figure 4.21 and Table 4.10, one can see that K_{θ_z} is becoming infinite while
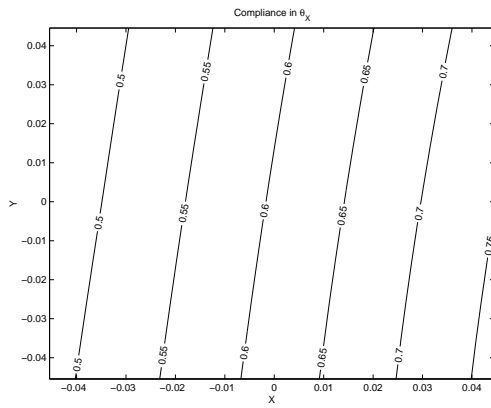
(a) Compliance in θ_x (1/Nm)
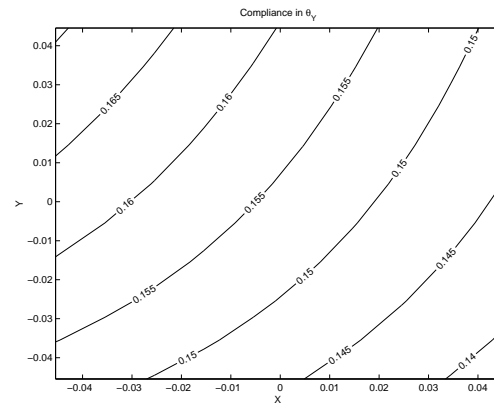
(b) Compliance in θ_y (1/Nm)
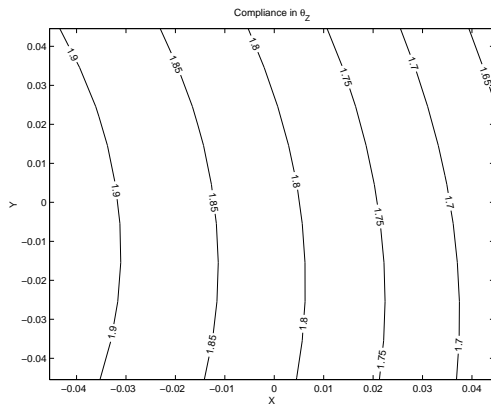
(c) Compliance in θ_z (1/Nm)
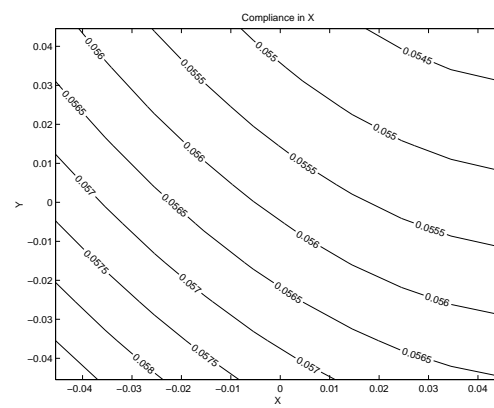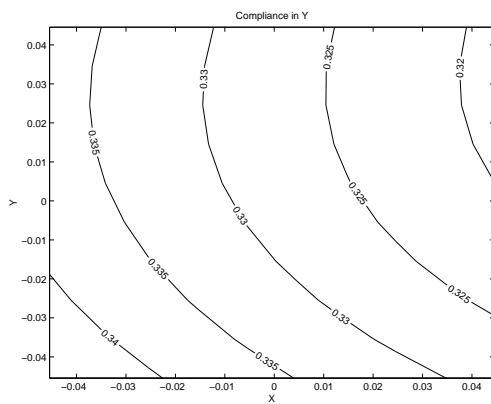
(d) Compliance in x (m/N)
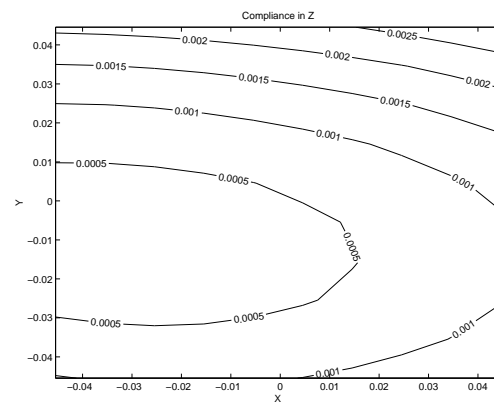
(e) Compliance in y (m/N)

(f) Compliance in z (m/N)

Figure 4.21: Compliance mappings of the spatial 5-dof parallel mechanism with prismatic actuators (all length units in m).

the flexible links are becoming stiffer. It corresponds to the motions prevented by the passive constraining leg. K_{θ_x} is also large enough because of the structure of the passive constraining leg. The stiffness in Z is higher near the center of the workspace, which is the best position for supporting vertical loads along the Z axis. All these can be obviously observed.

4.5.6 Design Guidelines

An example is now given to illustrate the effect of flexible links (virtual joints) on the parallel mechanism. The parameters of the reference configuration (Figure 4.2) used in this example are given as

$$\theta_p = 22.34°, \theta_b = 42.883°, R_p = 12\ cm, R_b = 22\ cm, k_{62} = 1000\ Nm,$$

$$k_{i1} = 1000\ N/m, \quad i = 1, \ldots, 5$$

$$l_{i1} = 46\ cm, l_{i2} = 36\ cm, \quad i = 1, \ldots, 5$$

where k_{i1} is the actuator stiffness, l_{i1}, l_{i2} are the link length for the 1st and 2nd link of each leg, and the Cartesian coordinates are given by

$$x \in [-4, 4]\ cm, y \in [-4, 4]\ cm, z = 68\ cm,$$

$$\theta_{64} = -\pi, \theta_{65} = 2\pi/3,$$

The configuration for this case is specified as

$$x = 0, y = 0, z = 68\ cm,$$

$$\theta_{64} = -\pi, \theta_{65} = 2\pi/3,$$

hence we have the expressions

$$
\begin{align}
K_{\theta_x} &= 0.0378863 K_a + K_{62} \tag{4.110}\\
K_{\theta_y} &= 0.0321798 K_a \tag{4.111}\\
K_{\theta_z} &= 0.000702041 K_a + 0.333333 K_{62} \tag{4.112}\\
K_x &= 0.0708594 K_a \tag{4.113}\\
K_y &= 0.0634428 K_a \tag{4.114}
\end{align}
$$

$$K_z = 4.8657K_a \tag{4.115}$$

where K_a represents the actuator stiffness, K_{62} represents the link's lumped stiffness located in the passive constraining leg.

With the results of the previous section and the expressions of eqs. (4.110) – (4.115), the following design guidelines can be obtained. The common design guidelines will be given in Section 4.7.

1. The global stiffness is increasing with the improvement of actuators, actuated links and the passive constraining leg's rigidity, and there is a critical stiffness value for actuated flexible links to keep the structure rigid. In this case, the passive constraining leg affects the stiffness around the X axis since the platform is not in the horizontal position, the projections of the direction which is orthogonal to the Hooke joint located at the platform are in XY and XZ planes, so while the Hooke joint at platform limits the rotation around the Z axis, it also limits the rotation around the X axis.

2. From the equations, one can find that the stiffness along the Z axis is the largest one among all the directions, and K_{θ_x} is larger than K_{θ_y} (in the case of the current configuration).

We also found the following facts about the mechanism after performing several tests and varying the parameters of the mechanism.

1. For a certain platform size, the larger the link length, the smaller the torsional stiffnesses around the X and Y, and the linear stiffnesses in X and Y, but the stiffness in the Z axis is becoming smaller.

2. For a given link length, the larger the platform size (within a certain range), the larger the torsional stiffnesses around the X and Y axes, and the smaller the stiffnesses along the X and Y axes.

4.6 The Tricept Machine Tool Family

4.6.1 Introduction of the Tricept Machine Tool Family

Figure 4.22: The Tricept machine tool prototype (Figure from Neos Robotics).

As shown in Figure 4.22, the Tricept machine tool family (including Tricept600, Tricept605, and Tricept805) are developed by Neos Robotics AB, a Swedish company which was one of the first machine tool builders to introduce a serious parallel machine.

The Tricept machine tool is designed as a vertical machining center. With such high rigidity for the machine, the range of applications include HSC-milling of aluminum, steel, structural parts, composites and riveting for the aerospace as well as large model making, plastic and foam machining for automation. The tricept concept is also very interesting for all types of laser cutting, water jet and welding applications.

The basic unit of the Tricept machine tool is a tripod with three servo actuators, which are free from backlash by pre-load. In its upper end, every single actuator is supported by a Hooke joint, in its lower end by a pre-loaded ball joint with three degrees of freedom. The upper Hooke joints of the actuators are placed on a hexagonal casting frame. The solution leads to a closed power flow between the components.

The center-tube of the machine eliminates the need of additional 3 actuators, which

is the conventional way of designing a hexapod. For optimal rigidity and accuracy, the center-tube does not have any telescopic feature, but is rigid and layered on a Hooke joint in the center of the machine. Such kind of design leads to great rigidity and high dynamic. Unlike a simple machine tool, the Tricept machine tool also can be integrated into an existing production line.

4.6.2 Inverse Kinematics

The schematic representation of the Tricept machine tool and the geometry of the joint distribution both on the base and on the platform are shown in Figures 4.23 and 4.24. This mechanism has the same kinematic chains as the 3-dof prismatic actuated parallel mechanism studied above except for the passive constraining leg. The passive constraining leg consists of a fixed Hooke joint, a moving link, a prismatic joint, and a second moving link fixed to the platform. This last leg is used to constrain the motion of the platform to only three degrees of freedom.
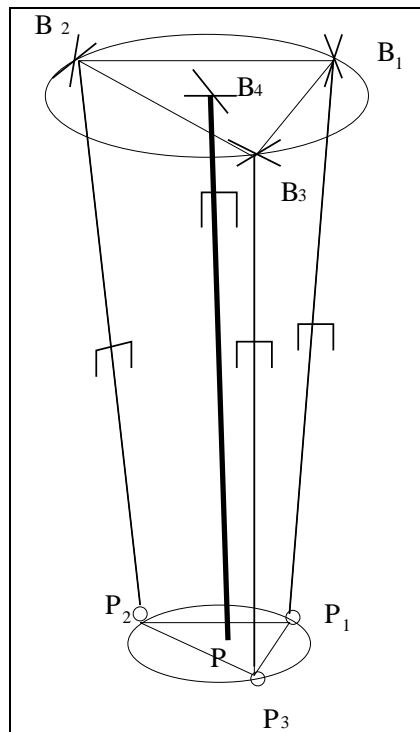
Figure 4.23: Schematic representation of the Tricept machine tool.

For the Tricept mechanism of Figure 4.23, the independent coordinates have been
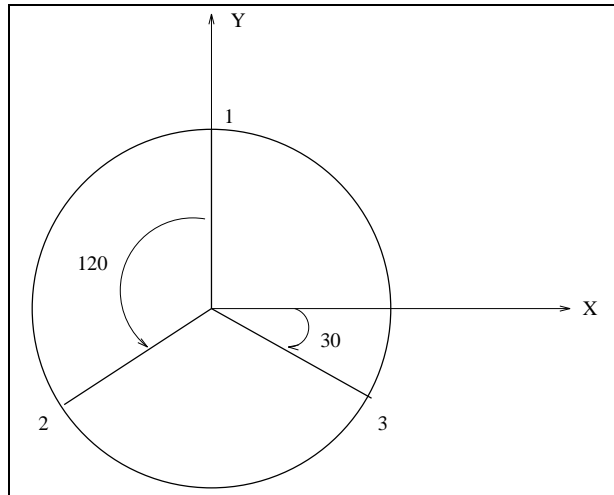
Figure 4.24: Position of the attachment points on the base and platform.

chosen for convenience as $(z, \theta_{41}, \theta_{42})$, where $(\theta_{41}, \theta_{42})$ are the joint angles of the Hooke joint attached to the base center at B_4, and z is the vertical coordinate of point P with respect to the fixed frame, for $i = 1, 2, 3$, one has

$$
\mathbf{r}'_i = \begin{bmatrix} R_p \cos \theta_{pi} \\ R_p \sin \theta_{pi} \\ 0 \end{bmatrix}, \quad \mathbf{b}_i = \begin{bmatrix} R_b \cos \theta_{bi} \\ R_b \sin \theta_{bi} \\ 0 \end{bmatrix} \tag{4.116}
$$

$$
\boldsymbol{\theta}_{bi} = \begin{bmatrix} \theta_{b1} \\ \theta_{b2} \\ \theta_{b3} \end{bmatrix} = \begin{bmatrix} \pi/2 \\ 7\pi/6 \\ -\pi/6 \end{bmatrix}, \quad \boldsymbol{\theta}_{pi} = \begin{bmatrix} \theta_{p1} \\ \theta_{p2} \\ \theta_{p3} \end{bmatrix} = \begin{bmatrix} \pi/2 \\ 7\pi/6 \\ -\pi/6 \end{bmatrix} \tag{4.117}
$$

The solution of the inverse kinematic problem for this Tricept mechanism can finally be written as

$$
\rho_i^2 = (\mathbf{p}_i - \mathbf{b}_i)^T (\mathbf{p}_i - \mathbf{b}_i), \quad i = 1, 2, 3 \tag{4.118}
$$

4.6.3 Jacobian Matrices

4.6.3.1 Rigid Model

The parallel mechanism studied here comprises two main components, namely, the constraining leg, which can be thought of as a serial mechanism and the actuated legs acting in parallel.
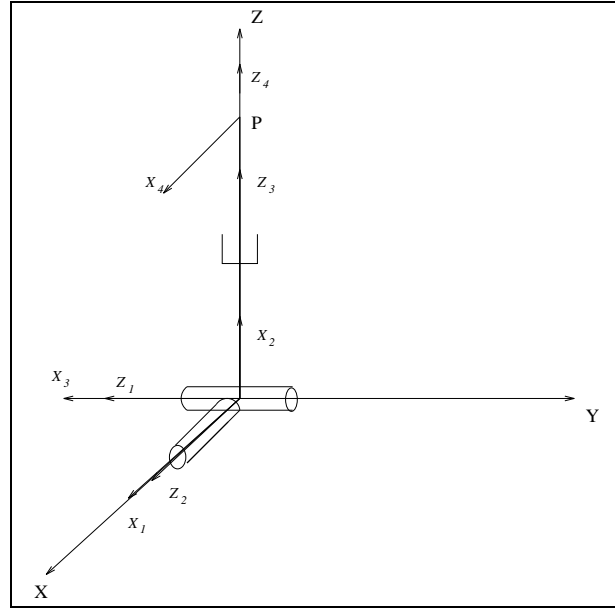
Figure 4.25: The passive constraining leg with rigid links.

Table 4.11: The DH parameters for the passive constraining leg with rigid links.

i	a_i	b_i	α_i	θ_i
0	0	0	$90°$	0
1	0	0	$90°$	θ_{41}
2	0	0	$90°$	θ_{42}
3	0	z	0	$90°$

Figure 4.25 illustrates the configuration of the passive constraining leg (compared to Figure 4.23, the mechanism is shown upside down). From the figure, one can obtain the Denavit-Hartenberg parameters given in Table 4.11. We take the fixed Cartesian coordinate frame as frame **0**, and define $\alpha_0 = 0, \theta_0 = 0$, then one obtains

$$\mathbf{Q}_{40} = \begin{bmatrix} 1 & 0 & 0 \\ 0 & 0 & -1 \\ 0 & 1 & 0 \end{bmatrix} \tag{4.119}$$

with the same method as in the other 3-dof case, one has the velocity equation of the 4th kinematic chain (passive constraining leg) as

$$\mathbf{J}_4 \dot{\boldsymbol{\theta}}_4 = \mathbf{t} \tag{4.120}$$

where

$$\dot{\boldsymbol{\theta}}_4 \;=\; \left[\begin{array}{ccc} \dot{\theta}_{41} & \dot{\theta}_{42} & \dot{z} \end{array}\right]^T \tag{4.121}$$

and $\mathbf{t}$ is the twist of the platform, $\mathbf{t} = \left[\begin{array}{cc} \boldsymbol{\omega}^T & \dot{\mathbf{p}}^{\mathbf{T}} \end{array}\right]^T$, $\boldsymbol{\omega}$ is the angular velocity of the platform. Then the Jacobian matrix of the passive constraining leg of the mechanism $\mathbf{J}_4$ can be expressed as

$$\mathbf{J}_4 = \left[\begin{array}{ccc} \mathbf{e}_{41} & \mathbf{e}_{42} & \mathbf{0} \\ \mathbf{e}_{41} \times \mathbf{r}_{41} & \mathbf{e}_{42} \times \mathbf{r}_{42} & \mathbf{e}_{41} \end{array}\right] \tag{4.122}$$

where $\mathbf{e}_{4i}$ is a unit vector defined in the direction of axis i while $\mathbf{r}_{4i}$ is a vector connecting the origin of frame i to point P.

4.6.3.2 Compliant Model

Figure 4.26: The passive constraining leg with flexible links.

Figure 4.26 illustrates the configuration of the passive constraining leg with flexible links, since there are forces and moments acting on the platform, the induced deformations are modeled using a virtual revolute joint on the base and two orthogonal virtual

Table 4.12: The DH parameters for the passive constraining leg with flexible links.

i	a_i	b_i	α_i	θ_i
0	0	0	90°	0
1	0	0	90°	θ_{41}
2	0	0	90°	θ_{42}
3	0	0	0	θ_{43}
4	0	$z/2$	90°	θ_{44}
5	0	0	90°	θ_{45}
6	$z/2$	0	0	θ_{46}

revolute joints in the middle of the passive constraining leg. These joints are represented using dashed lines in Figure 4.26. Then, one can obtain the Denavit-Hartenberg parameters given in Table 4.12 and obtains

$$\mathbf{J}'_4\dot{\boldsymbol{\theta}}'_4 = \mathbf{t} \tag{4.123}$$

where

$$\dot{\boldsymbol{\theta}}'_4 \;=\; \begin{bmatrix} \dot{\theta}_{41} & \dot{\theta}_{42} & \dot{\theta}_{43} & \dot{z}/2 & \dot{\theta}_{45} & \dot{\theta}_{46} \end{bmatrix}^T \tag{4.124}$$

and the Jacobian matrix of the passive constraining leg of the mechanism, noted $\mathbf{J}'_4$, can be obtained as

$$\mathbf{J}'_4 = \begin{bmatrix} \mathbf{e}_{41} & \mathbf{e}_{42} & \mathbf{e}_{43} & 0 & \mathbf{e}_{45} & \mathbf{e}_{46} \\ \mathbf{e}_{41} \times \mathbf{r}_{41} & \mathbf{e}_{42} \times \mathbf{r}_{42} & \mathbf{e}_{43} \times \mathbf{r}_{43} & \mathbf{e}_{44} & \mathbf{e}_{45} \times \mathbf{r}_{45} & \mathbf{e}_{46} \times \mathbf{r}_{46} \end{bmatrix} \tag{4.125}$$

4.6.4 Kinetostatic Models

The compliance matrix for the rigid model can be written as

$$\mathbf{C}_c = \mathbf{J}_4(\mathbf{A}\mathbf{J}_4)^{-1}\mathbf{B}\mathbf{C}\mathbf{B}^T(\mathbf{A}\mathbf{J}_4)^{-T}\mathbf{J}_4^T \tag{4.126}$$

where $\mathbf{C} = diag[c_1, c_2, c_3]$, with c_1, c_2 and c_3 are the compliances of the actuators and $\mathbf{J}_4$ is the Jacobian matrix of the constraining leg. Matrices $\mathbf{A}$ and $\mathbf{B}$ are the Jacobian matrices of the structure without the passive constraining leg.

Similarly, the stiffness matrix for the mechanism with flexible links can be written as

$$\mathbf{K} = [(\mathbf{J}_4')^{-T}\mathbf{K}_4(\mathbf{J}_4')^{-1} + \mathbf{A}^T\mathbf{B}^{-T}\mathbf{K}_J\mathbf{B}^{-1}\mathbf{A}] \tag{4.127}$$

with

$$\mathbf{K}_4 = diag[0, 0, k_{43}, 0, k_{45}, k_{46}] \tag{4.128}$$

where k_{43}, k_{45} and k_{46} are the stiffnesses of the virtual joints introduced to account for the flexibility of the links in the constraining leg. The architecture of the constraining leg including the virtual joints is represented in Figure 4.26, and $\mathbf{J}_4'$ is the Jacobian matrix of the constraining leg in this Tricept case, while $\mathbf{A}$ and $\mathbf{B}$ are the Jacobian matrices of the structure without the constraining leg.

4.6.5 Implementation

4.6.5.1 Stiffness Evolution and Compliance Comparison

The above model has been implemented for the Tricept machine tool for both cases — with flexible links and with rigid links. A program has been written using the software Mathematica and the stiffness trends are obtained in each direction with the variation of link stiffnesses (i.e, the link's flexibility). Figure 4.27 shows the Cartesian stiffness components of this mechanism as a function of the stiffness of the virtual springs (representing the stiffness of the links), for the reference (vertical) configuration.

The parameters used in this example are given by Neos Robotics AB as follows

$$\theta_{b1} = \pi/2, \theta_{b2} = 7\pi/6, \theta_{b3} = -\pi/6,$$
$$\theta_{p1} = \pi/2, \theta_{p2} = 7\pi/6, \theta_{p3} = -\pi/6,$$
$$R_p = 225 \; mm, R_b = 500 \; mm,$$
$$k_{i1} = 1000 \; N/m, \quad i = 1, \dots, 3$$

where k_{i1} is the actuator stiffness and the Cartesian coordinates are given as

$$x \in [-3, 3] \; cm, y \in [-3, 3] \; cm, z = 1300 \; mm,$$
$$\theta_{41} = \pi/2, \theta_{42} = \pi/2,$$

(a) Stiffness in θ_x
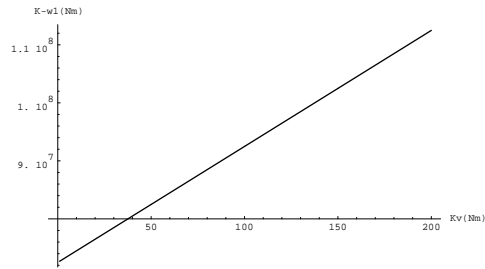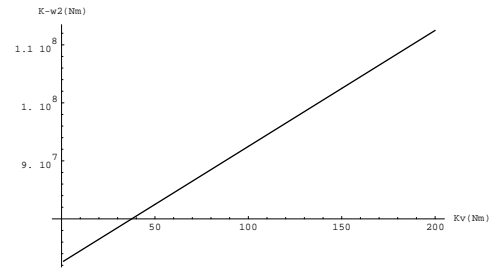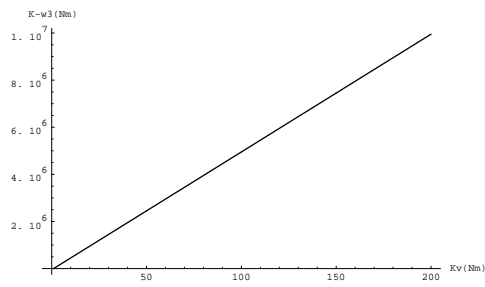
(b) Stiffness in θ_y

(c) Stiffness in θ_z
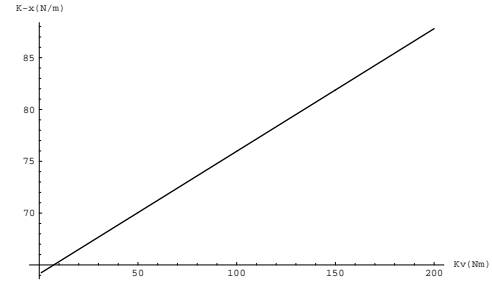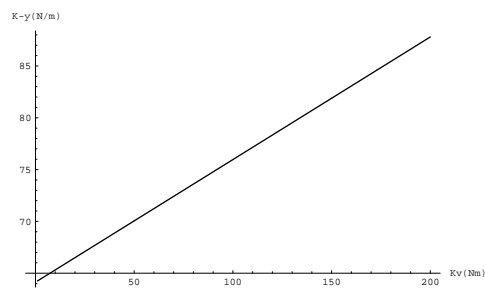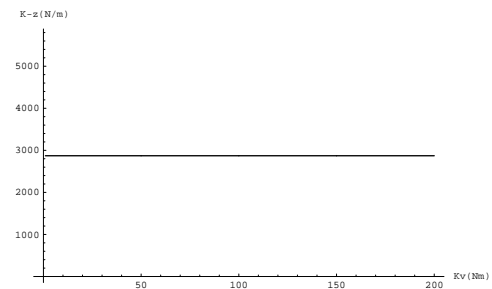
(d) Stiffness in x

(e) Stiffness in y

(f) Stiffness in z

Figure 4.27: Evolution of the stiffness as a function of the passive link's lumped stiffness in different directions.

From Figure 4.27, it is clear that the Cartesian stiffness is a linear function of the link stiffnesses. This result is consistent with eq. (4.69), where the stiffness terms appear linearly. The comparison between the parallel manipulator with rigid links (without virtual joints) and the parallel manipulator with flexible links (with virtual joints) is given in Table 4.13.

Table 4.13: Comparison of the mechanism compliance between the mechanism with rigid links and the mechanism with flexible links.

K_a	$K_{passive}$	κ_{θ_x}	κ_{θ_y}	κ_{θ_z}	κ_x	κ_y	κ_z
1000	1000	0.0028616	0.0028616	0.001	0.00479389	0.00479389	3.483×10^{-4}
1000	$10K_a$	0.00279356	0.00279356	0.0001	0.00471689	0.00471689	3.483×10^{-4}
1000	$10^2 K_a$	0.00278675	0.00278675	10^{-5}	0.00470919	0.00470919	3.483×10^{-4}
1000	$10^3 K_a$	0.00278607	0.00278607	10^{-6}	0.00470842	0.00470842	3.483×10^{-4}
1000	$10^4 K_a$	0.002786	0.002786	10^{-7}	0.00470834	0.00470834	3.483×10^{-4}
1000	$10^5 K_a$	0.002786	0.002786	10^{-8}	0.00470833	0.00470833	3.483×10^{-4}
1000	$10^6 K_a$	0.002786	0.002786	10^{-9}	0.00470833	0.00470833	3.483×10^{-4}
1000	$10^{10} K_a$	0.002786	0.002786	10^{-10}	0.00470833	0.00470833	3.483×10^{-4}
1000	rigid	0.002786	0.002786	0	0.00470833	0.00470833	3.483×10^{-4}

From Table 4.13, one can find that with the improvement of link stiffness, the mechanism's compliance with flexible link is very close to that of a mechanism with rigid links. This suggests that one can assume the flexible mechanism to be rigid only if the link stiffness reaches a high value. All results are obviously similar to the previous cases.

4.6.5.2   Compliance Mappings

The kinetostatic model is now used to obtain the compliance mappings for the Tricept machine tool. Figure 4.28 shows the compliance mappings on a section of the workspace of the platform. From the plots one can determine which regions of the workspace will satisfy some compliance criteria.

From Figure 4.27 and Table 4.13, it can be seen that K_{θ_x}, K_{θ_y}, K_{θ_z}, K_x and K_y are
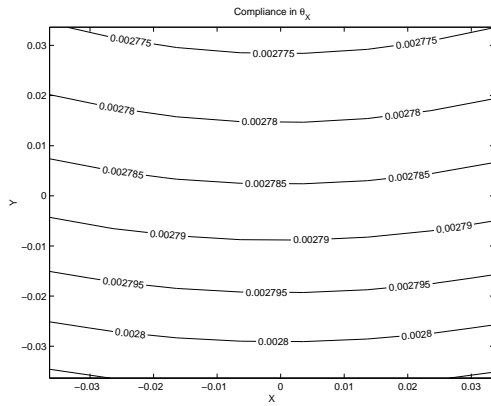
(a) Compliance in θ_x (1/Nm)
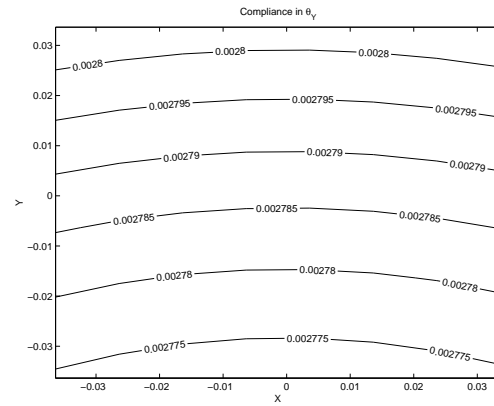
(b) Compliance in θ_y (1/Nm)
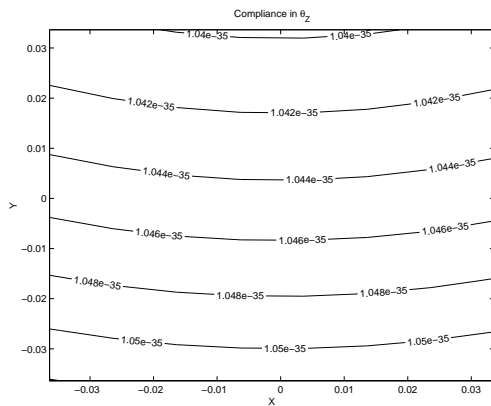
(c) Compliance in θ_z (1/Nm)
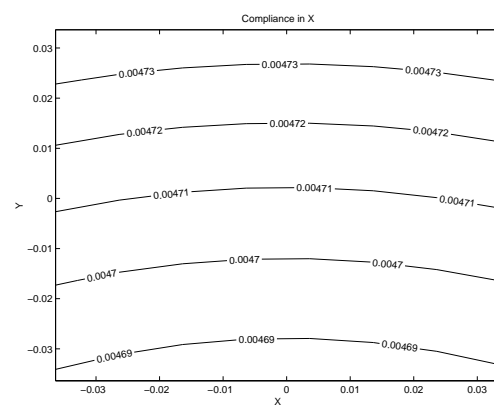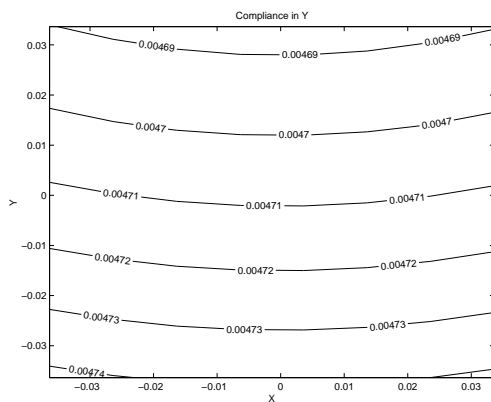
(d) Compliance in x (m/N)
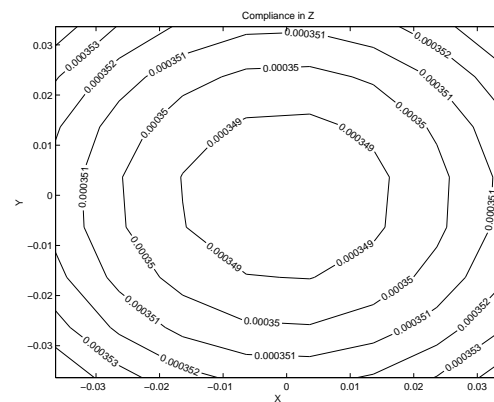
(e) Compliance in y (m/N)

(f) Compliance in z (m/N)

Figure 4.28: Compliance mappings of the Tricept machine tool (all length units in m).

becoming infinite while the flexible links are becoming rigid, and K_z is kept constant, it corresponds to the motions prevented by the passive constraining leg and at this configuration, the motions along the X and the Y are also limited (for passive leg is welded with platform).

4.6.6 Design Guidelines

For the configuration specified as

$$x = 0, y = 0, z = 1300 \ mm,$$
$$\theta_{41} = \pi/2, \theta_{42} = \pi/2,$$

one can find expressions for the Cartesian stiffnesses in all directions as a function of actuator stiffness and link stiffness (passive constraining leg) as

$$
\begin{align}
K_{\theta_x} &= 0.072685K_a + 4K_{46} \tag{4.129}\\
K_{\theta_y} &= 0.072685K_a + 4K_{45} \tag{4.130}\\
K_{\theta_z} &= K_{43} \tag{4.131}\\
K_x &= 0.0642478K_a + 2.36686K_{45} \tag{4.132}\\
K_y &= 0.0642478K_a + 2.36686K_{46} \tag{4.133}\\
K_z &= 2.8715K_a \tag{4.134}
\end{align}
$$

where K_a represents the stiffness of the actuators, while K_{43}, K_{45} and K_{46} represent the passive constraining leg's stiffness in X, Y and Z directions caused by the link bending (flexibility) and torsion. Since stiffnesses in eqs. (4.129) – (4.134) are pure stiffnesses in each direction, therefore, K_x, and K_y have relationship with passive leg stiffnesses.

Based on the results of the previous section and the expressions of eqs. (4.129) – (4.134), the following design guidelines can be established and used as reference for the design of this kind of mechanism (the common design guidelines will be given in Section 4.7).

1. The stiffness K_z is in direct proportion to the actuator stiffness and has no relationship with the rigidity of the passive constraining leg.

2. If $K_{45} = K_{46}$, i.e., the passive constraining leg's bending stiffness along the X and Y axes, play the equal role of limiting the movement of the platform along the X and Y. K_{43} — the passive constraining leg's stiffness around the Z axis — plays the function of limiting the rotation of the platform around the Z axis.

3. From the equations, one can find that the stiffness along the Z axis is the largest one among all the directions, and K_{θ_y} is equal to K_{θ_x} because of the structure's symmetrical configuration. This is clearly illustrated in Figure 4.27.

4. In Figure 4.28(a) and (b), the torsional compliances in θ_x and θ_y are shown, the compliances are symmetric to each other. In Figure 4.28(f) the stiffness in z is higher near the center of the workspace, which is the best position for supporting vertical loads. This is due to the architecture chosen, which aims at supporting heavy objects in an environment where the gravity is acting along the negative direction of the Z axis. All these are in accordance with what would be intuitively expected.

Some other facts about the mechanism are found after performing tests with the kinetostatic model.

1. For a certain platform size, the larger the link length, the larger the global stiffness values.

2. For a given link length, the smaller the platform size, the smaller the torsional stiffness values around the X and Y axes, and the larger the stiffness values along the Z axis.

4.7   Conclusions

A new family of n-DOF parallel mechanisms with one passive constraining leg has been introduced in this chapter. This type of architecture can be used in several applications including machine tools. The kinematic analysis of this family of spatial parallel n-degree-of-freedom mechanisms has been presented. The geometric configurations of the mechanisms are shown. In this chapter, only mechanisms with prismatic actuators

have been discussed. Solutions for the inverse kinematic problem have been given. The Jacobian matrices obtained have been used to establish the kinetostatic model of the mechanisms. The lumped link and joint compliances have been used for the study of the Cartesian compliance. Finally, examples have been investigated and numerical results have been obtained. The results clearly demonstrate the relevance of the kinetostatic analysis in the context of design of such mechanisms.

Additionally, there are some common design guidelines for this series of mechanisms, they are

1. With the improvement of link stiffness, the mechanism's compliance is very close to that of mechanism with rigid link, this suggests that we can assume the flexible mechanism to be rigid only if the link stiffness reaches a high value $(10^7 K_a)$.

2. The passive constraining leg's lumped stiffness does not affect all directional stiffnesses, it only plays the role of limiting the platform's motion to the desired ones.

3. the limitation of the platform's degree of freedom is dependent on the actuator stiffness and link stiffness.

4. If the passive constraining leg's lumped stiffness is fixed as the same value as actuator's (K_a), then it cannot adequately limit the motion to the desired degree-of-freedom, only if the passive constraining leg's lumped stiffness is large enough $(10^2 K_a)$, then it begins to efficiently play the role of limiting the platform motion to the desired ones.

Chapter 5

Kinetostatic Analysis of Spatial n-DOF Parallel Mechanisms with a Passive Constraining Leg and n Identical Legs with Revolute Actuators

5.1 Introduction

In chapter 4, we established and discussed a general kinetostatic model for parallel mechanisms with prismatic actuators whose degree of freedom (dof) is dependent on

117

a passive constraining leg connecting the base and the platform. In this chapter, the parallel mechanisms with revolute actuators are addressed. Together with the inverse kinematics and velocity equations for both rigid-link and flexible-link mechanisms, a general kinetostatic model is established for the analysis of the structural rigidity and accuracy of this family of mechanisms, some examples for 3-dof, 4-dof and 5-dof mechanisms are given in detail to illustrate the results.

5.2 General Kinetostatic Model for Spatial $n-$DOF Mechanisms with a Passive Constraining Leg and Revolute Actuators

5.2.1 Geometric Modeling

A 5-dof parallel mechanism with revolute actuators belonging to the family of mechanisms studied in this chapter is shown in Figures 5.1 and 5.2. It consists of six kinematic chains, including five actuated legs with identical topology and one passive constraining leg, connecting the fixed base to the moving platform. In this 5-dof parallel mechanism, the kinematic chains associated with the five identical legs consist — from base to platform — of an actuated revolute joint, a moving link, a Hooke joint, a second moving link and a spherical joint attached to the platform. The sixth chain (central leg) connecting the base to the platform is a passive leg and has the same architecture and function as 5-dof mechanism with prismatic actuators discussed in Chapter 4.

Similarly, families of 3-dof and 4-dof parallel mechanisms can be built using three or four identical legs with 6 degrees of freedom and one passive constraining leg with 3 degrees of freedom or 4 degrees of freedom, respectively.

5.2.2 Inverse Kinematics

With the same independent coordinates $(x, y, z, \theta_i, \theta_j)$, vectors $\mathbf{p}_i$, $\mathbf{r}'_i$, $\mathbf{p}$ and rotation matrix $\mathbf{Q}_0$ are the same as for the mechanisms discussed in Chapter 4. The inverse kinematics for both rigid-link and flexible-link mechanisms can be obtained as follows.
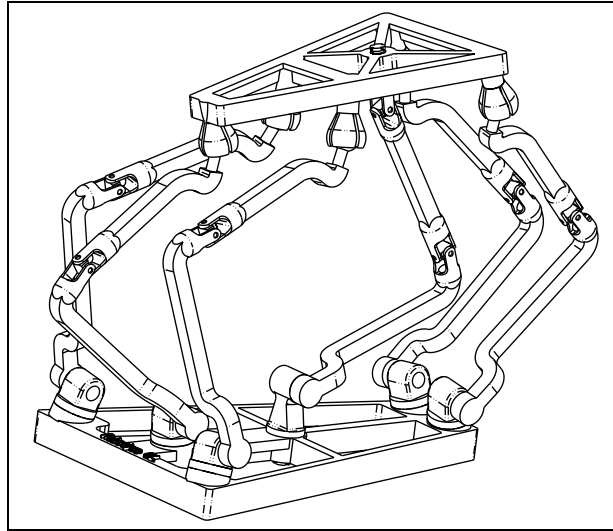
Figure 5.1: CAD model of the spatial 5-dof parallel mechanism with revolute actuators (Figure by Gabriel Coté).

5.2.2.1 Solution for the Mechanisms with Rigid Links

In order to solve the inverse kinematic problem, the passive constraining leg should be taken as a serial n-dof mechanism whose n Cartesian coordinates are known, which is a well known problem. Once the solution to the inverse kinematics of this n-dof serial mechanism is found, the complete pose (position and orientation) of the platform can be determined using the direct kinematic equations for this serial mechanism.

Figure 5.3 illustrates the configuration of the ith actuated joint of the mechanism with revolute actuators. Point B_i' is defined as the center of the Hooke joint connecting the two moving links of the ith actuated leg. Moreover, the Cartesian coordinates of point B_i' expressed in the fixed coordinate frame are represented as $(b_{ix}', b_{iy}', b_{iz}')$, and the position vector of point B_i' in the fixed frame is given by vector $\mathbf{b}_i'$. Since the axis of the fixed revolute joint of the ith actuated leg is assumed to be parallel to the xy plane of the fixed coordinate frame, one can write

$$b_{ix}' = b_{ix} - l_{i1}\sin(\theta_{bi} + \beta_i)\cos\theta_{i1}, \quad i = 1, \ldots, n, \quad n = 3, 4, \text{ or } 5 \tag{5.1}$$

$$b_{iy}' = b_{iy} + l_{i1}\cos(\theta_{bi} + \beta_i)\cos\theta_{i1}, \quad i = 1, \ldots, n, \quad n = 3, 4, \text{ or } 5 \tag{5.2}$$

$$b_{iz}' = b_{iz} + l_{i1}\sin\theta_{i1}, \quad i = 1, \ldots, n, \quad n = 3, 4, \text{ or } 5 \tag{5.3}$$

where θ_{bi} is the angle between the positive direction of the x axis of the base coordinate
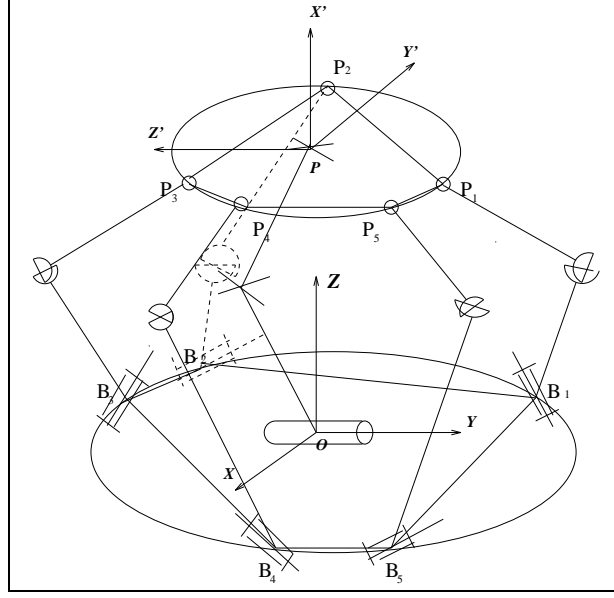
Figure 5.2: Schematic representation of the spatial 5-dof parallel mechanism with revolute actuators.

frame and the line connecting points O and B_i and θ_{i1} is the joint variable — rotation angle around the fixed revolute joint — associated with the ith actuated leg, β_i is the angle between the positive direction of the line connecting points O and B_i and the axis of the ith actuated joint. Moreover, l_{i1} is the length of the first link of the ith actuated leg. From the configuration of Figure 5.3, the relationships between the parameters can be written as

$$(b'_{ix} - x_i)^2 + (b'_{iy} - y_i)^2 + (b'_{iz} - z_i)^2 = l_{i2}^2, \quad i = 1, \ldots, n, \quad n = 3, 4, \text{ or } 5 \qquad (5.4)$$

where x_i, y_i, z_i are the coordinates of point P_i and l_{i2} is the length of the second link of the ith actuated leg.

Substituting eqs. (5.1) – (5.3) into eq. (5.4), one has
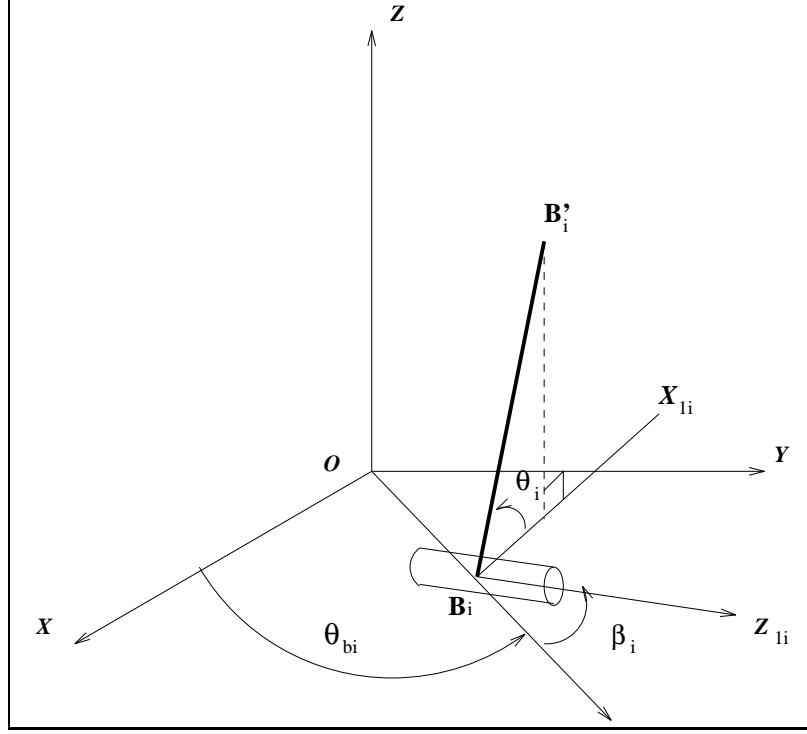
$$E_i \cos \theta_{i1} + F_i \sin \theta_{i1} = G_i, \quad i = 1, \ldots, n, \quad n = 3, 4, \text{ or } 5 \qquad (5.5)$$

where

$$E_i = (y_i - b_{iy}) \cos(\theta_{bi} + \beta_i) - (x_i - b_{ix}) \sin(\theta_{bi} + \beta_i) \qquad (5.6)$$

$$F_i = z_i - b_{iz} \qquad (5.7)$$

$$G_i = \frac{(x_i - b_{ix})^2 + (y_i - b_{iy})^2 + (z_i - b_{iz})^2 + l_{i1}^2 - l_{i2}^2}{2l_{i1}} \qquad (5.8)$$

Figure 5.3: The ith actuated revolute joint.

and angle θ_{i1} can be obtained by

$$\sin \theta_{i1} = \frac{F_i G_i + K_i E_i \sqrt{H_i}}{E_i^2 + F_i^2}, \quad i = 1, \ldots, n, \quad n = 3, \, 4, \text{ or } 5 \tag{5.9}$$

$$\cos \theta_{i1} = \frac{E_i G_i - K_i F_i \sqrt{H_i}}{E_i^2 + F_i^2}, \quad i = 1, \ldots, n, \quad n = 3, \, 4, \text{ or } 5 \tag{5.10}$$

where $K_i = \pm 1$ is the branch index of the mechanism associated with the configuration of the ith leg, and

$$H_i = E_i^2 + F_i^2 - G_i^2, \quad i = 1, \ldots, n, \quad n = 3, \, 4, \text{ or } 5 \tag{5.11}$$

Finally, the solution of the inverse kinematic problem is completed by performing

$$\theta_{i1} = atan2[\sin \theta_{i1}, \cos \theta_{i1}], \quad i = 1, \ldots, n, \quad n = 3, \, 4, \text{ or } 5 \tag{5.12}$$

Meanwhile, referring to Figure 5.3, the vector of leg length can be written as

$$\mathbf{b}_i' = \mathbf{b}_i + l_{i1} \mathbf{Q}_{ti1} \mathbf{d}_i, \quad i = 1, \ldots, n, \quad n = 3, \, 4, \text{ or } 5 \tag{5.13}$$

with

$$\mathbf{Q}_{ti1} = \begin{bmatrix} \cos(\theta_{bi} + \beta_i) & -\sin(\theta_{bi} + \beta_i) & 0 \\ \sin(\theta_{bi} + \beta_i) & \cos(\theta_{bi} + \beta_i) & 0 \\ 0 & 0 & 1 \end{bmatrix}, \quad i = 1, \dots, n, \quad n = 3, 4, \text{ or } 5 \quad (5.14)$$

and

$$\mathbf{d}_{i1} = \begin{bmatrix} 0 \\ \cos\theta_{i1} \\ \sin\theta_{i1} \end{bmatrix}, \quad i = 1, \dots, n, \quad n = 3, 4, \text{ or } 5 \quad (5.15)$$

assuming that the distance between points P_i and B_i' is noted l_{i2}, then one has

$$l_{i2}^2 = (\mathbf{p}_i - \mathbf{b}_i)^T (\mathbf{p}_i - \mathbf{b}_i), \quad i = 1, \dots, n, \quad n = 3, 4, \text{ or } 5 \quad (5.16)$$

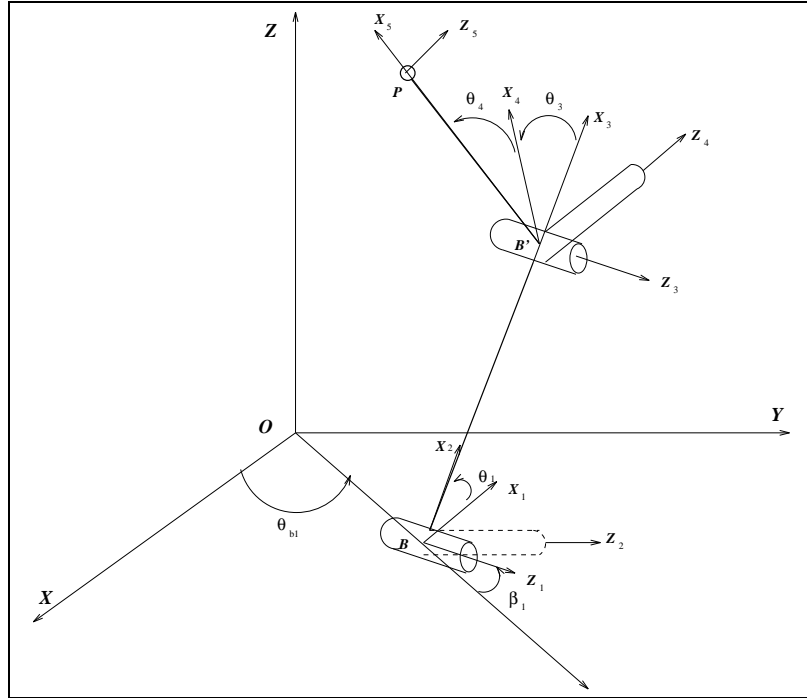### 5.2.2.2 Solutions for the Mechanisms with Flexible Links

Figure 5.4: One of the identical kinematic chains with flexible links.

Based on the lumped compliance model both for link and joint described in Section 4.2.2, we lumped one of the identical kinematic chains for the n-dof parallel mechanism discussed above in Figure 5.4. Joint 2 is a virtual joint used to model the

compliance of the driven link. From Figure 5.4, one can obtain $\theta_{i2} = 0$, when there is no deflection. Angles θ_{i3} and θ_{i4} can be obtained by writing the coordinates of point P in Frame 3 as

$$x_{i3} \;=\; l_{i2} \cos \theta_{i4} \cos \theta_{i3}, \quad i = 1, \ldots, n, \quad n = 3, 4, \text{ or } 5 \tag{5.17}$$

$$y_{i3} \;=\; l_{i2} \cos \theta_{i4} \sin \theta_{i3}, \quad i = 1, \ldots, n, \quad n = 3, 4, \text{ or } 5 \tag{5.18}$$

$$z_{i3} \;=\; l_{i2} \sin \theta_{i4}, \quad i = 1, \ldots, n, \quad n = 3, 4, \text{ or } 5 \tag{5.19}$$

and

$$[\mathbf{p}]_3 = \mathbf{Q}_{i2}^T \mathbf{Q}_{i1}^T \mathbf{Q}_{i0}^T [\mathbf{p}_i - \mathbf{b}'_i], \quad i = 1, \ldots, n, \quad n = 3, 4, \text{ or } 5 \tag{5.20}$$

then, combining eqs. (5.17) – (5.19) and (5.20), one can find θ_{i3} and θ_{i4} easily.

From Figure 5.4, one can express the position of point B'_i as

$$\mathbf{b}'_i = \mathbf{b}_i + \mathbf{Q}_{i0}\mathbf{a}_{i1} + \mathbf{Q}_{i0}\mathbf{Q}_{i1}\mathbf{a}_{i2}, \quad i = 1, \ldots, n, \quad n = 3, 4, \text{ or } 5 \tag{5.21}$$

where $\mathbf{Q}_{i0}$, $\mathbf{a}_{i1}$, $\mathbf{a}_{i2}$ and $\mathbf{Q}_{i1}$ can be expressed as

$$\mathbf{a}_{i1} = \begin{bmatrix} 0 \\ 0 \\ 0 \end{bmatrix}, \quad \mathbf{a}_{i2} = \begin{bmatrix} l_{i1} \cos \theta_{i2} \\ l_{i1} \sin \theta_{i2} \\ 0 \end{bmatrix}, \quad \mathbf{Q}_{i1} = \begin{bmatrix} \cos \theta_{i1} & 0 & \sin \theta_{i1} \\ \sin \theta_{i1} & 0 & -\cos \theta_{i1} \\ 0 & 1 & 0 \end{bmatrix} \tag{5.22}$$

$$\mathbf{Q}_{i0} = \begin{bmatrix} -\sin(\theta_{bi} + \beta_i) & 0 & \cos(\theta_{bi} + \beta_i) \\ \cos(\theta_{bi} + \beta_i) & 0 & \sin(\theta_{bi} + \beta_i) \\ 0 & 1 & 0 \end{bmatrix} \tag{5.23}$$

5.2.3 Jacobian Matrices

5.2.3.1 Rigid Model

The parallel mechanisms studied here comprise two main components, namely, the passive constraining leg — which can be thought of as a serial mechanism — and the actuated legs acting in parallel.

Considering the passive constraining leg, one can write

$$\mathbf{J}_{n+1}\dot{\boldsymbol{\theta}}_{n+1} = \mathbf{t}, \quad n = 3, 4, \text{ or } 5 \tag{5.24}$$

where $\mathbf{J}_{n+1}$ consists of $\mathbf{e}_i$ and $\mathbf{r}_i$ as represented in Appendix C, and $\mathbf{t} = \begin{bmatrix} \boldsymbol{\omega}^T & \dot{\mathbf{p}}^T \end{bmatrix}^T$ is the twist of the platform, $\boldsymbol{\omega}$ is the angular velocity of the platform and $\dot{\boldsymbol{\theta}}_{n+1} = \begin{bmatrix} \dot{\theta}_{n+1,1} & \cdots & \dot{\theta}_{n+1,n} \end{bmatrix}^T, (n = 3, 4, \text{ or } 5)$ is the joint velocity vector associated with the passive constraining leg. Matrix $\mathbf{J}_{n+1}$ is the Jacobian matrix of the passive constraining leg which is taken as a serial n-dof mechanism.

5.2.3.2 Compliant Model

If the compliances of the links and joints are included, $(6-n)$ virtual joints will then be added to the passive constraining leg in order to account for the compliance of the links (Gosselin and Zhang 1999). Hence, the Jacobian matrix of the passive constraining leg becomes

$$\mathbf{J}'_{n+1}\dot{\boldsymbol{\theta}}'_{n+1} = \mathbf{t}, \quad n = 3, 4, \text{ or } 5 \tag{5.25}$$

where $\mathbf{J}'_{n+1}$ consists of $\mathbf{e}_i$ and $\mathbf{r}_i$ as represented in Appendix C, and

$$\dot{\boldsymbol{\theta}}'_{n+1} = \begin{bmatrix} \dot{\theta}_{n+1,1} & \cdots & \dot{\theta}_{n+1,6} \end{bmatrix}^T, \quad n = 3, 4, \text{ or } 5 \tag{5.26}$$

5.2.4 Global Velocity Equations

1. Rigid Model

   Now, considering the parallel component of the mechanism, the parallel Jacobian matrix can be obtained by differentiating eqs. (5.13), (5.15), and (5.16) with respect to time. One has

$$\dot{\mathbf{b}}'_i = l_{i1}\mathbf{Q}_{ti1}\dot{\mathbf{d}}_i, \quad i = 1, \ldots, n, \quad n = 3, 4, \text{ or } 5 \tag{5.27}$$

$$\dot{\mathbf{d}}_{i1} = \begin{bmatrix} 0 \\ -\sin\theta_{i1} \\ \cos\theta_{i1} \end{bmatrix} \dot{\theta}_{i1}, \quad i = 1, \ldots, n, \quad n = 3, 4, \text{ or } 5 \tag{5.28}$$

$$(\mathbf{p}_i - \mathbf{b}'_i)^T\dot{\mathbf{b}}'_i - (\mathbf{p}_i - \mathbf{b}'_i)^T\dot{\mathbf{p}}_i = 0, \quad i = 1, \ldots, n, \quad n = 3, 4, \text{ or } 5 \tag{5.29}$$

   differentiating eq. (4.3), one obtains

$$\dot{\mathbf{p}}_i = \dot{\mathbf{p}} + \dot{\mathbf{Q}}\mathbf{r}'_i, \quad i = 1, \ldots, n, \quad n = 3, 4, \text{ or } 5 \tag{5.30}$$

assuming

$$\mathbf{e}_i = l_{i1}\mathbf{Q}_{ti1}\begin{bmatrix} 0 \\ -\sin\theta_{i1} \\ \cos\theta_{i1} \end{bmatrix}, \quad i=1,\ldots,n, \quad n=3,\,4,\text{ or }5 \tag{5.31}$$

then

$$\dot{\mathbf{b}}'_i = \mathbf{e}_i\dot{\theta}_{i1}, \quad i=1,\ldots,n, \quad n=3,\,4,\text{ or }5 \tag{5.32}$$

therefore eq. (5.29) can be rewritten as (for $i=1,\ldots,n, \quad n=3,\,4,\text{ or }5$)

$$\begin{aligned}
(\mathbf{p}_i-\mathbf{b}'_i)^T\mathbf{e}_i\dot{\theta}_{i1} &= (\mathbf{p}_i-\mathbf{b}'_i)^T\dot{\mathbf{p}}_i \\
&= (\mathbf{p}_i-\mathbf{b}'_i)^T(\dot{\mathbf{p}}+\dot{\mathbf{Q}}\mathbf{r}'_i) \\
&= (\mathbf{p}_i-\mathbf{b}'_i)^T(\dot{\mathbf{p}}+\mathbf{\Omega}\mathbf{Q}\mathbf{r}'_i) \\
&= (\mathbf{p}_i-\mathbf{b}'_i)^T\dot{\mathbf{p}}+(\mathbf{p}_i-\mathbf{b}'_i)^T\mathbf{\Omega}\mathbf{Q}\mathbf{r}'_i \\
&= (\mathbf{p}_i-\mathbf{b}'_i)^T\dot{\mathbf{p}}+(\mathbf{p}_i-\mathbf{b}'_i)^T[\boldsymbol{\omega}\times(\mathbf{Q}\mathbf{r}'_i)] \\
&= (\mathbf{p}_i-\mathbf{b}'_i)^T\dot{\mathbf{p}}+[(\mathbf{Q}\mathbf{r}'_i)\times(\mathbf{p}_i-\mathbf{b}'_i)]^T\boldsymbol{\omega} \tag{5.33}
\end{aligned}$$

Hence one has the velocity equation

$$\mathbf{A}\mathbf{t}=\mathbf{B}\dot{\boldsymbol{\theta}} \tag{5.34}$$

where vector $\dot{\boldsymbol{\theta}}$ and $\mathbf{t}$ are defined as

$$\dot{\boldsymbol{\theta}} = \begin{bmatrix} \dot{\theta}_1 & \cdots & \dot{\theta}_n \end{bmatrix}^T, \quad n=3,\,4,\text{ or }5 \tag{5.35}$$

$$\mathbf{t} = \begin{bmatrix} \boldsymbol{\omega}^T & \dot{\mathbf{p}}^T \end{bmatrix}^T \tag{5.36}$$

and

$$\mathbf{A}=\begin{bmatrix} \mathbf{m}_1^T \\ \mathbf{m}_2^T \\ \vdots \\ \mathbf{m}_n^T \end{bmatrix}, \quad \mathbf{B}=diag[(\mathbf{p}_1-\mathbf{b}'_1)^T\mathbf{e}_1,\ldots,(\mathbf{p}_n-\mathbf{b}'_n)^T\mathbf{e}_n] \tag{5.37}$$

with $\mathbf{m}_i$ is a six-dimensional vector, which can be expressed as

$$\mathbf{m}_i=\begin{bmatrix} (\mathbf{Q}\mathbf{r}'_i)\times(\mathbf{p}_i-\mathbf{b}'_i) \\ (\mathbf{p}_i-\mathbf{b}'_i) \end{bmatrix}, \quad i=1,\ldots,n, \quad n=3,\,4,\text{ or }5 \tag{5.38}$$

2. Compliant Model

Differentiating eqs. (5.21) and (5.22) with respect to time, one has

$$\dot{\mathbf{b}}'_i = \mathbf{Q}_{i0}\dot{\mathbf{Q}}_{i1}\mathbf{a}_{i2} + \mathbf{Q}_{i0}\mathbf{Q}_{i1}\dot{\mathbf{a}}_{i2}, \quad i = 1, \ldots, n, \quad n = 3, 4, \text{ or } 5 \tag{5.39}$$

$$\dot{\mathbf{a}}_{i2} = \begin{bmatrix} -l_{i1}\sin\theta_{i2} \\ l_{i1}\cos\theta_{i2} \\ 0 \end{bmatrix}\dot{\theta}_{i2}, \quad i = 1, \ldots, n \tag{5.40}$$

$$\dot{\mathbf{Q}}_{i1} = \begin{bmatrix} -\sin\theta_{i1} & 0 & \cos\theta_{i1} \\ \cos\theta_{i1} & 0 & \sin\theta_{i1} \\ 0 & 0 & 0 \end{bmatrix}\dot{\theta}_{i1}, \quad i = 1, \ldots, n, \quad n = 3, 4, \text{ or } 5 \tag{5.41}$$

For $i = 1, \ldots, n, \quad n = 3, 4, \text{ or } 5$, assuming

$$\mathbf{d}_{i1} = \mathbf{Q}_{i0}\begin{bmatrix} -\sin\theta_{i1} & 0 & \cos\theta_{i1} \\ \cos\theta_{i1} & 0 & \sin\theta_{i1} \\ 0 & 0 & 0 \end{bmatrix}\mathbf{a}_{i2}, \quad \mathbf{d}_{i2} = \mathbf{Q}_{i0}\mathbf{Q}_{i1}\begin{bmatrix} -l_{i1}\sin\theta_{i2} \\ l_{i1}\cos\theta_{i2} \\ 0 \end{bmatrix} \tag{5.42}$$

then one has

$$\dot{\mathbf{b}}'_i = \mathbf{d}_{i1}\dot{\theta}_{i1} + \mathbf{d}_{i2}\dot{\theta}_{i2}, \quad i = 1, \ldots, n, \quad n = 3, 4, \text{ or } 5 \tag{5.43}$$

Differentiating eq. (5.16) with respect to time, one obtains eq. (5.29), and hence, differentiating eq. (4.3), and following a derivation similar to the one presented above for the mechanism with rigid links, for $i = 1, \ldots, n, \quad n = 3, 4, \text{ or } 5$, one has

$$(\mathbf{p}_i - \mathbf{b}'_i)^T(\mathbf{d}_{i1}\dot{\theta}_{i1} + \mathbf{d}_{i2}\dot{\theta}_{i2}) = (\mathbf{p}_i - \mathbf{b}'_i)^T\dot{\mathbf{p}} + [(\mathbf{Q}\mathbf{r}'_i) \times (\mathbf{p}_i - \mathbf{b}'_i)]^T\boldsymbol{\omega} \tag{5.44}$$

Hence one has the velocity equation as

$$\mathbf{At} = \mathbf{B}_1\dot{\boldsymbol{\theta}}_1 + \mathbf{B}_2\dot{\boldsymbol{\theta}}_2 \tag{5.45}$$

where vectors $\dot{\boldsymbol{\theta}}_1$ and $\dot{\boldsymbol{\theta}}_2$ are defined as

$$\dot{\boldsymbol{\theta}}_1 = \begin{bmatrix} \dot{\theta}_{11} & \ldots & \dot{\theta}_{n1} \end{bmatrix}^T, \quad n = 3, 4, \text{ or } 5 \tag{5.46}$$

$$\dot{\boldsymbol{\theta}}_2 = \begin{bmatrix} \dot{\theta}_{12} & \ldots & \dot{\theta}_{n2} \end{bmatrix}^T, \quad n = 3, 4, \text{ or } 5 \tag{5.47}$$

matrices $\mathbf{A}$, $\mathbf{B}_1$ and $\mathbf{B}_2$ are given as

$$\mathbf{A} = \begin{bmatrix} \mathbf{m}_1 & \mathbf{m}_2 & \mathbf{m}_3 & \mathbf{m}_4 & \mathbf{m}_5 & \mathbf{m}_6 \end{bmatrix}^T \tag{5.48}$$

$$\mathbf{B}_1 = diag[b_{11}, \ldots, b_{n,2n-1}], \quad n = 3, 4, \text{ or } 5 \tag{5.49}$$

$$\mathbf{B}_2 = diag[b_{12}, \ldots, b_{n,2n}], \quad n = 3, 4, \text{ or } 5 \tag{5.50}$$

where $\mathbf{m}_i$ is a six-dimensional vector, $\mathbf{b}_{i,2i-1}$, $\mathbf{b}_{i,2i}$ are the diagonal items of $\mathbf{B}_1$ and $\mathbf{B}_2$, respectively. They can be expressed as

$$\mathbf{m}_i = \begin{bmatrix} (\mathbf{Q}\mathbf{r}'_i) \times (\mathbf{p}_i - \mathbf{b}'_i) \\ (\mathbf{p}_i - \mathbf{b}'_i) \end{bmatrix}, \quad i = 1, \ldots, n, \quad n = 3, 4, \text{ or } 5 \tag{5.51}$$

$$b_{i,2i-1} = (\mathbf{p}_i - \mathbf{b}'_i)^T \mathbf{d}_{i,1}, \quad i = 1, \ldots, n, \quad n = 3, 4, \text{ or } 5 \tag{5.52}$$

$$b_{i,2i} = (\mathbf{p}_i - \mathbf{b}'_i)^T \mathbf{d}_{i,2}, \quad i = 1, \ldots, n, \quad n = 3, 4, \text{ or } 5 \tag{5.53}$$

5.2.5   Kinetostatic Model of the Mechanism with Rigid Links

According to the principle of virtual work, one can finally obtain the Cartesian compliance matrix with the same approach as in Chapter 4.

$$\mathbf{C}_c = \mathbf{J}_{n+1}(\mathbf{A}\mathbf{J}_{n+1})^{-1}\mathbf{B}\mathbf{C}\mathbf{B}^T(\mathbf{A}\mathbf{J}_{n+1})^{-T}\mathbf{J}_{n+1}^T \tag{5.54}$$

with

$$\Delta\mathbf{c} = \mathbf{C}_c\mathbf{w} \tag{5.55}$$

where $\mathbf{C}_c$ is a symmetric positive semi-definite (6×6) matrix, as expected.

5.2.6   Kinetostatic Model of the Mechanism with Flexible Links

Again, based on the principle of virtual work, one can write

$$\mathbf{w}^T\mathbf{t} = \boldsymbol{\tau}_{n+1}^T\dot{\boldsymbol{\theta}}'_{n+1} + \boldsymbol{\tau}_1^T\dot{\boldsymbol{\theta}}_1 + \boldsymbol{\tau}_2^T\dot{\boldsymbol{\theta}}_2 \tag{5.56}$$

where $\boldsymbol{\tau}_1$ and $\boldsymbol{\tau}_2$ correspond to a partition of vector $\boldsymbol{\tau}$, in components associated with $\dot{\boldsymbol{\theta}}_1$ and $\dot{\boldsymbol{\theta}}_2$, respectively, i.e., the first and second joint of each leg. $\boldsymbol{\tau}$ is the vector of actuator forces and $\dot{\boldsymbol{\theta}}$ is the vector of actuator velocities (actuated joints and joints with virtual springs), and $\boldsymbol{\tau}_{n+1}$ is the vector of joint torques in the passive constraining

leg. This vector is defined as follows, where $\mathbf{K}_{n+1}$ is the stiffness matrix of the passive constraining leg,

$$\boldsymbol{\tau}_{n+1} = \mathbf{K}_{n+1}\Delta\boldsymbol{\theta}'_{n+1} \tag{5.57}$$

$$\boldsymbol{\tau}_1 = \mathbf{K}_{j1}\Delta\boldsymbol{\theta}_1 \tag{5.58}$$

$$\boldsymbol{\tau}_2 = \mathbf{K}_{j2}\Delta\boldsymbol{\theta}_2 \tag{5.59}$$

$$\mathbf{K}_{j1} = diag[k_{11},\ldots,k_{n1}] \tag{5.60}$$

$$\mathbf{K}_{j2} = diag[k_{12},\ldots,k_{n2}] \tag{5.61}$$

Matrix $\mathbf{K}_{n+1}$ is a diagonal 6×6 matrix in which the ith diagonal entry is zero if it is associated with a real joint or it is equal to k_i if it is associated with a virtual joint, where k_i is the stiffness of the virtual spring located at the ith joint. $k_{11},\ldots,k_{n1}$ are the compound stiffnesses of actuators and first links stiffnesses while $k_{12},\ldots,k_{n2}$ are the first links stiffnesses. One can rewrite eq. (5.45) as

$$\dot{\boldsymbol{\theta}}_1 = \mathbf{B}_1^{-1}\mathbf{A}t - \mathbf{B}_1^{-1}\mathbf{B}_2\dot{\boldsymbol{\theta}}_2 \tag{5.62}$$

Substituting eqs. (5.62) and (5.25) into eq. (5.56), one can obtain

$$\mathbf{w}^T\mathbf{J}'_{n+1}\dot{\boldsymbol{\theta}}'_{n+1} = \boldsymbol{\tau}_{n+1}^T\dot{\boldsymbol{\theta}}'_{n+1} + \boldsymbol{\tau}_2^T\dot{\boldsymbol{\theta}}_2 + \boldsymbol{\tau}_1^T\mathbf{B}_1^{-1}\mathbf{A}\mathbf{J}'_{n+1}\dot{\boldsymbol{\theta}}'_{n+1} - \boldsymbol{\tau}_1^T\mathbf{B}_1^{-1}\mathbf{B}_2\dot{\boldsymbol{\theta}}_2 \tag{5.63}$$

Since there are 11 degrees of freedom in the compliant mechanism, this equation must be satisfied for any value of $\dot{\boldsymbol{\theta}}'_{n+1}$ and $\dot{\boldsymbol{\theta}}_2$. Therefore, one can equate the coefficients of the terms in $\dot{\boldsymbol{\theta}}'_{n+1}$ and the terms in $\dot{\boldsymbol{\theta}}_2$, hence one can obtain

$$(\mathbf{J}'_{n+1})^T\mathbf{w} = \boldsymbol{\tau}_{n+1} + (\mathbf{J}'_{n+1})^T\mathbf{A}^T\mathbf{B}_1^{-T}\boldsymbol{\tau}_1 \tag{5.64}$$

$$\boldsymbol{\tau}_2 = \mathbf{B}_2^T\mathbf{B}_1^{-T}\boldsymbol{\tau}_1 \tag{5.65}$$

Substituting eqs. (5.57), (5.58) and (5.59) into eqs. (5.64) and (5.65), one obtains

$$(\mathbf{J}'_{n+1})^T\mathbf{w} = \mathbf{K}_{n+1}\Delta\boldsymbol{\theta}'_{n+1} + (\mathbf{J}'_{n+1})^T\mathbf{A}^T\mathbf{B}_1^{-T}\mathbf{K}_{j1}\Delta\boldsymbol{\theta}_1 \tag{5.66}$$

$$\Delta\boldsymbol{\theta}_2 = \mathbf{K}_{j2}^{-1}\mathbf{B}_2^T\mathbf{B}_1^{-T}\mathbf{K}_{j1}\Delta\boldsymbol{\theta}_1 \tag{5.67}$$

Substituting eq. (5.67) into eq. (5.45), one obtains

$$\mathbf{A}t = \mathbf{W}\dot{\boldsymbol{\theta}}_1 \tag{5.68}$$

where

$$\mathbf{W} = \mathbf{B}_1 + \mathbf{B}_2\mathbf{K}_{j2}^{-1}\mathbf{B}_2^T\mathbf{B}_1^{-T}\mathbf{K}_{j1} \tag{5.69}$$

Substituting eq. (5.68) into eq. (5.66), one obtains

$$(\mathbf{J}'_{n+1})^T \mathbf{w} = \mathbf{K}_{n+1}(\mathbf{J}'_{n+1})^{-1}\Delta\mathbf{c} + (\mathbf{J}'_{n+1})^T \mathbf{A}^T \mathbf{B}_1^{-T} \mathbf{K}_{j1} \mathbf{W}^{-1} \mathbf{A}\Delta\mathbf{c} \qquad (5.70)$$

i.e.,

$$\mathbf{w} = ((\mathbf{J}'_{n+1})^{-T}\mathbf{K}_{n+1}(\mathbf{J}'_{n+1})^{-1} + \mathbf{A}^T \mathbf{B}_1^{-T} \mathbf{K}_{j1} \mathbf{W}^{-1} \mathbf{A})\Delta\mathbf{c} \qquad (5.71)$$

which is in the form

$$\mathbf{w} = \mathbf{K}\Delta\mathbf{c} \qquad (5.72)$$

where $\mathbf{K}$ is the stiffness matrix, which is equal to

$$\mathbf{K} = [(\mathbf{J}'_{n+1})^{-T}\mathbf{K}_{n+1}(\mathbf{J}'_{n+1})^{-1} + \mathbf{A}^T \mathbf{B}_1^{-T} \mathbf{K}_{j1} \mathbf{W}^{-1} \mathbf{A}] \qquad (5.73)$$

Matrix $\mathbf{K}$ is a symmetric (6×6) positive semi-definite matrix, as expected. Matrix $\mathbf{K}$ will be of full rank in non-singular configurations. Indeed, the sum of the two terms in eq. (5.73) will span the complete space of constraint wrenches.

5.3 Spatial Three-Degree-of-Freedom Mechanisms with Revolute Actuators

5.3.1 Geometric Modeling and Inverse Kinematics

A 3-dof parallel mechanism's CAD model, schematic representation and its joint distribution both on the base and on the platform are shown in Figures 5.5, 5.6 and 4.5. This mechanism consists of four kinematic chains, including three identical actuated legs and one passive constraining leg, connecting the fixed base to a moving platform. In this 3-dof parallel mechanism, the kinematic chains associated with the three identical legs consist — from base to platform — of an actuated revolute joint, a moving link, a Hooke joint, a second moving link and a spherical joint attached to the platform. The fourth chain (central leg) connecting the base center to the platform center is a passive constraining leg and has the same architecture as in the 3-dof mechanism with prismatic actuator discussed in Chapter 4.

Since the structure discussed here has a structure similar to the 3-dof mechanism with prismatic actuators, the independent Cartesian coordinates are specified as the
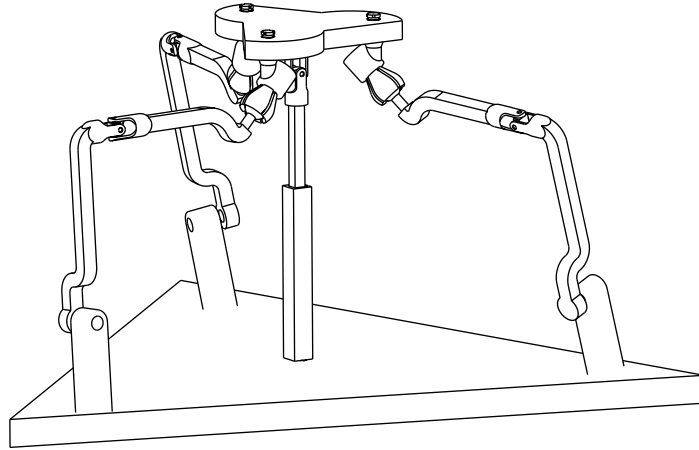
Figure 5.5: CAD model of the spatial 3-dof parallel mechanism with revolute actuators (Figure by Gabriel Coté).

same as in Chapter 4. The procedure for solving the inverse kinematics both for rigid-link and flexible-link has been presented for the general case of this family of mechanism in Section 5.2.2. With eqs. (5.1) – (5.16), one can solve the inverse kinematic problem easily. Therefore, it is not repeated here.

5.3.2 Jacobian Matrices

Considering the passive constraining leg, since it has an architecture identical to that of the 3-dof mechanism with prismatic actuators studied in Chapter 4, the Jacobian matrices of the passive constraining leg both for rigid-link and flexible-link are the same as the 3-dof mechanism with prismatic actuators of Chapter 4. Therefore, one can obtain the same Jacobian matrices as indicated in eqs. (4.64) and (4.67).

5.3.3 Global Velocity Equations

1. Rigid Model

   Considering the parallel component of the mechanism, the parallel Jacobian matrix can be obtained by eqs. (5.27) – (5.33), then one can obtain the velocity equation as

$$\mathbf{At} = \mathbf{B}\dot{\boldsymbol{\theta}} \tag{5.74}$$
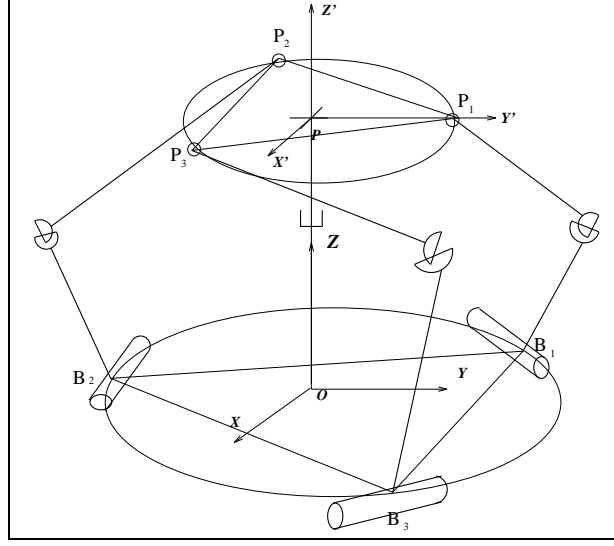
Figure 5.6: Schematic representation of the spatial 3-dof parallel mechanism with revolute actuators.

where vectors $\dot{\boldsymbol{\theta}}$ and $\mathbf{t}$ are defined as

$$\dot{\boldsymbol{\theta}} = \begin{bmatrix} \dot{\theta}_1 & \dot{\theta}_2 & \dot{\theta}_3 \end{bmatrix}^T \tag{5.75}$$

$$\mathbf{t} = \begin{bmatrix} \boldsymbol{\omega}^T & \dot{\mathbf{p}}^T \end{bmatrix}^T \tag{5.76}$$

and

$$\mathbf{A} = \begin{bmatrix} \mathbf{m}_1 & \mathbf{m}_2 & \mathbf{m}_3 \end{bmatrix}^T \tag{5.77}$$

$$\mathbf{B} = diag[(\mathbf{p}_1 - \mathbf{b}_1')^T \mathbf{e}_1, (\mathbf{p}_2 - \mathbf{b}_2')^T \mathbf{e}_2, (\mathbf{p}_3 - \mathbf{b}_3')^T \mathbf{e}_3] \tag{5.78}$$

with $\mathbf{m}_i$ is a six-dimensional vector, it can be expressed as

$$\mathbf{m}_i = \begin{bmatrix} (\mathbf{Q}\mathbf{r}'_i) \times (\mathbf{p}_i - \mathbf{b}_i') \\ (\mathbf{p}_i - \mathbf{b}_i') \end{bmatrix}, \quad i = 1, 2, 3 \tag{5.79}$$

2. Compliant Model

Referring to eqs. (5.39) – (5.44), one has the velocity equation as

$$\mathbf{At} = \mathbf{B}_1 \dot{\boldsymbol{\theta}}_1 + \mathbf{B}_2 \dot{\boldsymbol{\theta}}_2 \tag{5.80}$$

where vectors $\dot{\boldsymbol{\theta}}_1$ and $\dot{\boldsymbol{\theta}}_2$ are defined as

$$\dot{\boldsymbol{\theta}}_1 = \begin{bmatrix} \dot{\theta}_{11} & \dot{\theta}_{21} & \dot{\theta}_{31} \end{bmatrix}^T \tag{5.81}$$

$$\dot{\boldsymbol{\theta}}_2 = \begin{bmatrix} \dot{\theta}_{12} & \dot{\theta}_{22} & \dot{\theta}_{32} \end{bmatrix}^T \tag{5.82}$$

with $\dot{\mathbf{p}}$ and $\boldsymbol{\omega}$ are the linear and angular velocities of the platform, and

$$\mathbf{A} = \begin{bmatrix} \mathbf{m}_1 & \mathbf{m}_2 & \mathbf{m}_3 \end{bmatrix}^T \tag{5.83}$$

$$\mathbf{B}_1 = diag[b_{11}, b_{23}, b_{35}] \tag{5.84}$$

$$\mathbf{B}_2 = diag[b_{12}, b_{24}, b_{36}] \tag{5.85}$$

where $\mathbf{m}_i$ is a six-dimensional vector, $b_{i,2i-1}$, $b_{i,2i}$ are diagonal terms of $\mathbf{B}_1$ and $\mathbf{B}_2$, respectively, they can be expressed as

$$\mathbf{m}_i = \begin{bmatrix} (\mathbf{Q}\mathbf{r}'_i) \times (\mathbf{p}_i - \mathbf{b}'_i) \\ (\mathbf{p}_i - \mathbf{b}'_i) \end{bmatrix}, \quad i = 1, 2, 3 \tag{5.86}$$

$$b_{i,2i-1} = (\mathbf{p}_i - \mathbf{b}'_i)^T \mathbf{d}_{i,1}, \quad i = 1, 2, 3 \tag{5.87}$$

$$b_{i,2i} = (\mathbf{p}_i - \mathbf{b}'_i)^T \mathbf{d}_{i,2}, \quad i = 1, 2, 3 \tag{5.88}$$

5.3.4 Kinetostatic Models

The procedure for finding the compliance matrix for the rigid model is identical to what has been done in the computation of the compliance matrix of the 3-dof mechanism with prismatic actuators, and the compliance matrix can be written as

$$\mathbf{C}_c = \mathbf{J}_4 (\mathbf{A}\mathbf{J}_4)^{-1} \mathbf{B} \mathbf{C} \mathbf{B}^T (\mathbf{A}\mathbf{J}_4)^{-T} \mathbf{J}_4^T \tag{5.89}$$

where $\mathbf{C}_c = diag[c_1, c_2, c_3]$, with c_1, c_2 and c_3 are the compliances of the actuators, and $\mathbf{J}_4$ is the Jacobian matrix of the passive constraining leg in this 3-dof case. $\mathbf{A}$ and $\mathbf{B}$ are the Jacobian matrices of the structure without the passive constraining leg.

The same method described in Section 5.2.6 is applied for finding the stiffness matrix of the mechanism with flexible links, and this matrix can be written as

$$\mathbf{K} = [(\mathbf{J}'_4)^{-T} \mathbf{K}_4 (\mathbf{J}'_4)^{-1} + \mathbf{A}^T \mathbf{B}_1^{-T} \mathbf{K}_{j1} \mathbf{W}^{-1} \mathbf{A}] \tag{5.90}$$

where $\mathbf{W}$ is defined in eq. (5.69) and

$$\mathbf{K}_4 = diag[k_{41}, k_{42}, k_{43}, 0, 0, 0] \tag{5.91}$$

$$\mathbf{K}_{j1} = diag[k_{11}, k_{21}, k_{31}] \tag{5.92}$$

$$\mathbf{K}_{j2} = diag[k_{12}, k_{22}, k_{32}] \tag{5.93}$$

and $\mathbf{J}_4'$ is the Jacobian matrix of the passive constraining leg with virtual joints, k_{41}, k_{42} and k_{43} are the passive constraining leg's lumped stiffnesses, k_{11}, k_{21} and k_{31} are the compound stiffnesses of actuators and first links stiffnesses, k_{12}, k_{22} and k_{32} are the first links stiffnesses.

5.3.5 Implementation

The above model has been implemented for the 3-dof mechanism with revolute actuators for both cases, with rigid links and with flexible links. The results are given to illustrate the effect of the flexible links on the parallel mechanism. For the reference configuration of Figure 5.6, the parameters used in this example are given as

$$\theta_{b1} = \pi/3, \theta_{b2} = \pi, \theta_{b3} = -\pi/3,$$
$$\theta_{p1} = 0, \theta_{p2} = 2\pi/3, \theta_{p3} = -2\pi/3,$$
$$R_p = 9 \ cm, R_b = 22.73 \ cm,$$
$$K_i = -1, \quad i = 1, 2, 3$$
$$l_{i1} = 51.52 \ cm, l_{i2} = 69.7 \ cm, \quad i = 1, 2, 3$$
$$k_{i1}' = 1000 \ Nm, \quad i = 1, 2, 3$$

where k_{i1}' is the actuator stiffness, K_i is the branch index, and l_{i1}, l_{i2} are the link length for the 1st and 2nd link of each leg. The Cartesian coordinates are given by

$$x \in [-3, 3] \ cm, y \in [-3, 3] \ cm, z = 103 \ cm,$$
$$\theta_{42} = \pi/2, \theta_{43} = 0,$$

From Tables 5.1, 5.2 and Figure 5.7, one can find that with the improvement of the link stiffness, the mechanism's compliance is very close to that of mechanism with rigid links. This means that one can assume the flexible mechanism to be rigid only if the link stiffness reaches a high value.
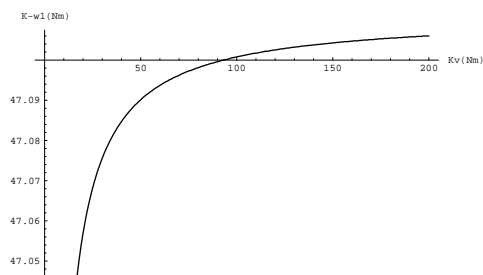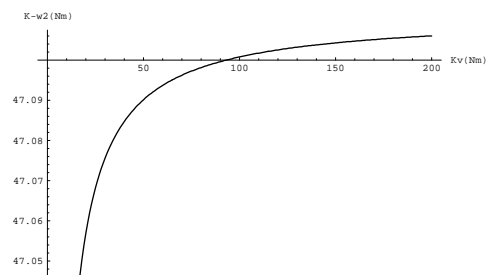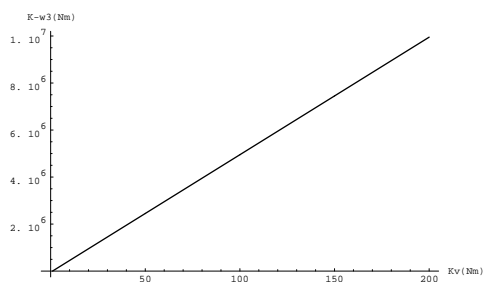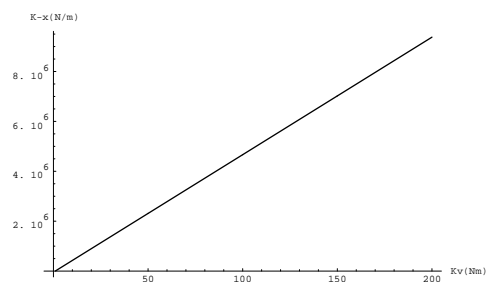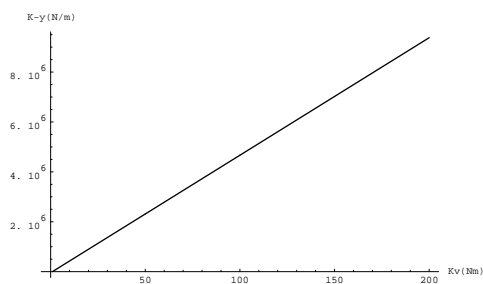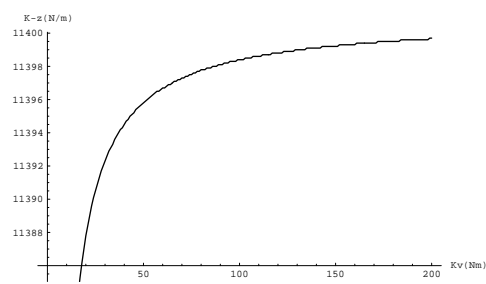
(a) Stiffness in θ_x

(b) Stiffness in θ_y

(c) Stiffness in θ_z

(d) Stiffness in x

(e) Stiffness in y

(f) Stiffness in z

Figure 5.7: Evolution of the stiffness as a function of the link's lumped stiffness in different directions.
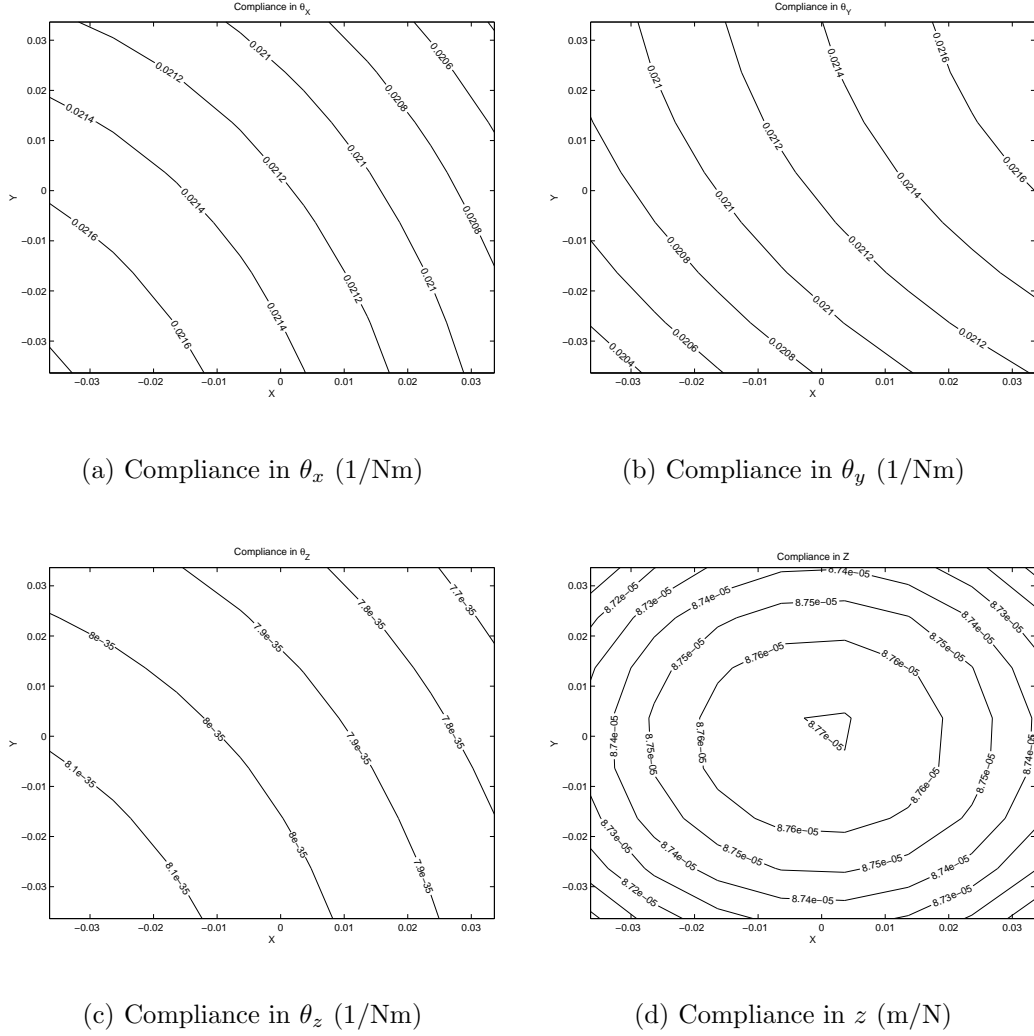
(a) Compliance in θ_x (1/Nm)

(b) Compliance in θ_y (1/Nm)

(c) Compliance in θ_z (1/Nm)

(d) Compliance in z (m/N)

Figure 5.8: Compliance mappings of the spatial 3-dof parallel mechanism with revolute actuators (all length units in m).

5.3.6 Design Guidelines

Given a certain configuration of the mechanism ($x = 0, y = 0, z = 103$ $cm, \theta_{42} = \pi/2, \theta_{43} = 0$), one can find expressions for the Cartesian stiffness in all directions as functions of the actuator stiffnesses and link stiffnesses. For the reference configuration, one obtains

$$K_{\theta_x} = \frac{141\lambda K_{b2}(0.895796 + 0.00859172\lambda^2 + 0.175459\lambda)}{(2681 + 2.51837\lambda^3 + 77.1446\lambda^2 + 787.717\lambda)} \tag{5.94}$$

$$K_{\theta_y} = \frac{141\lambda K_{b2}(0.895796 + 0.00859172\lambda^2 + 0.175459\lambda)}{(2681 + 2.51837\lambda^3 + 77.1446\lambda^2 + 787.717\lambda)} \tag{5.95}$$

Table 5.1: Comparison of the mechanism compliance between the mechanism with rigid links and the mechanism with flexible links.

$K_{actuator}$	K_{link}	κ_{θ_x}	κ_{θ_y}	κ_{θ_z}	κ_x	κ_y	κ_z
1000	1000	0.09937	0.09937	10^{-3}	1.06152×10^{-3}	1.06152×10^{-3}	0.000186579
1000	$10^1 K_a$	0.02904	0.02904	10^{-4}	1.06152×10^{-4}	1.06152×10^{-4}	0.0000975989
1000	$10^2 K_a$	0.02201	0.02201	10^{-5}	1.06152×10^{-5}	1.06152×10^{-5}	0.0000887009
1000	$10^3 K_a$	0.02131	0.02131	10^{-6}	1.06152×10^{-6}	1.06152×10^{-6}	0.0000878111
1000	$10^4 K_a$	0.02123	0.02123	10^{-7}	1.06152×10^{-7}	1.06152×10^{-7}	0.0000877221
1000	$10^5 K_a$	0.02123	0.02123	10^{-8}	1.06152×10^{-8}	1.06152×10^{-8}	0.0000877132
1000	$10^6 K_a$	0.02123	0.02123	10^{-9}	1.06152×10^{-9}	1.06152×10^{-9}	0.0000877123
1000	$10^7 K_a$	0.02123	0.02123	10^{-10}	1.06152×10^{-10}	1.06152×10^{-10}	0.0000877122
1000	rigid	0.02123	0.02123	0.0	0.0	0.0	0.0000877122

$$K_{\theta_z} = \frac{87497.6\lambda K_{b2}(0.0895796 + 0.000859172\lambda^2 + 0.0175459\lambda)}{(268111 + 251.837\lambda^3 + 7714.46\lambda^2 + 78771.7\lambda)} + K_{43} \qquad (5.96)$$

$$K_x = \frac{728387\lambda K_{b2}(0.895759 + 0.00859172\lambda^2 + 0.175459\lambda)}{(268111 + 251.837\lambda^3 + 7714.46\lambda^2 + 78771.7\lambda)} + K_{41} \qquad (5.97)$$

$$K_y = \frac{728387\lambda K_{b2}(0.0895759 + 0.000859172\lambda^2 + 0.0175459\lambda)}{(268111 + 251.837\lambda^3 + 7714.46\lambda^2 + 78771.7\lambda)} + K_{42} \qquad (5.98)$$

$$K_z = \frac{341228\lambda K_{b2}(8.95796 + 0.0859172\lambda^2 + 1.75459\lambda)}{(268111 + 251.837\lambda^3 + 7714.46\lambda^2 + 78771.7\lambda)} \qquad (5.99)$$

$$\lambda = \frac{K_a K_{b1}}{(K_a + K_{b1})K_{b2}} \qquad (5.100)$$

where K_a represents the actuator stiffness, and K_{b1}, K_{b2} represent actuated kinematic chain's 1st and 2nd link's stiffness, respectively, while K_{41}, K_{42} and K_{43} represent the passive constraining leg's lumped stiffnesses in X, Y and Z directions caused by the link bending and torsion.

Based on the results above, the following design guidelines can be established and used for designing this type of mechanism. The common design guidelines for this family of mechanisms will be given in Section 5.6.

1. The stiffnesses $K_{\theta_x}, K_{\theta_y}$ and K_z are dependent on the stiffnesses of the actuators and on the stiffnesses of the actuated links. They have no relationship with the rigidity of the passive constraining leg.

Table 5.2: The stiffness effect of the passive constraining leg.

$K_{actuator}$	K_{link}	$K_{passive}$	K_{θ_x}	K_{θ_y}	K_{θ_z}	K_x	K_y	K_z
1000	$10^2 K_a$	1000	46.5996	46.5996	1028.92	3349.26	3349.26	3349.26
1000	$10^2 K_a$	$10^1 K_a$	46.5996	46.5996	10028.9	11827.6	11827.6	3349.26
1000	$10^2 K_a$	$10^2 K_a$	46.5996	46.5996	100029	96611.4	96611.4	3349.26
1000	$10^2 K_a$	$10^3 K_a$	46.5996	46.5996	10^6	944449	944449	3349.26
1000	$10^2 K_a$	$10^4 K_a$	46.5996	46.5996	10^7	9.42282×10^6	9.42282×10^6	3349.26
1000	$10^2 K_a$	$10^5 K_a$	46.5996	46.5996	10^8	9.42066×10^7	9.42066×10^7	3349.26
1000	$10^2 K_a$	$10^6 K_a$	46.5996	46.5996	10^9	9.42044×10^8	9.42044×10^8	3349.26
1000	$10^2 K_a$	$10^7 K_a$	46.5996	46.5996	10^{10}	9.42042×10^9	9.42042×10^9	3349.26

2. K_{41} and K_{42}, i.e., the passive constraining leg's bending stiffnesses along the X and Y axes, play the same role of limiting the movement of the platform along the X and Y. K_{43}, i.e., the passive constraining leg's torsional stiffness around the Z axis, and plays the role of limiting the rotation of the platform around the Z axis.

3. From the above equations, one can find that the stiffness along the Z axis is the largest one among all the others, and K_{θ_y} is equal to K_{θ_x} because of the structural symmetrical configuration. This is clearly illustrated in Figure 5.7.

4. In Figures 5.8(a) and (b), these torsional compliances in θ_x and θ_y are shown, the compliances are symmetric to each other. In Figure 5.8(f), the stiffness in the z direction is increasing when the platform moves further from the center of the workspace. All these are in accordance with what would be intuitively expected.

One also finds the following facts regarding this 3-dof mechanism with revolute actuators after performing the tests with the kinetostatic model.

1. For a certain platform size, the larger the link length, the smaller the global stiffness.

2. For a given link length, the larger the platform size, the larger the torsional stiffness values around the X and Y axes, and the smaller the stiffness value along the Z axis.

5.4   Spatial Four-Degree-of-Freedom Mechanisms with Revolute Actuators

5.4.1   Geometric Modeling

Figures 5.9 and 5.10 represent a 4-dof parallel mechanism's CAD model and its schematic representation, the joints distribution both on the base and on the platform are the same as in Figure 4.12. This mechanism consists of five kinematic chains, including four actuated legs with identical topology and one passive constraining leg, connecting the fixed base to a moving platform. In this 4-dof parallel mechanism, the kinematic chains associated with the four identical legs, from base to platform, consist of an actuated revolute joint, a moving link, a Hooke joint, a second moving link and a spherical joint attached to the platform. The fifth chain (central leg) connecting the base center to the platform center is a passive constraining leg and has the same architecture as in the 4-dof mechanism with prismatic actuators.
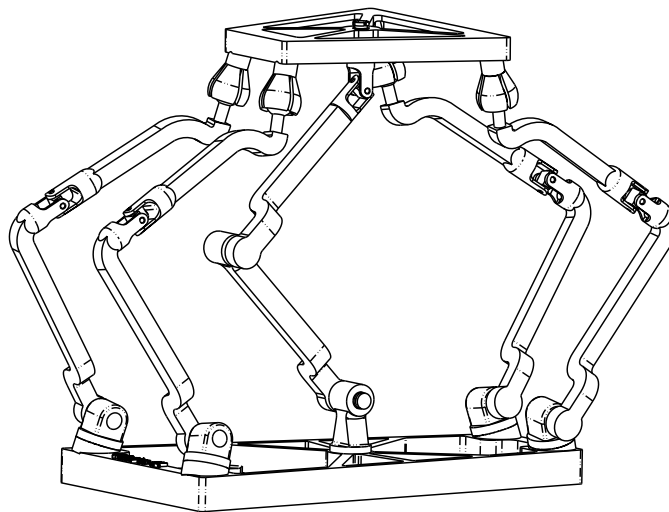
Figure 5.9: CAD model of the spatial 4-dof parallel mechanism with revolute actuators (Figure by Gabriel Coté).
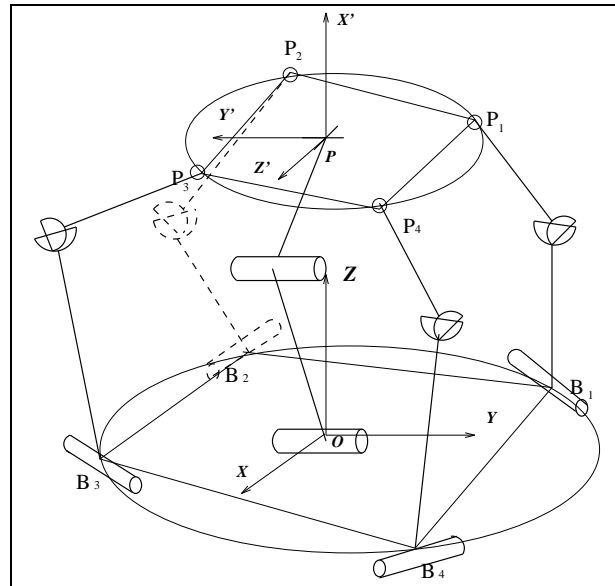
Figure 5.10: Schematic representation of the spatial 4-dof parallel mechanism with revolute actuators.

5.4.2 Inverse Kinematics

With the same independent coordinates $(x, z, \theta_{53}, \theta_{54})$, vectors $\mathbf{p}_i$, $\mathbf{r}'_i$, $\mathbf{p}$ and rotation matrix $\mathbf{Q}_0$ as in the 4-dof mechanisms with prismatic actuators discussed in Chapter 4, and eqs. (5.1) – (5.22), one can obtain the inverse kinematics easily. It is not repeated here.

5.4.3 Jacobian Matrices

The passive constraining leg has an architecture identical to that (Figures 4.13 and 4.14) of the 4-dof mechanism with prismatic actuators. Hence, the Jacobian matrices of the passive constraining leg both for rigid-link and flexible-link are the same as for the 4-dof mechanism with prismatic actuators developed in Chapter 4. One can obtain equations identical to eqs. (4.82) and (4.85).

5.4.4 Global Velocity Equations

1. Rigid Model

Now, the parallel component of the mechanism is considered, and the parallel Jacobian matrix, i.e., the velocity equation for the actuated part can be obtained through eqs. (5.27) – (5.33). Hence one has the velocity equation for rigid-link as follow

$$\mathbf{At} = \mathbf{B}\dot{\boldsymbol{\theta}} \tag{5.101}$$

where vectors $\dot{\boldsymbol{\theta}}$ and $\mathbf{t}$ are defined as

$$\dot{\boldsymbol{\theta}} = \begin{bmatrix} \dot{\theta}_1 & \dot{\theta}_2 & \dot{\theta}_3 & \dot{\theta}_4 \end{bmatrix}^T \tag{5.102}$$

$$\mathbf{t} = \begin{bmatrix} \boldsymbol{\omega}^T & \dot{\mathbf{p}}^T \end{bmatrix}^T \tag{5.103}$$

and

$$\mathbf{A} = \begin{bmatrix} \mathbf{m}_1 & \mathbf{m}_2 & \mathbf{m}_3 & \mathbf{m}_4 \end{bmatrix}^T \tag{5.104}$$

$$\mathbf{B} = diag[(\mathbf{p}_1 - \mathbf{b}_1')^T\mathbf{e}_1, (\mathbf{p}_2 - \mathbf{b}_2')^T\mathbf{e}_2, (\mathbf{p}_3 - \mathbf{b}_3')^T\mathbf{e}_3,$$
$$(\mathbf{p}_4 - \mathbf{b}_4')^T\mathbf{e}_4] \tag{5.105}$$

where $\mathbf{m}_i$ is a six-dimensional vector, it can be expressed as

$$\mathbf{m}_i = \begin{bmatrix} (\mathbf{Q}\mathbf{r}_i') \times (\mathbf{p}_i - \mathbf{b}_i') \\ (\mathbf{p}_i - \mathbf{b}_i') \end{bmatrix}, \quad i = 1, \ldots, 4 \tag{5.106}$$

2. Compliant Model

Similarly to the 3-dof mechanism studied in the preceding section, for the flexible-link case, one has the velocity equation as follows

$$\mathbf{At} = \mathbf{B}_1\dot{\boldsymbol{\theta}}_1 + \mathbf{B}_2\dot{\boldsymbol{\theta}}_2 \tag{5.107}$$

where vectors $\dot{\boldsymbol{\theta}}_1$ and $\dot{\boldsymbol{\theta}}_2$ are defined as

$$\dot{\boldsymbol{\theta}}_1 = \begin{bmatrix} \dot{\theta}_{11} & \dot{\theta}_{21} & \dot{\theta}_{31} & \dot{\theta}_{41} \end{bmatrix}^T \tag{5.108}$$

$$\dot{\boldsymbol{\theta}}_2 = \begin{bmatrix} \dot{\theta}_{12} & \dot{\theta}_{22} & \dot{\theta}_{32} & \dot{\theta}_{42} \end{bmatrix}^T \tag{5.109}$$

where $\mathbf{A}$ and its terms are the same as in eqs. (5.104) and (5.106) and

$$\mathbf{B}_1 = diag[b_{11}, b_{23}, b_{35}, b_{47}] \tag{5.110}$$

$$\mathbf{B}_2 = diag[b_{12}, b_{24}, b_{36}, b_{48}] \tag{5.111}$$

with $b_{i,2i-1}$, $b_{i,2i}$ are diagonal terms of $\mathbf{B}_1$ and $\mathbf{B}_2$, they can be expressed as

$$b_{i,2i-1} = (\mathbf{p}_i - \mathbf{b}_i')^T\mathbf{d}_{i,1}, \quad i = 1, \ldots, 4 \tag{5.112}$$

$$b_{i,2i} = (\mathbf{p}_i - \mathbf{b}_i')^T\mathbf{d}_{i,2}, \quad i = 1, \ldots, 4 \tag{5.113}$$

5.4.5 Kinetostatic Models

As illustrated in Figure 5.9, the compliance matrix for the 4-dof mechanism with rigid links will be

$$\mathbf{C}_c = \mathbf{J}_5(\mathbf{A}\mathbf{J}_5)^{-1}\mathbf{B}\mathbf{C}\mathbf{B}^T(\mathbf{A}\mathbf{J}_5)^{-T}\mathbf{J}_5^T \tag{5.114}$$

where

$$\mathbf{C} = diag[c_1, c_2, c_3, c_4] \tag{5.115}$$

with c_1, c_2, c_3 and c_4 are the compliances of the actuators, and $\mathbf{J}_5$ is the Jacobian matrix of the constraining leg in this 4-dof case. Matrices $\mathbf{A}$ and $\mathbf{B}$ are the Jacobian matrices of the structure without the passive constraining leg.

Referring to Section 5.2.6, one can obtain the stiffness matrix for this 4-dof mechanism with flexible links as

$$\mathbf{K} = (\mathbf{J}_5')^{-T}\mathbf{K}_5(\mathbf{J}_5')^{-1} + \mathbf{A}^T\mathbf{B}_1^{-T}\mathbf{K}_{j1}\mathbf{W}^{-1}\mathbf{A} \tag{5.116}$$

where $\mathbf{W}$ is defined in eq. (5.69) and

$$\mathbf{K}_5 = diag[0, k_{52}, 0, k_{54}, 0, 0] \tag{5.117}$$
$$\mathbf{K}_{j1} = diag[k_{11}, k_{21}, k_{31}, k_{41}] \tag{5.118}$$
$$\mathbf{K}_{j2} = diag[k_{12}, k_{22}, k_{32}, k_{42}] \tag{5.119}$$

where k_{52} and k_{54} are the passive constraining leg lumped stiffnesses, $k_{11}, k_{21}, k_{31}, k_{41}$ are the compound stiffnesses of the actuator's stiffness and the first link's stiffness, $k_{12}, k_{22}, k_{32}, k_{42}$ are the first link's stiffnesses. $\mathbf{J}_5'$ is the Jacobian matrix of the passive constraining leg with consideration of link flexibility, while $\mathbf{A}$ and $\mathbf{B}_1$, $\mathbf{B}_2$ are the Jacobian matrices of the structure without the passive constraining leg in this case.

5.4.6 Implementation

In order to illustrate the effect of the flexible links on the parallel mechanism, an example of 4-dof mechanism is presented. The parameters for Figure 5.10 are given as

$$\alpha = 30°, \beta = 60°,$$

$$R_p = 9 \ cm, R_b = 22.73 \ cm,$$

$$K_i = -1, \quad i = 1, \dots, 4$$

$$l_{i1} = 51.52 \ cm, l_{i2} = 69.7 \ cm, \quad i = 1, \dots, 4, \quad l_{51} = l_{52} = 103 \ cm$$

$$k_{i1} = 1000 \ Nm, \quad i = 1, \dots, 4$$

where k_{i1} is the actuator stiffness, K_i is the branch index, l_{51}, l_{52} are the link lengths of the passive leg and l_{i1}, l_{i2} are the link lengths for the 1st and 2nd link of each leg and the Cartesian coordinates are given by

$$x \in [-3, 3] \ cm, y \in [-3, 3] \ cm, z = 103 \ cm,$$

$$\theta_{53} = -\pi/3, \theta_{54} = 2\pi/3,$$

The comparison between the parallel mechanism with rigid links (without virtual joints) and the parallel mechanism with flexible links (with virtual joints) is given in Figure 5.11, Tables 5.3 and 5.4. Again, the effect of the link flexibility is clearly demonstrated from the Tables 5.3, 5.4 and Figure 5.11.

Table 5.3: Comparison of the mechanism compliance between the mechanism with rigid links and the mechanism with flexible links.

$K_{actuator}$	K_{link}	κ_{θ_x}	κ_{θ_y}	κ_{θ_z}	κ_x	κ_y	κ_z
1000	1000	3.46122	0.138363	1.5×10^{-3}	0.0146575	1.32691×10^{-3}	0.000271569
1000	$10^1 K_a$	1.49876	0.0703633	1.5×10^{-4}	0.00717397	1.32691×10^{-4}	0.000106446
1000	$10^2 K_a$	1.30251	0.0635633	1.5×10^{-5}	0.00642561	1.32691×10^{-5}	0.0000899335
1000	$10^3 K_a$	1.28289	0.0628833	1.5×10^{-6}	0.00635078	1.32691×10^{-6}	0.0000882822
1000	$10^4 K_a$	1.28093	0.0628153	1.5×10^{-7}	0.0063433	1.32691×10^{-7}	0.0000881171
1000	$10^5 K_a$	1.28073	0.0628085	1.5×10^{-8}	0.00634255	1.32691×10^{-8}	0.0000881006
1000	$10^6 K_a$	1.28071	0.0628079	1.5×10^{-9}	0.00634247	1.32691×10^{-9}	0.000088099
1000	$10^7 K_a$	1.28071	0.0628078	1.5×10^{-10}	0.00634246	1.32691×10^{-10}	0.0000880988
1000	rigid	1.28071	0.0628078	0.0	0.00634246	0.0	0.0000880988
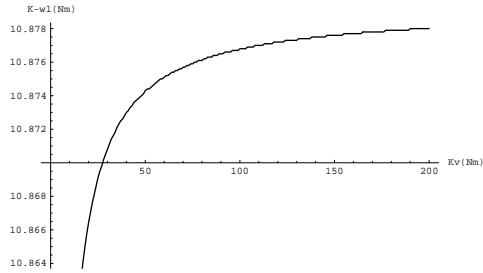
(a) Stiffness in θ_x
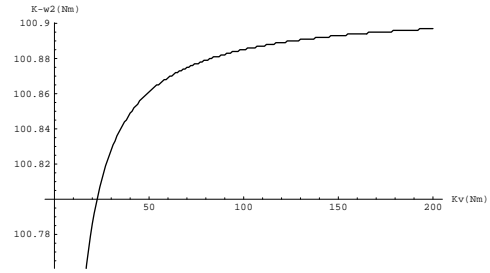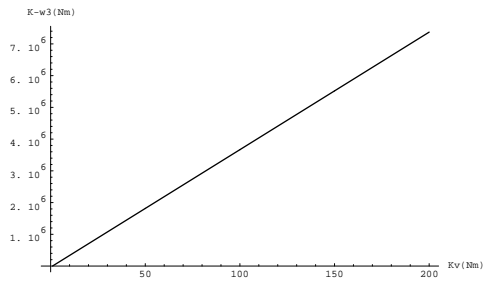
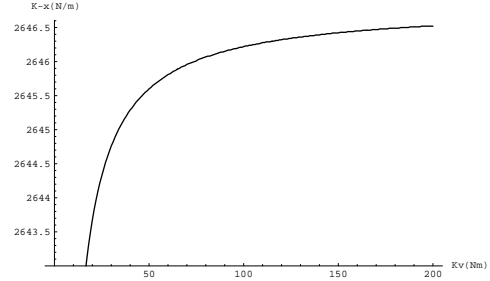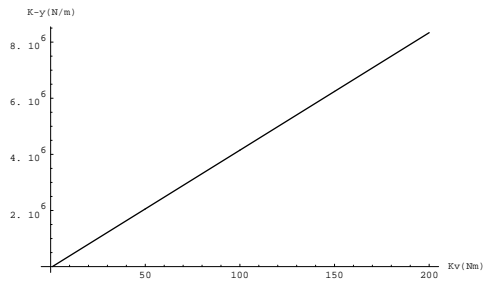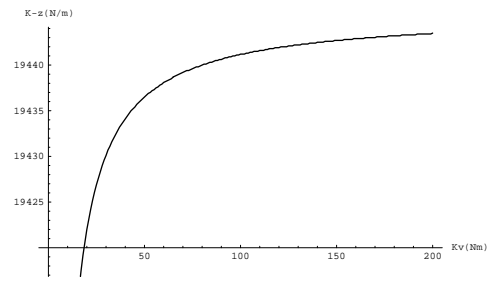(b) Stiffness in θ_y

(c) Stiffness in θ_z

(d) Stiffness in x

(e) Stiffness in y

(f) Stiffness in z

Figure 5.11: Evolution of the stiffness as a function of the link's lumped stiffness in different directions.
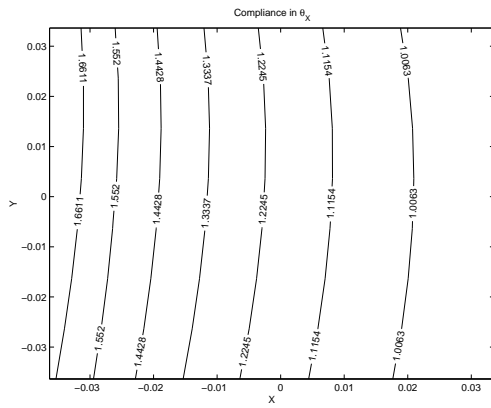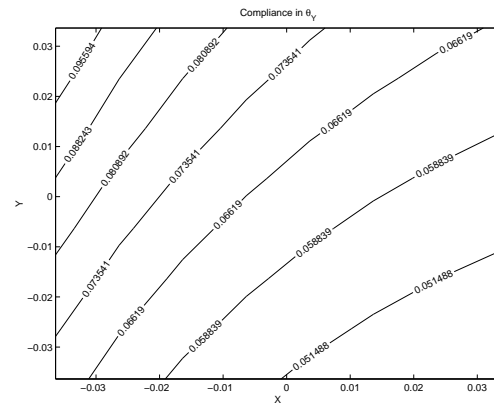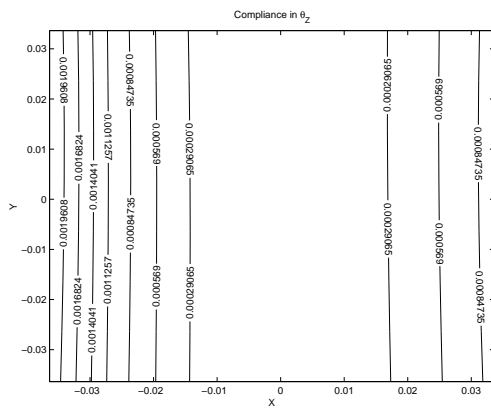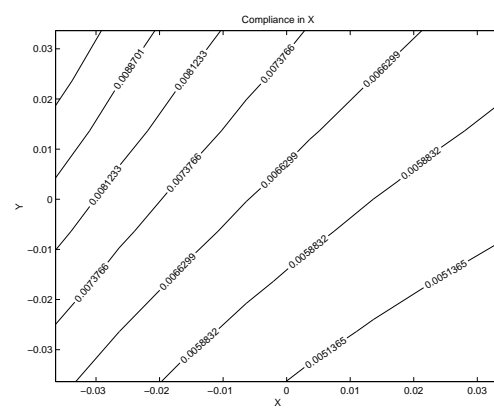
(a) Compliance in θ_x (1/Nm)

(b) Compliance in θ_y (1/Nm)

(c) Compliance in θ_z (1/Nm)
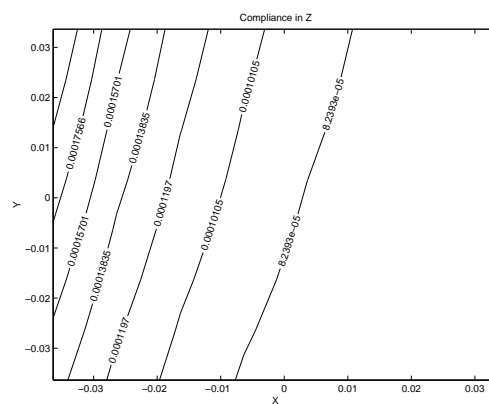
(d) Compliance in x (m/N)

(e) Compliance in z (m/N)

Figure 5.12: Compliance mappings of the spatial 4-dof parallel mechanism with revolute actuators (all length units in m).

Table 5.4: The stiffness effect of the passive constraining leg.

$K_{actuator}$	K_{link}	$K_{passive}$	K_{θ_x}	K_{θ_y}	K_{θ_z}	K_x	K_y	K_z
1000	$10^2 K_a$	1000	10.7582	99.7507	7420.66	2617.08	11818.2	19222
1000	$10^2 K_a$	$10^1 K_a$	10.7582	99.7507	74087.3	2617.08	87181.5	19222
1000	$10^2 K_a$	$10^2 K_a$	10.7582	99.7507	740754	2617.08	840815	19222
1000	$10^2 K_a$	$10^3 K_a$	10.7582	99.7507	7.40742×10^6	2617.08	8.37715×10^6	19222
1000	$10^2 K_a$	$10^4 K_a$	10.7582	99.7507	7.40741×10^7	2617.08	8.37405×10^7	19222
1000	$10^2 K_a$	$10^5 K_a$	10.7582	99.7507	7.40741×10^8	2617.08	8.37374×10^8	19222
1000	$10^2 K_a$	$10^6 K_a$	10.7582	99.7507	7.40741×10^9	2617.08	8.37371×10^9	19222
1000	$10^2 K_a$	$10^7 K_a$	10.7582	99.7507	7.40741×10^{10}	2617.08	8.3737×10^{10}	19222

5.4.7   Design Guidelines

For a given configuration ($x = 0, y = 0, z = 103\ cm, \theta_{53} = -\pi/3, \theta_{54} = 2\pi/3$), one can obtain the expressions for the Cartesian stiffness in each direction as follows

$$K_{\theta_x} = \frac{33146\lambda K_{b2}(0.892211 + 0.00273055\lambda^3 + 0.0577587\lambda^2 + 0.398016\lambda)}{(620383 + 275.726\lambda^4 + 7864.05\lambda^3 + 82287.2\lambda^2 + 373568\lambda)} \quad (5.120)$$

$$K_{\theta_y} = \frac{273173\lambda K_{b2}(0.892211 + 0.00273055\lambda^3 + 0.0577587\lambda^2 + 0.398016\lambda)}{(620383 + 275.726\lambda^4 + 7864.05\lambda^3 + 82287.2\lambda^2 + 373568\lambda)} \quad (5.121)$$

$$K_{\theta_z} = \frac{36776\lambda K_{b2}(0.892211 + 0.00273055\lambda^3 + 0.0577587\lambda^2 + 0.398016\lambda)}{(620383 + 275.726\lambda^4 + 7864.05\lambda^3 + 82287.2\lambda^2 + 373568\lambda)}$$
$$+ \ 0.592593 K_{52} + 0.148148 K_{54} \quad (5.122)$$

$$K_x = \frac{77904\lambda K_{b2}(89.2211 + 0.273055\lambda^3 + 5.77587\lambda^2 + 39.8016\lambda)}{(620383 + 275.726\lambda^4 + 7864.05\lambda^3 + 82287.2\lambda^2 + 373568\lambda)} \quad (5.123)$$

$$K_y = \frac{94298\lambda K_{b2}(89.2211 + 0.273055\lambda^3 + 5.77587\lambda^2 + 39.8016\lambda)}{(620383 + 275.726\lambda^4 + 7864.05\lambda^3 + 82287.2\lambda^2 + 373568\lambda)}$$
$$+ \ 0.418685 K_{52} + 0.418685 K_{54} \quad (5.124)$$

$$K_z = \frac{5264086\lambda K_{b2}(8.92211 + 0.0273055\lambda^3 + 0.577587\lambda^2 + 3.98016\lambda)}{(620383 + 275.726\lambda^4 + 7864.05\lambda^3 + 82287.2\lambda^2 + 373568\lambda)} \quad (5.125)$$

$$\lambda = \frac{K_a K_{b1}}{(K_a + K_{b1})K_{b2}} \quad (5.126)$$

where K_a represents the actuator stiffness, K_{b1}, K_{b2} are 1st and 2nd link's stiffnesses of the actuated leg, K_{52} and K_{54} represent the first and second (from bottom to platform) link's lumped stiffnesses of the passive constraining leg.

Besides the common design guidelines given in Section 5.6, the following design

guidelines can be established from the above results for designing this kind of mechanism.

1. The stiffnesses $K_{\theta_x}, K_{\theta_y}, K_x$ and K_z are dependent on the stiffnesses of actuators and actuated links and have no relationship with the rigidity of passive constraining leg's.

2. If $K_{52} \neq K_{54}$, i.e., the passive constraining leg's first link (from bottom to platform) is not as rigid as the second link, then the first link's rigidity is more important than the second link's for limiting the platform's degrees of freedom, this can be found from the coefficients of K_{52} and K_{54} in eqs. (5.122) and (5.124).

3. From the equations, one can find that the stiffness along the Z axis is the largest one among all the others, and K_{θ_y} is larger than K_{θ_x}. It is clearly illustrated in Figure 5.11.

4. For a certain platform size, the larger the link length, the larger the torsional stiffness values around the X and Y axes, and the smaller the translational stiffness along the Z axis.

5. For a given link length, the smaller the platform size, the larger the stiffness values along the X and Z axes.

6. From Figure 5.11 and Table 5.3, one can see that K_{θ_z} and K_y are becoming infinite while the flexible links are approaching rigid, it corresponds to the motions prevented by the passive constraining leg. K_{θ_x} is also large enough because of the structure of the passive constraining leg. The stiffness in Z is higher near the center of the workspace, which is the best position for supporting vertical loads along the Z axis. All these are in accordance with what would be intuitively expected.

5.5 Spatial Five-Degree-of-Freedom Mechanisms with Revolute Actuators

A 5-dof parallel mechanism and their joint distribution both on the base and on the platform are shown in Figures 5.1, 5.2 and 4.17. One can find the inverse kinematics for both the rigid-link and the flexible-link cases easily from eqs. (5.1) – (5.22)

5.5.1 Jacobian Matrices

Since the passive constraining leg has an architecture identical to that of the 5-dof mechanism with prismatic actuators, the Jacobian matrices for the constraining leg are the same as in eqs. (4.102) and (4.105). The Jacobian matrix for the parallel part will be computed in the next section.

5.5.2 Global Velocity Equations

1. Rigid Model

   Similarly, for the part of this mechanism without the passive constraining leg, one can obtain the velocity equation for rigid links as

   $$\mathbf{At} = \mathbf{B}\dot{\boldsymbol{\theta}} \tag{5.127}$$

   where vectors $\dot{\boldsymbol{\theta}} = \begin{bmatrix} \dot{\theta}_1 & \dot{\theta}_2 & \dot{\theta}_3 & \dot{\theta}_4 & \dot{\theta}_5 \end{bmatrix}^T$, and

   $$\begin{aligned} \mathbf{A} &= \begin{bmatrix} \mathbf{m}_1 & \mathbf{m}_2 & \mathbf{m}_3 & \mathbf{m}_4 & \mathbf{m}_5 \end{bmatrix}^T \\ \mathbf{B} &= diag[(\mathbf{p}_1 - \mathbf{b}'_1)^T \mathbf{e}_1, (\mathbf{p}_2 - \mathbf{b}'_2)^T \mathbf{e}_2, (\mathbf{p}_3 - \mathbf{b}'_3)^T \mathbf{e}_3, \\ &\qquad (\mathbf{p}_4 - \mathbf{b}'_4)^T \mathbf{e}_4, (\mathbf{p}_5 - \mathbf{b}'_5)^T \mathbf{e}_5] \end{aligned}$$

   $$(5.128)$$
   $$(5.129)$$

   where $\mathbf{m}_i$ is a six-dimensional vector that can be expressed as

   $$\mathbf{m}_i = \begin{bmatrix} (\mathbf{Qr}'_i) \times (\mathbf{p}_i - \mathbf{b}'_i) \\ (\mathbf{p}_i - \mathbf{b}'_i) \end{bmatrix}, \quad i = 1, \ldots, 5 \tag{5.130}$$

2. Compliant Model

One also has the velocity equation for the 5-dof parallel mechanism with flexible links as

$$\mathbf{A}\dot{\mathbf{t}} = \mathbf{B}_1\dot{\boldsymbol{\theta}}_1 + \mathbf{B}_2\dot{\boldsymbol{\theta}}_2 \tag{5.131}$$

where vectors $\dot{\boldsymbol{\theta}}_1$ and $\dot{\boldsymbol{\theta}}_2$ are defined as

$$\dot{\boldsymbol{\theta}}_1 = \begin{bmatrix} \dot{\theta}_{11} & \dot{\theta}_{21} & \dot{\theta}_{31} & \dot{\theta}_{41} & \dot{\theta}_{51} \end{bmatrix}^T \tag{5.132}$$

$$\dot{\boldsymbol{\theta}}_2 = \begin{bmatrix} \dot{\theta}_{12} & \dot{\theta}_{22} & \dot{\theta}_{32} & \dot{\theta}_{42} & \dot{\theta}_{52} \end{bmatrix}^T \tag{5.133}$$

and $\mathbf{A}$ and its terms are identical to eqs. (5.128) and (5.130), Jacobian matrices $\mathbf{B}_1$ and $\mathbf{B}_2$ can be written as

$$\mathbf{B}_1 = diag[b_{11}, b_{23}, b_{35}, b_{47}, b_{59}] \tag{5.134}$$

$$\mathbf{B}_2 = diag[b_{12}, b_{24}, b_{36}, b_{48}, b_{510}] \tag{5.135}$$

where $b_{i,2i-1}$, $b_{i,2i}$ are diagonal terms of $\mathbf{B}_1$ and $\mathbf{B}_2$, they can be expressed as

$$b_{i,2i-1} = (\mathbf{p}_i - \mathbf{b}_i')^T \mathbf{d}_{i,1}, \quad i = 1, \ldots, 5 \tag{5.136}$$

$$b_{i,2i} = (\mathbf{p}_i - \mathbf{b}_i')^T \mathbf{d}_{i,2}, \quad i = 1, \ldots, 5 \tag{5.137}$$

5.5.3   Kinetostatic Models

This mechanism is illustrated in Figure 5.1, the compliance matrix for the mechanism with rigid links can be written as

$$\mathbf{C}_c = \mathbf{J}_6(\mathbf{A}\mathbf{J}_6)^{-1}\mathbf{B}\mathbf{C}\mathbf{B}^T(\mathbf{A}\mathbf{J}_6)^{-T}\mathbf{J}_6^T \tag{5.138}$$

where

$$\mathbf{C} = diag[c_1, c_2, c_3, c_4, c_5] \tag{5.139}$$

with c_1, c_2, c_3, c_4 and c_5 the compliances of the actuators, and $\mathbf{J}_6$ is the Jacobian matrix of the passive constraining leg in this 5-dof case. Matrices $\mathbf{A}$ and $\mathbf{B}$ are the Jacobian matrices of the structure without the passive constraining leg.

Similarly, the stiffness matrix for the mechanism with flexible links can be written as

$$\mathbf{K} = (\mathbf{J}_6')^{-T}\mathbf{K}_6(\mathbf{J}_6')^{-1} + \mathbf{A}^T\mathbf{B}_1^{-T}\mathbf{K}_{j1}\mathbf{W}^{-1}\mathbf{A} \tag{5.140}$$

with

$$\mathbf{K}_6 = diag[0, k_{62}, 0, 0, 0, 0] \tag{5.141}$$

$$\mathbf{K}_{j1} = diag[k_{11}, k_{21}, k_{31}, k_{41}, k_{51}] \tag{5.142}$$

$$\mathbf{K}_{j2} = diag[k_{12}, k_{22}, k_{32}, k_{42}, k_{52}] \tag{5.143}$$

where $\mathbf{W}$ is defined in eq. (5.69) and k_{62} is the lumped stiffness of the passive constraining leg, $\mathbf{K}_{j1}$ includes the compound stiffness items of the actuated links and actuator's stiffnesses while $\mathbf{K}_{j2}$ only includes actuated link's stiffnesses, and $\mathbf{J}'_6$ is the Jacobian matrix of the passive constraining leg in this 5-dof case. Matrices $\mathbf{A}$ and $\mathbf{B}_1$, $\mathbf{B}_2$ are the Jacobian matrices of the structure without the passive constraining leg in this case with flexible links.

5.5.4 Implementation

An example is now given to illustrate the effect of the link flexibility on the parallel mechanism. The parameters used in this example are given as

$$\theta_p = 22.34°, \theta_b = 42.883°,$$

$$R_p = 18.18 \ cm, R_b = 33.3 \ cm,$$

$$K_i = -1, \quad i = 1, \ldots, 5$$

$$l_{i1} = 69.7 \ cm, l_{i2} = 51.52 \ cm, \quad i = 1, \ldots, 5$$

$$k_{i1} = 1000 \ Nm, \quad i = 1, \ldots, 5$$

$$k_{62} = 1000 \ Nm, \quad l_{61} = l_{62} = 103 \ cm$$

where k_{i1} is the actuator stiffness, K_i is the branch index, l_{61}, l_{62} are the passive leg's link length, l_{i1}, l_{i2} are the link lengths for the 1st and 2nd link of each leg and the Cartesian coordinates are given by

$$x \in [-3, 3] \ cm, y \in [-3, 3] \ cm, z = 103 \ cm,$$

$$\theta_{64} = -\pi, \theta_{65} = 2\pi/3,$$

The comparison between the parallel mechanism with rigid links (without virtual joints) and the parallel mechanism with flexible links (with virtual joints) is given in Figure 5.13, Tables 5.5 and 5.6. The results are similar to those obtained in the previous cases.
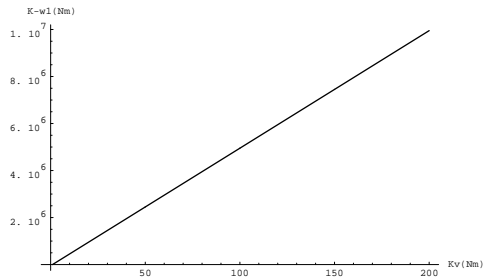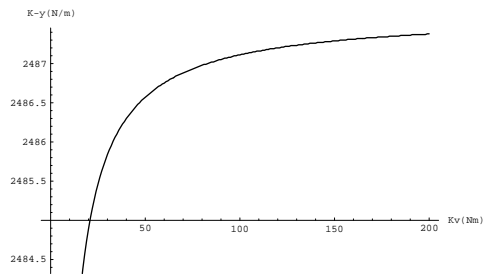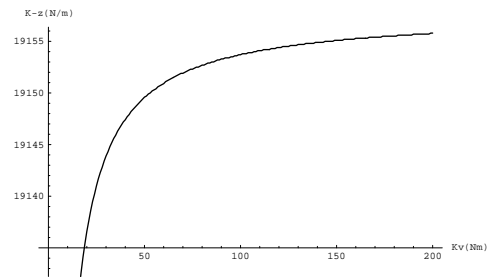
(a) Stiffness in θ_x
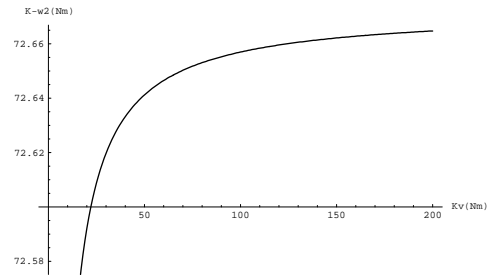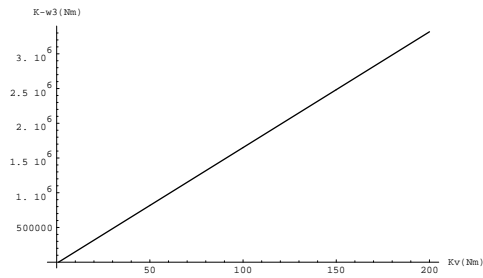
(b) Stiffness in θ_y
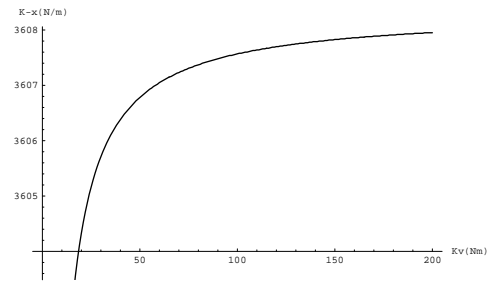
(c) Stiffness in θ_z

(d) Stiffness in x

(e) Stiffness in y

(f) Stiffness in z

Figure 5.13: Evolution of the stiffness as a function of the link's lumped stiffness in different directions.
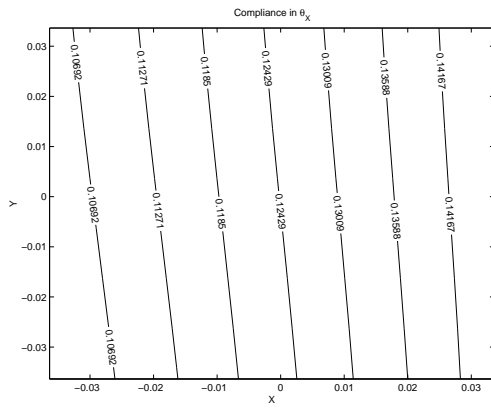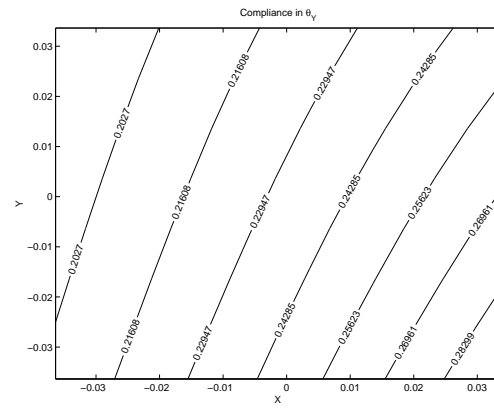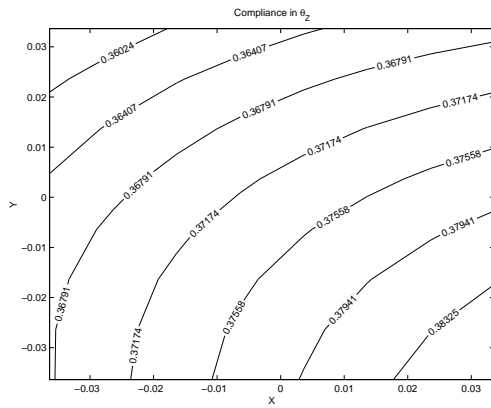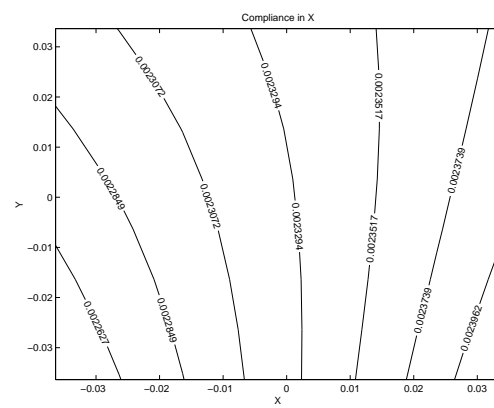
(a) Compliance in θ_x (1/Nm)

(b) Compliance in θ_y (1/Nm)

(c) Compliance in θ_z (1/Nm)
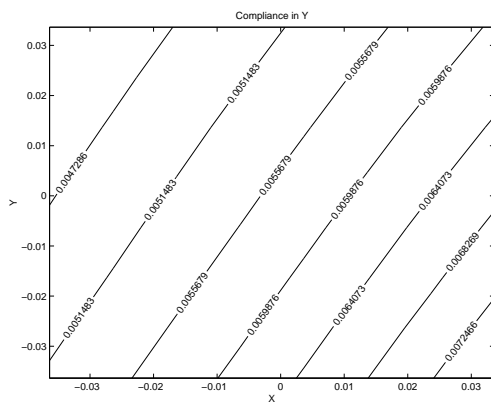
(d) Compliance in x (m/N)
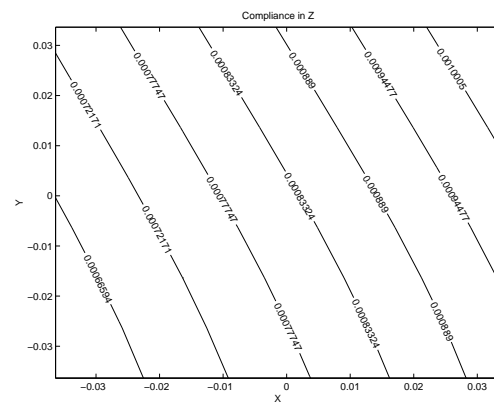
(e) Compliance in y (m/N)

(f) Compliance in z (m/N)

Figure 5.14: Compliance mappings of the spatial 5-dof parallel mechanism with revolute actuators (all length units in m).

Table 5.5: Comparison of the mechanism compliance between the mechanism with rigid links and the mechanism with flexible links.

$K_{actuator}$	K_{link}	κ_{θ_x}	κ_{θ_y}	κ_{θ_z}	κ_x	κ_y	κ_z
1000	1000	0.255808	0.478997	0.766154	0.00479741	0.0116413	0.00169207
1000	$10^1 K_a$	0.137552	0.257339	0.412528	0.00257412	0.00625667	0.000910745
1000	$10^2 K_a$	0.125726	0.235173	0.377165	0.0023518	0.0057182	0.000832613
1000	$10^3 K_a$	0.124543	0.232956	0.373629	0.00232956	0.00566435	0.000824799
1000	$10^4 K_a$	0.124425	0.232734	0.373275	0.00232734	0.00565897	0.000824018
1000	$10^5 K_a$	0.124413	0.232712	0.37324	0.00232712	0.00565843	0.00082394
1000	$10^6 K_a$	0.124412	0.23271	0.373236	0.00232709	0.00565838	0.000823932
1000	$10^7 K_a$	0.124412	0.23271	0.373236	0.00232709	0.00565837	0.000823931
1000	rigid	0.124412	0.23271	0.373236	0.00232709	0.00565837	0.000823931

5.5.5 Design Guidelines

Given a certain configuration of the mechanism ($x = 0, y = 0, z = 68, \theta_{64} = -\pi, \theta_{65} = 2\pi/3$), one can find its Cartesian stiffnesses in all directions as the function of actuator stiffness and link stiffness, they are

$$K_{\theta_x} = \frac{26.51898\lambda K_{b2}(1858 + 1.57723 \times 10^{-2}\lambda^4 + 1.17094\lambda^3 + 33\lambda^2 + 402\lambda)}{(286914 + 0.142572\lambda^5 + 13.0695\lambda^4 + 477.977\lambda^3 + 8700\lambda^2 + 79200\lambda)}$$
$$+ K_{62} \tag{5.144}$$

$$K_{\theta_y} = \frac{2.258838\lambda K_{b2}(27820 + 0.24232\lambda^4 + 17.9065\lambda^3 + 495\lambda^2 + 6069\lambda)}{(286914 + 0.142572\lambda^5 + 13.0695\lambda^4 + 477.977\lambda^3} \tag{5.145}$$

$$K_{\theta_z} = \frac{1.224386\lambda K_{b2}(27820 + 0.24232\lambda^4 + 17.9065\lambda^3 + 495\lambda^2 + 6069\lambda)}{(286914 + 0.142572\lambda^5 + 13.0695\lambda^4 + 477.977\lambda^3}$$
$$+ 0.333333K_{62} \tag{5.146}$$

$$K_x = \frac{111.65681\lambda K_{b2}(27820 + 0.242321\lambda^4 + 17.9065\lambda^3 + 495\lambda^2 + 6069\lambda)}{(286914 + 0.142572\lambda^5 + 13.0695\lambda^4 + 477.977\lambda^3} \tag{5.147}$$

$$K_y = \frac{77.312363\lambda K_{b2}(27820 + 0.242321\lambda^4 + 17.9065\lambda^3 + 495\lambda^2 + 6069\lambda)}{(286914 + 0.142572\lambda^5 + 13.0695\lambda^4 + 477.977\lambda^3} \tag{5.148}$$

$$K_z = \frac{594.198\lambda K_{b2}(27820 + 0.242321\lambda^4 + 17.9065\lambda^3 + 495\lambda^2 + 6069\lambda)}{(286914 + 0.142572\lambda^5 + 13.0695\lambda^4 + 477.977\lambda^3} \tag{5.149}$$

$$\lambda = \frac{K_a K_{b1}}{(K_a + K_{b1})K_{b2}} \tag{5.150}$$

where K_a represents the stiffness of actuators and K_{b1}, K_{b2} represent 1st and 2nd link's stiffness of the actuated leg, K_{62} represents the first (from bottom to platform) link's

Table 5.6: The stiffness effect of the passive constraining leg.

$K_{actuator}$	K_{link}	$K_{passive}$	K_{θ_x}	K_{θ_y}	K_{θ_z}	K_x	K_y	K_z
1000	$10^2 K_a$	1000	1701.29	605.472	645.359	3213.34	2553.71	17568.7
1000	$10^2 K_a$	$10^1 K_a$	10701.3	605.472	3645.36	3213.34	2553.71	17568.7
1000	$10^2 K_a$	$10^2 K_a$	100701	605.472	33645.4	3213.34	2553.71	17568.7
1000	$10^2 K_a$	$10^3 K_a$	10^6	605.472	333645	3213.34	2553.71	17568.7
1000	$10^2 K_a$	$10^4 K_a$	10^7	605.472	3.33365×10^6	3213.34	2553.71	17568.7
1000	$10^2 K_a$	$10^5 K_a$	10^8	605.472	3.33336×10^7	3213.34	2553.71	17568.7
1000	$10^2 K_a$	$10^6 K_a$	10^9	605.472	3.33334×10^8	3213.34	2553.71	17568.7
1000	$10^2 K_a$	$10^7 K_a$	10^{10}	605.472	3.33333×10^9	3213.34	2553.71	17568.7

stiffness of the passive constraining leg.

Based on the results of the preceding section and the expression of eqs. (5.144) – (5.149), the following design guidelines can be established and as reference for designing such kind of mechanisms.

1. The stiffnesses (except K_{θ_z}) are increasing with the increase of actuator stiffness, actuated link stiffness and the passive constraining leg's rigidity, and there is a critical stiffness value for the actuated flexible links to keep the structure virtually rigid. In this case, the passive constraining leg affects the stiffness around the X axis since the platform is not in the horizontal position, the projections of the direction which is orthogonal to the Hooke joint located at the platform are in the XY and XZ planes, when the Hooke joint at platform limits the rotation around the Z axis, it also limits the rotation around the X axis.

2. The limitation of the platform's rotation around the Z axis is dependent on the stiffnesses of the actuators, actuated links and of passive constraining leg's.

3. From the equations, one can find that the stiffness along the Z axis is the largest one among all the directions, and K_{θ_x} is larger than K_{θ_y} (in the reference configuration).

4. For a certain platform size, the larger the link length is, the smaller the global

stiffness values will be in all directions.

5. For a given link length, the larger the platform size (within a certain range, less than the size of the base platform), the larger the torsional stiffness values around the X and Y axes, and the smaller the stiffness values along the X and Y axes.

6. From Figure 5.13 and Table 5.5, one can see that K_{θ_z} is approaching infinite while the flexible links are approaching rigid, which corresponds to the motions prevented by the passive constraining leg. K_{θ_x} is also large enough because of the structure of the passive constraining leg. The stiffness in Z is higher near the center of the workspace, which is the best position for supporting vertical loads along the Z axis. All these results can be obviously observed.

5.6   Conclusions

A new type of n-DOF parallel mechanism with one passive constraining leg is presented in this chapter. This type of architecture can be used in several applications including machine tools. The kinematic analysis of this class of spatial parallel n-degree-of-freedom mechanisms has been presented. The geometric configurations of the mechanisms have first been shown. In this chapter, mechanisms with revolute actuators have been considered. Solutions for the inverse kinematic problem have been given. The Jacobian matrices obtained have been used to establish the kinetostatic model of the mechanisms. The lumped models of the link and joint compliances have been used for the study of the Cartesian compliance. It has been shown that the kinetostatic analysis can be used to assess the stiffness properties of this family of mechanisms. Finally, examples have been investigated and numerical results have been obtained, the results clearly demonstrate the relevance of the kinetostatic analysis in the context of design of such mechanisms.

Additionally, there exist some common design guidelines for this series of mechanisms, they are

1. With the increase of link stiffnesses, the mechanism's compliance is very close to that of the mechanism with rigid links. This suggests that one can assume

the flexible mechanism to be rigid only if the link stiffness reaches a high value $(10^7 K_{actuator})$.

2. The passive constraining leg's lumped stiffness(es) does not affect all directional stiffnesses, it plays a very important role in limiting the platform's motion to the desired ones.

3. The limitation of the platform's degrees of freedom are dependent on the actuator stiffness and link stiffness.

4. If the passive constraining leg's stiffness(es) is fixed as the same value as actuator's (e.g. 1000), then it cannot adequately limit the motion to the desired degree of freedom. Only if the passive constraining leg's lumped stiffness(es) is large enough $(10^2 K_{actuator})$, then it begins to efficiently play the role of limiting the platform motions to the desired ones.

Chapter 6

Kinetostatic Analysis of Spatial Fully-Parallel 6-dof Mechanisms

6.1 Introduction

This chapter presents the kinetostatic modeling and the stiffness analysis of spatial fully-parallel 6-dof mechanisms. The lumped models for the joints and links have been introduced in Sections 3.3.2 and 4.2.2. According to these models, the compliance of the links can be replaced by virtual compliant joints and rigid links. Two different methods are presented for the derivation of the stiffness equations suitable respectively for rigid model and flexible model, and the corresponding Jacobian matrices are derived. The variation of the link parameters is then briefly discussed. Finally, stiffness contour graphs are obtained using the stiffness equations and examples are given to

illustrate the results. It is shown that if the link stiffnesses are large enough, then the stiffness of the parallel mechanism with flexible links is very close to that of the parallel mechanism with rigid links which suggests that one can rely on this model to estimate and improve the stiffness of the flexible mechanism. Spatial six-degree-of-freedom parallel mechanisms can be used in several robotic applications as well as in machine tools. The stiffness analysis and the determination of the most rigid areas of the mechanism's workspace are very important design issues. In this chapter, examples of 3-leg and 6-leg fully-parallel mechanisms with revolute actuators and 6-leg fully-parallel mechanism with prismatic actuators are given respectively. The objective is also to provide some comparative results for the mechanisms analyzed in the previous chapters.

6.2 Spatial Six-Degree-of-Freedom Mechanisms with Prismatic Actuators

6.2.1 Geometric Modeling and Inverse Kinematics

A 6-dof parallel mechanism and its joint distributions both on the base and on the platform are shown in Figures 6.1, 6.2 and 6.3. This mechanism consists of six identical variable length links, connecting the fixed base to a moving platform. The kinematic chains associated with the six legs, from base to platform, consist of a fixed Hooke joint, a moving link, an actuated prismatic joint, a second moving link and a spherical joint attached to the platform. It is also assumed that the vertices on the base and on the platform are located on circles of radii R_b and R_p, respectively.

A fixed reference frame $O - xyz$ is connected to the base of the mechanism and a moving coordinate frame $P - x'y'z'$ is connected to the platform. In Figure 6.2, the points of attachment of the actuated legs to the base are represented with B_i and the points of attachment of all legs to the platform are represented with P_i, with $i = 1, \ldots, 6$, while point P is located at the center of the platform with the coordinate of $P(x, y, z)$.

The Cartesian coordinates of the platform are given by the position of point P with respect to the fixed frame, and the orientation of the platform (orientation of frame
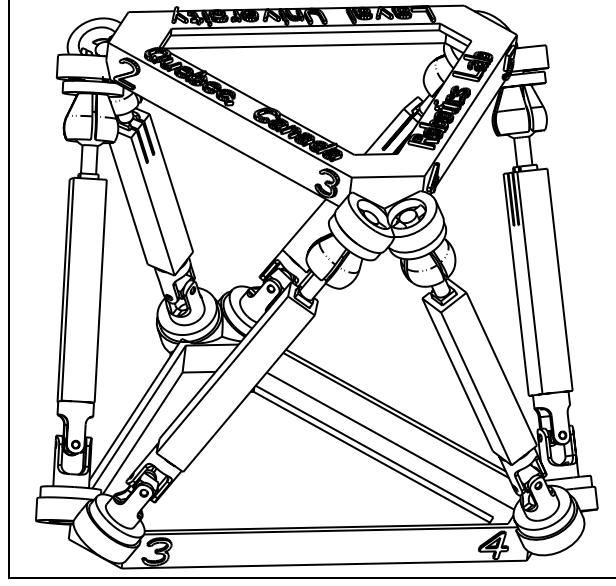
Figure 6.1: CAD model of the spatial 6-dof parallel mechanism with prismatic actuators (Figure by Thierry Laliberté and Gabriel Coté).

$P - x'y'z'$ with respect to the fixed frame), represented by three Euler angles ϕ, θ and ψ or by the rotation matrix $\mathbf{Q}$.

If the coordinates of point B_i in the fixed frame are represented by vector $\mathbf{b}_i$, then we have

$$\mathbf{p}_i = \begin{bmatrix} x_i \\ y_i \\ z_i \end{bmatrix}, \quad \mathbf{r}'_i = \begin{bmatrix} R_p \cos\theta_{pi} \\ R_p \sin\theta_{pi} \\ 0 \end{bmatrix}, \quad \mathbf{p} = \begin{bmatrix} x \\ y \\ z \end{bmatrix}, \quad \mathbf{b}_i = \begin{bmatrix} R_b \cos\theta_{bi} \\ R_b \sin\theta_{bi} \\ 0 \end{bmatrix} \quad (6.1)$$

where $\mathbf{p}_i$ is the position vector of point P_i expressed in the fixed coordinate frame whose coordinates are defined as (x_i, y_i, z_i), $\mathbf{r}'_i$ is the position vector of point P_i expressed in the moving coordinate frame, and $\mathbf{p}$ is the position vector of point P expressed in the fixed frame as defined above, and

$$\boldsymbol{\theta}_{bi} = \begin{bmatrix} \theta_{b1} \\ \theta_{b2} \\ \theta_{b3} \\ \theta_{b4} \\ \theta_{b5} \\ \theta_{b6} \end{bmatrix} = \begin{bmatrix} \theta_b \\ 2\pi/3 - \theta_b \\ 2\pi/3 + \theta_b \\ 4\pi/3 - \theta_b \\ 4\pi/3 + \theta_b \\ -\theta_b \end{bmatrix}, \quad \boldsymbol{\theta}_{pi} = \begin{bmatrix} \theta_{p1} \\ \theta_{p2} \\ \theta_{p3} \\ \theta_{p4} \\ \theta_{p5} \\ \theta_{p6} \end{bmatrix} = \begin{bmatrix} \theta_p \\ 2\pi/3 - \theta_p \\ 2\pi/3 + \theta_p \\ 4\pi/3 - \theta_p \\ 4\pi/3 + \theta_p \\ -\theta_p \end{bmatrix} \quad (6.2)$$
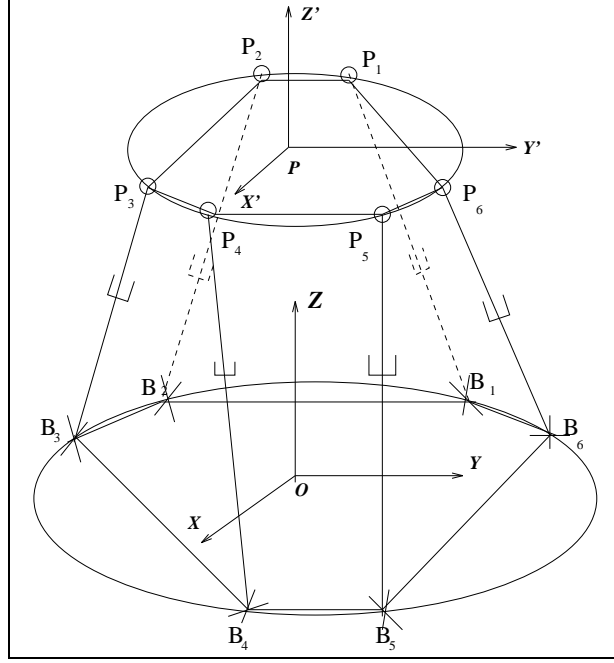
Figure 6.2: Schematic representation of the spatial 6-dof parallel mechanism with prismatic actuators.

Similarly to the procedures in Section 4.2.3, the solution of the inverse kinematic of this mechanism can be written as

$$\rho_i^2 = (\mathbf{p}_i - \mathbf{b}_i)^T (\mathbf{p}_i - \mathbf{b}_i), \quad i = 1, \ldots, 6 \tag{6.3}$$

6.2.2 Global Velocity Equation

Since the mechanism is actuated in parallel, its global velocity equation can be obtained using the same method as in Section 4.2.5. Based on eqs. (4.18) – (4.23), one has the velocity equation as

$$\mathbf{A}\mathbf{t} = \mathbf{B}\dot{\boldsymbol{\rho}} \tag{6.4}$$

where vectors $\dot{\boldsymbol{\rho}}$ and $\mathbf{t}$ are defined as

$$\dot{\boldsymbol{\rho}} = \begin{bmatrix} \dot{\rho}_1 & \ldots & \dot{\rho}_6 \end{bmatrix}^T \tag{6.5}$$

$$\mathbf{t} = \begin{bmatrix} \boldsymbol{\omega}^T & \dot{\mathbf{p}}^T \end{bmatrix}^T \tag{6.6}$$
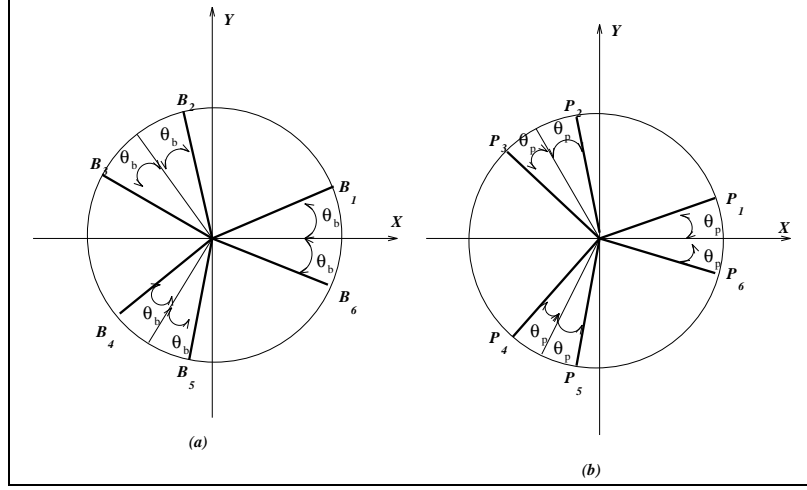
Figure 6.3: Position of the attachment points: (a)on the base, (b)on the platform.

where $\boldsymbol{\omega}$ and $\dot{\mathbf{p}}$ are the angular velocity and velocity of one point of the platform, respectively, and

$$\mathbf{A} = \begin{bmatrix} \mathbf{m}_1 & \mathbf{m}_2 & \mathbf{m}_3 & \mathbf{m}_4 & \mathbf{m}_5 & \mathbf{m}_6 \end{bmatrix}^T \tag{6.7}$$

$$\mathbf{B} = diag[\rho_1, \rho_2, \rho_3, \rho_4, \rho_5, \rho_6] \tag{6.8}$$

and $\mathbf{m}_i$ is a six-dimensional vector expressed as

$$\mathbf{m}_i = \begin{bmatrix} (\mathbf{Q}\mathbf{r}'_i) \times (\mathbf{p}_i - \mathbf{b}_i) \\ (\mathbf{p}_i - \mathbf{b}_i) \end{bmatrix} \tag{6.9}$$

Therefore, Jacobian matrix $\mathbf{J}$ can be written as

$$\mathbf{J} = \mathbf{B}^{-1}\mathbf{A} \tag{6.10}$$

The derivation of the relationship between Cartesian velocities and joint rates is thereby completed.

6.2.3   Stiffness Model

Since the mechanism is fully parallel, the stiffness of the mechanism has been obtained in Section 3.2

$$\mathbf{K} = \mathbf{J}^T \mathbf{K}_J \mathbf{J} \tag{6.11}$$

6.2.4   Implementation and Results

Given the geometric properties as

$$\theta_p = 22.34°, \theta_b = 42.883°,$$

$$R_p = 6 \ cm, R_b = 15 \ cm,$$

$$K_i = -1, \quad i = 1, \ldots, 6$$

$$k_{i1} = 1000 \ N/m, \quad i = 1, \ldots, 6$$

where k_{i1} is the actuator stiffness, and the Cartesian coordinates are given by

$$x \in [-4, 4] \ cm, y \in [-4, 4] \ cm, z = 51 \ cm,$$

$$\phi = 0, \theta = 0, \psi = 0,$$

The stiffness model described above is now used to obtain the stiffness mappings. Figure 6.4 shows the stiffness mappings on a section of the workspace of the platform. From such plots one can determine which regions of the workspace will satisfy some stiffness criteria.

Another example of mechanism is the INRIA "left-hand" prototype described in (Gosselin 1990). The dimensions are given in Table 6.1, the stiffness mappings and mesh graphs are illustrated in Figures 6.5 and A.11, the results show the same trends of stiffness as in (Gosselin 1990).

Table 6.1: Geometric properties of the INRIA prototype (all lengths are in centimeters)

i	1	2	3	4	5	6
b_{ix}	9.258	13.258	4.000	-4.000	-13.258	-9.258
b_{iy}	9.964	3.036	-13.000	-13.000	3.036	9.964
b_{iz}	2.310	2.310	2.310	2.310	2.310	2.310
x_i	3.000	7.822	4.822	-4.822	-7.822	-3.000
y_i	7.300	-1.052	-6.248	-6.248	-1.052	7.300
z_i	-3.710	-3.710	-3.710	-3.710	-3.710	-3.710
L_i	51	51	51	51	51	51
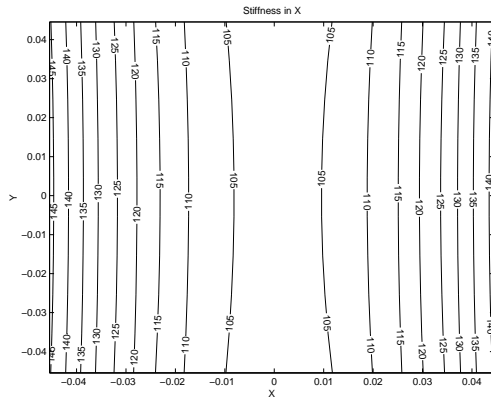
(a) Stiffness in x (N/m)
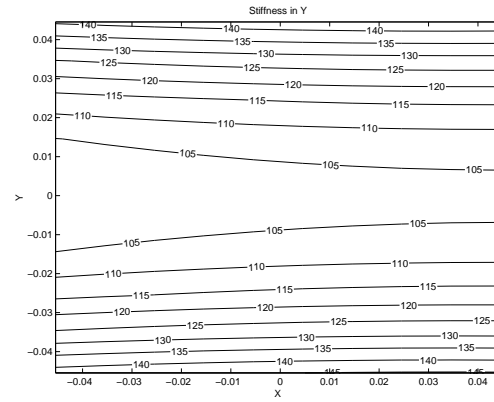
(b) Stiffness in y (N/m)
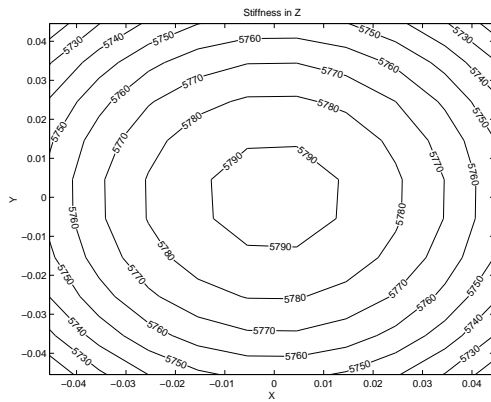
(c) Stiffness in z (N/m)
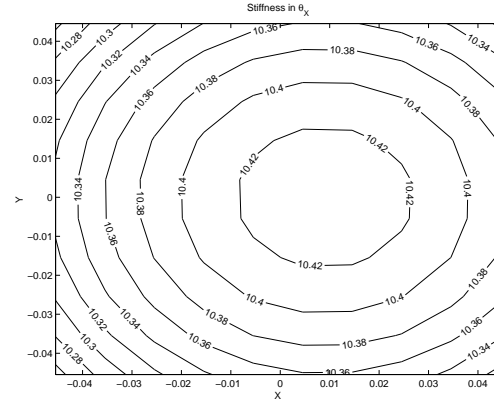
(d) Stiffness in θ_x (Nm)
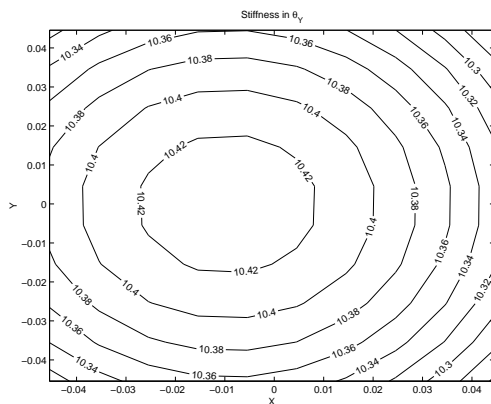
(e) Stiffness in θ_y (Nm)
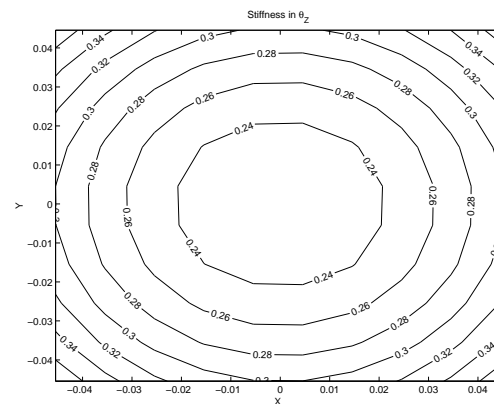
(f) Stiffness in θ_z (Nm)

Figure 6.4: Stiffness mappings of the spatial 6-dof parallel mechanism with prismatic actuators (all length units in m).
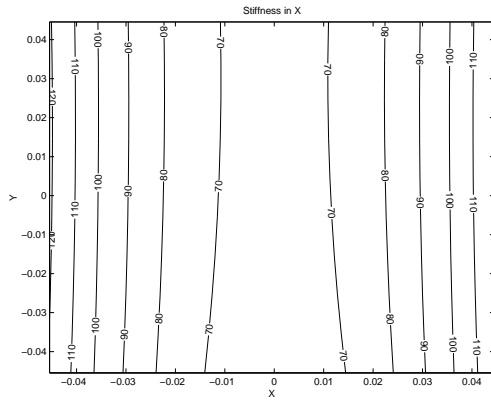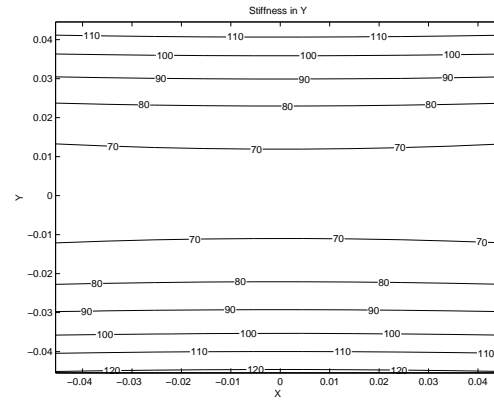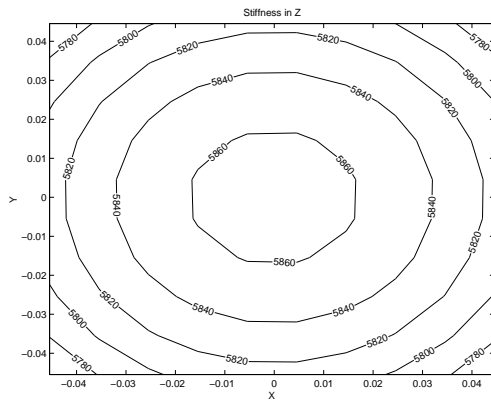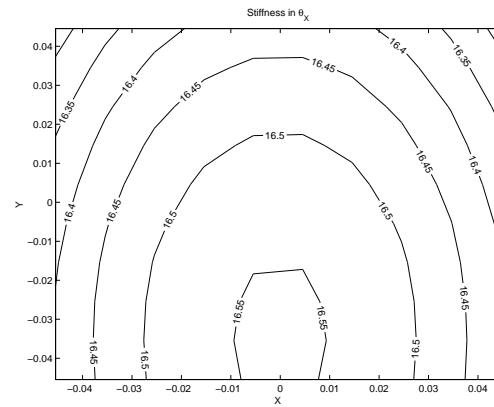
(a) Stiffness in x (N/m)

(b) Stiffness in y (N/m)

(c) Stiffness in z (N/m)

(d) Stiffness in θ_x (Nm)
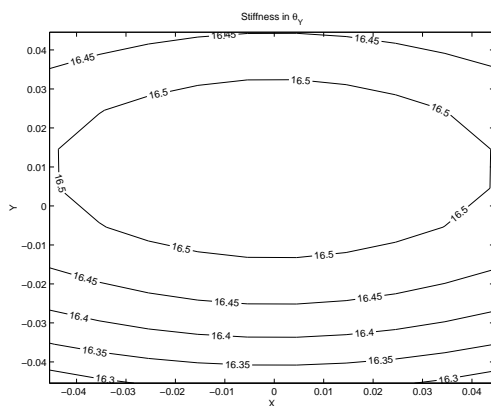
(e) Stiffness in θ_y (Nm)
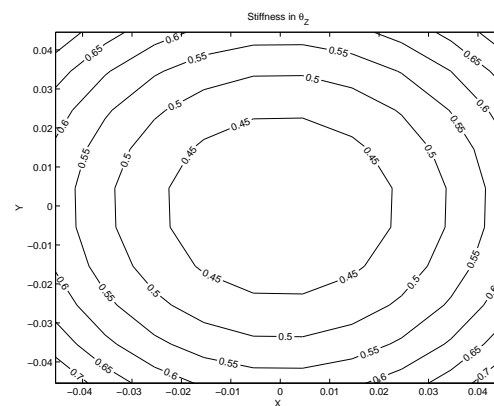
(f) Stiffness in θ_z (Nm)

Figure 6.5: Stiffness mappings of the spatial 6-dof parallel mechanism with prismatic actuators (using data of INRIA prototype) (all length units in m).

From the graphs, one observes that K_{θ_x} and K_{θ_y}, K_x and K_y are symmetric with respect to each other, and in Figure 6.4(a) the stiffness in X becomes higher when the platform moves further from the Y axis. This was to be expected because when the platform moves aside along the X axis, the projection of the legs on this axis becomes larger, and the mechanism is stiffer in Y. The same reasoning applies to Figure 6.4(b) for the stiffness in Y.

In Figures 6.4(d) and 6.4(e), the torsional stiffnesses in θ_x and θ_y are shown, the stiffness is larger when it moves further from the Y axis. In Figure 6.4(c) the stiffness in Z is higher near the center of the workspace, which is the best position for supporting vertical loads. It can also be noted that the stiffness in Z is much larger than the stiffness in the X or Y directions. This is due to the architecture chosen, which aims at supporting heavy objects in an environment where the gravity is acting along the negative direction of Z axis. All these are in accordance with what would be intuitively expected.

Table 6.2 shows the variation of the stiffness with $K_{actuator}$. Clearly, the Cartesian stiffnesses in each direction are increased with the improvement of the actuator stiffness.

Table 6.2: The Cartesian stiffness as a function of the actuator stiffness.

$K_{actuator}$	K_x	K_y	K_z	K_{θ_x}	K_{θ_y}	K_{θ_z}
200	20.5936	20.5936	1158.81	2.08586	2.08586	0.0444375
600	61.7809	61.7809	3476.44	6.25759	6.25759	0.133313
1000	102.968	102.968	5794.06	10.4293	10.4293	0.222188
2000	205.936	205.936	11588.1	20.8586	20.8586	0.444375
3000	308.904	308.904	17382.2	31.2879	31.2879	0.666563
4000	411.872	411.872	23176.3	41.7173	41.7173	0.888751
6000	617.809	617.809	34764.4	62.5759	62.5759	1.33313

6.3 Spatial Six-Degree-of-Freedom Mechanisms with Revolute Actuators

6.3.1 Geometric Modeling

Figures 6.6 and 6.7 represent a 6-dof parallel mechanism with revolute actuators. The joint distribution is the same as in Figure 6.3. This mechanism consists of six actuated legs with identical topology, connecting the fixed base to a moving platform. The kinematic chains consist — from base to platform — of an actuated revolute joint, a moving link, a Hooke joint, a second moving link and a spherical joint attached to the platform.
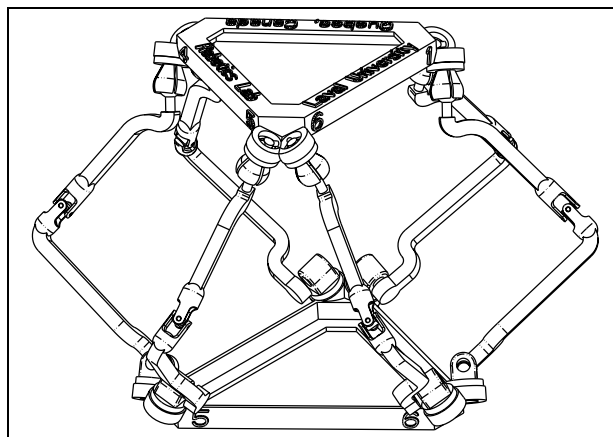
Figure 6.6: CAD model of the spatial 6-dof parallel mechanism with revolute actuators (Figure by Thierry Laliberté and Gabriel Coté).

6.3.2 Global Velocity Equations

6.3.2.1 Rigid Model

A fixed reference frame $O - xyz$ is connected to the base of the mechanism and a moving coordinate frame $P - x'y'z'$ is connected to the platform. We use the same Cartesian coordinates of the platform P as in Section 6.2 and the orientation of the platform (orientation of frame $P - x'y'z'$ with respect to the fixed frame), represented by three Euler angles ϕ, θ and ψ or by the matrix $\mathbf{Q}$.
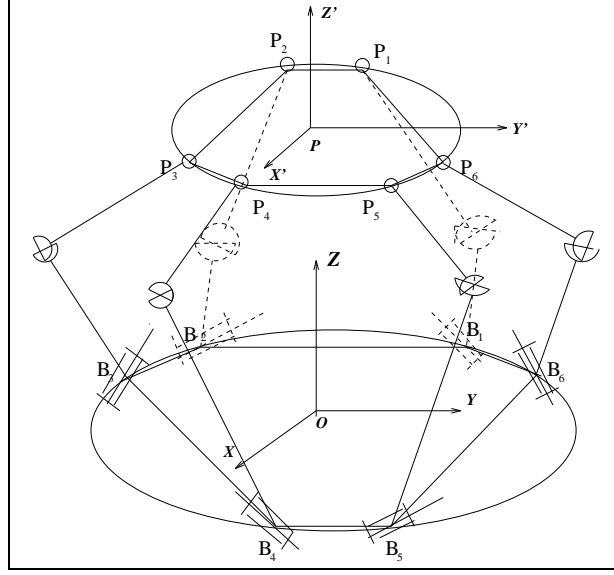
Figure 6.7: Schematic representation of the spatial 6-dof parallel mechanism with revolute actuators.

Based on the same inverse kinematics as in Section 5.2.2 and eqs. (5.1) – (5.34), one obtains the global velocity equation as

$$\mathbf{A}\mathbf{t} = \mathbf{B}\dot{\boldsymbol{\theta}} \tag{6.12}$$

where vectors $\dot{\boldsymbol{\theta}}$ and $\mathbf{t}$ are defined as

$$\dot{\boldsymbol{\theta}} = \begin{bmatrix} \dot{\theta}_1 & \dots & \dot{\theta}_6 \end{bmatrix}^T \tag{6.13}$$

$$\mathbf{t} = \begin{bmatrix} \boldsymbol{\omega}^T & \dot{\mathbf{p}}^T \end{bmatrix}^T \tag{6.14}$$

and

$$\mathbf{A} = \begin{bmatrix} \mathbf{m}_1 & \mathbf{m}_2 & \mathbf{m}_3 & \mathbf{m}_4 & \mathbf{m}_5 & \mathbf{m}_6 \end{bmatrix}^T \tag{6.15}$$

$$\mathbf{B} = diag[(\mathbf{p}_1 - \mathbf{b}'_1)^T \mathbf{e}_1, (\mathbf{p}_2 - \mathbf{b}'_2)^T \mathbf{e}_2, (\mathbf{p}_3 - \mathbf{b}'_3)^T \mathbf{e}_3,$$
$$(\mathbf{p}_4 - \mathbf{b}'_4)^T \mathbf{e}_4, (\mathbf{p}_5 - \mathbf{b}'_5)^T \mathbf{e}_5, (\mathbf{p}_6 - \mathbf{b}'_6)^T \mathbf{e}_6] \tag{6.16}$$

and $\mathbf{m}_i$ is a six-dimensional vector expressed as

$$\mathbf{m}_i = \begin{bmatrix} (\mathbf{Q}\mathbf{r}'_i) \times (\mathbf{p}_i - \mathbf{b}'_i) \\ (\mathbf{p}_i - \mathbf{b}'_i) \end{bmatrix}, \quad i = 1, \dots, 6 \tag{6.17}$$

and again, the Jacobian matrix $\mathbf{J}$ can be written as

$$\mathbf{J} = \mathbf{B}^{-1}\mathbf{A} \tag{6.18}$$

6.3.2.2 Compliant Model

Figure 5.4 represents one of the kinematic chains for the 6-dof parallel mechanism above. Based on eqs. (5.17) – (5.19) in Section 5.2.2.2, one can find θ_{i3} and θ_{i4} easily. Similarly to Section 5.2.2.2, one can obtain the global velocity equation as

$$\mathbf{At} = \mathbf{B}\dot{\boldsymbol{\theta}} \qquad (6.19)$$

where vector $\dot{\boldsymbol{\theta}}$ is defined as

$$\dot{\boldsymbol{\theta}} = \begin{bmatrix} \dot{\theta}_{11} & \dot{\theta}_{12} & \dot{\theta}_{21} & \dot{\theta}_{22} & \dot{\theta}_{31} & \dot{\theta}_{32} & \dot{\theta}_{41} & \dot{\theta}_{42} & \dot{\theta}_{51} & \dot{\theta}_{52} & \dot{\theta}_{61} & \dot{\theta}_{62} \end{bmatrix}^T \qquad (6.20)$$

matrix $\mathbf{A}$ and its terms are as given in eqs. (6.15) and (6.17) and

$$\mathbf{B}_{6\times 12} = \begin{bmatrix} b_{11} & b_{12} & 0 & 0 & 0 & 0 & 0 & 0 & 0 & 0 & 0 & 0 \\ 0 & 0 & b_{21} & b_{22} & 0 & 0 & 0 & 0 & 0 & 0 & 0 & 0 \\ 0 & 0 & 0 & 0 & b_{31} & b_{32} & 0 & 0 & 0 & 0 & 0 & 0 \\ 0 & 0 & 0 & 0 & 0 & 0 & b_{41} & b_{42} & 0 & 0 & 0 & 0 \\ 0 & 0 & 0 & 0 & 0 & 0 & 0 & 0 & b_{51} & b_{52} & 0 & 0 \\ 0 & 0 & 0 & 0 & 0 & 0 & 0 & 0 & 0 & 0 & b_{61} & b_{62} \end{bmatrix} \qquad (6.21)$$

where

$$b_{ij} = (\mathbf{p}_i - \mathbf{b}'_i)^T \mathbf{d}_{ij}, \quad i = 1, \ldots, 6, \quad j = 1, 2 \qquad (6.22)$$

The derivation of the relationship between Cartesian velocities and joint rates is thereby completed.

6.3.3 Stiffness Model of the Mechanism with Rigid Links

Again, the stiffness of the structure has been obtained in Section 3.2

$$\mathbf{K} = \mathbf{J}^T \mathbf{K}_J \mathbf{J} \qquad (6.23)$$

6.3.4 Kinetostatic Model of the Mechanism with Flexible Links

From eq. (6.12), one obtains

$$\mathbf{t} = \mathbf{J}' \dot{\boldsymbol{\theta}} \qquad (6.24)$$

where

$$\mathbf{J}' = \mathbf{A}^{-1}\mathbf{B} \tag{6.25}$$

according to the principle of virtual work, one has

$$\boldsymbol{\tau}^T \dot{\boldsymbol{\theta}} = \mathbf{w}^T \mathbf{t} \tag{6.26}$$

where $\boldsymbol{\tau}$ is a vector of the actuator torques applied at each actuated joint or joint with spring. If we assume that no gravitational forces act on any of the intermediate links, and $\mathbf{w}$ is a vector composed of forces and moments (hereafter called wrench) applied by the end-effector. Substituting eq. (6.24) into (6.26) one can obtain

$$\boldsymbol{\tau} = \mathbf{J}'^T \mathbf{w} \tag{6.27}$$

The joint forces and displacements of each joint can be related by Hooke's law, i.e.,

$$\boldsymbol{\tau} = \mathbf{K}_J \Delta \boldsymbol{\theta} \tag{6.28}$$

$\Delta\boldsymbol{\theta}$ only includes the actuated joints and joint with springs i.e.,

$$\mathbf{K}_J \Delta \boldsymbol{\theta} = \mathbf{J}'^T \mathbf{w} \tag{6.29}$$

hence

$$\Delta \boldsymbol{\theta} = \mathbf{K}_J^{-1} \mathbf{J}'^T \mathbf{w} \tag{6.30}$$

pre-multiplying by $\mathbf{J}'$ on both sides, one obtains

$$\mathbf{J}' \Delta \boldsymbol{\theta} = \mathbf{J}' \mathbf{K}_J^{-1} \mathbf{J}'^T \mathbf{w} \tag{6.31}$$

Substituting eq. (6.24) into eq. (6.31), one obtains

$$\mathbf{t} = \mathbf{J}' \mathbf{K}_J^{-1} \mathbf{J}'^T \mathbf{w} \tag{6.32}$$

therefore, one obtains the compliance matrix of the mechanism $\boldsymbol{\kappa}$ as follow

$$\boldsymbol{\kappa} = \mathbf{J}' \mathbf{K}_J^{-1} \mathbf{J}'^T \tag{6.33}$$

and the system stiffness matrix is

$$\mathbf{K} = \left[\mathbf{J}' \mathbf{K}_J^{-1} \mathbf{J}'^T\right]^{-1} \tag{6.34}$$

where

$$\mathbf{K}_J = diag[k_{11}, k_{12}, k_{21}, k_{22}, k_{31}, k_{32}, k_{41}, k_{42}, k_{51}, k_{52}, k_{61}, k_{62}] \tag{6.35}$$

where k_{i1} is stiffness of the ith actuator, and k_{i2} is the lumped stiffness of each leg.

6.3.5 Implementation and Results

In order to illustrate the effect of the flexible links on the parallel mechanism, an example of 6-dof mechanism is presented. The parameters for Figure 5.3 are given as

$$\theta_p = 22.34°, \theta_b = 42.883°,$$

$$R_p = 6\ cm, R_b = 15\ cm,$$

$$l_{i1} = 46\ cm, l_{i2} = 36\ cm, \quad i = 1, \ldots, 6$$

$$k_{i1} = 1000\ Nm, \quad i = 1, \ldots, 6$$

where k_{i1} is the stiffness of each leg, l_{i1}, l_{i2} are the link lengths for the 1st and 2nd link of each leg, and the Cartesian coordinates are given by

$$x \in [-3, 3]\ cm, y \in [-3, 3]\ cm, z = 68\ cm,$$

$$\phi = 0, \theta = 0, \psi = 0,$$

Figure 6.8 shows the variation of the stiffness for the above example. The comparison between the parallel mechanism with rigid link and the parallel mechanism with flexible links is given in Table 6.3. The results are similar to those obtained in previous cases.

Table 6.3: Comparison of the mechanism stiffness between the mechanism with rigid links and the mechanism with flexible links.

| $K_{actuator}$	K_{link}	K_x	K_y	K_z	K_{θ_x}	K_{θ_y}	K_{θ_z}
1000	1000	3700.65	3700.65	10082.1	18.1478	18.1478	20.633
1000	$10K_a$	6967.15	6967.15	18981.4	34.1665	34.1665	38.8454
1000	$100K_a$	7641.67	7641.67	20819.1	37.4743	37.4743	42.6062
1000	$1000K_a$	7716.37	7716.37	21022.6	37.8406	37.8406	43.0227
1000	$10000K_a$	7723.92	7723.92	21043.2	37.8777	37.8777	43.0648
1000	$100000K_a$	7724.68	7724.68	21045.2	37.8814	37.8814	43.069
1000	$1000000K_a$	7724.76	7724.76	21045.4	37.8818	37.8818	43.0694
1000	$10000000K_a$	7724.76	7724.76	21045.4	37.8818	37.8818	43.0695
1000	rigid	7724.76	7724.76	21045.4	37.8818	37.8818	43.0695
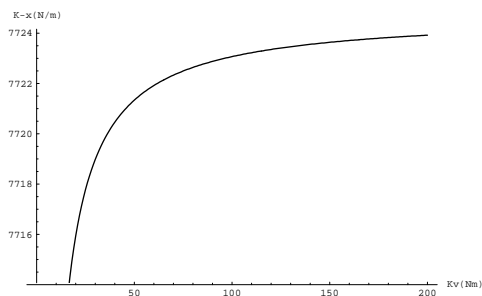
(a) Stiffness in x
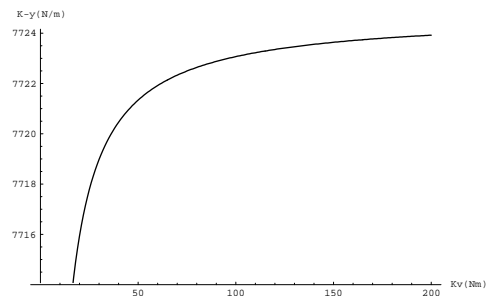
(b) Stiffness in y
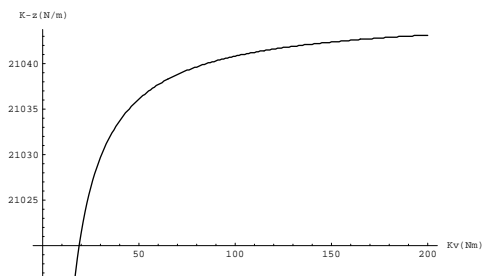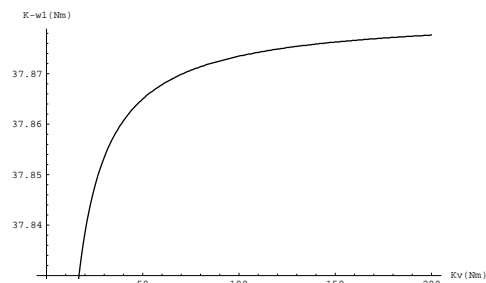
(c) Stiffness in z
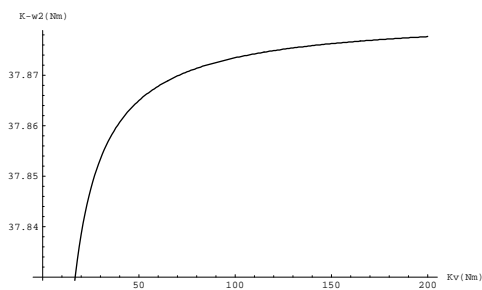
(d) Stiffness in θ_x
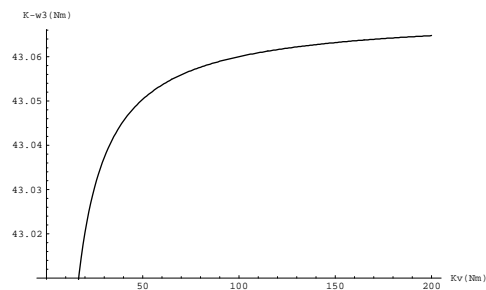
(e) Stiffness in θ_y

(f) Stiffness in θ_z

Figure 6.8: Evolution of the stiffness as a function of the link's lumped stiffness in different directions.

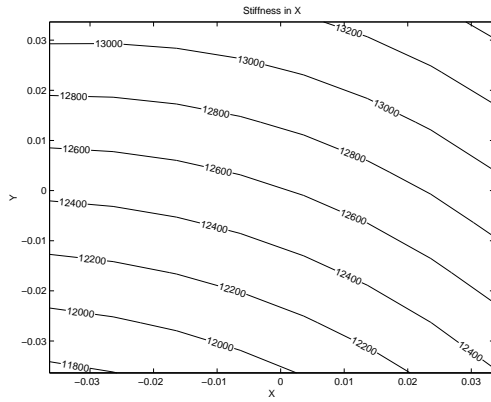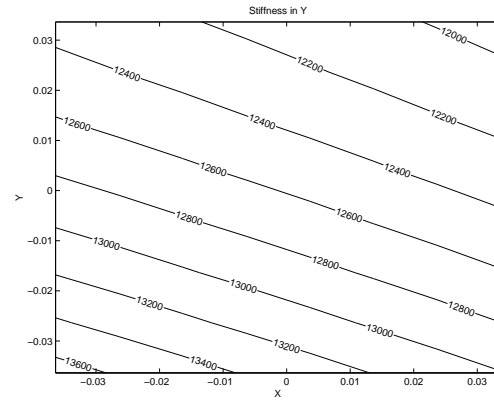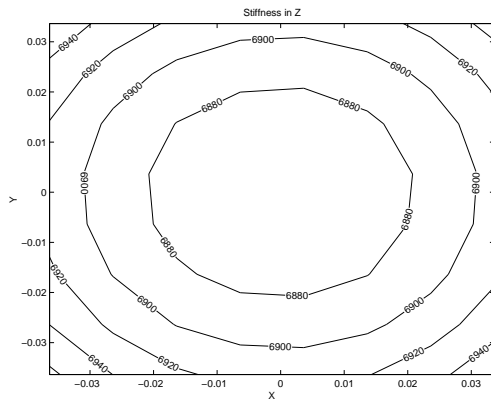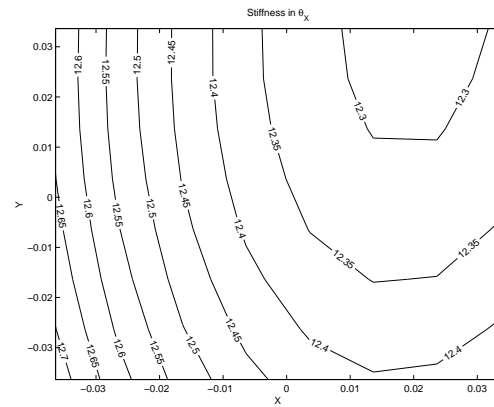(a) Stiffness in x (N/m)

(b) Stiffness in y (N/m)

(c) Stiffness in z (N/m)

(d) Stiffness in θ_x (Nm)
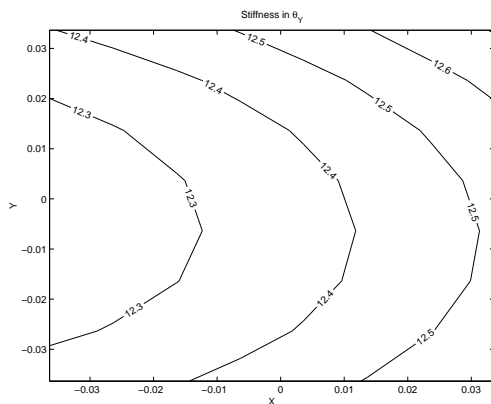
(e) Stiffness in θ_y (Nm)
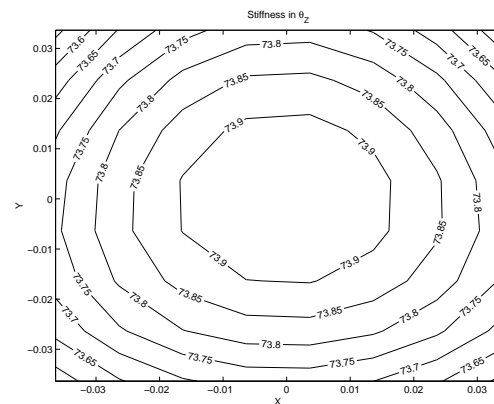
(f) Stiffness in θ_z (Nm)

Figure 6.9: Stiffness mappings of the spatial 6-dof parallel mechanism with revolute actuators (6 legs) (all length units in m).

From Figure 6.9, one can find that K_x and K_y, K_{θ_x} and K_{θ_y} are symmetric with respect to each other. In Figure 6.9(a), the stiffness in X becomes higher when the platform moves further from the Y axis. This was to be expected because when the platform moves aside along the X axis, the projection of the legs on this axis becomes larger, and the mechanism is stiffer in Y. And the same reasoning applies to Figure 6.9(b) for the stiffness in Y.

In Figures 6.9(d) and (e), the torsional stiffnesses in θ_x and θ_y are shown, the stiffness is larger when the platform moves further from the Y axis. However, in the center of the workspace, the K_z is at its minimum, and the stiffness in the Z becomes higher when the platform moves further from the center of the workspace. On the other hand, from Figure 6.9(f), the stiffness in θ_z is higher near the center of the workspace, which is the best position for supporting torsional loads around Z axis. All these are in accordance with what would be intuitively expected.

6.4 Six-Degree-of-Freedom Spatial Parallel Mechanisms with Three Legs

A 6-dof parallel mechanism with 3 legs is shown in Figure 6.10. This mechanism consists of three kinematic chains, connecting the fixed base to a moving platform, all the kinematic chains have the identical topology. In this 6-dof parallel mechanism, the kinematic chains associated with the three legs consist of a fixed revolute actuator, a moving link, then a second revolute actuator, a moving link, a revolute joint, a third moving link and a passive spherical joint attached to the platform.

6.4.1 Stiffness Model of the Mechanism with Rigid Links

6.4.1.1 Inverse Kinematics

From Figure 6.11, one can find θ_{i1} as

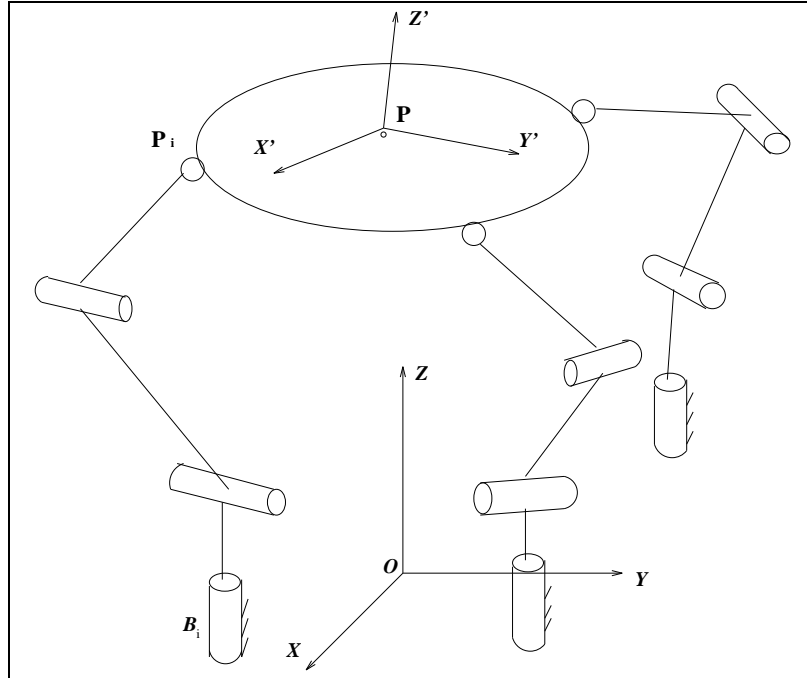$$\tan\theta_{i1} = \frac{y_i - y_{bi}}{x_i - x_{bi}} \quad i = 1, 2, 3 \tag{6.36}$$

Figure 6.10: Schematic representation of the 6-dof parallel mechanism with 3 legs.

where (x_{bi}, y_{bi}, z_{bi}) are the coordinates of point B_i while (x_i, y_i, z_i) are the coordinates of point P_i. Knowing θ_{i1}, one can obtain θ_{i2} from eq. (6.44)

$$\sin\theta_{i2} = \frac{B_{2i}C_{2i} + KA_{2i}\sqrt{A_{2i}^2 + B_{2i}^2 - C_{2i}^2}}{A_{2i}^2 + B_{2i}^2} \quad i = 1, 2, 3 \tag{6.37}$$

$$\cos\theta_{i2} = \frac{A_{2i}C_{2i} - KB_{2i}\sqrt{A_{2i}^2 + B_{2i}^2 - C_{2i}^2}}{A_{2i}^2 + B_{2i}^2} \quad i = 1, 2, 3 \tag{6.38}$$

where $K = \pm1$ is the branch index associated with the kinematic chain of the mechanism and where A_{2i}, B_{2i} and C_{2i} are defined in eqs. (6.45) to (6.47). Therefore, one can find the inverse kinematics from the equations above.

6.4.1.2   Global Velocity Equation

Figure 6.11 represents the ith actuated leg of the mechanism with two revolute actuators distributed in the first and second joint (from base). The Cartesian coordinates of point O_{i3} are expressed in the fixed coordinate frame and noted as (x_{i3}, y_{i3}, z_{i3}). Assuming that all the coordinates attached to the base actuators are in the same orientations with the fixed coordinates frame. Therefore, one has

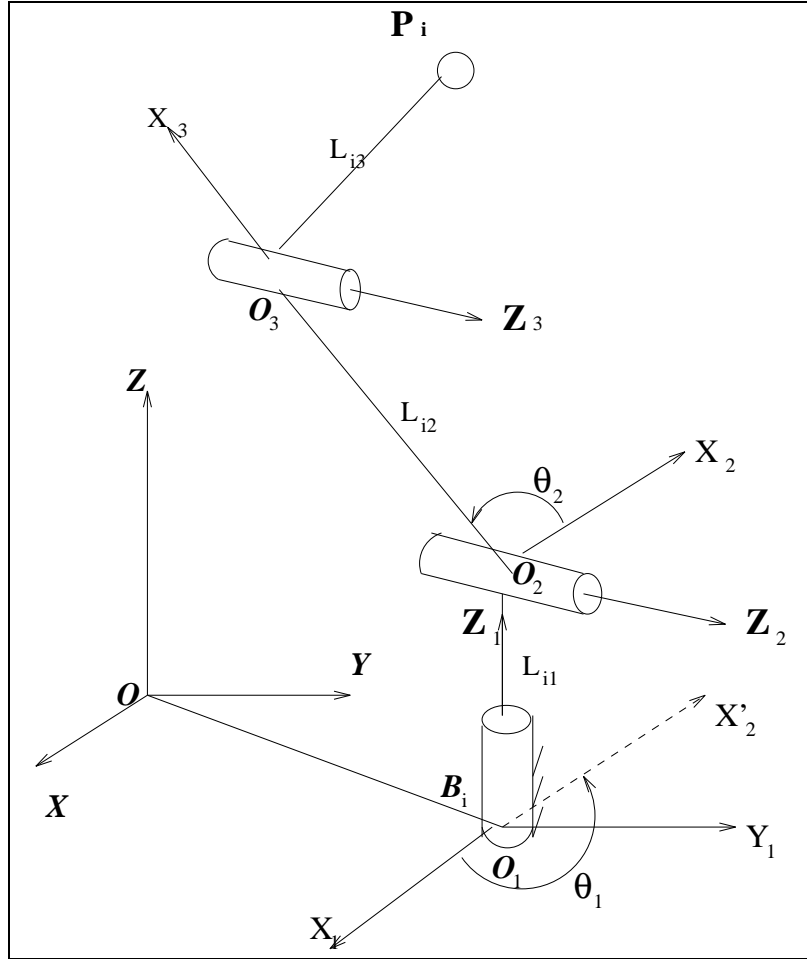$$x_{i3} = l_{i2}\cos\theta_{i2}\cos\theta_{i1} + x_{bi} \quad i = 1, 2, 3 \tag{6.39}$$

Figure 6.11: One of the kinematic chains with rigid links.

$$y_{i3} = l_{i2}\cos\theta_{i2}\sin\theta_{i1} + y_{bi} \quad i = 1, 2, 3 \tag{6.40}$$

$$z_{i3} = l_{i2}\sin\theta_{i2} + l_{i1} + z_{bi} \quad i = 1, 2, 3 \tag{6.41}$$

where θ_{i1}, θ_{i2} are the joint variables, i.e., rotation angle around the revolute joints defined by the DH nomenclature, and l_{i2} is the length of the second link of the ith leg. The coordinates of the base joints are given by $(x_{bi}, y_{bi}, z_{bi}, i = 1, 2, 3)$, from the geometry of the mechanism, one can write

$$(x_{i3} - x_i)^2 + (y_{i3} - y_i)^2 + (z_{i3} - z_i)^2 = l_{i3}^2 \tag{6.42}$$

where $x_i, y_i, z_i, (i = 1, 2, 3)$ have been previously defined as the coordinates of point P_i and l_{i3} is the length of the third link of each leg. Substituting eqs. (6.39) – (6.41) into eq. (6.42), one obtains the equation as

$$2l_{i2}\cos\theta_{i2}\cos\theta_{i1}(x_{bi} - x_i) + 2l_{i2}\sin\theta_{i1}\cos\theta_{i2}(y_{bi} - y_i) + 2l_{i2}\sin\theta_{i2}(z_{bi} + l_{i1} - z_i)$$

$$= l_{i3}^2 - l_{i2}^2 - (x_{bi} - x_i)^2 - (y_{bi} - y_i)^2 - (z_{bi} + l_{i1} - z_i)^2 \tag{6.43}$$

This equation can be rewritten as

$$A_{2i} \cos \theta_{i2} + B_{2i} \sin \theta_{i2} = C_{2i} \quad i = 1, 2, 3 \tag{6.44}$$

with

$$A_{2i} = 2l_{i2} \cos \theta_{i1}(x_{bi} - x_i) + 2l_{i2} \sin \theta_{i1}(y_{bi} - y_i) \quad i = 1, 2, 3 \tag{6.45}$$

$$B_{2i} = 2l_{i2}(z_{bi} + l_{i1} - z_i) \quad i = 1, 2, 3 \tag{6.46}$$

$$C_{2i} = l_{i3}^2 - l_{i2}^2 - (x_{bi} - x_i)^2 - (y_{bi} - y_i)^2 - (z_{bi} + l_{i1} - z_i)^2 \quad i = 1, 2, 3 \tag{6.47}$$

Differentiating eq. (6.43) with respect to time, one obtains

$$A_i \dot{\theta}_{i1} + B_i \dot{\theta}_{i2} = \mathbf{r}_i^T \dot{\mathbf{p}_i} \quad i = 1, 2, 3 \tag{6.48}$$

where $\mathbf{r}_i^T = \begin{bmatrix} C_{i21}' & C_{i22}' & C_{i23}' \end{bmatrix}^T$ and where for $i = 1, 2, 3$

$$A_i = 2l_{i2} \cos \theta_{i1} \cos \theta_{i2}(y_{bi} - y_i) - 2l_{i2} \cos \theta_{i2} \sin \theta_{i1}(x_{bi} - x_i) \tag{6.49}$$

$$B_i = 2l_{i2} \cos \theta_{i2}(z_{bi} + l_{i1} - z_i) - 2l_{i2} \sin \theta_{i2} \sin \theta_{i1}(y_{bi} - y_i)$$
$$-2l_{i2} \sin \theta_{i2} \cos \theta_{i1}(x_{bi} - x_i) \tag{6.50}$$

$$C_{i21}' = 2(x_{bi} - x_i) + 2l_{i2} \cos \theta_{i2} \cos \theta_{i1} \tag{6.51}$$

$$C_{i22}' = 2(y_{bi} - y_i) + 2l_{i2} \cos \theta_{i2} \sin \theta_{i1} \tag{6.52}$$

$$C_{i23}' = 2(z_{bi} + l_{i1} - z_i) + 2l_{i2} \sin \theta_{i2} \tag{6.53}$$

$$\dot{\mathbf{p}}_i = [\dot{x}_i, \dot{y}_i, \dot{z}_i]^T \tag{6.54}$$

Differentiating eq. (6.36) with respect to time, one obtains

$$\dot{\theta}_{i1} = \begin{bmatrix} C_{i11} & C_{i12} & C_{i13} \end{bmatrix}^T \dot{\mathbf{p}_i} \quad i = 1, 2, 3 \tag{6.55}$$

for $i = 1, 2, 3$, with

$$C_{i11} = \frac{-\cos^2 \theta_{i1}(y_i - y_{bi})}{(x_i - x_{bi})^2} \tag{6.56}$$

$$C_{i12} = \frac{\cos^2 \theta_{i1}}{x_i - x_{bi}} \tag{6.57}$$

$$C_{i13} = 0 \tag{6.58}$$

Substituting eq. (6.55) into eq. (6.48), one obtains the equation for $\dot{\theta}_{i2}$ as

$$\dot{\theta}_{i2} = \begin{bmatrix} C_{i21} & C_{i22} & C_{i23} \end{bmatrix}^T \dot{\mathbf{p}_i}, \quad i = 1, 2, 3 \tag{6.59}$$

where for $i = 1, 2, 3$,

$$C_{i21} = \frac{1}{B_i}(C'_{i21} - A_i C_{i11}) \tag{6.60}$$

$$C_{i22} = \frac{1}{B_i}(C'_{i22} - A_i C_{i12}) \tag{6.61}$$

$$C_{i23} = \frac{1}{B_i}(C'_{i23} - A_i C_{i13}) \tag{6.62}$$

therefore, one has

$$\begin{bmatrix} \dot{\theta}_{i1} \\ \dot{\theta}_{i2} \end{bmatrix} = \begin{bmatrix} C_{i11} & C_{i12} & C_{i13} \\ C_{i21} & C_{i22} & C_{i23} \end{bmatrix} \begin{bmatrix} \dot{x}_i \\ \dot{y}_i \\ \dot{z}_i \end{bmatrix} \tag{6.63}$$

i.e.,

$$\begin{bmatrix} \dot{\theta}_{11} \\ \dot{\theta}_{12} \\ \dot{\theta}_{21} \\ \dot{\theta}_{22} \\ \dot{\theta}_{31} \\ \dot{\theta}_{32} \end{bmatrix} = \begin{bmatrix} C_{111} & C_{112} & C_{113} & 0 & 0 & 0 & 0 & 0 & 0 \\ C_{121} & C_{122} & C_{123} & 0 & 0 & 0 & 0 & 0 & 0 \\ 0 & 0 & 0 & C_{211} & C_{212} & C_{213} & 0 & 0 & 0 \\ 0 & 0 & 0 & C_{221} & C_{222} & C_{223} & 0 & 0 & 0 \\ 0 & 0 & 0 & 0 & 0 & 0 & C_{311} & C_{312} & C_{313} \\ 0 & 0 & 0 & 0 & 0 & 0 & C_{321} & C_{322} & C_{323} \end{bmatrix} \begin{bmatrix} \dot{x}_1 \\ \dot{y}_1 \\ \dot{z}_1 \\ \dot{x}_2 \\ \dot{y}_2 \\ \dot{z}_2 \\ \dot{x}_3 \\ \dot{y}_3 \\ \dot{z}_3 \end{bmatrix} \tag{6.64}$$

which can be written as

$$\dot{\boldsymbol{\theta}} = \mathbf{D}\dot{\mathbf{p}} \tag{6.65}$$

Moreover, considering the platform as a rigid body, one can write

$$\dot{\mathbf{P}} = \mathbf{Rt} \tag{6.66}$$

where

$$\mathbf{R} = \begin{bmatrix} \mathbf{R}_1 \\ \mathbf{R}_2 \\ \mathbf{R}_3 \end{bmatrix} \tag{6.67}$$

with $\mathbf{R}_i$ a 3×6 matrix written as

$$\mathbf{R}_i = \begin{bmatrix} (\mathbf{P} - \mathbf{P}_i) & \mathbf{1} \end{bmatrix} \tag{6.68}$$

where $\mathbf{1}$ is a 3×3 identity matrix, and $\mathbf{P} = \mathbf{1} \times \mathbf{p}$, $\mathbf{P}_i = \mathbf{1} \times \mathbf{p}_i$. Substituting eq. (6.66) into (6.65), one then has

$$\dot{\boldsymbol{\theta}} = \mathbf{Jt} \tag{6.69}$$

with

$$\mathbf{J} = \mathbf{DR} \tag{6.70}$$

6.4.1.3 Stiffness Model

The stiffness model of the structure with rigid links can be expressed as

$$\mathbf{K} = \mathbf{J}^T \mathbf{K}_J \mathbf{J} \tag{6.71}$$

where $\mathbf{K}_J = diag[k_{j1}, \ldots, k_{j6}]$ is the joint stiffness matrix.

6.4.2 Kinetostatic Model of the Mechanism with Flexible Links

6.4.2.1 The DH Table for Each Kinematic Chain

Figure 6.12 represents one of the legs with flexible links, one can obtain the Denavit-Hartenberg parameters as in Table 6.4.

Table 6.4: The DH parameters for the ith leg with flexible links.

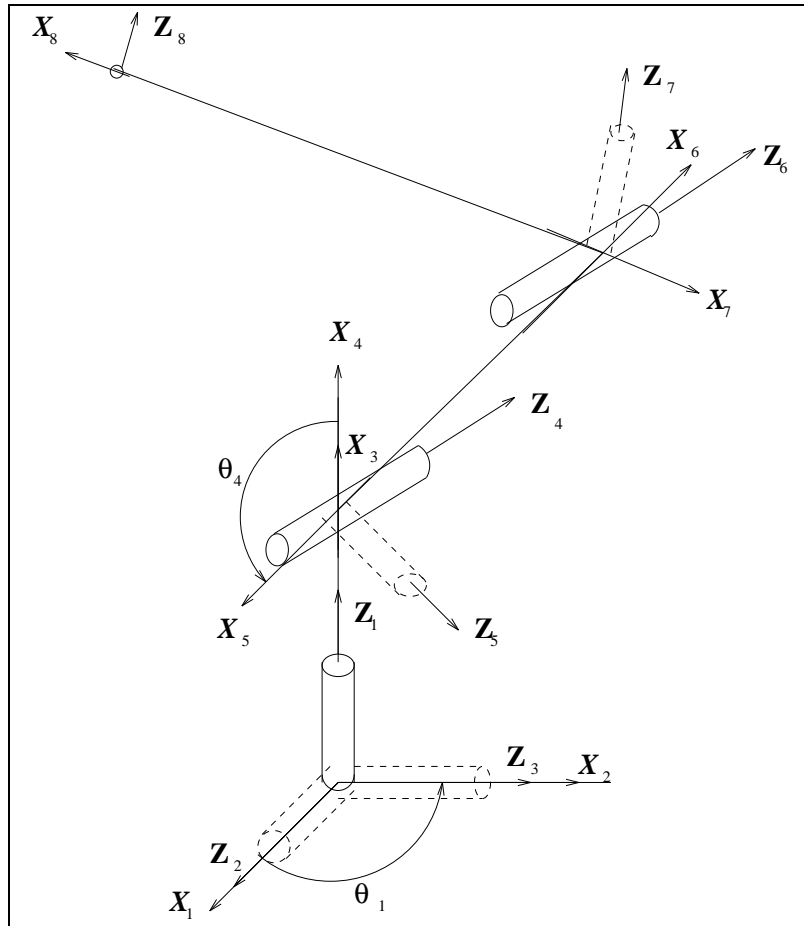| i	a_i	b_i	α_i	θ_i
1	0	0	$90°$	θ_{i1}
2	0	0	$90°$	θ_{i2}
3	l_1	0	$90°$	θ_{i3}
4	0	0	$90°$	θ_{i4}
5	l_2	0	$90°$	θ_{i5}
6	0	0	$90°$	θ_{i6}
7	l_3	0	0	θ_{i7}

Figure 6.12: One of the kinematic chains with flexible links.

6.4.2.2 Jacobian Matrix for Each Kinematic Chain

The Jacobian matrix of the ith leg of the mechanism $\mathbf{J}_i$ can be expressed as

$$\mathbf{J}_i = \left[\mathbf{e}_{i1} \times \mathbf{r}_{i1}, \quad \mathbf{e}_{i2} \times \mathbf{r}_{i2}, \quad \mathbf{e}_{i3} \times \mathbf{r}_{i3}, \quad \mathbf{e}_{i4} \times \mathbf{r}_{i4}, \quad \mathbf{e}_{i5} \times \mathbf{r}_{i5}, \quad \mathbf{e}_{i6} \times \mathbf{r}_{i6}, \quad \mathbf{e}_{i7} \times \mathbf{r}_{i7} \right] \tag{6.72}$$

therefore, the Jacobian matrix of the mechanism can be written as

$$\mathbf{J} = diag[\mathbf{J}_1, \mathbf{J}_2, \mathbf{J}_3] \tag{6.73}$$

for the 6-dof parallel mechanism being discussed, one has

$$\mathbf{J}\dot{\boldsymbol{\theta}} = \dot{\mathbf{p}} \tag{6.74}$$

where $\mathbf{J}$ is a 9×21 matrix, $\dot{\boldsymbol{\theta}}$ is the vector of 21 joint rates, i.e., $\dot{\boldsymbol{\theta}} = \left[\dot{\boldsymbol{\theta}}_1^T \quad \dot{\boldsymbol{\theta}}_2^T \quad \dot{\boldsymbol{\theta}}_3^T \right]^T$, and $\dot{\mathbf{p}}$ is the velocity vector of points P_1, P_2 and P_3, i.e., $\dot{\mathbf{p}} = \left[\dot{\mathbf{p}}_1^T \quad \dot{\mathbf{p}}_2^T \quad \dot{\mathbf{p}}_3^T \right]^T$.

6.4.2.3   Elimination of the Unactuated Joints

In this mechanism, some of the joints are unactuated while the system's stiffness matrix should be established on the basis of joints with actuation or with springs. The procedure to eliminate all these unactuated joints is as follow.

Based on the theorem of velocity compatibility (Angeles 1997), the velocities of three points of a rigid body satisfy the compatibility condition, i.e.,

$$\dot{\mathbf{C}}^T\mathbf{C} + \mathbf{C}^T\dot{\mathbf{C}} = \mathbf{0} \tag{6.75}$$

where matrices $\mathbf{C}$ and $\dot{\mathbf{C}}$ are defined as in eqs. (6.76) and (6.77), $\mathbf{0}$ denoting the 3×3 zero matrix.

$$\mathbf{C} = \begin{bmatrix} \mathbf{p}_1 - \mathbf{c} & \mathbf{p}_2 - \mathbf{c} & \mathbf{p}_3 - \mathbf{c} \end{bmatrix} \tag{6.76}$$

$$\dot{\mathbf{C}} = \begin{bmatrix} \dot{\mathbf{p}}_1 - \dot{\mathbf{c}} & \dot{\mathbf{p}}_2 - \dot{\mathbf{c}} & \dot{\mathbf{p}}_3 - \dot{\mathbf{c}} \end{bmatrix} \tag{6.77}$$

Eq. (6.75) states that for given velocities of three points of a rigid body to be compatible, the product $\dot{\mathbf{C}}^T\mathbf{C}$ must be skewsymmetric and it represents six independent scalar equations that the data of the problem must satisfy. The three diagonal entries represent the distance between any pair of points (kinematic chain constraints) while the off-diagonal entries represent the angles between the pairs of lines formed by each pair of points (shape constraints). Assuming $\mathbf{c} = \mathbf{p}_1$, substituting eqs. (6.76) and (6.77) into eq. (6.75), one obtains

$$(\mathbf{p}_2 - \mathbf{p}_1)^T(\dot{\mathbf{p}}_2 - \dot{\mathbf{p}}_1) = 0 \tag{6.78}$$

$$(\mathbf{p}_3 - \mathbf{p}_1)^T(\dot{\mathbf{p}}_3 - \dot{\mathbf{p}}_1) = 0 \tag{6.79}$$

$$(\mathbf{p}_2 - \mathbf{p}_1)^T(\dot{\mathbf{p}}_3 - \dot{\mathbf{p}}_1) + (\mathbf{p}_3 - \mathbf{p}_1)^T(\dot{\mathbf{p}}_2 - \dot{\mathbf{p}}_1) = 0 \tag{6.80}$$

Hence, one can eliminate the passive joints from the Jacobian through a partitioning of the equations. Finally, one can obtain

$$\mathbf{A}\dot{\boldsymbol{\theta}}' = \mathbf{B}\dot{\boldsymbol{\theta}}'' \tag{6.81}$$

where $\dot{\boldsymbol{\theta}}'$ is the vector of joint rates without passive joints and $\dot{\boldsymbol{\theta}}''$ is the vector of joint rates with only passive joints. Hence

$$\dot{\boldsymbol{\theta}}'' = \mathbf{B}^{-1}\mathbf{A}\dot{\boldsymbol{\theta}}' \tag{6.82}$$

Since vector $\dot{\boldsymbol{\theta}}$ contains all joint rates, the objective is to obtain the relationship between $\dot{\boldsymbol{\theta}}$ and $\dot{\boldsymbol{\theta}}'$ as

$$\dot{\boldsymbol{\theta}} = \mathbf{V}\dot{\boldsymbol{\theta}}' \tag{6.83}$$

In this 6-dof parallel mechanism, the unactuated joint parameter distributed in three legs is θ_{i6}, $i = 1, 2, 3$. One can eliminate all these unactuated joints as follows. Substituting eq. (6.74) into eqs. (6.78) to (6.80), one obtains

$$(\mathbf{p}_2 - \mathbf{p}_1)^T \mathbf{J}_2 \dot{\boldsymbol{\theta}}_2 = (\mathbf{p}_2 - \mathbf{p}_1)^T \mathbf{J}_1 \dot{\boldsymbol{\theta}}_1 \tag{6.84}$$

$$(\mathbf{p}_3 - \mathbf{p}_1)^T \mathbf{J}_3 \dot{\boldsymbol{\theta}}_3 = (\mathbf{p}_3 - \mathbf{p}_1)^T \mathbf{J}_1 \dot{\boldsymbol{\theta}}_1 \tag{6.85}$$

$$(\mathbf{p}_2 - \mathbf{p}_1)^T \mathbf{J}_3 \dot{\boldsymbol{\theta}}_3 + (\mathbf{p}_3 - \mathbf{p}_1)^T \mathbf{J}_2 \dot{\boldsymbol{\theta}}_2 = [(\mathbf{p}_2 - \mathbf{p}_1)^T + (\mathbf{p}_3 - \mathbf{p}_1)^T]\mathbf{J}_1 \dot{\boldsymbol{\theta}}_1 \tag{6.86}$$

where $\dot{\boldsymbol{\theta}}_i$ is the vector of joint rates of the ith leg. One can partition the equations and take the unactuated joints out of the matrix as

$$(\mathbf{p}_2 - \mathbf{p}_1)^T (\mathbf{J}_2' \dot{\boldsymbol{\theta}}_2' + [\mathbf{e}_{26} \times \mathbf{r}_{26}][\dot{\theta}_{26}]) = (\mathbf{p}_2 - \mathbf{p}_1)^T (\mathbf{J}_1' \dot{\boldsymbol{\theta}}_1' + [\mathbf{e}_{16} \times \mathbf{r}_{16}][\dot{\theta}_{16}]) \tag{6.87}$$

$$(\mathbf{p}_3 - \mathbf{p}_1)^T (\mathbf{J}_3' \dot{\boldsymbol{\theta}}_3' + [\mathbf{e}_{36} \times \mathbf{r}_{36}][\dot{\theta}_{36}]) = (\mathbf{p}_3 - \mathbf{p}_1)^T (\mathbf{J}_1' \dot{\boldsymbol{\theta}}_1' + [\mathbf{e}_{16} \times \mathbf{r}_{16}][\dot{\theta}_{16}]) \tag{6.88}$$

$$(\mathbf{p}_2 - \mathbf{p}_1)^T (\mathbf{J}_3' \dot{\boldsymbol{\theta}}_3' + [\mathbf{e}_{36} \times \mathbf{r}_{36}][\dot{\theta}_{36}]) + (\mathbf{p}_3 - \mathbf{p}_1)^T (\mathbf{J}_2' \dot{\boldsymbol{\theta}}_2' + [\mathbf{e}_{26} \times \mathbf{r}_{26}][\dot{\theta}_{26}])$$
$$= [(\mathbf{p}_2 - \mathbf{p}_1)^T + (\mathbf{p}_3 - \mathbf{p}_1)^T](\mathbf{J}_1' \dot{\boldsymbol{\theta}}_1' + [\mathbf{e}_{16} \times \mathbf{r}_{16}][\dot{\theta}_{16}]) \tag{6.89}$$

where for $i = 1, 2, 3$

$$\mathbf{J}_i' = \begin{bmatrix} \mathbf{e}_{i1} \times \mathbf{r}_{i1}, & \mathbf{e}_{i2} \times \mathbf{r}_{i2}, & \mathbf{e}_{i3} \times \mathbf{r}_{i3}, & \mathbf{e}_{i4} \times \mathbf{r}_{i4}, & \mathbf{e}_{i5} \times \mathbf{r}_{i5}, & \mathbf{e}_{i7} \times \mathbf{r}_{i7} \end{bmatrix} \tag{6.90}$$

$$\dot{\boldsymbol{\theta}}_i' = \begin{bmatrix} \dot{\theta}_{i1} & \dot{\theta}_{i2} & \dot{\theta}_{i3} & \dot{\theta}_{i4} & \dot{\theta}_{i5} & \dot{\theta}_{i7} \end{bmatrix}^T \tag{6.91}$$

from eqs. (6.87), (6.88) and (6.89), one can obtain eq. (6.81) with

$$\mathbf{A}_{3\times18} = \begin{bmatrix} \mathbf{A}_{11} & \mathbf{A}_{12} & \mathbf{A}_{13} \\ \mathbf{A}_{21} & \mathbf{A}_{22} & \mathbf{A}_{23} \\ \mathbf{A}_{31} & \mathbf{A}_{32} & \mathbf{A}_{33} \end{bmatrix}, \quad \mathbf{B}_{3\times3} = \begin{bmatrix} \mathbf{B}_{11} & \mathbf{B}_{12} & \mathbf{B}_{13} \\ \mathbf{B}_{21} & \mathbf{B}_{22} & \mathbf{B}_{23} \\ \mathbf{B}_{31} & \mathbf{B}_{32} & \mathbf{B}_{33} \end{bmatrix} \tag{6.92}$$

$$\dot{\boldsymbol{\theta}}' = \begin{bmatrix} \dot{\boldsymbol{\theta}}_1^T & \dot{\boldsymbol{\theta}}_2^T & \dot{\boldsymbol{\theta}}_3^T \end{bmatrix}^T \tag{6.93}$$

$$\dot{\boldsymbol{\theta}}'' = \begin{bmatrix} \dot{\theta}_{16} & \dot{\theta}_{26} & \dot{\theta}_{36} \end{bmatrix}^T \tag{6.94}$$

and

$$\mathbf{A}_{11} = (\mathbf{p}_2 - \mathbf{p}_1)^T \mathbf{J}_1' \tag{6.95}$$

$$\mathbf{A}_{12} = -(\mathbf{p}_2 - \mathbf{p}_1)^T \mathbf{J}'_2 \tag{6.96}$$

$$\mathbf{A}_{13} = \mathbf{0}_{1\times 6} \tag{6.97}$$

$$\mathbf{A}_{21} = (\mathbf{p}_3 - \mathbf{p}_1)^T \mathbf{J}'_1 \tag{6.98}$$

$$\mathbf{A}_{22} = \mathbf{0}_{1\times 6} \tag{6.99}$$

$$\mathbf{A}_{23} = -(\mathbf{p}_3 - \mathbf{p}_1)^T \mathbf{J}'_3 \tag{6.100}$$

$$\mathbf{A}_{31} = [(\mathbf{p}_2 - \mathbf{p}_1)^T + (\mathbf{p}_3 - \mathbf{p}_1)^T]\mathbf{J}'_1 \tag{6.101}$$

$$\mathbf{A}_{32} = -(\mathbf{p}_3 - \mathbf{p}_1)^T \mathbf{J}'_2 \tag{6.102}$$

$$\mathbf{A}_{33} = -(\mathbf{p}_2 - \mathbf{p}_1)^T \mathbf{J}'_3 \tag{6.103}$$

$$\mathbf{B}_{11} = -(\mathbf{p}_2 - \mathbf{p}_1)^T[\mathbf{e}_{16} \times \mathbf{r}_{16}] \tag{6.104}$$

$$\mathbf{B}_{12} = (\mathbf{p}_2 - \mathbf{p}_1)^T[\mathbf{e}_{26} \times \mathbf{r}_{26}] \tag{6.105}$$

$$\mathbf{B}_{13} = 0 \tag{6.106}$$

$$\mathbf{B}_{21} = -(\mathbf{p}_3 - \mathbf{p}_1)^T[\mathbf{e}_{16} \times \mathbf{r}_{16}] \tag{6.107}$$

$$\mathbf{B}_{22} = 0 \tag{6.108}$$

$$\mathbf{B}_{23} = (\mathbf{p}_3 - \mathbf{p}_1)^T[\mathbf{e}_{36} \times \mathbf{r}_{36}] \tag{6.109}$$

$$\mathbf{B}_{31} = -[(\mathbf{p}_2 - \mathbf{p}_1)^T + (\mathbf{p}_3 - \mathbf{p}_1)^T][\mathbf{e}_{16} \times \mathbf{r}_{16}] \tag{6.110}$$

$$\mathbf{B}_{32} = (\mathbf{p}_3 - \mathbf{p}_1)^T[\mathbf{e}_{26} \times \mathbf{r}_{26}] \tag{6.111}$$

$$\mathbf{B}_{33} = (\mathbf{p}_2 - \mathbf{p}_1)^T[\mathbf{e}_{36} \times \mathbf{r}_{36}] \tag{6.112}$$

hence

$$\dot{\boldsymbol{\theta}}'' = \mathbf{B}^{-1}\mathbf{A}\dot{\boldsymbol{\theta}}' \tag{6.113}$$

assume

$$[\mathbf{B}^{-1}\mathbf{A}]_{3\times 18} = \begin{bmatrix} \mathbf{M}_{1\times 18} \\ \mathbf{N}_{1\times 18} \\ \mathbf{S}_{1\times 18} \end{bmatrix} \tag{6.114}$$

One has then

$$\dot{\boldsymbol{\theta}}_{21\times 1} = \mathbf{V}_{21\times 18}\dot{\boldsymbol{\theta}}'_{18\times 1} \tag{6.115}$$

where

$$
\mathbf{V} = \begin{bmatrix}
\mathbf{I}_{5\times5} & \mathbf{0}_{5\times13} \\
\mathbf{M}_{1\times18} \\
\mathbf{0}_{6\times5} & \mathbf{I}_{6\times6} & \mathbf{0}_{6\times7} \\
\mathbf{N}_{1\times18} \\
\mathbf{0}_{6\times11} & \mathbf{I}_{6\times6} & \mathbf{0}_{6\times1} \\
\mathbf{S}_{1\times18} \\
\mathbf{0}_{1\times17} & \mathbf{I}_{1\times1}
\end{bmatrix}
\tag{6.116}
$$

Finally, the joint stiffness matrix is defined as

$$
\mathbf{K}_J = diag[k_{11}, \ldots, k_{15}, k_{17}, k_{21}, \ldots, k_{25}, k_{27}, k_{31} \ldots, k_{35}, k_{37}]
\tag{6.117}
$$

6.4.2.4 Kinetostatic Model

From eqs. (6.74) and (6.66) one can obtain

$$
\mathbf{J}\dot{\boldsymbol{\theta}} = \mathbf{R}\mathbf{t}
\tag{6.118}
$$

since matrix $\mathbf{R}$ represents a system of 9 compatible linear equations in 6 unknowns, one can use the least square solution to this equation, to obtain an exact solution. Using eq. (6.83), one obtains

$$
\mathbf{t} = (\mathbf{R}^T\mathbf{R})^{-1}\mathbf{R}^T\mathbf{J}\mathbf{V}\dot{\boldsymbol{\theta}}'
\tag{6.119}
$$

let $\mathbf{J}'$ be represented as

$$
\mathbf{J}' = (\mathbf{R}^T\mathbf{R})^{-1}\mathbf{R}^T\mathbf{J}\mathbf{V}
\tag{6.120}
$$

then one has

$$
\mathbf{t} = \mathbf{J}'\dot{\boldsymbol{\theta}}'
\tag{6.121}
$$

According to the principle of virtual work, one has

$$
\boldsymbol{\tau}^T\dot{\boldsymbol{\theta}}' = \mathbf{w}^T\mathbf{t}
\tag{6.122}
$$

where $\boldsymbol{\tau}$ is a vector of the actuator torques applied at each actuated joint or joints with spring. It is assumed that no gravitational forces act on any of the intermediate links, and $\mathbf{w}$ is a vector composed of forces and moments (wrench) applied by the end-effector. Equating these two powers, one obtains substituting eq. (6.121) to (6.122) one can obtain

$$
\boldsymbol{\tau} = \mathbf{J}'^T\mathbf{w}
\tag{6.123}
$$

The joint forces and displacements of each joint can be related by Hooke's law, i.e.,

$$\boldsymbol{\tau}_i = \mathbf{k}_i \Delta \boldsymbol{\theta}_i \tag{6.124}$$

and for the whole structure, one has

$$\boldsymbol{\tau} = \mathbf{K}_J \Delta \boldsymbol{\theta}' \tag{6.125}$$

$\Delta \boldsymbol{\theta}'$ only includes the actuated joints and joints with springs i.e.,

$$\mathbf{K}_J \Delta \boldsymbol{\theta}' = \mathbf{J}'^T \mathbf{w} \tag{6.126}$$

hence

$$\Delta \boldsymbol{\theta}' = \mathbf{K}_J^{-1} \mathbf{J}'^T \mathbf{w} \tag{6.127}$$

pre-multiplying both sides by $\mathbf{J}'$, one obtains

$$\mathbf{J}' \Delta \boldsymbol{\theta}' = \mathbf{J}' \mathbf{K}_J^{-1} \mathbf{J}'^T \mathbf{w} \tag{6.128}$$

substituting eq. (6.121) into eq. (6.128), one obtains

$$\mathbf{t} = \mathbf{J}' \mathbf{K}_J^{-1} \mathbf{J}'^T \mathbf{w} \tag{6.129}$$

therefore, one obtains the compliance matrix of the mechanism $\boldsymbol{\kappa}$ as follows

$$\boldsymbol{\kappa} = \mathbf{J}' \mathbf{K}_J^{-1} \mathbf{J}'^T \tag{6.130}$$

and the Cartesian stiffness matrix is

$$\mathbf{K} = \left(\mathbf{J}' \mathbf{K}_J^{-1} \mathbf{J}'^T \right)^{-1} \tag{6.131}$$

6.4.3   Implementation and Results

Based on the model above, an example is now given to illustrate the effect of flexible links on the precision of the mechanism. A reference configuration is given below (all lengths are in centimeters)

$$x_{b1} = 0, y_{b1} = 32, z_{b1} = 0,$$
$$x_{b2} = -16\sqrt{3}, y_{b2} = -16, z_{b2} = 0,$$

$$x_{b3} = 16\sqrt{3}, y_{b3} = -16, z_{b3} = 0,$$
$$a_1 = -8\sqrt{3}, b_1 = 8, c_1 = 0,$$
$$a_2 = 0, b_2 = -16, c_2 = 0,$$
$$a_3 = 8\sqrt{3}, b_3 = 8, c_3 = 0,$$
$$l_{11} = l_{21} = l_{31} = 6,$$
$$l_{12} = l_{22} = l_{32} = 26,$$
$$l_{13} = l_{23} = l_{33} = 12,$$
$$K_i = \pm 1, (i = 1, 2, 3)$$

where

x_{bi}, y_{bi}, z_{bi} are the coordinates of the base attachment points in a local coordinate frame,

a_i, b_i, c_i are the coordinates of the platform attachment points in their local coordinate frame,

$l_{1i}, l_{2i}, l_{3i}, (i = 1, 2, 3)$ are the length of each link,

K_i is the branch index.

and the Cartesian coordinates are given as

$$x = 0, y = 0, z = 22 \ cm,$$
$$\phi = 0, \theta = 0, \psi = -\pi/6,$$

and

$$k_{ai1} = k_{ai4} = 1, \quad i = 1, 2, 3$$
$$k_{i2} = k_{i3} = k_{i5} = k_{i7} \in [1, 50000], \quad i = 1, 2, 3$$
$$k_{bi4} \in [1, 50000], \quad i = 1, 2, 3$$

where k_{ai1} and k_{ai4} are the actuator stiffnesses of joints $i1$ and $i4$, respectively, k_{i2}, k_{i3}, k_{i5} and k_{i7} are the lumped link stiffnesses induced by bending, k_{bi4} is also lumped link stiffness induced by torsion.

Figure 6.13 shows the variation of the stiffness as a function of link stiffness and Table 6.5 exhibits the Cartesian stiffness of the 6-dof mechanism with flexible links and with rigid links. All these results are similar to that obtained in previous sections.
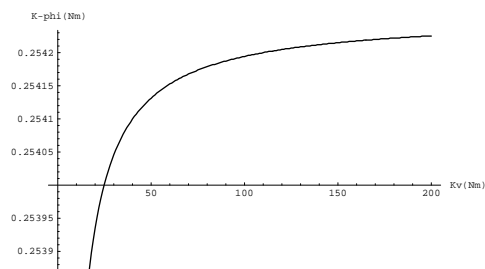
(a) Stiffness in ϕ
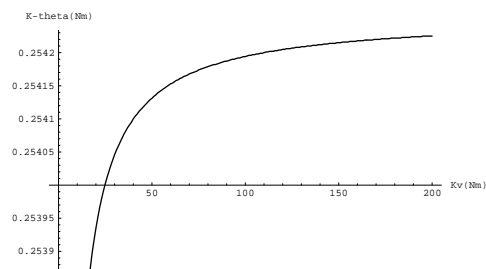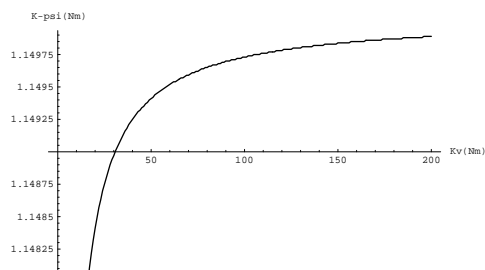
(b) Stiffness in θ
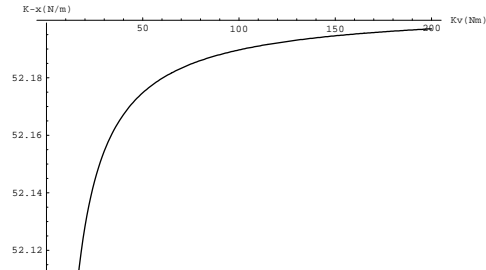
(c) Stiffness in ψ
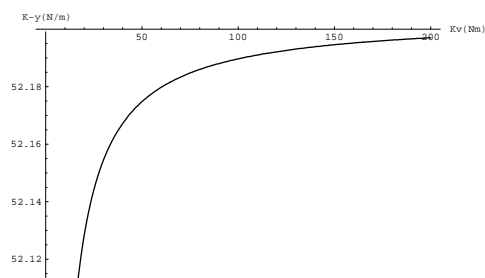
(d) Stiffness in X
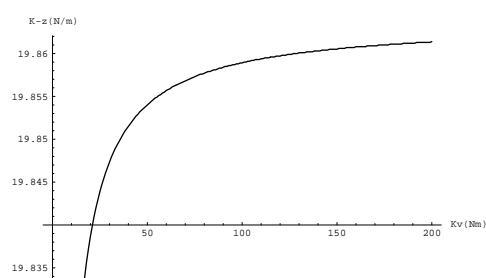
(e) Stiffness in Y

(f) Stiffness in Z

Figure 6.13: Evolution of the stiffness as a function of the link's stiffness in different directions.

Table 6.5: Comparison of Cartesian stiffness between the mechanism with flexible links and the mechanism with rigid links.

$K_{actuator}$	K_{link}	K_ϕ	K_θ	K_ψ	K_x	K_y	K_z
1	1	0.074758	0.074758	0.312083	13.8907	13.8907	5.84047
1	10	0.205028	0.205028	0.905732	40.8851	40.8851	16.0178
1	1000	0.253647	0.253647	1.14695	52.06	52.06	19.8162
1	5000	0.254134	0.254134	1.14942	52.1754	52.1754	19.8542
1	10000	0.254195	0.254195	1.14973	52.1898	52.1898	19.859
1	50000	0.254244	0.254244	1.14998	52.2014	52.2014	19.8628
1	10000000	0.254256	0.254256	1.15004	52.2043	52.2043	19.8637
1	rigid	0.254256	0.254256	1.15004	52.2043	52.2043	19.8637

Assuming that the cross section of the first link (from base to platform) is progressively increased, the stiffness progressively increases as shown in Table 6.6, the same for the 2nd and 3rd links in each leg, for which the results are shown in Tables 6.7 and 6.8. The results are also illustrated in Figures 6.14 and 6.15.

From Tables 6.6 – 6.8 and Figures 6.14 and 6.15, one can observe that the 1st link in each leg (from base to platform) has the largest effects on the stiffness of the mechanism, then the 2nd link of each leg, but the 3rd link of each leg has no effect on K_ϕ, K_θ, K_z, and has very little effect on K_ψ, K_x and K_y. Anyhow, the smallest link stiffness should not be less than that of the actuator's.

The stiffness model described above is now used to obtain the stiffness mappings for this spatial six-degree-of-freedom parallel mechanism. As shown in Figure 6.16, from such plots one can determine which regions of the workspace will satisfy some stiffness criteria.

From the stiffness mappings, one can observe that K_ϕ and K_θ, K_x and K_y are symmetric, and in Figure 6.16(d) the stiffness in X becomes higher when the platform moves further from the Y axis. This was to be expected because when the platform moves aside along the X axis, the projection of the legs on this axis becomes larger, and the mechanism is more rigid in Y. The same reasoning applies to Figure 6.16(e) for the stiffness in Y.

Table 6.6: Comparison of Cartesian stiffness between the mechanism with rigid links and the mechanism with flexible links. (The cross section of the 1st link in each leg is progressively increased, all the other $K_{link} = 20000 \ Nm$.)

$K_{actuator}$	K_{link}	K_ϕ	K_θ	K_ψ	K_x	K_y	K_z
1	1	0.105891	0.105891	0.486243	21.9064	22.3921	8.27276
1	10	0.223001	0.223001	1.01132	45.8274	46.0434	17.422
1	100	0.250731	0.250731	1.1344	51.4837	51.511	19.5883
1	1000	0.253888	0.253888	1.14839	52.1281	52.1308	19.835
1	5000	0.254172	0.254172	1.14965	52.1862	52.1866	19.8572
1	10000	0.254208	0.254208	1.14981	52.1934	52.1936	19.86
1	20000	0.254225	0.254225	1.14989	52.1971	52.1971	19.8614
1	50000	0.254236	0.254236	1.14994	52.1992	52.1992	19.8622
1	100000	0.25424	0.25424	1.14995	52.2	52.1999	19.8625
1	1000000	0.254243	0.254243	1.14997	52.2006	52.2005	19.8627
1	rigid	0.254256	0.254256	1.15004	52.2043	52.2043	19.8637

In Figures 6.16(a) and (b), the torsional stiffnesses in ϕ and θ are shown, the stiffness is larger when the platform moves further from the Y axis. However, in the center of the workspace, K_z and K_ψ are at their minimum when $\psi = -\pi/6$. This is due to the singularity which may appear with a rotation around the Z axis. On the other hand, from Figure 6.17 when $\phi = \theta = \psi = 0$, the stiffness in Z is higher near the center of the workspace, which is the best position for supporting vertical loads. It can also be noted that the stiffness in Z is much larger than the stiffness in the X or Y directions. This is due to the architecture chosen, which aims at supporting heavy objects in an environment where the gravity is acting along the negative direction of Z axis. All these are in accordance with what would be intuitively expected.

6.5 Conclusions

The kinetostatic analysis and the general stiffness model of spatial parallel six-degree-of-freedom mechanisms have been addressed in this chapter. Solutions for the inverse

Table 6.7: Comparison of the mechanism stiffness between the mechanism with rigid links and the mechanism with flexible links. (The stiffness of the 2nd link in each leg is progressively increased, all the other $K_{link} = 20000 \ Nm$.)

$K_{actuator}$	K_{link}	K_ϕ	K_θ	K_ψ	K_x	K_y	K_z
1	1	0.127124	0.127124	0.528982	23.5252	23.5252	9.93153
1	10	0.231127	0.231127	1.02832	46.4978	46.4978	18.0568
1	100	0.251721	0.251721	1.13649	51.5671	51.5671	19.6657
1	1000	0.253984	0.253984	1.1486	52.1362	52.1362	19.8425
1	5000	0.254187	0.254187	1.14968	52.1875	52.1875	19.8584
1	10000	0.254213	0.254213	1.14982	52.1939	52.1939	19.8604
1	20000	0.254225	0.254225	1.14989	52.1971	52.1971	19.8614
1	50000	0.254233	0.254233	1.14993	52.199	52.199	19.862
1	100000	0.254236	0.254236	1.14994	52.1996	52.1996	19.8622
1	1000000	0.254238	0.254238	1.14996	52.2002	52.2002	19.8623
1	rigid	0.254256	0.254256	1.15004	52.2043	52.2043	19.8637

kinematic problem have been given and the methods for the derivation of the general stiffness model have been presented. The effects of flexible links on the mechanism have been demonstrated. Finally, plots of the stiffness mappings have been given in order to illustrate the results. Six-degree-of-freedom mechanisms are of interest for many applications in robotics and other fields such as machine tools. The determination of the stiffness mappings is an important design issue which can be efficiently handled with the procedures described in this chapter.

Based on the results included in Figures and Tables of this chapter, the following conclusions can be drawn:

1. The flexibility of links has obvious effects on the stiffness of the mechanism.

2. The larger the link's stiffness, the larger the mechanism's stiffness in each direction.

3. If the link stiffness is large enough, then the mechanism's stiffness with flexible beams is very close to that of rigid model which suggests that one can depend on

Table 6.8: Comparison of the mechanism stiffness between the mechanism with rigid links and the mechanism with flexible links. (The stiffness of the 3rd link in each leg is progressively increased, all the other $K_{link} = 20000\ Nm$.)

$K_{actuator}$	K_{link}	K_ϕ	K_θ	K_ψ	K_x	K_y	K_z
1	1	0.254225	0.254225	0.967253	41.9736	41.9736	19.8614
1	10	0.254225	0.254225	1.12583	50.8503	50.8503	19.8614
1	100	0.254225	0.254225	1.14742	52.0586	52.0586	19.8614
1	1000	0.254225	0.254225	1.14965	52.1838	52.1838	19.8614
1	5000	0.254225	0.254225	1.14985	52.195	52.195	19.8614
1	10000	0.254225	0.254225	1.14988	52.1964	52.1964	19.8614
1	20000	0.254225	0.254225	1.14989	52.1971	52.1971	19.8614
1	50000	0.254225	0.254225	1.1499	52.1975	52.1975	19.8614
1	100000	0.254225	0.254225	1.1499	52.1976	52.1976	19.8614
1	1000000	0.254225	0.254225	1.1499	52.1977	52.1977	19.8614
1	rigid	0.254256	0.254256	1.15004	52.2043	52.2043	19.8637

such a method to estimate the stiffness of the compliant model.

4. If the mechanism has symmetric structure, then $K_\phi = K_\theta$ and $K_x = K_y$.

5. For a uniform cross section beam or circular cylinder with homogeneous material, $EI = constant$, therefore, for a required beam stiffness, one can design the beam or circular cylinder structure according to their area moments of inertia equations.

6. From the flexible beam stiffness values obtained from the real case, one finds that proper sizes and material of flexible beams are required to reduce the effects of flexible beams for the stiffness of the mechanism.

7. For the 6-dof parallel mechanism with three legs, the most serious effect on the mechanism stiffness is the first link's stiffness in each leg, followed by the 2nd and 3rd link. The 3rd link's stiffness has almost no effect on the system stiffness as long as it is larger or equal to the actuator's stiffness.
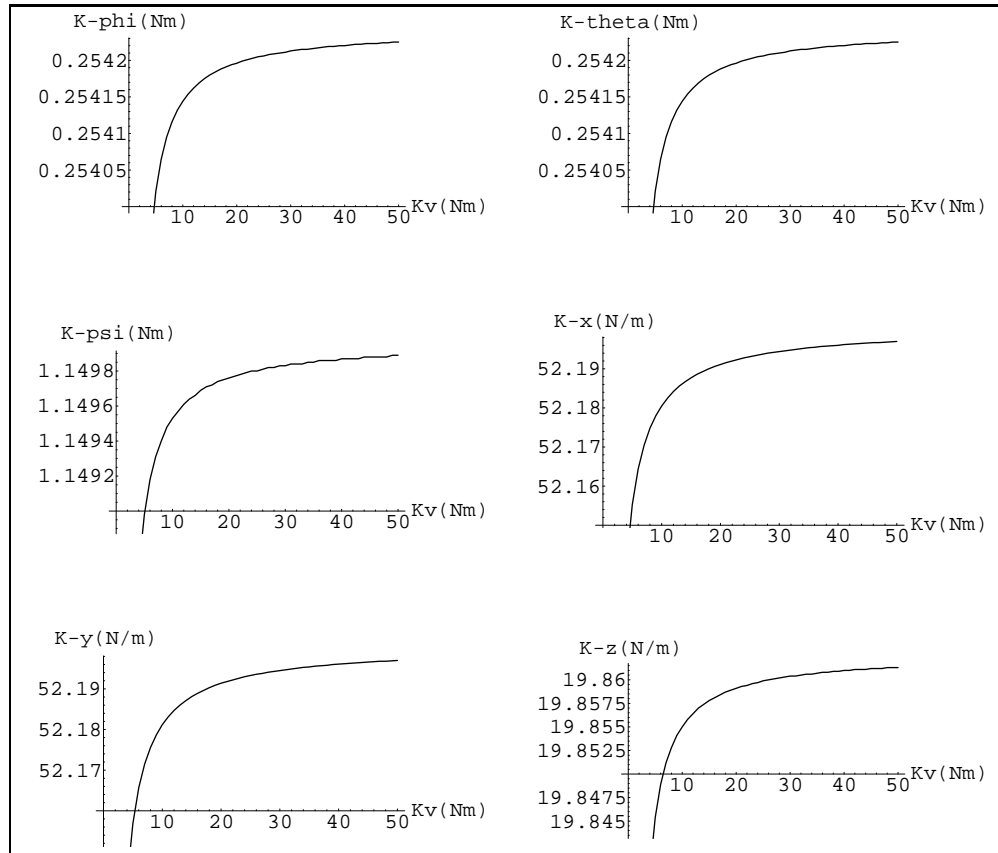
Figure 6.14: Cartesian stiffness as a function of the link's stiffness. ($K_{actuator} = 1 \ Nm, K_{link} = 20000 \ Nm$, the stiffness of the first link (from base to platform) is progressively increasing.)
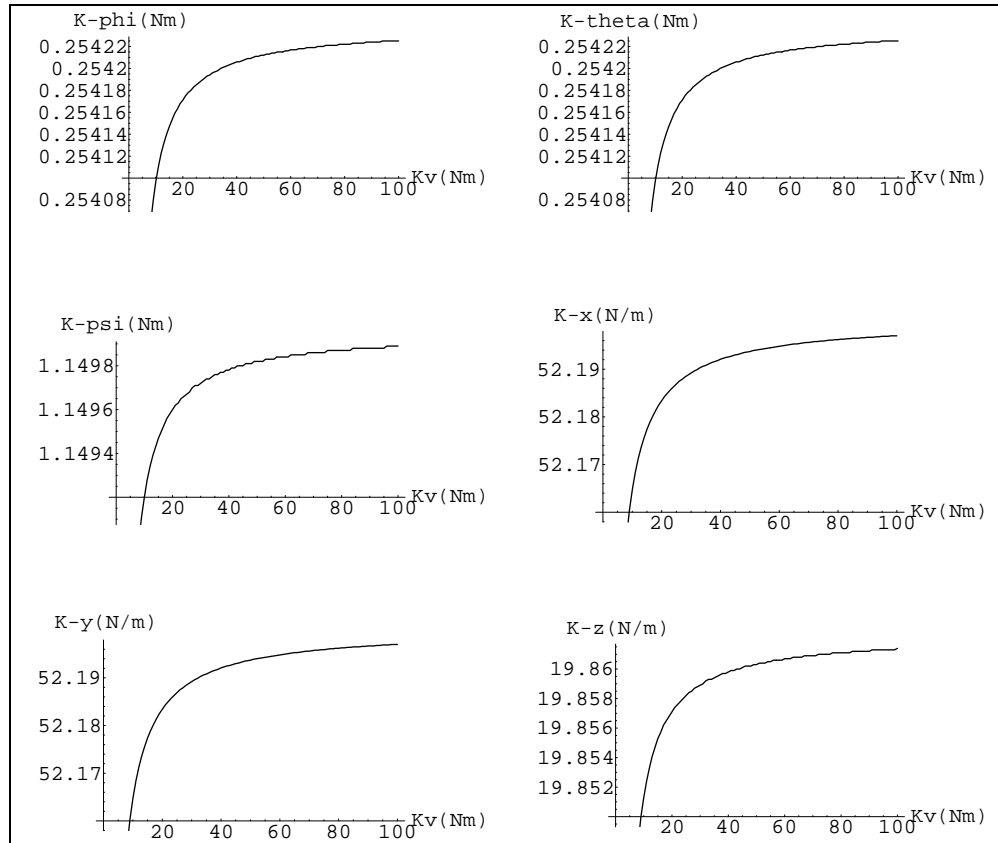
Figure 6.15: Cartesian stiffness as a function of the link's stiffness. ($K_{actuator} = 1\ Nm, K_{link} = 20000\ Nm$, the stiffness of the second link (from base to platform) is progressively increasing.)
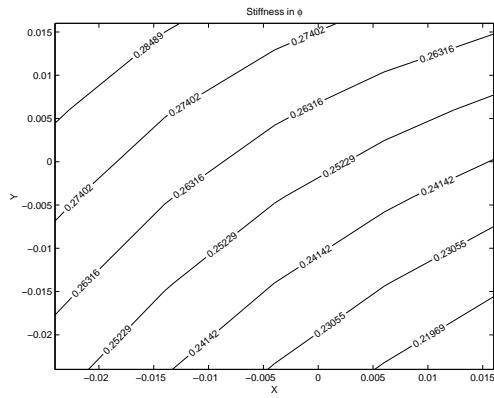
(a) Stiffness in ϕ (Nm)
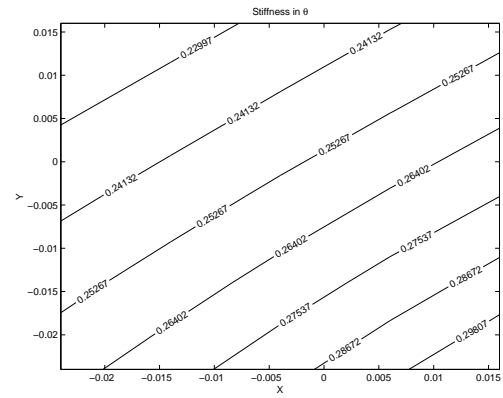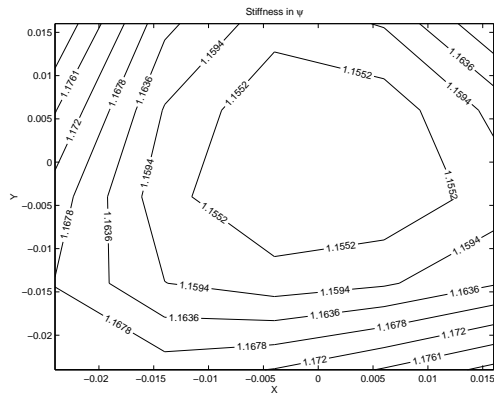
(b) Stiffness in θ (Nm)
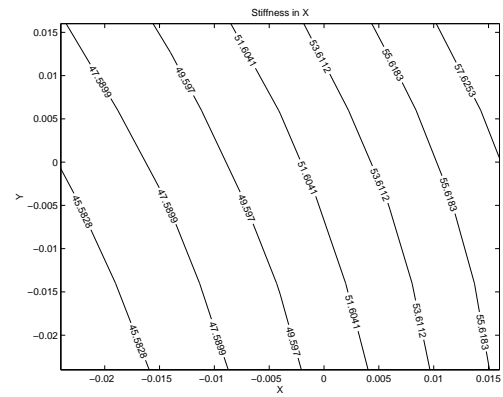
(c) Stiffness in ψ (Nm)
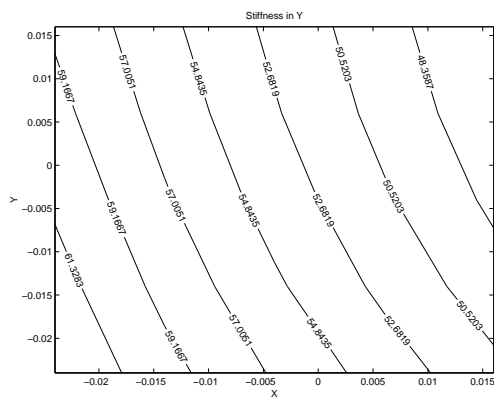
(d) Stiffness in X (N/m)
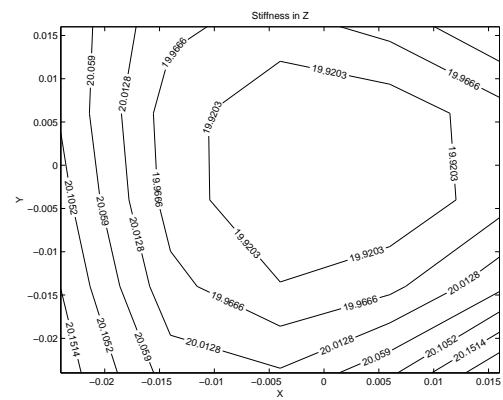
(e) Stiffness in Y (N/m)

(f) Stiffness in Z (N/m)

Figure 6.16: Stiffness mappings of the spatial 6-dof parallel mechanism with revolute actuators (3 legs). ($\phi = \theta = 0, \psi = -\pi/6, z = 22\ cm$) (all length units in m)

(a) Stiffness in ϕ (Nm)

(b) Stiffness in θ (Nm)

(c) Stiffness in ψ (Nm)

(d) Stiffness in X (N/m)

(e) Stiffness in Y (N/m)

(f) Stiffness in Z (N/m)

Figure 6.17: Stiffness mappings of the spatial 6-dof parallel mechanism with revolute actuators (3 legs). ($\phi = \theta = \psi = 0, z = 22\ cm$) (all length units in m)

Chapter 7

Optimization of the Global Stiffness

7.1 Introduction

Optimization plays an important role in engineering design problems, it deals with problems of minimizing or maximizing a function with several variables. For the mechanisms studied here, the highest global stiffnesses are desired so as to reach the high rigidity and high precision. This can be achieved either through maximizing the global stiffnesses or through minimizing the global compliances for a certain parallel mechanism by selecting mechanism's geometric parameters (link length, height, etc.) and behavior parameters (link stiffnesses). In this chapter, the optimization criteria are first established. In order to address the optimization issue, an optimization technique

must be selected. Considering the complexity of the problems, a novel optimization technique called genetic algorithms is applied, and the rationale for using this method together with the determination of parameters and objective function are addressed as well. The detailed analysis of the kinetostatics of the parallel mechanisms conducted in previous chapters will now be used to define and optimize their geometric sizes and properties. Finally, the implementation and optimal results for all kinds of mechanisms discussed in this thesis are given.

7.1.1   Optimization Criteria

In this thesis, the main consideration for the optimization criteria is to maximize global stiffnesses (or minimize the global compliances). The global stiffness/compliance used here is the diagonal entry of the Cartesian stiffness/compliance matrix. It represents the pure stiffness/compliance in each direction.

Genetic algorithm methods are used to conduct the optimal design of the system in terms of a better system stiffness. The objective functions are established and maximized/minimized in order to find the suitable geometric parameters (coordinates of the attachment points, coordinates of the moving platform, link length, vertex distributions at base and moving platform, platform height, etc.) and behavior parameters (actuator stiffness, actuated link stiffness, and kinetostatic model stiffness, etc.) of the mechanisms. Since the objective function is closely related to the topology and geometry of the structure, the general optimization methodology can be described as follows:

- analyze the requirements including the stiffness, the mechanical interferences, the workspace properties and the singularities.

- analyze the constraints including geometric size and properties.

- establish a reasonable initial guess of the geometry of the mechanism, then use a numerical optimization to further improve the kinematic properties and ensure the optimum characteristics are obtained. Finally, a program gives a potential solution to allow the verification of other important properties.

7.1.2 Genetic Algorithms

Introduced in the 1970s by John Holland (Holland 1975), genetic algorithms are part of the larger class of evolutionary algorithms that also include evolutionary programming (Fogel *et al.* 1966), evolution strategies (Rechenberg 1973) and genetic programming (Koza 1991). The genetic algorithms (GAs) are powerful and broadly applicable stochastic search and optimization techniques based on the evolutionary principle of natural chromosomes (Goldberg 1989). Specifically, the evolution of chromosomes due to the operation of crossover and mutation and natural selection of chromosomes based on Darwin's survival-of-the-fittest principles are all artificially simulated to constitute a robust search and optimization procedure. The genetic algorithms are the computer simulation of such evolution where the user provides the environment (function) in which the population must evolve.

A comparison between conventional optimization methods and genetic algorithms is now given. The conventional methods are usually limited to convex regular functions while the genetic algorithm is robust, global and generally more straightforward to apply to all kinds of functions including multi-modal, discontinuous, and non-differentiable functions. Goldberg (1989) has summarized the differences as follows:

1. Genetic algorithms work with a coding of the solution set, not the solutions themselves.

2. Genetic algorithms search from a population of solutions, not a single solution.

3. Genetic algorithms use payoff information (fitness function), not derivatives or other auxiliary knowledge.

4. Genetic algorithms use probabilistic transition rules, not deterministic rules.

In recent years, the GAs have been applied to a broad range of real-world problems (Boudreau and Turkkan 1996; Davis 1991; Gen and Cheng 1997; Boudreau and Gosselin 1998; Michalewicz 1994; Winter *et al.* 1995; Nearchou 1998; Davidor 1991; Goldberg and Samtani 1986) such as ecosystem modeling, combinatorial and parametric optimization, reliability design, vehicle routing and scheduling, machine intelligence,

robotic trajectory optimization, neural networks implementations, pattern recognition, analysis of complex systems and financial prediction.

The basic procedure of genetic algorithms can be described as follows:

1. Create an initial population

   The initial population of chromosomes is created randomly.

2. Evaluate all of the individuals (apply some function or formula to the individuals)

   The fitness is computed in this step. The goal of the fitness function is to numerically encode the performance of the chromosomes.

3. Selection

   Select a new population from the old population based on the fitness of the individuals as given by the evaluation function. In this step, the chromosomes with the largest fitness rates are selected while the chromosomes with low fitness rates are removed from the population.

4. Genetic operations (mutation and crossover)

   If the parents are allowed to mate, a recombination operator is employed to exchange genes between the two parents to produce two children. If they are not allowed to mate, the parents are placed into the next generation unchanged. A mutation simply changes the value for a particular gene.

5. Evaluate these newly created individuals.

6. Repeat steps 3-5 (one generation) until the termination criteria has been satisfied.

Suppose $P(t)$ and $C(t)$ are parents and children in current generation t, then a genetic algorithm is expressed in Figure 7.1,

From Figure 7.1, one can find that there are only two kinds of operations included in genetic algorithms, i.e., genetic operations (crossover and mutation) and evolution operation (selection).

```
begin
    t  =  0;
    initialize P(t);
    evaluate P(t);
    while  (unfinished condition)    do
        select P ' (t) from P(t);
        reproduce C(t) from P ' (t);
        mutate C(t);
        evaluate  C(t);
        t  =  t + 1;
    end
 end
```

Figure 7.1: The structure of genetic algorithms.

7.1.3   Rationale for Using Genetic Algorithms

Genetic algorithms have the advantages of robustness and good convergence properties, namely:

- They require no knowledge or gradient information about the optimization problems. They can solve any kind of objective functions and any kind of constraints (i.e., linear or nonlinear) defined on discrete, continuous, or mixed search spaces.

- Discontinuities present on the optimization problems have little effect on the overall optimization performance.

- They are effective at performing global search (in probability) instead of local optima.

- They perform very well for large-scale optimization problems.

- They can be employed for a wide variety of optimization problems.

Genetic algorithms have been shown to solve linear and nonlinear problems by exploring all regions of state space and exponentially exploiting promising areas through mutation, crossover, and selection operations applied to individuals in the population (Michalewicz 1994).

In the present work, there are many optimization parameters (up to 13 variables, depending on mechanism, make up the optimization problem) and complex matrix computations. Hence, it is very difficult to write out the analytical expressions for each stiffness element. Moreover, with traditional optimization methods, only a few geometric parameters (Gosselin and Guillot 1991) could be handled due to the lack of convergence of the optimization algorithm when used with more complex problems. This arises from the fact that traditional optimization methods use a local search by a convergent stepwise procedure (e.g. gradient, Hessians, linearity, and continuity), which compares the values of the next points and moves to the relative optimal points. Global optima can be found only if the problem possesses certain convexity properties that essentially guarantee that any local optima is a global optimal. Therefore, genetic algorithms are the best candidate for the optimization problems studied here.

7.1.4 Determination of Parameter Settings for Genetic Algorithms

In order to use genetic algorithms properly, several parameter settings have to be determined, they are: chromosome representation, selection function, genetic operators, the creation of the population size, mutation rate, crossover rate, and the evaluation function.

1. Chromosome representation

   This is a basic issue for the GA representation, it is used to describe each individual in the population of interest. In the original algorithm, each individual or chromosome used to be expressed as a sequence of genes from binary digits (0 and 1) (Holland 1975). However, it has been shown that more natural representations are more efficient and produce better solutions (Michalewicz 1994). Michalewicz

(1994) has done extensive experimentation comparing real-valued and binary genetic algorithms and shows that the real-valued genetic algorithm is an order of magnitude more efficient in terms of CPU time. He also shows that a real-valued representation moves the problem closer to the problem representation which offers higher precision with more consistent results across replications (Michalewicz 1994). It outperformed binary genetic algorithm and simulated annealing in terms of computational efficiency and solution quality (Houck *et al.* 1995). Hence, real-valued expressions are used in our case to represent each individual or chromosome for function optimization. For the problem studied here, the chromosomes consist of the architecture parameters (coordinates of the attachment points, coordinates of the moving platform, link lengths, vertex distributions at base and moving platform, platform height, etc.) and behavior parameters (actuator stiffness, actuated link stiffness, and kinetostatic model stiffness, etc.) of the mechanisms.

2. Selection function

This step is a key procedure to produce the successive generations. It determines which of the individuals will survive and continue on to the next generation. A probabilistic selection is performed based on the individual's fitness such that the better individuals have an increased chance of being selected. There are several methods for selection: roulette wheel selection and its extensions, scaling techniques, tournament, elitist models, and ranking methods (Goldberg 1989; Michalewicz 1994). In our case, the normalized geometric ranking method (Joines and Houck 1994) is used since it only requires the evaluation function to map the solutions to a partially ordered set and it tends to eliminate chromosomes with extreme values, thus allowing for minimization and negativity. In normalized geometric ranking methods, Joines and Houck (1994) define a probability of selection P_i for each individual as

$$P[\text{ selecting the } i\text{th individual }] = q'(1 - q)^{(r-1)} \tag{7.1}$$

where

q represents the probability of selecting the best individual,

r represents the rank of the individual, where 1 is the best,

P is the population size.

$$q' = \frac{q}{1-(1-q)^P}.$$

3. Genetic operators

The operators are used to create new children based on the current generation in the population. Basically, there are two types of operators: crossover and mutation. Crossover takes two individuals and produces two new individuals while mutation alters one individual to produce a single new solution.

In binary representations, the applications of these two types of operators are only binary mutation and simple crossover.

In real-valued representations, the applications of these two types of operators have been developed by Michalewicz (1994), they are: uniform mutation, non-uniform mutation, multi-non-uniform mutation, boundary mutation, simple crossover, arithmetic crossover, and heuristic crossover (Michalewicz 1994).

Uniform mutation randomly selects one variable and sets it equal to a uniform random number while boundary mutation randomly selects one variable and sets it equal to either its lower or upper bound.

Non-uniform mutation randomly selects one variable and sets it equal to a non-uniform random number, according to Michalewicz (1994), it is defined as follows: if $s_x{}^t = (x_1, x_2, x_3, \ldots, x_m)$ is a chromosome (t is the generation number) and the element x_j was selected for non-uniform mutation, the result is a vector $s_x{}^{t+1} = (x_1, x_2, x_3, \ldots, x'_j, \ldots, x_m)$, where

$$x'_j = x_j + \Delta(t, UB - x_j), \quad \text{if a random digit is 0} \tag{7.2}$$
$$x'_j = x_j - \Delta(t, x_j - LB), \quad \text{if a random digit is 1} \tag{7.3}$$

where UB and UL are the upper and lower bounds for the variable, and $\Delta(t, y)$ is given by

$$\Delta(t, y) = y(1 - r^{(1-\frac{t}{G})^b}) \tag{7.4}$$

where

r is a uniform random number between (0,1),

G represents the maximum number of generations,

t is the current generation.

b is a parameter determining the degree of dependency on the generation number.

4. Population size

   The population size represents the number of individuals or chromosomes in the population. Usually, larger population sizes increase the amount of variation present in the initial population, it requires more fitness evaluations. If the population loses diversity, the population is said to have premature convergence and little exploration is being done. For longer chromosomes and challenging optimization problems, larger population sizes are needed to maintain diversity — higher diversity can also be achieved through higher mutation rates and uniform crossover — and hence better exploration. Usually, the population size is determined by the rule of thumb of seven to eight times the number of the optimization parameters.

5. Mutation rate

   The mutation rate is defined as the percentage of the total number of genes in the population (Gen and Cheng 1997), it determines the probability that a mutation will occur. Mutation is employed to give new information to the population and also prevents the population from becoming saturated with similar chromosomes (premature convergence). Large mutation rates increase the probability that good schemata will be destroyed, but increase population diversity. The best mutation rate is application dependent but for most applications is between 0.001 and 0.1.

6. Crossover rate

   The crossover rate (denoted by p_c) is defined as the ratio of the number of offspring produced in each generation to the population size, P (Gen and Cheng 1997). This ratio controls the expected number $p_c \times P$ of chromosomes to undergo the crossover operation. The best crossover rate is application dependent but for most applications is between 0.80 and 0.95.

7. Evaluation functions

   Evaluation functions are subject to the minimal requirement that the function can map the population into a partially ordered set. In the present work, the sum of diagonal elements in stiffness/compliance matrix with relative weight factors for each direction is set as the evaluation function.

7.2 Implementation

In this research work, the stiffness for certain mechanism configurations is expressed by a (6×6) matrix, as discussed before. The diagonal elements of the matrix are the mechanism's pure stiffness in each Cartesian direction. To obtain the optimal stiffness in each direction, one can write an objective function, eq. (7.5), with stiffness element to maximize or write an objective function, eq. (7.6), with compliance elements whose negative is to be maximized, i.e., maximize(val) where

$$val = \eta_1 K_{11} + \eta_2 K_{22} + \eta_3 K_{33} + \eta_4 K_{44} + \eta_5 K_{55} + \eta_6 K_{66} \tag{7.5}$$

or

$$val = -(\lambda_1 \kappa_{11} + \lambda_2 \kappa_{22} + \lambda_3 \kappa_{33} + \lambda_4 \kappa_{44} + \lambda_5 \kappa_{55} + \lambda_6 \kappa_{66}) \tag{7.6}$$

where, for $i = 1, \ldots, 6$

K_{ii} represents the diagonal elements of the mechanism's stiffness matrix,

κ_{ii} represents the diagonal elements of mechanism's compliance matrix,

η_i is the weight factor for each directional stiffness, which characterizes the priority of the stiffness in this direction.

λ_i is the weight factor for each directional compliance, which characterizes the priority of the compliance in this direction.

This would maximize/minimize the SUM of the diagonal elements. Although we could not maximize/minimize each diagonal element individually, we always can optimize each stiffness by distributing the weighting factors. Once the objective function is written, a search domain for each optimization variable (lengths, angles, etc.) should be specified to create an initial population. The limits of the search domain are set by a specified maximum number of generations or population convergence criteria, since the GAs will force much of the entire population to converge to a single solution.

For the optimization of the stiffness, a real-valued method is used combined with the selection, mutation and crossover operators with their optional parameters used for all these type of parallel mechanism stiffness/compliance function optimization as shown

in Table 7.1. The first optional parameter is the number of times to apply the operators for real-valued representation, G_m represents the maximum number of generations, b is a parameter determining the degree of dependency on the generation number, we use 3 in our case (Michalewicz 1994). The other optional parameters depend on the operators we are using. Since Matlab requires matrices to have the same length in all rows, many of the parameters are 0 indicating that they are really place holders only. In the following sections, we will describe it in more detail.

Table 7.1: Genetic algorithm parameters used for real-valued stiffness function optimization.

Name	Parameters
Uniform Mutation	[4 0 0]
Non-Uniform Mutation	[4 G_m b]
Multi-Non-Uniform Mutation	[6 G_m b]
Boundary Mutation	[4 0 0]
Simple Crossover	[2 0]
Arithmetic Crossover	[2 0]
Heuristic Crossover	[2 3]
Normalized Geometric Selection	0.08

7.2.1 Spatial Six-Degree-of-Freedom Mechanism with Prismatic Actuators

7.2.1.1 Parameters Selection

The spatial six-degree-of-freedom mechanism with prismatic actuators is shown in Figures 6.2 and 6.3. In order to obtain the maximum global stiffness, five architecture and behavior parameters are used as optimization parameters, the vector of optimization variables is

$$\mathbf{s} = [R_p, R_b, z, T_p, T_b] \tag{7.7}$$

where R_p is the radius of the platform, R_b is the radius of the base, z is the height of the platform, T_p, T_b are the angles to determine the attachment points on the base and on the platform, and their bounds are

$$R_p \in [5, 10] \; cm, R_b \in [12, 22] \; cm,$$

$$z \in [45, 56] \; cm,$$

$$T_p \in [18, 26]°, T_b \in [38, 48]°,$$

In this research work, the objective function of eq. (7.5) is maximized where the following is assumed

$$
\begin{aligned}
\eta_i &= 1 \quad i = 1, \ldots, 6, \\
P &= 80 \\
G_{max} &= 100
\end{aligned}
$$

where P is the population size and G_{max} is the maximum number of generations.

7.2.1.2 Results

The genetic algorithm is implemented in Matlab to search for the best solutions. The results are given only for one case with $\phi = 0, \theta = 0, \psi = 0$. Figure 7.2 shows the evolution of the best individual for 100 generations. The architectural and behavior parameters found by the GA after 100 generations are

$$\mathbf{s} = [R_p, R_b, z, T_p, T_b] = [10, 12, 56, 18, 48]$$

and the stiffnesses in each direction are

$$
\begin{aligned}
\mathbf{K} &= [K_x, K_y, K_z, K_{\theta_x}, K_{\theta_y}, K_{\theta_z}] \\
&= [34.1918, 34.1918, 5931.6164, 29.65808182, 29.65808182, 0.68092535]
\end{aligned}
$$

the sum of the stiffnesses is 6059.997.

Before optimization, the parameters for this mechanism were given as

$$\mathbf{s}' = [R_p, R_b, z, T_p, T_b] = [6, 15, 51, 22.34, 42.88]$$

and the stiffness in each direction was

$$\mathbf{K}' = [K'_x, K'_y, K'_z, K'_{\theta_x}, K'_{\theta_y}, K'_{\theta_z}]$$
$$= [102.968, 102.968, 5794.06, 10.4293, 10.4293, 0.222188]$$

and the stiffness sum is 6021.08. Hence, after optimization, the stiffness sum is improved 1.01 times.
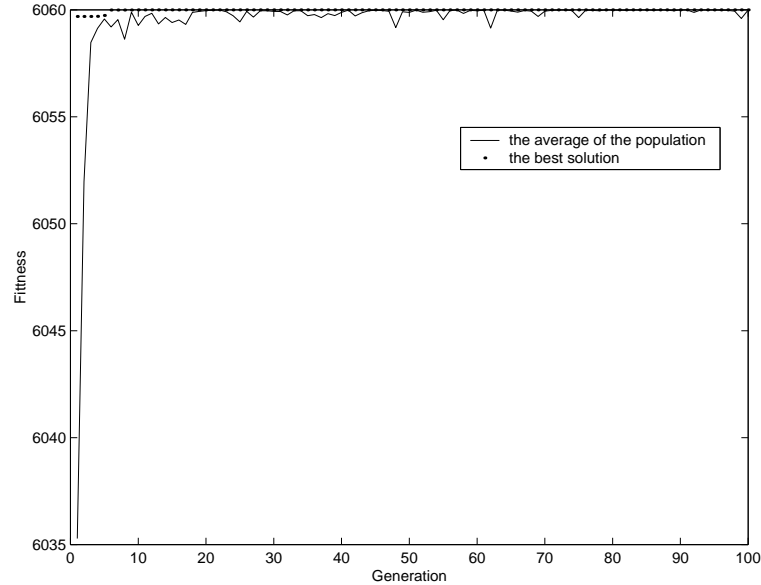
Figure 7.2: The evolution of the performance of the 6-dof mechanism with prismatic actuators.

From Figure 7.2, it can be seen that after a sufficient number of generations (around 30 generations), the track of the best solution and the track of the average of the population converge to the final best solution.

7.2.2 Spatial Six-Degree-of-Freedom Mechanism with Revolute Actuators

7.2.2.1 Parameters Selection

A spatial six-degree-of-freedom mechanism with revolute actuators is represented in Figure 6.7. The vertex distribution is the same as in Figure 6.3. From Figure 6.8, it is clear that the Cartesian stiffness is a monotonically increasing function of the link

stiffnesses (for all the case with revolute actuators). Nevertheless, there exists a critical link stiffness, which has tiny effects on mechanism's Cartesian stiffness when it is larger than the critical link stiffness, therefore, for all mechanisms with revolute actuators, link stiffnesses are also included as optimization parameters. Nine (9) optimization parameters are specified in this mechanism for maximizing the mechanism's global stiffnesses. The vector of optimization variables can be expressed as

$$\mathbf{s} = [R_p, R_b, z, T_p, T_b, l_1, l_2, K_2, K_b] \qquad (7.10)$$

where R_p is the radius of the platform, R_b is the radius of the base, z is the height of the platform, T_p, T_b are the angles to determine the attachment points on the base and on the platform, l_1, l_2 are the link lengths and K_b, K_2 are the link stiffnesses of the 1st and 2nd link of each leg, respectively, and the bound for each parameter is

$$R_p \in [5, 7] \ cm, R_b \in [14, 16] \ cm,$$
$$z \in [66, 70] \ cm,$$
$$T_p \in [20, 26]°, T_b \in [40, 45]°,$$
$$l_1 \in [42, 48] \ cm, l_2 \in [32, 40] \ cm,$$
$$K_2 \in [10^6, 10^{10}], K_b \in [10^6, 10^{10}],$$

In this case, the objective function of eq. (7.5) is maximized assuming

$$\eta_i \ = \ 1 \quad i = 1, \ldots, 6,$$
$$P \ = \ 80$$
$$G_{max} \ = \ 100$$

where P is the population size and G_{max} is the maximum number of generations.

7.2.2.2 Results

A program based on the genetic algorithm is applied to search for the best solutions. The results are given only for one configuration with $\theta = 0, \phi = 0, \psi = 0$. Figure 7.3 shows the evolution of the best individual and the average of the population for 100 generations. The optimal geometric and behavior parameters obtained by the GA after 100 generations are

$$\mathbf{s} = [R_p, R_b, z, T_p, T_b, l_1, l_2, K_2, K_b] = [5, 16, 70, 20, 45, 42, 32, 10^{10}, 10^{10}]$$

and the stiffnesses in each direction are

$$\begin{aligned}
\mathbf{K} &= [K_x, K_y, K_z, K_{\theta_x}, K_{\theta_y}, K_{\theta_z}] \\
&= [18873.14, 18873.14, 159835.85, 199.79, 199.79, 41.04]
\end{aligned}$$

the sum of the stiffnesses is 198022.766.

Initially, the geometric and behavior values were given for this mechanism as

$$\begin{aligned}
\mathbf{s}' &= [R_p, R_b, z, T_p, T_b, l_1, l_2, K_2, K_b] \\
&= [6, 15, 68, 22.34, 42.883, 46, 36, 10^{10}, 10^{10}]
\end{aligned}$$

and the stiffnesses in each direction were

$$\begin{aligned}
\mathbf{K}' &= [K'_x, K'_y, K'_z, K'_{\theta_x}, K'_{\theta_y}, K'_{\theta_z}] \\
&= [7725, 7725, 21045, 37.8818, 37.8818, 43.0695]
\end{aligned}$$

the stiffness sum is 36613.8. Therefore, after optimization, the stiffness sum is improved 5.4 times.
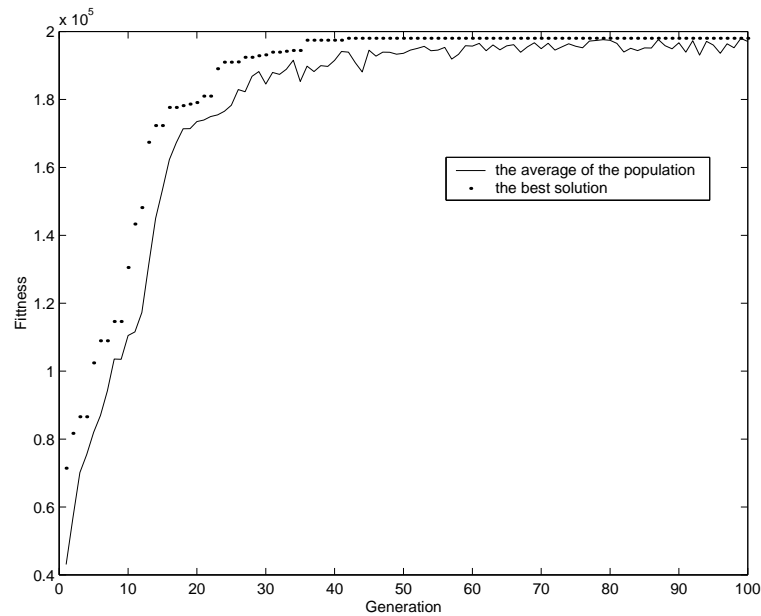
Figure 7.3: The evolution of the performance of the 6-dof mechanism with revolute actuators.

Figure 7.3 shows that after 34 generations, the track of the best solution and the track of the average of the population converge to the final best solution.

7.2.3 Spatial Five-Degree-of-Freedom Mechanism with Prismatic Actuators

7.2.3.1 Parameters Selection

The spatial five-degree-of-freedom mechanism with prismatic actuators is shown in Figure 4.2 and the position of the attachment points both on the base and on the platform is shown in Figure 4.17. In order to obtain the maximum global stiffness, the global compliance (since there are infinite terms among the diagonal stiffness elements) is minimized. However, from eqs. $(4.110) - (4.115)$, it is clear that the Cartesian stiffness is a monotonically increasing function of the link and actuator stiffnesses (for all the case with prismatic actuators). Hence, the optimum solution always corresponds to the maximum link or actuator stiffnesses and these parameters are not included in the optimization variables. Seven (7) parameters are specified as optimization parameters, they are

$$\mathbf{s} = [R_p, R_b, l_{61}, l_{62}, z, T_p, T_b] \tag{7.12}$$

where R_p is the radius of the platform, R_b is the radius of the base, l_{61}, l_{62} are the link length for the 1st and 2nd link of the passive leg, respectively, z is the height of the platform, T_p, T_b are the angles to determine the attachment points on the base and on the platform, and their bounds are

$$R_p \in [10, 14] \ cm, R_b \in [20, 26] \ cm,$$

$$l_{61} \in [52, 70] \ cm, l_{62} \in [52, 70] \ cm,$$

$$z \in [66, 70] \ cm$$

$$T_p \in [18, 26]°, T_b \in [38, 48]°,$$

In this work, the objective function of eq. (7.6) is minimized assuming

$$\lambda_i = 1 \quad i = 1, \ldots, 6,$$

$$P = 80$$

$$G_{max} = 100$$

7.2.3.2 Results

Results are given here only for the case with $\theta_{65} = -\pi, \theta_{66} = 2\pi/3$. Figure 7.4 shows the evolution of the best individual for 100 generations. The architectural and behavior parameters found by the GA after 100 generations are

$$
\begin{aligned}
\mathbf{s} &= [R_p, R_b, l_{61}, l_{62}, z, T_p, T_b] \\
&= [14, 21.2, 52, 70, 66, 18, 48]
\end{aligned}
$$

and the compliances in each direction are

$$
\begin{aligned}
\boldsymbol{\kappa} &= [\kappa_{\theta_x}, \kappa_{\theta_y}, \kappa_{\theta_z}, \kappa_x, \kappa_y, \kappa_z] \\
&= [0.03687, 0.03113, 0.03646, 0.03962, 0.01657, 2.46 \times 10^{-4}]
\end{aligned}
$$

the sum of the compliances is 0.16.

Before optimization, the parameter values of the mechanism were given as

$$
\begin{aligned}
\mathbf{s}' &= [R_p, R_b, l_{61}, l_{62}, z, T_p, T_b] \\
&= [12, 22, 68, 68, 68, 22.34, 42.883]
\end{aligned}
$$

and the compliances in each direction were

$$
\begin{aligned}
\boldsymbol{\kappa}' &= [\kappa'_{\theta_x}, \kappa'_{\theta_y}, \kappa'_{\theta_z}, \kappa'_x, \kappa'_y, \kappa'_z] \\
&= [0.08627, 0.0981, 0.2588, 0.07342, 0.030325, 2.55 \times 10^{-4}]
\end{aligned}
$$

the compliance sum is 0.54714. After optimization, the compliance sum is improved 3.4 times.

7.2.4 Spatial Five-Degree-of-Freedom Mechanism with Revolute Actuators

7.2.4.1 Parameters Selection

The schematic representation of this type mechanism and its vertex distribution are shown in Figures 5.2 and 4.17, respectively. Twelve architecture and behavior parameters are specified as optimization parameters to minimize the compliances, they can
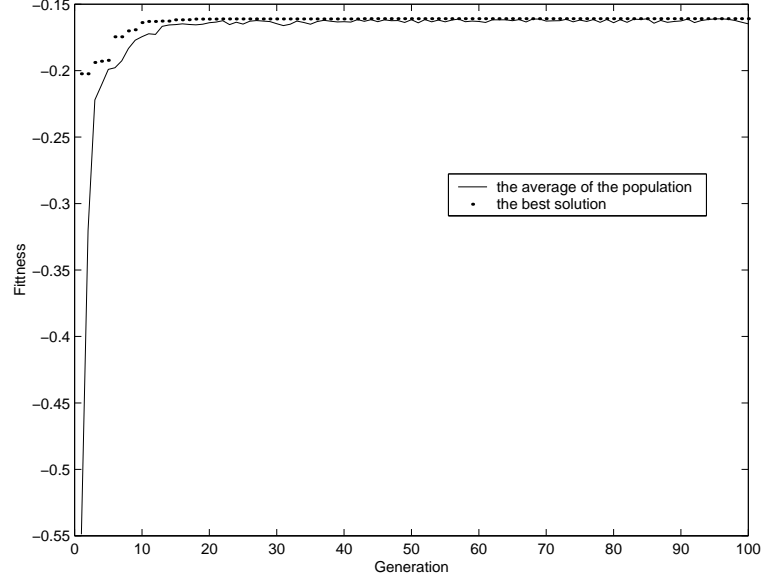
Figure 7.4: The evolution of the performance of the 5-dof mechanism with prismatic actuators.

be represented as a vector of $\mathbf{s}$

$$\mathbf{s} = [R_p, R_b, l_{61}, l_{62}, l_1, l_2, z, k_b, k_{62}, k_2, T_p, T_b] \tag{7.13}$$

where R_p is the radius of the platform, R_b is the radius of the base, l_{61}, l_{62} are the link lengths for the 1st and 2nd link of the passive leg, respectively, l_1, l_2 are the link length for the 1st and 2nd link of the each actuated leg, respectively, z is the height of the platform, T_p, T_b are the angles to determine the attachment points on the base and on the platform, and the bound of each optimization parameter is

$$R_p \in [5, 7] \ cm, R_b \in [14, 18] \ cm,$$
$$l_{61} \in [67, 70] \ cm, l_{62} \in [67, 70] \ cm,$$
$$l_1 \in [33, 35] \ cm, l_2 \in [45, 47] \ cm,$$
$$z \in [66, 70] \ cm, T_p \in [18, 30]°, T_b \in [38, 50]°,$$
$$k_b, k_{62}, k_2 \in [10^6, 10^{10}]$$

For this mechanism, the objective function of eq. (7.6) is minimized with

$$\lambda_i = 1 \quad (i = 1, \ldots, 6), \quad P = 80, \quad G_{max} = 200$$

7.2.4.2 Results

Results are given here for the case with $\theta_{65} = -\pi, \theta_{66} = 2\pi/3$. Figure 7.5 shows the evolution of the best individual for 200 generations. The mechanism's geometric and behavior parameters found by the GA after 200 generations are

$$
\begin{aligned}
\mathbf{s} &= [R_p, R_b, l_{61}, l_{62}, l_1, l_2, z, k_b, k_{62}, k_2, T_p, T_b] \\
&= [7, 16, 68.622, 67.208, 33, 45, 69, 9.126 \times 10^9, 9.968 \times 10^9, 7.99 \times 10^9, 19.97, 47.97]
\end{aligned}
$$

and the compliances in each direction are

$$
\begin{aligned}
\boldsymbol{\kappa} &= \left[\kappa_{\theta_x}, \kappa_{\theta_y}, \kappa_{\theta_z}, \kappa_x, \kappa_y, \kappa_z \right] \\
&= [7.77 \times 10^{-2}, 0.10345, 0.24256, 1.116 \times 10^{-3}, 1.87 \times 10^{-3}, 2.67 \times 10^{-4}]
\end{aligned}
$$

the sum of the compliances is 0.426999.

The initial guess of the geometric and structure behavior parameters of the mechanism were given as

$$
\begin{aligned}
\mathbf{s}' &= [R_p, R_b, l_{61}, l_{62}, l_1, l_2, z, k_b, k_{62}, k_2, T_p, T_b] \\
&= [6, 15, 68, 68, 34, 46, 68, 10^{10}, 10^{10}, 10^{10}, 22.34, 42.883]
\end{aligned}
$$

and the compliances in each direction were

$$
\begin{aligned}
\boldsymbol{\kappa}' &= \left[\kappa'_{\theta_x}, \kappa'_{\theta_y}, \kappa'_{\theta_z}, \kappa'_x, \kappa'_y, \kappa'_z \right] \\
&= [0.1244, 0.2327, 0.3732, 0.001, 0.002464, 3.589 \times 10^{-4}]
\end{aligned}
$$

the compliance sum is 0.734195. Hence after optimization, the compliance sum is improved 1.72 times.

7.2.5 Spatial Four-Degree-of-Freedom Mechanism with Prismatic Actuators

7.2.5.1 Parameters Selection

Figure 4.11 shows the spatial four-degree-of-freedom mechanism with prismatic actuators, and Figure 4.12 represents position of the attachment points. For this mechanism,
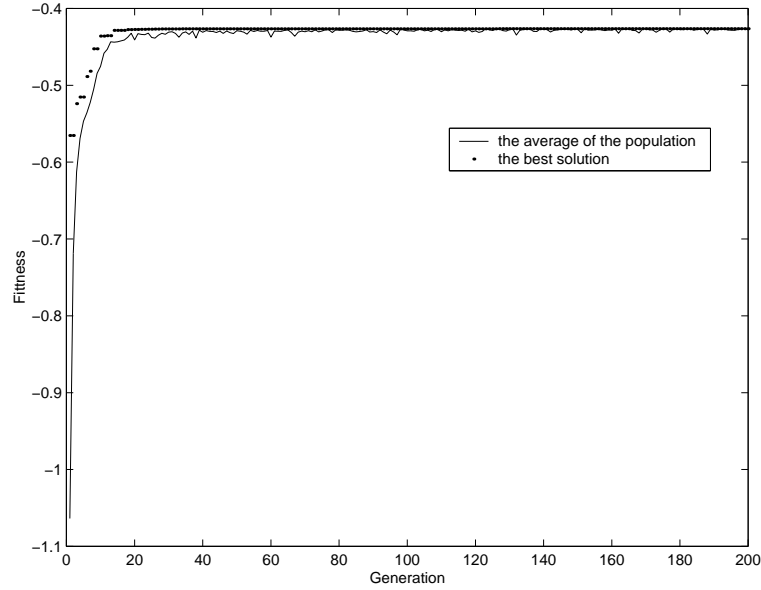
Figure 7.5: The evolution of the performance of the 5-dof mechanism with revolute actuators.

the optimization parameters are

$$\mathbf{s} = [R_p, R_b, l_{51}, l_{52}, z, T_p, T_b] \tag{7.15}$$

where R_p is the radius of the platform, R_b is the radius of the base, l_{51}, l_{52} are the link lengths for the 1st and 2nd link of the passive leg, respectively, z is the height of the platform, T_a, T_b are the angles to determine the attachment points on the base and on the platform, and their bounds are

$$R_p \in [10, 14] \ cm, R_b \in [20, 26] \ cm,$$
$$l_{51} \in [52, 70] \ cm, l_{52} \in [52, 70] \ cm,$$
$$z \in [66, 70] \ cm, T_a \in [25, 35]°, T_b \in [55, 65]°,$$

Again, the compliances are minimized as above.

7.2.5.2   Results

Results are given here only for one case with $\theta_{55} = -\pi/3, \theta_{56} = 2\pi/3$. Figure 7.6 shows the evolution of the best individual for 100 generations. The geometric and behavior parameters found by the GA after 100 generations are

$$\mathbf{s} = [R_p, R_b, l_{51}, l_{52}, z, T_a, T_b]$$

$$= [14, 26, 70, 55, 66, 35, 55]$$

and the compliances in each direction are

$$
\begin{aligned}
\boldsymbol{\kappa} &= \left[\kappa_{\theta_x}, \kappa_{\theta_y}, \kappa_{\theta_z}, \kappa_x, \kappa_y, \kappa_z\right] \\
&= [0.12, 0.5742, 3.747 \times 10^{-3}, 0.3165, 5.006 \times 10^{-11}, 3.345 \times 10^{-3}]
\end{aligned}
$$

the sum of the compliances is 1.017897.

Initially, the parameters for this mechanism were given as

$$
\begin{aligned}
\mathbf{s}' &= [R_p, R_b, l_{51}, l_{52}, z, T_a, T_b] \\
&= [12, 22, 68, 68, 68, 30, 60]
\end{aligned}
$$

and the compliances in each direction were

$$
\begin{aligned}
\boldsymbol{\kappa}' &= \left[\kappa'_{\theta_x}, \kappa'_{\theta_y}, \kappa'_{\theta_z}, \kappa'_x, \kappa'_y, \kappa'_z\right] \\
&= [0.5164, 1.4046, 1.5 \times 10^{-10}, 0.9087, 5.78 \times 10^{-11}, 0.011139]
\end{aligned}
$$

the compliance sum is 2.84085. Therefore, after optimization the compliance sum has been improved 2.8 times.
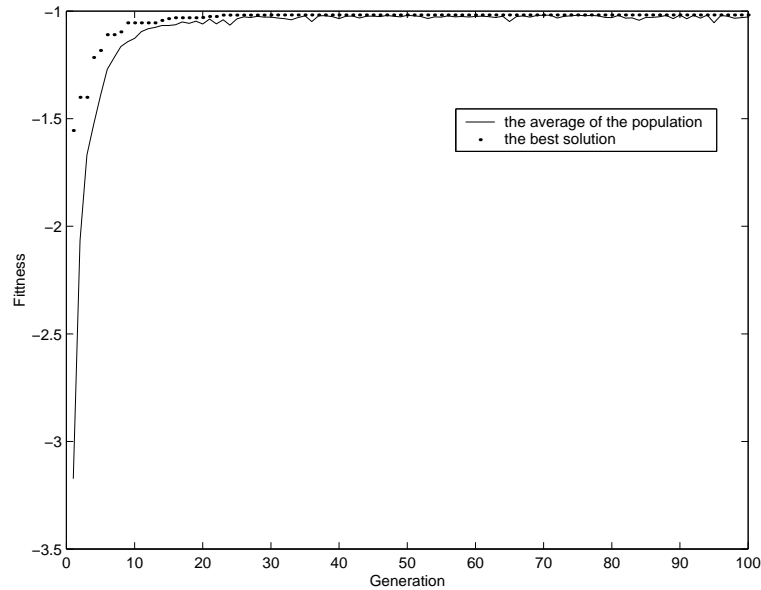
Figure 7.6: The evolution of the performance of the 4-dof mechanism with prismatic actuators.

7.2.6 Spatial Four-Degree-of-Freedom Mechanism with Revolute Actuators

7.2.6.1 Parameters Selection

A spatial four-degree-of-freedom mechanism with revolute actuators is shown in Figure 5.10 and the vertex distributions both on the base and on the platform are the same as in Figure 4.12. The parameters are

$$\mathbf{s} = [R_p, R_b, l_{51}, l_{52}, L_1, L_2, z, k_b, k_{52}, k_{54}, K_2, T_p, T_b] \tag{7.16}$$

where R_p is the radius of the platform, R_b is the radius of the base, l_{51}, l_{52} are the link lengths for the 1st and 2nd link of the passive leg, respectively, L_1, L_2 are the link lengths for the 1st and 2nd link of the actuated leg, respectively, z is the height of the platform, k_b and K_2 are the stiffnesses of the 1st and 2nd link of the actuated leg, k_{52}, k_{54} are the stiffnesses of the 1st and 2nd link of the passive leg, T_a, T_b are the angles to determine the attachment points on the base and on the platform, and their bounds are

$$R_p \in [5, 7] \ cm, R_b \in [14, 16] \ cm,$$
$$l_{51} \in [67, 69] \ cm, l_{52} \in [67, 69] \ cm,$$
$$L_1 \in [33, 35] \ cm, L_2 \in [45, 47] \ cm,$$
$$z \in [66, 70] \ cm,$$
$$T_a \in [25, 35]^\circ, T_b \in [55, 65]^\circ,$$
$$k_b, k_{52}, k_{54}, K_2 \in [10^6, 10^{10}]$$

7.2.6.2 Results

Results are given here for one case with $\theta_{55} = -\pi/3, \theta_{56} = 2\pi/3$. Figure 7.7 shows the evolution of the best individual for 100 generations. After 100 generations, the optimum geometric and behavior parameters for this configuration are

$$\begin{aligned} \mathbf{s} &= [R_p, R_b, l_{51}, l_{52}, L_1, L_2, z, k_b, k_{52}, k_{54}, K_2, T_a, T_b] \\ &= [7, 16, 67, 69, 35, 47, 67, 10^{10}, 9.9958 \times 10^9, 10^{10}, 9.9844 \times 10^9, 35, 55] \end{aligned}$$

and the compliances in each direction are

$$\begin{aligned}
\boldsymbol{\kappa} &= \left[\kappa_{\theta_x}, \kappa_{\theta_y}, \kappa_{\theta_z}, \kappa_x, \kappa_y, \kappa_z\right] \\
&= [0.28857, 0.019376, 8.66 \times 10^{-5}, 9.39 \times 10^{-4}, 5.751 \times 10^{-11}, 3.646 \times 10^{-5}]
\end{aligned}$$

the sum of the compliances is 0.309.

The initial guess for this mechanism was

$$\begin{aligned}
\mathbf{s}' &= [R_p, R_b, l_{51}, l_{52}, L_1, L_2, z, k_b, k_{52}, k_{54}, K_2, T_a, T_b] \\
&= [6, 15, 68, 68, 34, 46, 68, 10^{10}, 10^{10}, 10^{10}, 10^{10}, 30, 60]
\end{aligned}$$

and the compliances in each direction were

$$\begin{aligned}
\boldsymbol{\kappa}' &= \left[\kappa'_{\theta_x}, \kappa'_{\theta_y}, \kappa'_{\theta_z}, \kappa'_x, \kappa'_y, \kappa'_z\right] \\
&= [1.2807, 0.0628078, 0, 0.00276278, 0, 0.00003838]
\end{aligned}$$

the compliance sum is 1.3463. Hence, after optimization, the total compliance is improved 4.36 times.
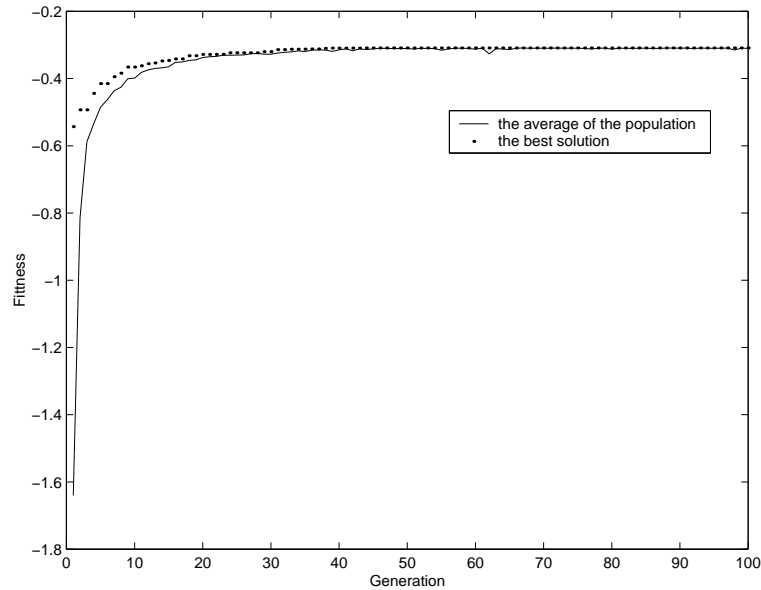
Figure 7.7: The evolution of the performance of the 4-dof mechanism with revolute actuators.

7.2.7 Spatial Three-Degree-of-Freedom Mechanism with Prismatic Actuators

7.2.7.1 Parameters Selection

The spatial three-degree-of-freedom mechanism with prismatic actuators is shown in Figure 4.4 and the position of the attachment points both on the base and on the platform is shown in Figure 4.5. The parameters are

$$\mathbf{s} = [R_p, R_b, z] \tag{7.17}$$

where R_p is the radius of the platform, R_b is the radius of the base, z is the height of the platform, and their bounds are set as

$$R_p \in [5, 10] \; cm, R_b \in [12, 14] \; cm,$$

$$z \in [66, 70] \; cm,$$

7.2.7.2 Results

Here only the case with $\theta_{45} = \pi/2, \theta_{46} = 0$ is discussed. Figure 7.8 shows the evolution of the best individual for 100 generations. After 100 generations, the optimal geometric and behavior parameters found by the GA are

$$\begin{aligned} \mathbf{s} &= [R_p, R_b, z] \\ &= [10, 12, 70] \end{aligned}$$

and the compliances in each direction are

$$\begin{aligned} \boldsymbol{\kappa} &= \left[\kappa_{\theta_x}, \kappa_{\theta_y}, \kappa_{\theta_z}, \kappa_x, \kappa_y, \kappa_z\right] \\ &= [6.8355 \times 10^{-2}, 6.8355 \times 10^{-2}, 0, 0, 0, 3.4177 \times 10^{-4}] \end{aligned}$$

the sum of the compliances is 0.137.

The initial geometric and behavior values for this mechanism were given as

$$\begin{aligned} \mathbf{s}' &= [R_p, R_b, z] \\ &= [6, 15, 68] \end{aligned}$$

and the compliances in each direction were

$$\boldsymbol{\kappa'} = [\kappa'_{\theta_x}, \kappa'_{\theta_y}, \kappa'_{\theta_z}, \kappa'_x, \kappa'_y, \kappa'_z]$$
$$= [0.192, 0.192, 0, 0, 0, 3.4566 \times 10^{-4}]$$

the compliance sum is 0.3844. Therefore, after optimization, the total compliance is improved 2.81 times which is a minor gain.
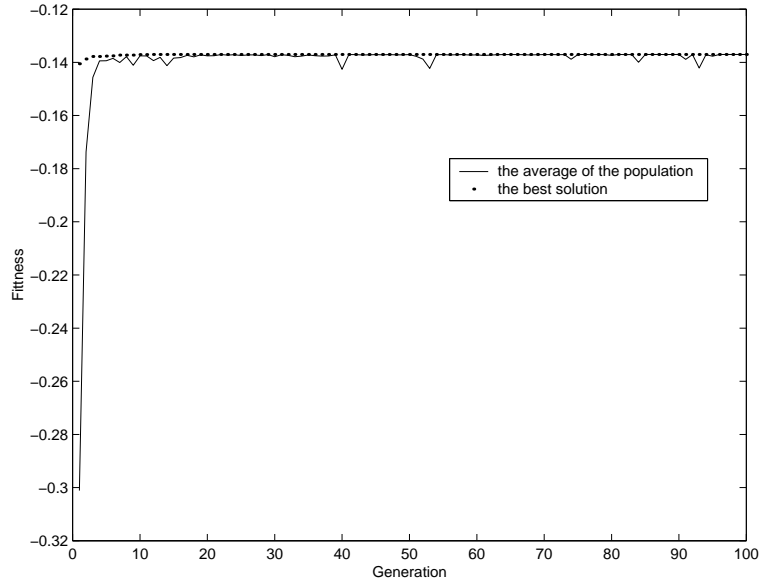
Figure 7.8: The evolution of the performance of the 3-dof mechanism with prismatic actuators.

7.2.8 Spatial Three-Degree-of-Freedom Mechanism with Revolute Actuators

7.2.8.1 Parameters Selection

The spatial three-degree-of-freedom mechanism with revolute actuators is shown in Figure 5.6 and the vertex distributions are the same as in Figure 4.5. The parameters are

$$\mathbf{s} = [R_p, R_b, l_1, l_2, z, k_2, k_b, k_{41}, k_{42}, k_{43}] \tag{7.18}$$

where R_p is the radius of the platform, R_b is the radius of the base, l_1, l_2 are the link length and k_b, k_2 are the stiffnesses for the 1st and 2nd link of the actuated leg,

respectively, k_{41}, k_{42} are the bending stiffnesses of the passive leg along x and y axes, and k_{43} is the torsional stiffness of the passive leg, z is the height of the platform, and their bounds are

$$R_p \in [5, 7] \ cm, R_b \in [14, 16] \ cm,$$

$$l_1 \in [33, 35] \ cm, l_2 \in [45, 47] \ cm,$$

$$z \in [66, 70] \ cm,$$

$$k_2, k_b, k_{41}, k_{42}, k_{43} \in [10^6, 10^{10}]$$

7.2.8.2 Results

Here only one case with $\theta_{45} = \pi/2, \theta_{46} = 0$ is analyzed. Figure 7.9 shows the evolution of the best individual for 100 generations. After running the program for 100 generations, the optimal architectural and behavior parameters can be found as

$$
\begin{aligned}
\mathbf{s} &= [R_p, R_b, l_1, l_2, z, k_2, k_b, k_{41}, k_{42}, k_{43}] \\
&= [7, 16, 33, 45, 69, 10^{10}, 10^{10}, 10^{10}, 10^{10}, 10^{10}]
\end{aligned}
$$

and the compliances in each direction are

$$
\begin{aligned}
\boldsymbol{\kappa} &= [\kappa_{\theta_x}, \kappa_{\theta_y}, \kappa_{\theta_z}, \kappa_x, \kappa_y, \kappa_z] \\
&= [1.0782 \times 10^{-2}, 1.0782 \times 10^{-2}, 0, 0, 0, 2.64 \times 10^{-5}]
\end{aligned}
$$

the sum of the compliances is 0.02159.

Before optimization, a series of parameters were guessed as

$$
\begin{aligned}
\mathbf{s}' &= [R_p, R_b, l_1, l_2, z, k_2, k_b, k_{41}, k_{42}, k_{43}] \\
&= [6, 15, 34, 46, 68, 10^{10}, 10^{10}, 10^{10}, 10^{10}, 10^{10}]
\end{aligned}
$$

and the compliance in each direction can be computed as

$$
\begin{aligned}
\boldsymbol{\kappa}' &= [\kappa'_{\theta_x}, \kappa'_{\theta_y}, \kappa'_{\theta_z}, \kappa'_x, \kappa'_y, \kappa'_z] \\
&= [2.12264 \times 10^{-2}, 2.12264 \times 10^{-2}, 0, 0, 0, 3.82 \times 10^{-5}]
\end{aligned}
$$

the compliance sum is 0.04249. Hence, after optimization, the total compliances is improved 1.97 times.
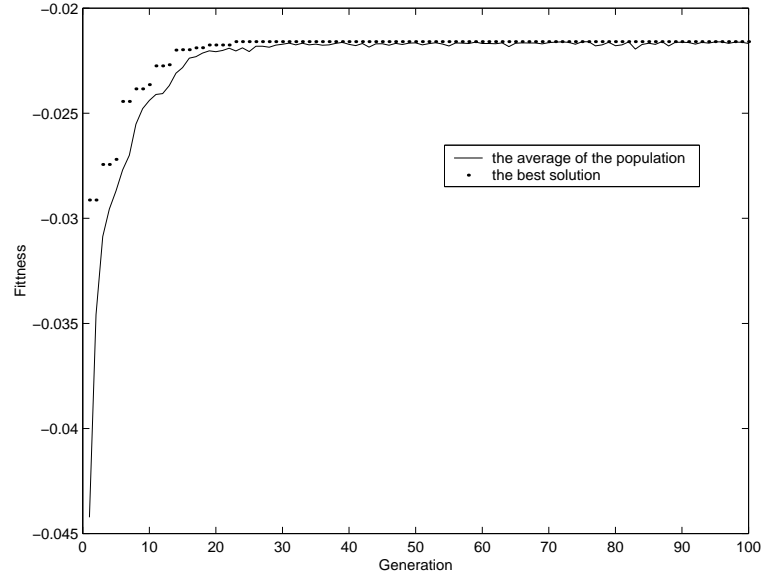
Figure 7.9: The evolution of the performance of the 3-dof mechanism with revolute actuators.

7.2.9 The Tricept Machine Tool Family

7.2.9.1 Parameters Selection

The schematic representation of the Tricept machine tool and the geometry of the joint distribution both on the base and platform are shown in Figures 4.23 and 4.24, respectively. The vector of optimization variables is therefore

$$\mathbf{s} = [R_p, R_b, z] \tag{7.19}$$

where R_p is the radius of the platform, R_b is the radius of the base, z is the height of the platform, and their bounds are specified based on the dimensions of the Tricept machine tool

$$R_p \in [200, 300] \ mm, R_b \in [400, 600] \ mm,$$

$$z \in [900, 1500] \ mm,$$

7.2.9.2 Results

The case with $\theta_{41} = \pi/2, \theta_{42} = 0$ is discussed here. Figure 7.10 shows the evolution of the best individual for 100 generations. The optimal architectural and behavior

parameters found by the GA after 100 generations are

$$\mathbf{s} = [R_p, R_b, z] = [300, 600, 900]$$

and the compliances in each direction are

$$
\begin{aligned}
\kappa &= \left[\kappa_{\theta_x}, \kappa_{\theta_y}, \kappa_{\theta_z}, \kappa_x, \kappa_y, \kappa_z\right] \\
&= [2.0576 \times 10^{-3}, 2.0576 \times 10^{-3}, 0, 1.667 \times 10^{-3}, 1.667 \times 10^{-3}, 3.703 \times 10^{-4}]
\end{aligned}
$$

the sum of the compliances is 0.0078189. Before optimization, the dimensions of the Tricept machine tool provided by Neos Robotics AB were

$$\mathbf{s}' = [R_p, R_b, z] = [225, 500, 1300]$$

and the compliances in each direction were

$$
\begin{aligned}
\kappa' &= \left[\kappa'_{\theta_x}, \kappa'_{\theta_y}, \kappa'_{\theta_z}, \kappa'_x, \kappa'_y, \kappa'_z\right] \\
&= [2.786 \times 10^{-3}, 2.786 \times 10^{-3}, 0, 4.708 \times 10^{-3}, 4.708 \times 10^{-3}, 3.4825 \times 10^{-4}]
\end{aligned}
$$

The sum of the compliances is 0.0153369. Hence, after optimization, the sum of the compliances is improved by a factor of 1.96 just by slightly enlarging the radius of the base and platform.
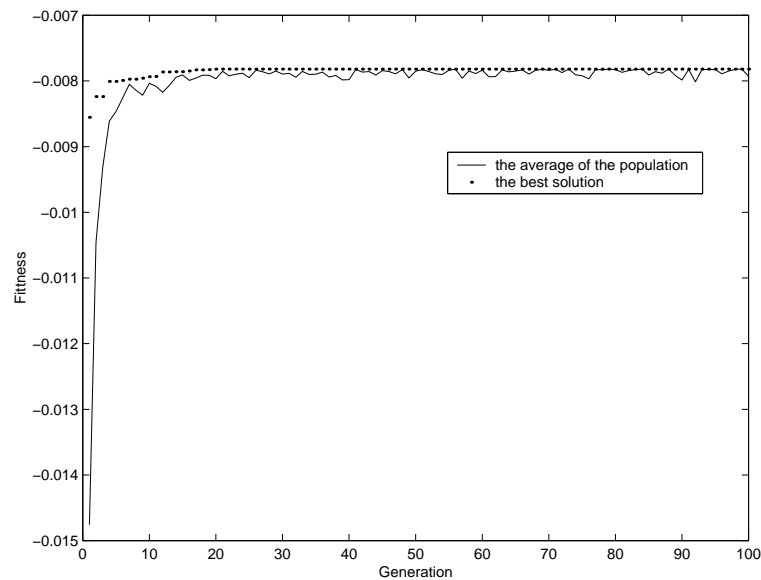
Figure 7.10: The evolution of the performance of the Tricept machine tool.

7.3 Conclusions

The kinetostatic model with its underlying design principles has been made more explicit through the implementation of optimization based on genetic algorithms in this chapter. A very remarkable implementation is the optimization of the Tricept machine tool family. After slightly adjusting the radius of the platform and the base, the total global stiffness can be improved 1.96 times. For the other mechanisms, the global stiffness are all obviously improved (normally 1.01 to 5.4 times). The kinetostatic model analyzed and obtained in previous chapters is employed for optimal structure design. From the results which have been achieved, it can be seen that the kinetostatic model can be applied for flexible mechanism analysis and global stiffness analysis, it can be further used as an optimization tool for parallel mechanisms. Moreover, the versatility of genetic algorithm compare to the conventional optimization methods is shown in this chapter, it is quite appropriate for dealing with multi-parameters problem.

Chapter 8

Conclusions and Future Work

8.1 Conclusions

Design of a parallel mechanism for machine tools which can achieve the desired rigidity and precision is a difficulty issue. This issue can now be addressed using a kineto-static modeling method. The research described in this thesis is aimed at developing a kinetostatic model which can be used for kinematic analysis, design and optimization of parallel kinematic machines. Both a theoretical study and implementation have been carried out. The theoretical study has resulted in new observations and design guidelines for parallel kinematic machines, which have been verified through the implementation of the kinetostatic modeling.

This thesis also demonstrates how the kinetostatic modeling can be applied in the design and optimization of the parallel kinematic machines with the consideration of

the characteristics of joint and link flexibilities and shows the idea that flexible links have significant effects on the parallel kinematic machines' stiffness and accuracy. Link flexibility cannot be neglected in machine tool design.

In this last chapter, a number of conclusions already drawn in the preceding chapters are now highlighted again with some concluding remarks.

1. **Degree-of-freedom issue for PKMs**

   Most of the work in the literature proposes a general architecture based on the concept of traditional "Gough-Stewart" mechanism type. This suggests that their parallel kinematic mechanisms have six degrees of freedom. However, in many applications such as axisymmetric machining — which requires at most five dofs — six degrees of freedom are not required. Moreover, most machining operations can be performed with 3 or 4 dofs. Hence, there is a need for efficient parallel mechanisms with less than six degrees of freedom. By contrast, the new types of PKMs described in Chapters 4 and 5 of this thesis represent a different view on a proper kinematic architecture design of PKMs. The mechanisms introduced in this thesis are a series of n-dof parallel mechanisms which consist of n identical actuated legs with six degrees of freedom and one passive leg with n degrees of freedom connecting the platform and the base. The degrees of freedom of the mechanism are dependent on the passive leg's degree of freedom. The purpose of using the passive leg is to limit the degrees of freedom to the desired ones. Since the external loads on the platform will induce bending and/or torsion in the passive leg, its mechanical design is a very important issue which can be addressed using the kinetostatic model proposed in this thesis.

2. **The most promising architectures**

   A topological study of different combinations of kinematic chain structures which correspond to the requirements — provide 5 degrees of freedom between the tool and the workpiece — is completed and the most promising kinematic structures are generated based on the Chebychev-Grübler-Kutzbach criterion and some other design criteria.

3. **The general stiffness model**

The general stiffness model for fully-parallel mechanisms with various actuator stiffnesses is established. The reliability of the general stiffness model is verified both in numerical method and in the software Pro/Engineer with the examples of a planar 2-dof parallel mechanisms with revolute actuators and a planar 3-dof parallel mechanism with prismatic actuators.

4. **Lumped modeling**

The sensitivity analysis — the errors on the platform positioning in the presence of the manufacturing tolerances, joint clearances and leg flexibility — has received less attention in the past. However, these influences could not be neglected in practice, and it has been shown that if the mechanism flexibility is considered, then the performances may become very poor and the main feature of the mechanism vanishes. Also there may exist singular mechanism configurations which must be avoided during motion, but that cannot be found from the mobility analysis of the rigid mechanism model. Therefore, a new method to analyze the effect of the link and joint flexibility on the mechanism's stiffness and precision is provided in this thesis. With this model, a significant effect on the mechanism's precision has been demonstrated. The influence of the structure parameters including material properties on the system behavior is discussed. The relationships between the mechanism stiffness and the flexibility of the links are derived and the necessity of taking the links' flexibility into account is demonstrated.

5. **Kinetostatic analysis of new types of parallel mechanisms**

Several new types of parallel mechanisms with prismatic/revolute actuators whose degrees of freedom are dependent on a constraining passive leg connecting the base and the platform are introduced. A general lumped kinetostatic model is proposed in order to account for joint and link compliances and for the analysis of the structural rigidity and accuracy of spatial parallel mechanisms which can be used for machine tool design. One can improve the rigidity of parallel kinematic mechanisms through optimization of the link rigidities and geometric dimensions to reach the maximized global stiffness and precision. Examples for 3-dof, 4-dof, 5-dof, 6-dof and the Tricept machine tool families are given in detail to illustrate the results. The discussions are given to account for the influence of the structure

parameters including material properties on the system behavior, and the behavior *vs* structural parameters. Stiffness/Compliance mappings are obtained as a visualization tool to aid in the use of the kinetostatic model. From plots, one can determine which regions of the workspace will satisfy some stiffness/compliance criteria.

6. **Establishment of the kinetostatic modeling**

   While establishing the kinetostatic model of the parallel kinematic mechanisms, two methods are applied, one is the principle of virtual work while the other is based on the theorem of velocity compatibility, both methods are verified.

7. **Optimization issue**

   Genetic algorithms have the advantages of robustness and good convergence properties. Since there are many optimization parameters and complex matrix computations, it is very difficulty to write the analytical expressions for each stiffness element. Hence, GAs are selected to fulfill the optimization issue. Interesting optimization results for the Tricept machine tool family are obtained: after slightly adjusting the radius of platform and base, the total global stiffness can be improved 1.96 times. The kinetostatic model analyzed and obtained in previous chapters is employed for optimum structure design. From the results which have been achieved, it can be seen that kinetostatic model can be applied for flexible mechanism analysis and global stiffness analysis. It can be further used as an optimization design tool for parallel manipulators.

Although the procedures are developed in particular for the new type of spatial parallel mechanisms proposed in this thesis, the approaches can be extended to all kinds of mechanisms.

8.2   Future Work

The work presented in this thesis was primarily concerned with kinematic structure design, analysis, optimization and establishment of the general kinetostatic model for parallel kinematic machines. No consideration was given to PKMs' dynamic behavior,

simulation and control issues. These are by no means neglected research topics. In order to make the parallel kinematic mechanisms into the parallel kinematic machines in reality, the future work is recommended.

1. A natural extension of this thesis work is the implementation of dynamic analysis, simulation, workspace volume optimization and control of PKMs with the consideration of flexible links. Such that an integrated design environment for configuration, design and analysis of parallel kinematic machines can be built. It can provide a concurrent synthesis of the physical machine prototype, the virtual machine (with virtual reality) and control algorithms. The kinetostatic analysis and optimization conducted in this thesis can be the basis for such an integration. The final results can further be evaluated by experimentation.

2. It is noted that the advantages of high speed machining of PKMs will be lost if the machine is not fully integrated into the overall manufacturing system. The integrated flexible infrastructure consists of each of the manufacturing support functions, i.e. CAD/CAM, inspection, fixturing, etc. Here, the simulation can be used to bridge the gaps between CAD, CAM and machine tool.

3. The reconfigurability (modularity) of PKMs is worth further research. Components of PKMs are simple and consist of standard units such as joints and links, which can be efficiently configured into the most suitable leg geometry for desired tasks. The modularity design of PKMs can lead to product sustainability.

Bibliography

Abbasi, W. A., Ridgeway, S. C., Adsit, P. D., Crane, C. D., and Duffy, J., 1997, "Investigation of a special 6-6 parallel platform for contour milling," in *Proceedings of the ASME - Manufacturing Science and Engineering Division*, pp. 373–380.

Advani, S. K., 1998, *The Kinematic Design of Flight Simulator Motion-Bases*. Delft University Press.

Alizade, R. I. and Tagiyev, N. R., 1994, "A forward and reverse displacement analysis of a 6-dof in-parallel manipulator," *Mechanism and Machine Theory*, Vol. 29, No. 1, pp. 115–124.

Angeles, J., 1997, *Fundamentals of Robotic Mechanical Systems: Theory, Methods, and Algorithms*. Springer-Verlag New York, Inc.

Arai, T., Cleary, K., Homma, K., Adachi, H., and Nakamura, T., 1991, "Development of parallel link manipulator for underground excavation task," in *1991 International Symposium on Advanced Robot Technology*, pp. 541–548.

Aronson, R. B., 1997, "Hexapods: Hot or ho hum?," *Manufacturing Engineering*, pp. 60–67.

Asada, H. and Granito, J. A. C., 1985, "Kinematics and statics characterization of wrist joints and their optimal design," in *Proc. IEEE Int. Conf. Robotics Automat.*, pp. 244–250.

Asada, H. and Slotine, J. J. E., 1986, *Robot Analysis and Control*. John Wiley & Sons.

Bailey, P., 1994, "The merits of hexapods for robotics applications," in *Conference on next steps for industrial Robotics*, pp. 11/8–16/8, London.

Baker, J. E., 1992, "On mobility and relative freedoms in multiloop linkages and structures," *Mechanism and Machine Theory*, Vol. 16, No. 6, pp. 583–597.

Behi, F., 1988, "Kinematic analysis for a six-degree-of-freedom 3-prps parallel mechanism," *IEEE Journal of Robotics and Automation*, Vol. 4, No. 5, pp. 561–565.

Bianchi, G., Fassi, I., and Molinari-Tosatti, L., 2000, "A virtual prototyping environment for pkm analysis and design," in *Proceedings of Year 2000 Parallel Kinematic Machines International Conference*.

Boër, C. R., Molinari-Tosatti, L., and Smith, K. S., 1999, *Parallel Kinematic Machines*. Springer-Verlag London Limited.

Boudreau, R. and Gosselin, C. M., 1998, "The synthesis of planar parallel manipulators with a genetic algorithm," in *Proceedings of the ASME Design Engineering Technical Conference*, Atlanta, GA.

Boudreau, R. and Turkkan, N., 1996, "Solving the forward kinematics of parallel manipulators with a genetic algorithm," *Journal of Robotic Systems*, Vol. 13, No. 2, pp. 111–125.

Caenen, J. and Angue, J., 1990, "Identification of geometric and non geometric parameters of robots," *Proceedings of the 1990 IEEE International Conference on Robotics and Automation*, pp. 1032–1037.

Chang, L. W. and Hamilton, J. F., 1991a, "Dynamics of robotic manipulator with flexible links," *ASME Journal of Dynamic Systems, Measurement, and Control*, Vol. 113, pp. 54–59.

Chang, L. W. and Hamilton, J. F., 1991b, "The kinematics of robotic manipulator with flexible links using an equivalent rigid link system(erls) model," *ASME Journal of Dynamic Systems, Measurement, and Control*, Vol. 113, pp. 48–53.

Chen, I.-M., 1994, *Theory and application of modular reconfigurable robotic systems*. Ph. D thesis, California Institute of Technology.

Chen, J. and Chao, L. M., 1986, "Positioning error analysis for robotic manipulator with all rotary joints," in *Proceedings of IEEE International Conference on Robotics and Automation*, pp. 1011–1016.

Chen, N. and Song, S. M., 1992, "Direct position analysis of the 4-6 stewart platform," *Robotics, Spatial Mechanisms, and Mechanical Systems*, Vol. 45, pp. 75–80.

Chi, Y. L., 1999, *Systems and Methods Employing a Rotary Track For Machining and Manufacturing*. WIPO Patent No. WO 99/38646.

Cléroux, L. and Gosselin, C. M., 1996, "Modeling and identification of non-geometric parameters in semi-flexible serial robotic mechanisms," in *Proceedings of the ASME Mechanisms Conference*, Irvine, California.

Cléroux, L., Gourdeau, R., and Cloutier, G. M., 1995, "A semi-flexible geometric model for serial manipulators," *Robotica*, Vol. 13, pp. 385–395.

Clinton, C. M., Zhang, G., and Wavering, A. J., 1997, *Stiffness Modeling of a Stewart-Platform-Based Milling Machine*. http://isd.cme.nist.gov/cgi-bin/document-search.pl.

Cohen, R., 1992, "Conceptual design of a modular robot," *ASME Journal of Mechanical Design*, Vol. 112, pp. 117–125.

Davidor, Y., 1991, *Genetic algorithms and robotics: a heuristic strategy for optimization*. World Scientific Publishing Co. Pte. Ltd.

Davis, L., 1991, *Handbook of genetic algorithms*. Van Nostrand Reinhold, New York.

Denavit, J. and Hartenberg, R., 1955, "A kinematic notation for lower-pair mechanisms based on matrices," *ASME Journal of Applied Mechanics*, pp. 215–221.

Earl, C. F. and Rooney, J., 1983, "Some kinematic structures for robot manipulator designs," *Journal of Mechanisms, Transmissions, and Automation in Design*, Vol. 105, No. 1, pp. 15–22.

El-Khasawneh, B. S. and Ferreira, P. M., 1999, "Computation of stiffness and stiffness bounds for parallel link manipulators," *International journal of Machine Tools & Manufacture*, Vol. 39, pp. 321–342.

Everett, L. J. and Hsu, T. W., 1989, "The theory of kinematic parameter identification for industrial robots," *ASME Journal of Dynamic Systems, Measurement, and Control*, Vol. 111, No. 2, pp. 96 – 100.

Fassi, I., Molinari-Tosatti, L., Negri, S., Bernardo, G. D., and Bianchi, G., 1999, "A concept for a computer aided configuration tool for parallel kinematic machines," in *ICAR'99*, pp. 563–567.

Fattah, A., Angeles, J., and Misra, A. K., 1994, "Direct kinematics of a 3-dof spatial parallel manipulator with flexible legs," *Proceedings of the ASME Mechanisms Conference*, pp. 285–291.

Fichter, E., 1986, "A stewart platform-based manipulator: General theory and practical construction," *The International Journal of Robotics Research*, Vol. 5, No. 2, pp. 157–182.

Fogel, L. J., Owens, A. J., and Walsh, M. J., 1966, *Artificial Intelligence Through Simulated Evolution*. John Wiley & Sons, Inc.

Gen, M. and Cheng, R., 1997, *Genetic algorithms and engineering design*. John Wiley & Sons.

Goldberg, D., 1989, *Genetic Algorithms in Search, Optimization and Machine Learning*. Addison-Wesley.

Goldberg, D. E. and Samtani, M. P., 1986, "Engineering optimization via genetic algorithm," in *Ninth Conference on Electronic Computation*, pp. 471–482.

Gopalakrishnan, V. and Kota, S., 1998, "A parallely actuated work support module for reconfigurable machining systems," in *Proceedings of 1998 ASME Design Engineering Technical Conferences*, pp. 1–9.

Gosselin, C. M., 1988, *Kinematic Analysis,Optimization and Programming of Parallel Robotic Manipulators*. Ph. D thesis, McGill University.

Gosselin, C. M., 1990, "Stiffness mapping for parallel manipulators," *IEEE Transactions on Robotics and Automation*, Vol. 6, No. 3, pp. 377–382.

Gosselin, C. M. and Angeles, J., 1988, "The optimum kinematic design of a planar three-degree-of-freedom parallel manipulator," *ASME Journal of Mechanisms, Transmissions, and Automation in Design*, Vol. 110, No. 1, pp. 35–41.

Gosselin, C. M. and Angeles, J., 1990, "Singularity analysis of closed-loop kinematic chains," *IEEE Transactions on Robotics and Automation*, Vol. 6, No. 3, pp. 281–290.

Gosselin, C. M. and Guillot, M., 1991, "The synthesis of manipulators with prescribed workspace," *ASME Journal of Mechanical Design*, Vol. 113, pp. 451–455.

Gosselin, C. M. and Hamel, J., 1994, "The agile eye: A high-performance three-degree-of-freedom camera-orienting device," in *Proceedings of the IEEE International Conference on Robotics and Automation*, pp. 781–786.

Gosselin, C. M. and Wang, J., 1997, "Singularity loci of planar parallel manipulators with revolute actuators," *Journal of Robotics and Autonomous System*, Vol. 21, pp. 377–398.

Gosselin, C. M. and Zhang, D., 1999, "Stiffness analysis of parallel mechanisms using a lumped model,". Technical report, Département de Génie Mécanique, Université Laval.

Gough, V., 1956, "Contribution to discussion to papers on research in automobile stability and control and in tire performance," in *Proceedings of the Auto. Div. Instn mech. Engrs*, p. 392.

Gregorio, R. D. and Parenti-Castelli, V., 1999, "Influence of leg flexibility on the kinetostatic behavior of a 3-dof fully-parallel manipulator," in *Proceedings of Tenth World Congress on the Theory of Machines and Mechanisms*, pp. 1091–1098.

Griffis, M. and Duffy, J., 1989, "A forward displacement analysis of a class of stewart platform," *Journal of Robotics Systems*, Vol. 6, No. 6, pp. 703–720.

Harary, F., 1969, *Graph Theory*. Addison-Wesley.

Hayati, S. A., Tso, K., and Roston, G., 1988, "Robot geometry calibration," in *Proceedings of the IEEE International Conference on Robotics and Automation*, pp. 947–951.

Heisel, U., 1999, "Precision requirements of hexapod-machines and investigation results," in *"Parallel Kinematic Machines — Theoretical Aspects and Industrial Requirements", editors: C. R. Boër, L. Molinari-Tosatti and K. S. Smith, Springer Publishers*, pp. 131–150.

Holland, J. H., 1975, *Adaptation in Natural and Artificial Systems*. The University of Michigan Press.

Hollingum, J., 1997, "Features: Hexapods to take over?," *Industrial Robot*, Vol. 24, pp. 428–431.

Honegger, M., Codourey, A., and Burdet, E., 1997, "Adaptive control of the hexaglide, a 6 dof parallel manipulator," in *Proceedings of the IEEE International Conference on Robotics and Automation, Albuquerque*, USA.

Hong, K.-S., Kim, Y.-M., Choi, C., and Shin, K., 1997, "Inverse kinematics of a serial manipulator: Kinematic redundancy and two approaches for closed-form solutions," in *Proceedings of IEEE International Conference on Robotics and Automation*, pp. 780–785.

Houck, C. R., Joines, J. A., and Kay, M. G., 1995, "A genetic algorithm for function optimization: A matlab implementation,". Technical report, North Carolina State University.

Hsu, T. W. and Everett, L. J., 1985, "Identification of the kinematic parameters of robot manipulator for positional accuracy improvement," in *Proceedings of the ASME Conference on Computers in Engineering*, pp. 263–267.

Huber, R., 1993, "This man wants to change the way you machine part," *Production*.

Hunt, K., 1983, "Structural kinematics of in-parallel-actuated robot-arms," *ASME Journal of Mechanisms, Transmissions and Automation in Design*, Vol. 105, No. 4, pp. 705–712.

Hunt, K. H., 1978, *Kinematic Geometry of Mechanisms*. Clarendon Press, Oxford.

Joines, J. and Houck, C., 1994, "On the use of non-stationary penalty functions to solve constrained optimization problems with genetic algorithms," in *1994 IEEE International Symposium Evolutionary Computation*, pp. 579–584, Orlando, FL.

Jonker, B., 1990, "A finite element dynamic analysis of flexible manipulators," *The International Journal of Robotics Research*, Vol. 9, pp. 59–74.

Judd, R. P. and Knasinski, A. B., 1990, "A technique to calibrate industrial robots with experimental verification," *IEEE Transactions on Robotics and Automation*, Vol. 6, No. 1, pp. 20–30.

Kempfer, L., 1994, "The cutting edge of solids," *Computer Aided Engineering*, Vol. 13, pp. 40–42.

Kerr, D. R., 1989, "Analysis, properties, and design of a stewart-platform transducer," *ASME Journal of Mechanisms, Transmissions and Automation in Design*, Vol. 111, pp. 25–28.

Klein, C. A. and Blaho, B. E., 1987, "Dexterity measures for the design and control of kinematically redundant manipulators," *International journal of Robotics Research*, Vol. 6, No. 2, pp. 72–83.

Kohli, D. and Osvatic, M., 1993, "Inverse kinematics of general 6r and 5r, p serial manipulators," *Transactions Of the ASME Journal of Mechanical Design*, Vol. 115, No. 4, pp. 922–931.

Koza, J. R., 1991, "Evolving a computer program to generate random numbers using the genetic programming paradigm," in *Proceedings of 4th Int. Conf. on Genetic Algorithms*, pp. 37–44.

Lauffer, J., Hinnerichs, T., Kuo, C. P., Wada, B., Ewaldz, D., Winfough, B., and Shankar, N., 1996, "Milling machine for the 21st century - goals, approach, characterization and modeling," in *Proceedings of SPIE - The International Society for Optical Engineering Smart Structures and Materials 1996: Industrial and Commercial Applications of Smart Structures Technologies*, Vol. 2721, pp. 326–340, San Diego.

Lee, H.-Y. and Reinholtz, C. F., 1996, "Inverse kinematics of serial-chain manipulators," *Transactions Of the ASME Journal of Mechanical Design*, Vol. 118, No. 3, pp. 396–403.

Lee, S. and Kim, S., 1993, "Efficient inverse kinematics for serial connections of serial and parallel manipulators," in *Proceedings of the 1993 IEEE/RSJ International Conference on Intelligent Robots and Systems*, pp. 1635–1641.

Lin, W., Crane III, C. D., and Griffis, M., 1994, "Closed-form forward displacement analyses of the 4-5 in-parallel platforms," *ASME Journal of Mechanical Design*, Vol. 116, pp. 47–53.

Manocha, D. and Canny, J. F., 1992, "Efficient inverse kinematics for general serial manipulators," in *Proceedings of the 1992 Japan - USA Symposium on Flexible Automation*, pp. 125–129.

Martin, H. C., 1966, *Introduction to matrix methods of structural analysis.* McGraw-Hill Book Company.

Matar, G., 1997, "Hexapod: Application-led technology," *Prototyping Technology International*, pp. 70–72.

Meghdari, A., 1991, "A variational approach for modeling flexibility effects in manipulator arms," *Robotica*, Vol. 9, pp. 213–217.

Merlet, J. P., 1987, "Parallel manipulators, part i: Theory, design, kinematics, dynamics and control," *Technical report, 646, INRIA, France.*

Merlet, J.-P., 1997, *6 Degrees of Freedom robots.* http://www.inria.fr/prisme/.../subsection324.htm.

Michalewicz, Z., 1994, *Genetic Algorithms + Data Structures = Evolution Programs.* AI Series. Springer-Verlag, New York.

Molinari-Tosatti, L., Bianchi, G., Fassi, I., Boër, C. R., and Jovane, F., 1997, "An integrated methodology for the design of parallel kinematic machines," *Annals of CIRP*, pp. 341–345.

Nearchou, A., 1998, "Solving the inverse kinematics problem of redundant robots operating in complex environments via a modified genetic algorithm," *Mechanism and Machine Theory*, Vol. 33, No. 3, pp. 273–292.

Owen, J., 1999, "Tomorrow's machines in paris," *SME Manufacturing Engineering*, Vol. 123, No. 2, pp. 118 – 129.

Physik-Instrumente, 1997, "Hexapod 6 axis micropositioning system," in *Supplement to the catalog No. 111/112*, pp. 36–37.

Pierrot, F. and Shibukawa, T., 1999, "From hexa to hexam," in *"Parallel Kinematic Machines — Theoretical Aspects and Industrial Requirements", editors: C. R. Boër, L. Molinari-Tosatti and K. S. Smith, Springer Publishers*, pp. 357–364.

Pouliot, N. A., Gosselin, C. M., and Nahon, M. A., 1998, "Motion simulation capabilities of three-degree-of-freedom flight simulators," *AIAA Journal of Aircraft*, Vol. 35, No. 1, pp. 9–17.

Powell, N. P., Whittingham, B. D., and Gindy, N. N. Z., 1999, "Parallel link mechanism machine tools: acceptance testing and performance analysis," in *"Parallel*

Kinematic Machines — Theoretical Aspects and Industrial Requirements", editors: C. R. Boër, L. Molinari-Tosatti and K. S. Smith, Springer Publishers, pp. 327–344.

Pritschow, G., 1999, "Research and development in the field of parallel kinematic systems in europe," in *"Parallel Kinematic Machines — Theoretical Aspects and Industrial Requirements", editors: C. R. Boër, L. Molinari-Tosatti and K. S. Smith, Springer Publishers*, pp. 3–15.

Pritschow, G. and Wurst, K.-H., 1997, "Systematic design of hexapods and other parallel link systems," *CIRP Annals - Manufacturing Technology*, Vol. 46, No. 1, pp. 291–295.

Rechenberg, L., 1973, *Evolutionsstrategie: Optimierung Technischer Systeme nach Prinzipien der Biologischen Evolution*. Frommann-Holzboog, Stuttgart.

Rehsteiner, F., Neugebauer, R., Spiewak, S., and Wieland, F., 1999, "Putting parallel kinematics machines (pkm) to productive work," *Annals of CIRP*, pp. 345–350.

Reinholz, C. and Gokhale, D., 1987, "Design and analysis of variable geometry truss robot," in *Proc. 9th Applied Mechanisms Conference*, U.S.A.

Rey, L. and Clavel, R., 1999, "The delta parallel robot," in *"Parallel Kinematic Machines — Theoretical Aspects and Industrial Requirements", editors: C. R. Boër, L. Molinari-Tosatti and K. S. Smith, Springer Publishers*, pp. 401–418.

Ryu, S. J., Kim, J. W., Hwang, J. C., Park, C., Cao, H. S., Lee, K., Lee, Y., Cornel, U., Park, F. C., and Kim, J., 1999, "Eclipse: an overactuated parallel mechanism for rapid machining," in *"Parallel Kinematic Machines — Theoretical Aspects and Industrial Requirements", editors: C. R. Boër, L. Molinari-Tosatti and K. S. Smith, Springer Publishers*, pp. 441–455.

Sefrioui, J. and Gosselin, C. M., 1993, "Singularity analysis of representation of planar parallel manipulators," *Journal of Robotics and Autonomous System*, Vol. 10, pp. 209–224.

Stewart, D., 1965, "A platform with six degrees of freedom," in *Proceedings of the Institution of Mechanical Engineers*, Vol. 180, pp. 371–378.

Stone, H. W., 1987, *Kinematic Modeling, Identification, and Control of Robotic Manipulators*. Kluwer Academic Publishers.

Tahmasebi, F., 1993, *Kinematic Synthesis and Analysis of a Novel Class of Six-DOF Parallel Minimanipulators*. Ph. D thesis, University of Maryland.

Tahmasebi, F. and Tsai, L. W., 1994, *Six-degree-of-freedom parallel "minimanipulator" with three inextensible limbs*. United States Patent, Patent Number: 5,279,176.

Tang, S. and Wang, C., 1987, "Computation of the effects of link deflections and joint compliance on robot positioning," *Proceeding of the 1987 IEEE International Conference on Robotics and Automation*, pp. 910–915.

Timoshenko, S. P. and Gere, J. M., 1972, *Mechanics of materials*. PWS publication company.

Tönshoff, H. K., Grendel, H., and Kaak, R., 1999, "Structure and characteristics of the hybrid manipulator georg v," in *"Parallel Kinematic Machines — Theoretical Aspects and Industrial Requirements", editors: C. R. Boër, L. Molinari-Tosatti and K. S. Smith, Springer Publishers*, pp. 365–376.

Tsai, L. and Lee, J. J., 1989, "Kinematic analysis of tendon-driven robotics mechanisms using graph theory," *ASME Journal of Mechanisms, Transmissions and Automation in Design*, Vol. 111, pp. 59–65.

Uchiyama, M., 1994, "A 6 d.o.f. parallel robot hexa," *Advanced Robotics: The International Journal of the Robotics Society of Japan*, Vol. 8, p. 601.

Wang, C. K., 1966, *Matrix methods of structural analysis*. International Textbook Company.

Wang, Q. Y., Zou, H., Zhao, M. Y., and Li, Q. M., 1997, "Design and kinematics of a parallel manipulator for manufacturing," *Annals of CIRP*, pp. 297–300.

Warnecke, H. J., Neugebauer, R., and Wieland, F., 1998, "Development of hexapod based machine tool," *Annals of CIRP*, pp. 337–340.

Wavering, A. J., 1999, "Parallel kinematic machine research at nist: Past, present, and future," in *"Parallel Kinematic Machines — Theoretical Aspects and Industrial Requirements", editors: C. R. Boër, L. Molinari-Tosatti and K. S. Smith, Springer Publishers*, pp. 17–31.

Weck, M., Giesler, M., Meylahn, A., and Staimer, D., 1999, "Parallel kinematics: the importance of enabling technologies," in *"Parallel Kinematic Machines*

— *Theoretical Aspects and Industrial Requirements", editors: C. R. Boër, L. Molinari-Tosatti and K. S. Smith, Springer Publishers*, pp. 283–294.

Whitney, D. E., Lozinski, C. A., and Rourke, J. M., 1986, "Industrial robot forward calibration method and results," *ASME Journal of Dynamic Systems, Measurement and Control*, pp. 1–8.

Winter, G., Periaux, Galan, M., and Cuesta, P., 1995, *Genetic algorithms in engineering and computer science.* Chichester: John Wiley & Sons.

Wurst, K. H., 1999, "Linapod - machine tools as parallel link systems based on a modular design," in *"Parallel Kinematic Machines — Theoretical Aspects and Industrial Requirements", editors: C. R. Boër, L. Molinari-Tosatti and K. S. Smith, Springer Publishers*, pp. 377–394.

Xi, J. and Mechefske, C., 2000, "Integrated development of lightweight reconfigurable parallel mechanisms," in *Proceedings of International Conference on Integrated Design and Manufacturing in Mechanical Engineering.*

Yoshikawa, T., 1984, "Analysis and control of robot manipulators with redundancy," in *Proceedings of First International Symposium on Robotics Research*, pp. 735–747.

Zhang, C. D. and Song, S. M., 1992, "Forward position analysis of nearly general stewart platform," *Robotics, Spatial Mechanisms, and Mechanical Systems*, Vol. 45, pp. 81–87.

Zhang, W., 1994, *An Integrated Environment for CADCAM of Mechanical Systems.* Ph.D. thesis, Delft University of Technology.

Zhang, W. J. and Li, Q., 1999, "On a new approach to mechanism topology identification," *ASME Journal of Mechanical Design*, Vol. 121, pp. 57–64.

Appendix   A

Stiffness/Compliance Mesh Graphs
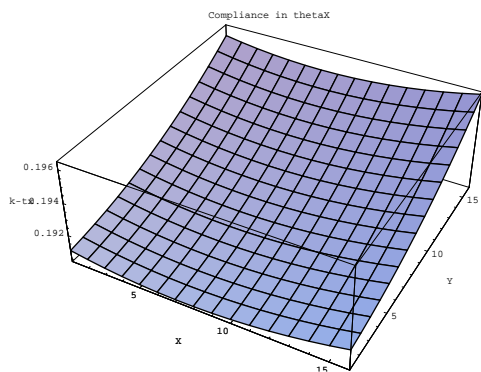
(a) Compliance in θ_x
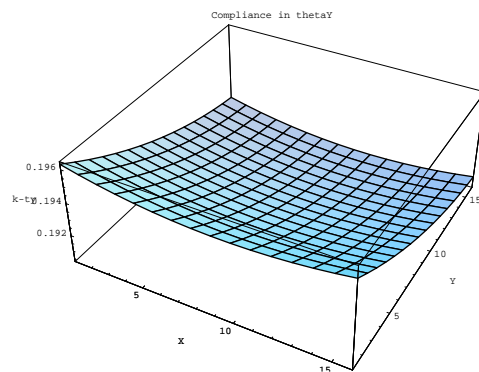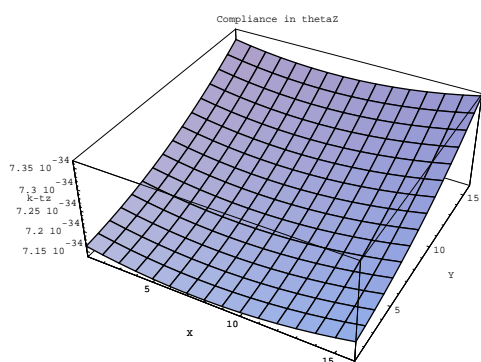
(b) Compliance in θ_y
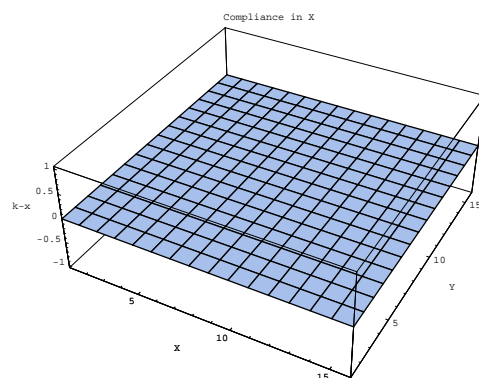
(c) Compliance in θ_z
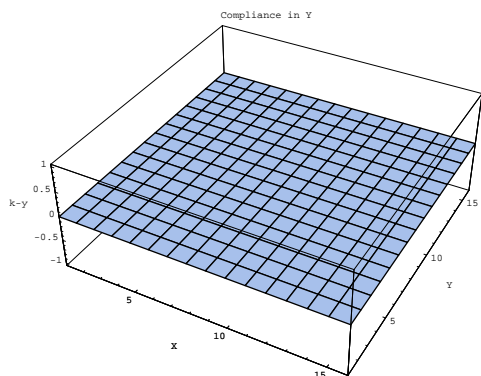
(d) Compliance in x
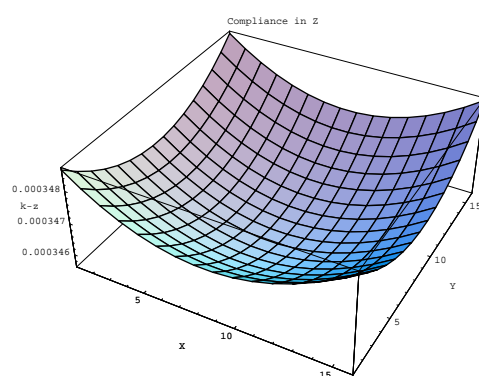
(e) Compliance in y

(f) Compliance in z

Figure A.1: Compliance mesh maps for the spatial 3-dof parallel mechanism with prismatic actuators.
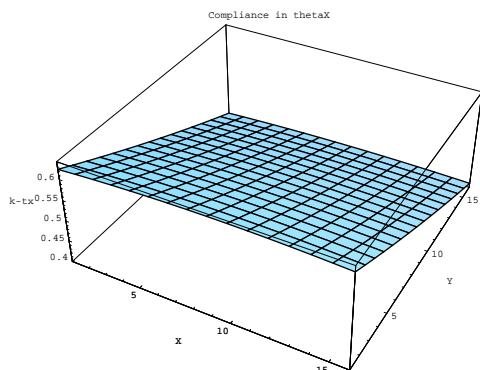
(a) Compliance in θ_x
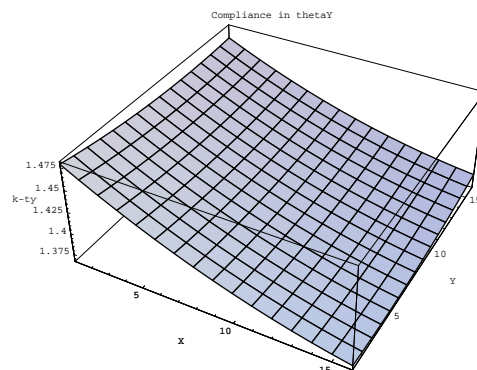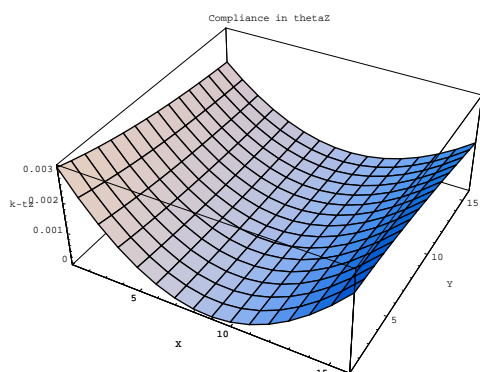
(b) Compliance in θ_y
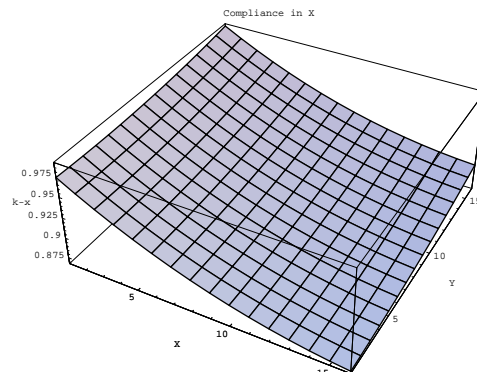
(c) Compliance in θ_z
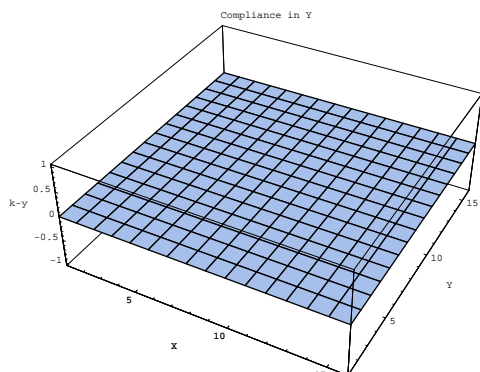
(d) Compliance in x
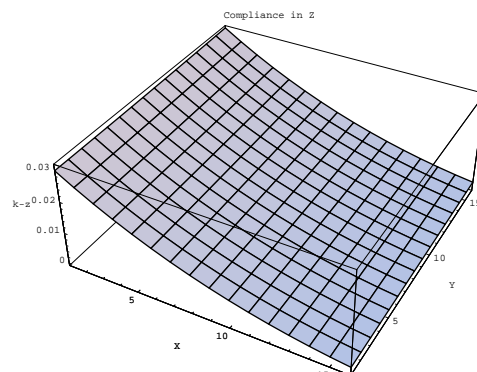
(e) Compliance in y

(f) Compliance in z

Figure A.2: Compliance mesh maps for the spatial 4-dof parallel mechanism with prismatic actuators.
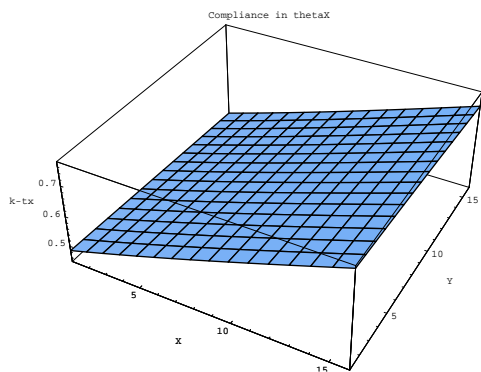
(a) Compliance in θ_x
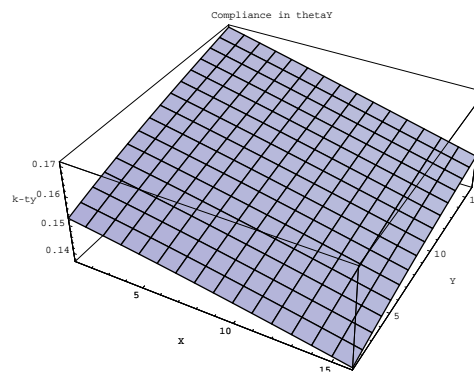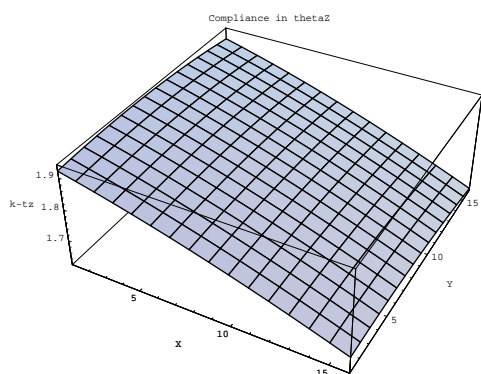
(b) Compliance in θ_y
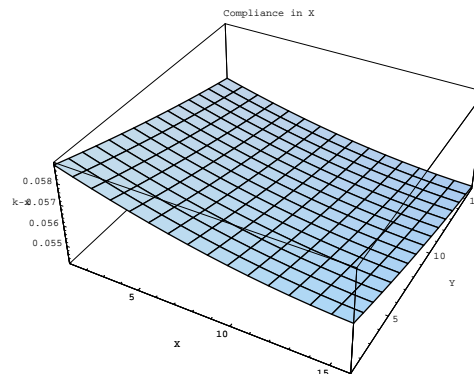
(c) Compliance in θ_z
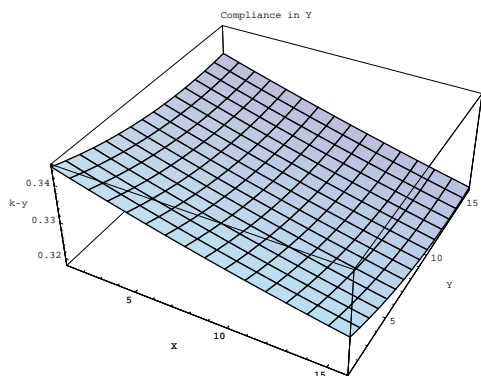
(d) Compliance in x
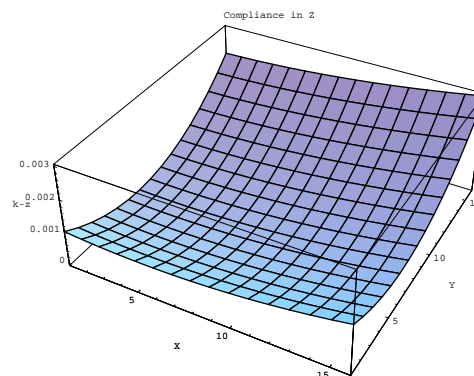
(e) Compliance in y

(f) Compliance in z

Figure A.3: Compliance mesh maps for the spatial 5-dof parallel mechanism with prismatic actuators.
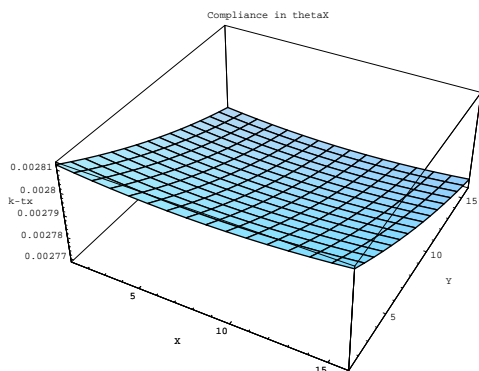
(a) Compliance in θ_x
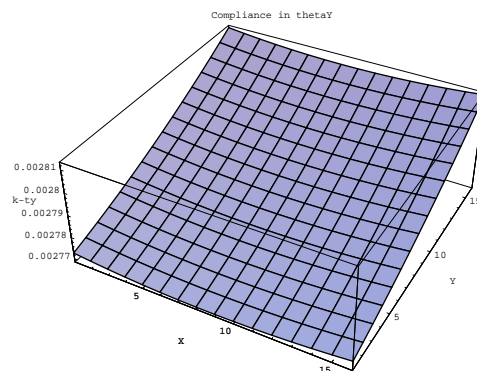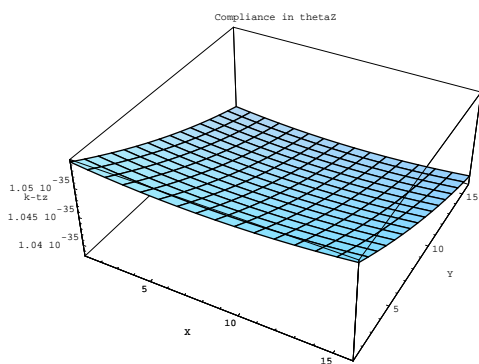
(b) Compliance in θ_y
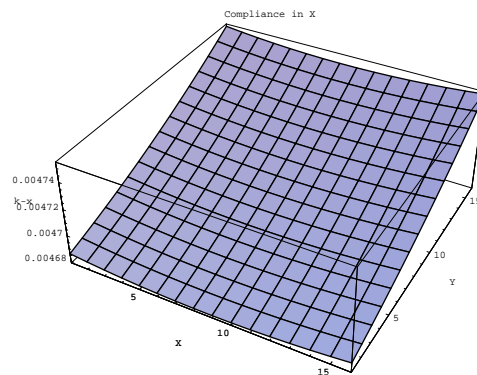
(c) Compliance in θ_z
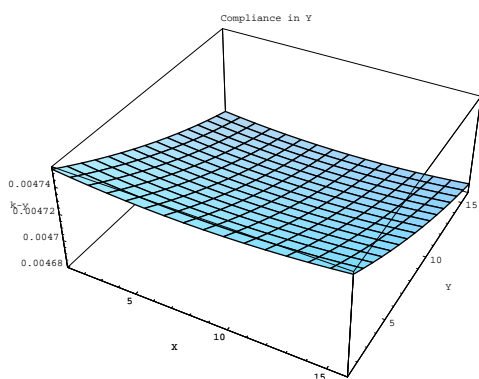
(d) Compliance in x
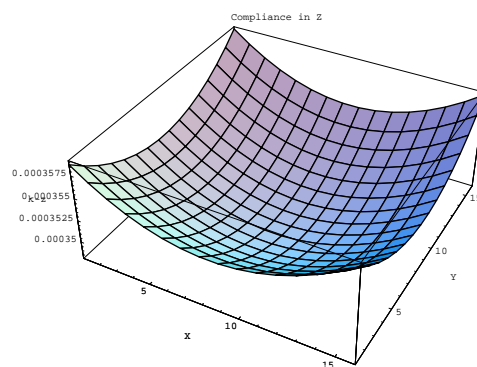
(e) Compliance in y

(f) Compliance in z

Figure A.4: Compliance mesh maps for the Tricept machine tool.
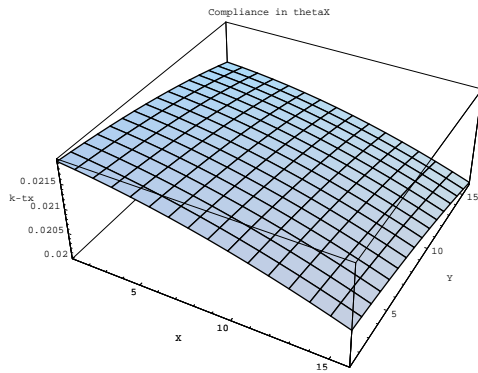
(a) Compliance in θ_x
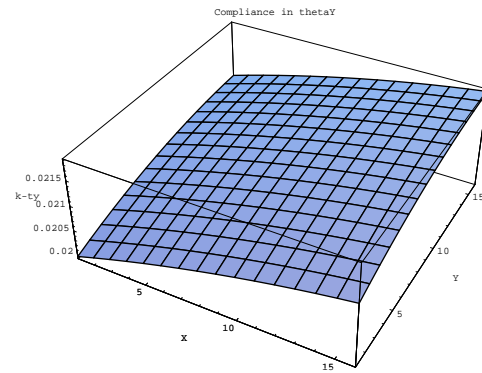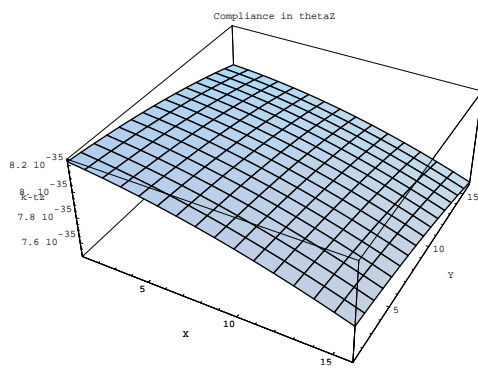
(b) Compliance in θ_y
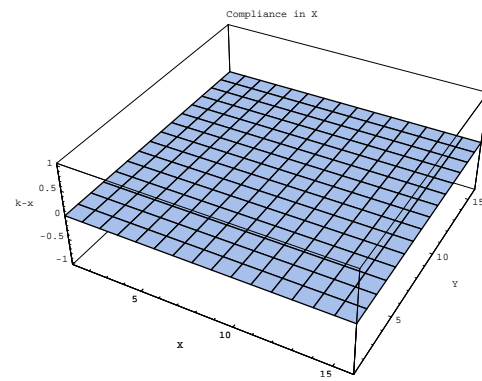
(c) Compliance in θ_z
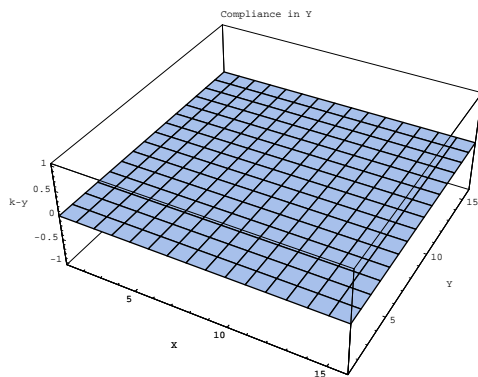
(d) Compliance in x
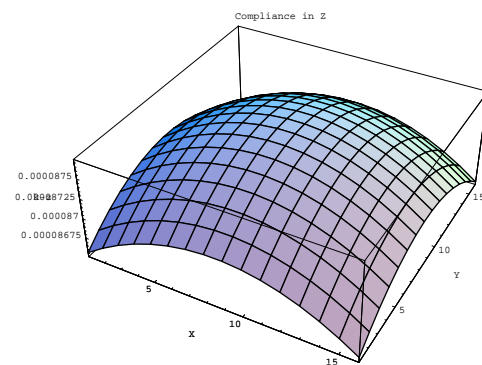
(e) Compliance in y

(f) Compliance in z

Figure A.5: Compliance mesh maps for the spatial 3-dof parallel mechanism with revolute actuators.
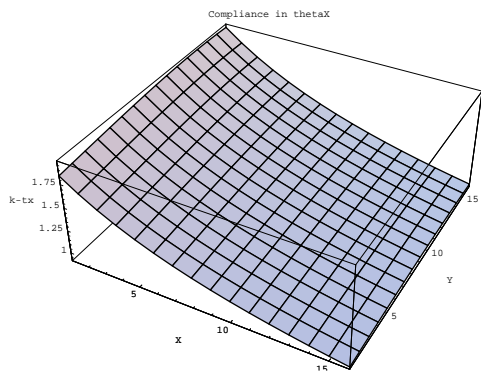
(a) Compliance in θ_x
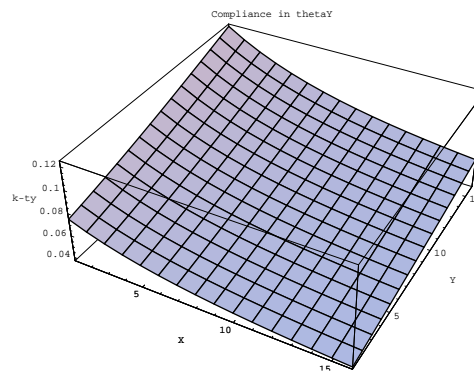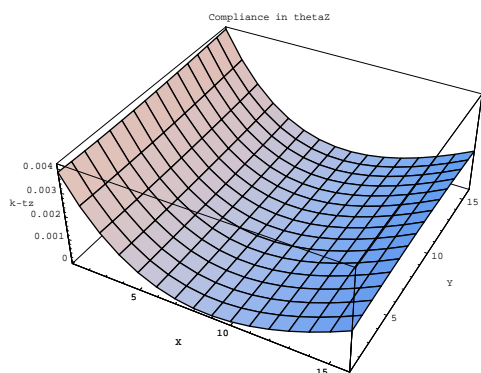
(b) Compliance in θ_y
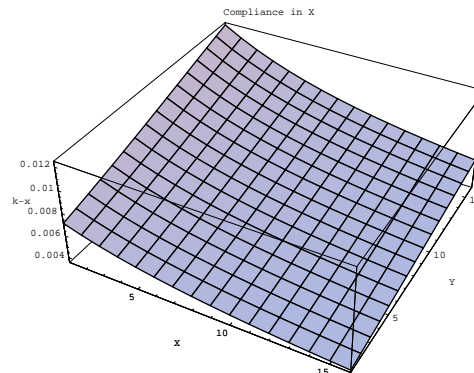
(c) Compliance in θ_z
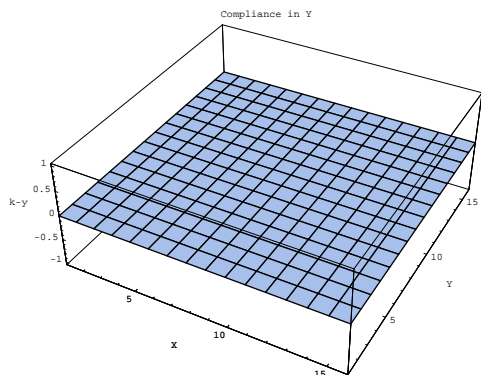
(d) Compliance in x
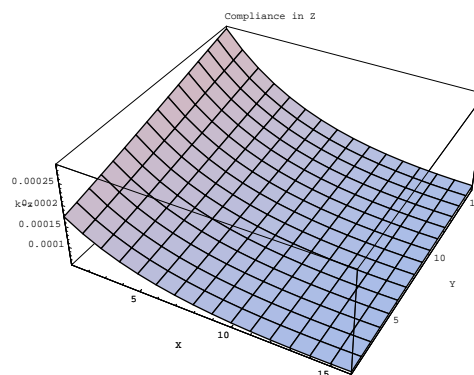
(e) Compliance in y

(f) Compliance in z

Figure A.6: Compliance mesh maps for the spatial 4-dof parallel mechanism with revolute actuators.
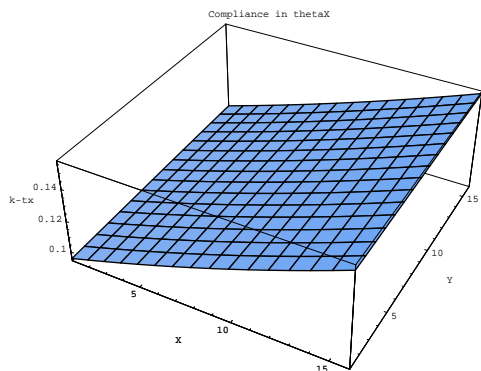
(a) Compliance in θ_x
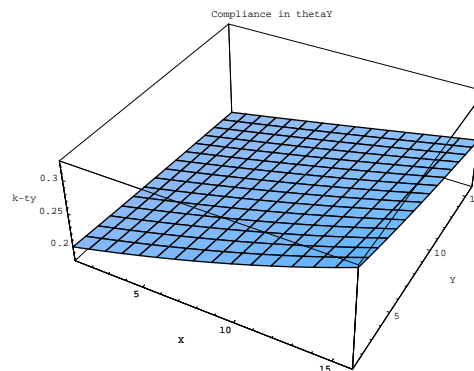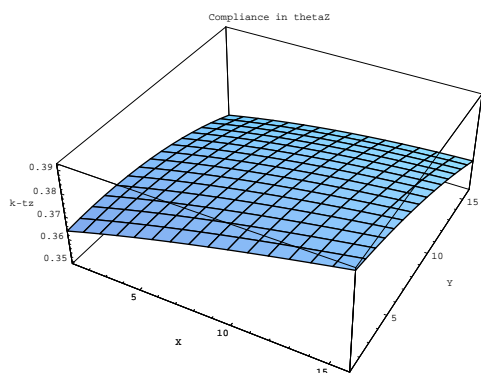
(b) Compliance in θ_y
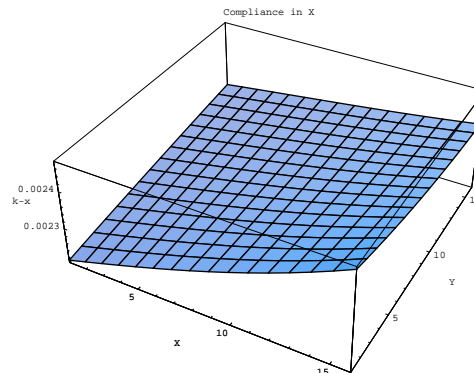
(c) Compliance in θ_z
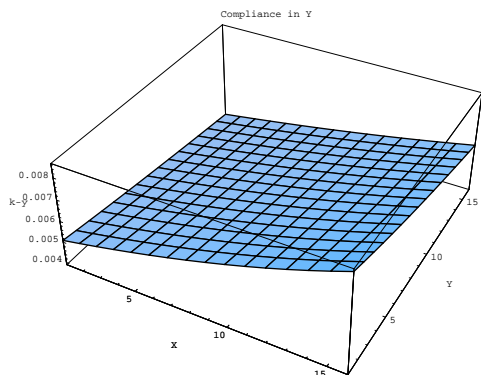
(d) Compliance in x
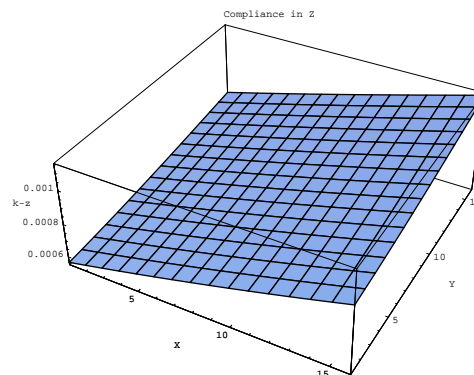
(e) Compliance in y

(f) Compliance in z

Figure A.7: Compliance mesh maps for the spatial 5-dof parallel mechanism with revolute actuators.
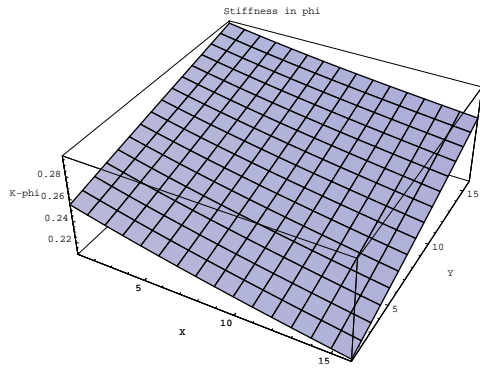
(a) Stiffness in ϕ axis
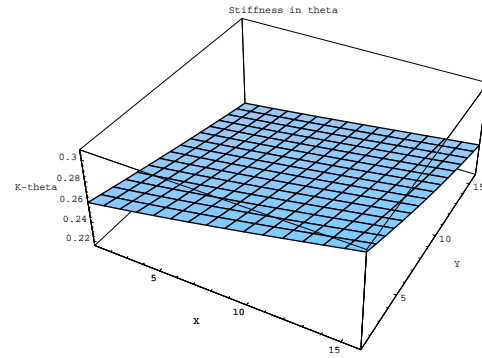
(b) Stiffness in θ axis
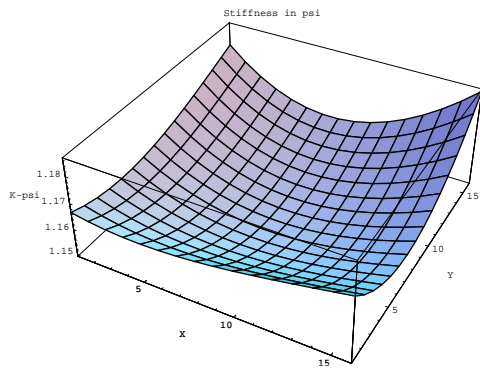
(c) Stiffness in ψ axis
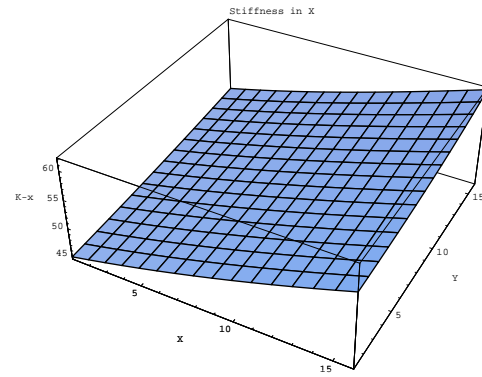
(d) Stiffness in X axis
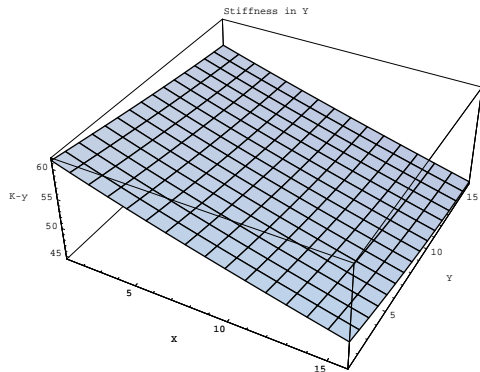
(e) Stiffness in Y axis
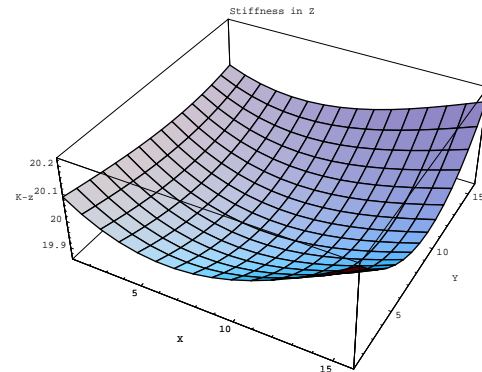
(f) Stiffness in Z axis

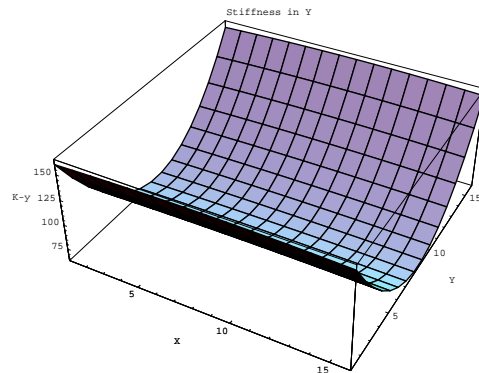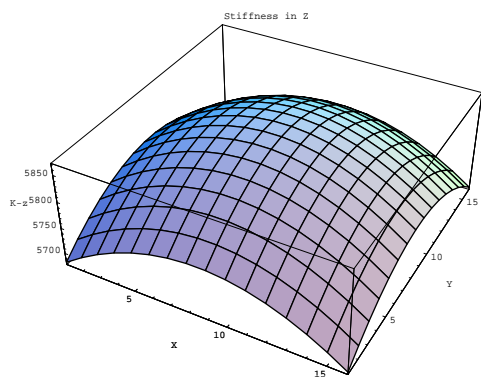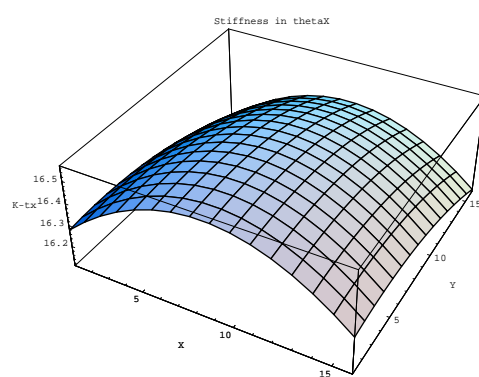Figure A.8: Stiffness mesh maps for the spatial 6-dof fully-parallel mechanism with revolute actuators (3 legs). ($\phi = \theta = 0, \psi = -\pi/6, z = 22\ cnm$)
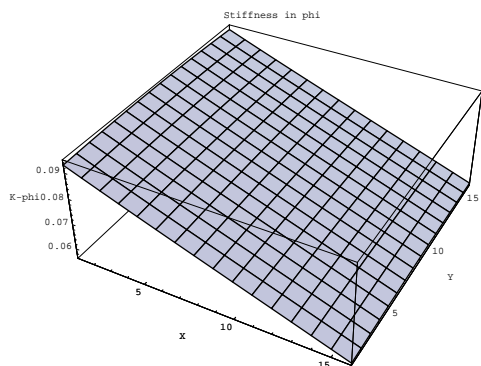
(a) Stiffness in ϕ axis
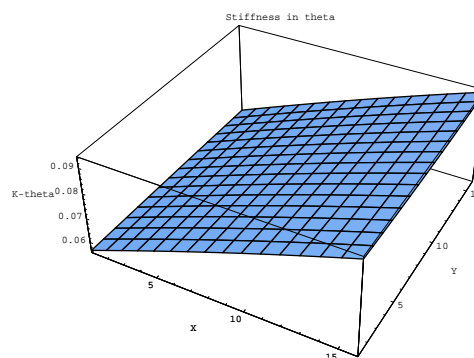
(b) Stiffness in θ axis
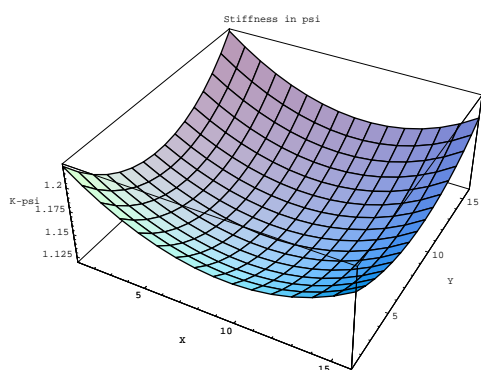
(c) Stiffness in ψ axis
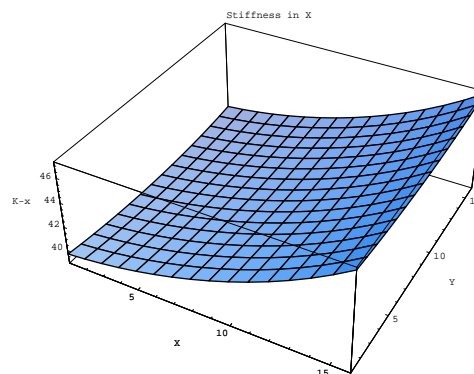
(d) Stiffness in X axis
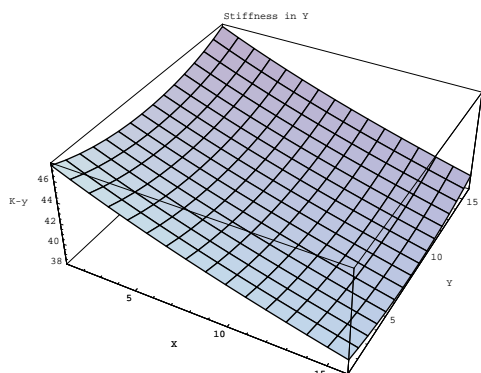
(e) Stiffness in Y axis
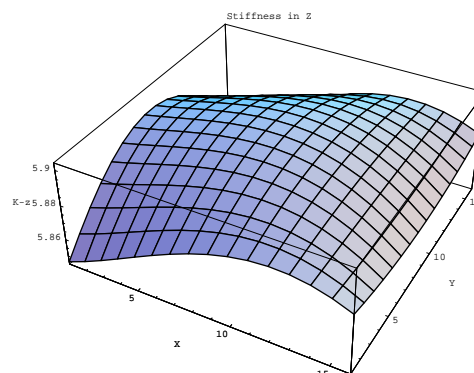
(f) Stiffness in Z axis

Figure A.9: Stiffness mesh maps for the spatial 6-dof fully-parallel mechanism with revolute actuators (3 legs). ($\phi = \theta = \psi = 0, z = 22\ cm$)
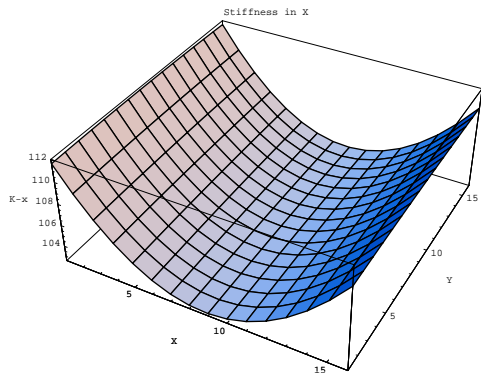
(a) Stiffness in x
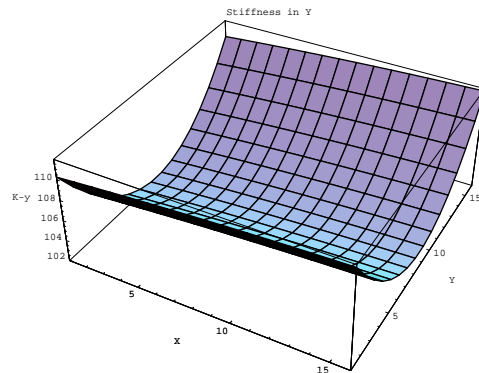
(b) Stiffness in y
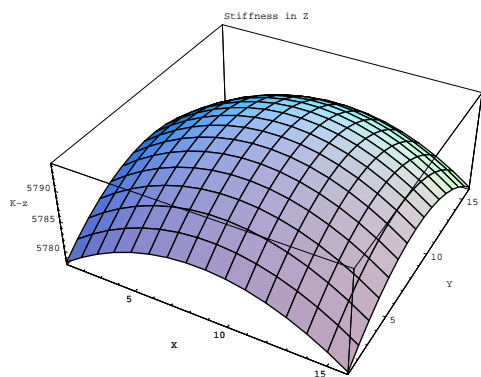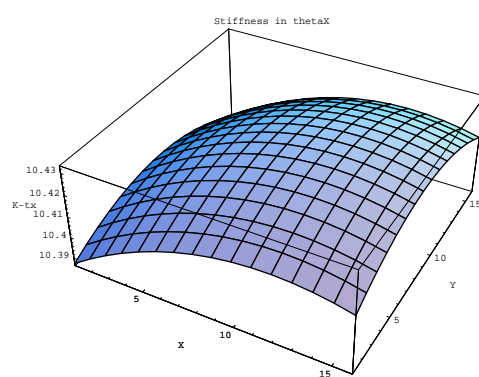
(c) Stiffness in z
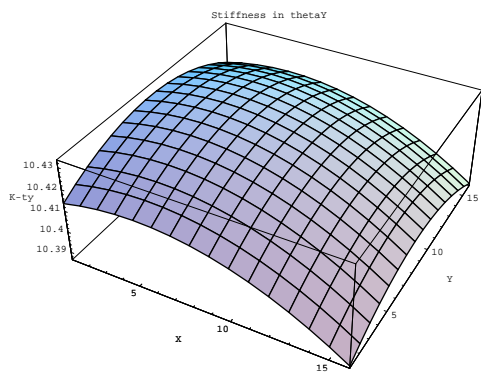
(d) Stiffness in θ_x
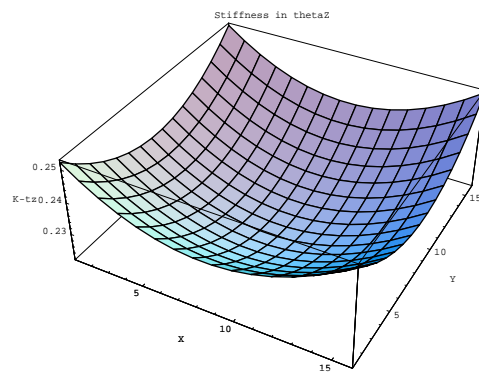
(e) Stiffness in θ_y

(f) Stiffness in θ_z

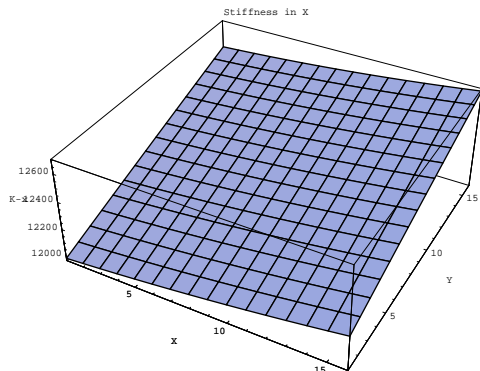Figure A.10: Stiffness mesh maps for the spatial 6-dof fully-parallel mechanism with prismatic actuators (6 legs).
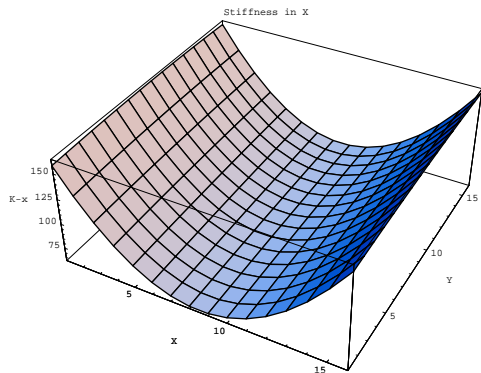
(a) Stiffness in x

(b) Stiffness in y

(c) Stiffness in z
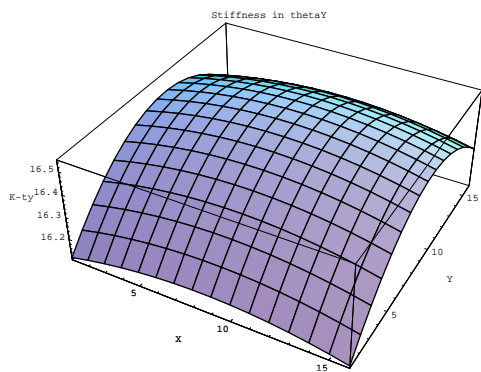
(d) Stiffness in θ_x
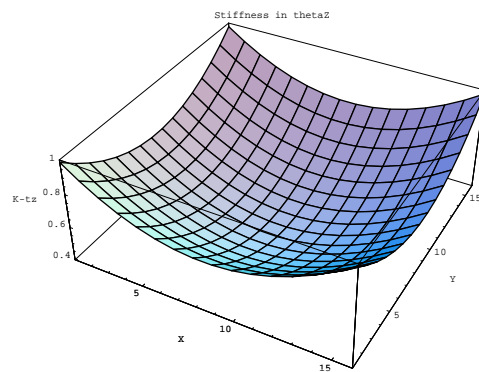
(e) Stiffness in θ_y

(f) Stiffness in θ_z

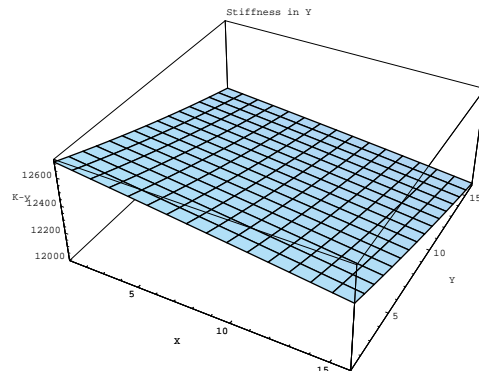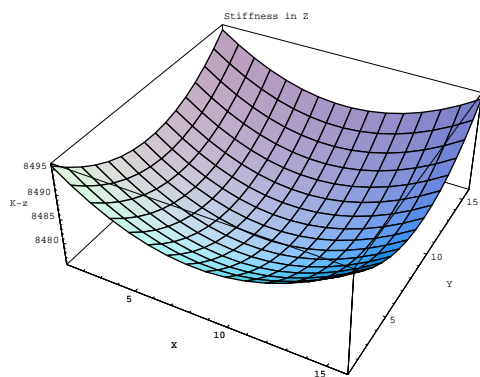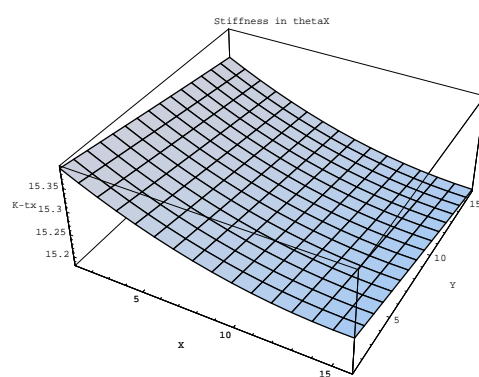Figure A.11: Stiffness mesh maps for the spatial 6-dof fully-parallel mechanism with prismatic actuators (6 legs).

(a) Stiffness in x

(b) Stiffness in y

(c) Stiffness in z
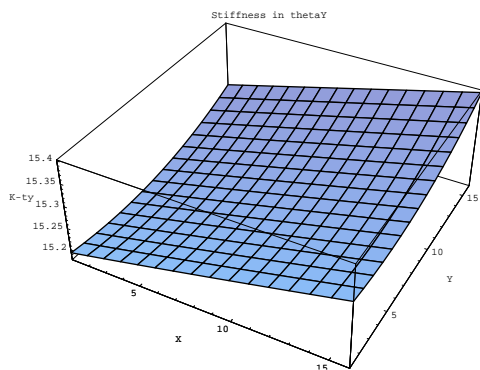
(d) Stiffness in θ_x
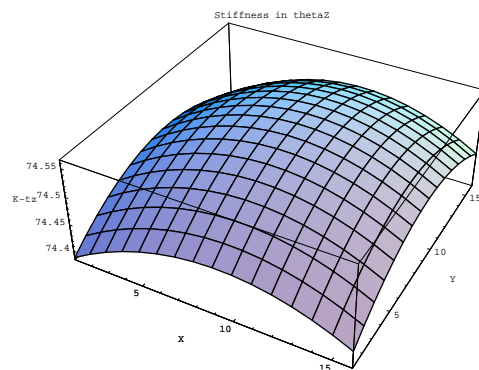
(e) Stiffness in θ_y

(f) Stiffness in θ_z

Figure A.12: Stiffness mesh maps for the spatial 6-dof fully-parallel mechanism with revolute actuators (6 legs).

Appendix B

Inverse Kinematics of the Passive Constraining Leg

B.1   Spatial 4-dof Parallel Mechanism with Prismatic Actuators

Figure 4.13 illustrates the configuration of the passive leg with rigid joints. Point B_5' is defined as the center of the Hooke joint connecting the two moving links of the passive leg. Moreover, the Cartesian coordinates of the points B_i' expressed in the fixed coordinate frame are represented as $(b_{5x}', b_{5y}', b_{5z}')$, the coordinates of the point B_5' in the fixed frame are represented by vector $\mathbf{b}_5'$. Since the axis of the fixed revolute joint of the 5th leg is assumed to be parallel to the xy plane of the fixed coordinate frame,

one can write

$$b'_{5x} = l_{51} \cos \theta_{51} \tag{B.1}$$

$$b'_{5y} = 0 \tag{B.2}$$

$$b'_{5z} = l_{51} \sin \theta_{51} \tag{B.3}$$

where θ_{51} is the joint variable – rotation angle around the fixed revolute joint – associated with 5th leg. Moreover, l_{51} is the length of the first link of the 5th leg. From the configuration of Figure 4.13, we can write the relationships of the parameters as

$$(b'_{5x} - x)^2 + (b'_{5y} - y)^2 + (b'_{5z} - z)^2 = l_{52}^2 \tag{B.4}$$

where x, y, z are the coordinates of point P_5 and l_{52} is the length of the second link of the passive leg.

Substituting eqs. (B.1) – (B.3) into eq. (B.4), one has

$$E \cos \theta_{51} + F \sin \theta_{51} = G \tag{B.5}$$

where

$$E = 2l_{51}x \tag{B.6}$$

$$F = 2l_{51}z \tag{B.7}$$

$$G = x^2 + y^2 + z^2 + l_{51}^2 - l_{52}^2 \tag{B.8}$$

therefore θ_{51} can be obtained as

$$\sin \theta_{51} = \frac{FG + KE\sqrt{H}}{E^2 + F^2} \tag{B.9}$$

$$\cos \theta_{51} = \frac{EG - KF\sqrt{H}}{E^2 + F^2} \tag{B.10}$$

where $K = \pm 1$ is the branch index of the mechanism associated with the configuration of the passive leg and

$$H = E^2 + F^2 - G^2 \tag{B.11}$$

hence the solution of the inverse kinematic problem is then completed by the expression

$$\theta_{51} = atan2[\sin \theta_{51}, \cos \theta_{51}] \tag{B.12}$$

from Figure 4.13, one can also obtain the θ_{52} simply using Cosine function.

B.2 Spatial 5-dof Parallel Mechanism with Prismatic Actuators

Figure 4.18 illustrates the configuration of the passive leg. Point B_6' is defined as the center of the Hooke joint connecting the two moving links of the passive leg. Moreover, the Cartesian coordinates of the points B_i' expressed in the fixed coordinate frame are represented as $(b_{6x}', b_{6y}', b_{6z}')$, the coordinates of the point B_6' in the fixed frame are represented by vector $\mathbf{b}_6'$. Since the axis of the fixed revolute joint of the passive leg is assumed to be parallel to the xy plane of the fixed coordinate frame, we can write

$$b_{6x}' = l_{61} \cos \theta_{61} \tag{B.13}$$

$$b_{6y}' = 0 \tag{B.14}$$

$$b_{6z}' = l_{61} \sin \theta_{61} \tag{B.15}$$

where θ_{61} is the joint variable – rotation angle around the fixed revolute joint – associated with passive leg. Moreover, l_{61} is the length of the first link of the passive leg. From the configuration of Figure 4.18, we can write the relationships of the parameters as

$$(b_{6x}' - x)^2 + (b_{6y}' - y)^2 + (b_{6z}' - z)^2 = l_{62}^2 \tag{B.16}$$

where x, y, z are the coordinates of point P_6 and l_{62} is the length of the second link of the 6th leg.

Substituting eqs. (B.13) – (B.15) into eq. (B.16), we have

$$E \cos \theta_{61} + F \sin \theta_{61} = G \tag{B.17}$$

where

$$E = 2l_{61}x \tag{B.18}$$

$$F = 2l_{61}z \tag{B.19}$$

$$G = x^2 + y^2 + z^2 + l_{61}^2 - l_{62}^2 \tag{B.20}$$

and we also can find the θ_{61} as

$$\sin \theta_{61} = \frac{FG + KE\sqrt{H}}{E^2 + F^2} \tag{B.21}$$

$$\cos\theta_{61} \quad = \quad \frac{EG - KF\sqrt{H}}{E^2 + F^2} \tag{B.22}$$

where $K = \pm 1$ is the branch index of the mechanism associated with the configuration of the 6th leg and

$$H = E^2 + F^2 - G^2 \tag{B.23}$$

hence the solution of the inverse kinematic problem is then completed by the perform

$$\theta_{61} = atan2[\sin\theta_{61}, \cos\theta_{61}] \tag{B.24}$$

From Figure 4.18, we can also obtain the θ_{62} and θ_{63}, we can write point P in Frame2 as

$$x_{62} \quad = \quad l_{62}\cos\theta_{63}\cos\theta_{62} \tag{B.25}$$
$$y_{62} \quad = \quad l_{62}\cos\theta_{63}\sin\theta_{62} \tag{B.26}$$
$$z_{62} \quad = \quad l_{62}\sin\theta_{63} \tag{B.27}$$

since we have

$$\mathbf{PB'} = \mathbf{p} - \mathbf{b'}_6 \tag{B.28}$$

and

$$[\mathbf{P}]_2 = \mathbf{Q}_{61}^T \mathbf{Q}_{60}^T [\mathbf{p} - \mathbf{b'}_6] \tag{B.29}$$

then combine eqs. (B.25) – (B.27) and (B.29), we can find θ_{62} and θ_{63} easily.

Appendix C

Expressions of e and r for the Compliant Model

C.1 Spatial Three Degrees of Freedom Mechanisms

$$\mathbf{e}_{4i} \;=\; \mathbf{Q}_{40} \cdots \mathbf{Q}_{4(i-1)}\mathbf{e}_{40}, \quad i = 1, \ldots, 6 \tag{C.1}$$

and the position vectors are expressed as follows

$$\mathbf{r}_{4i} \;=\; \sum_{j=i}^{6} \mathbf{Q}_{40} \cdots \mathbf{Q}_{4(i-1)}\mathbf{a}_{4i}, \quad i = 1, \ldots, 6 \tag{C.2}$$

C.2   Spatial Four Degrees of Freedom Mechanisms

$$\mathbf{e}_{5i} \;=\; \mathbf{Q}_{50}\cdots\mathbf{Q}_{5(i-1)}\mathbf{e}_{50}, \quad i = 1,\ldots,6 \tag{C.3}$$

and the position vectors are expressed as follows

$$\mathbf{r}_{5i} \;=\; \sum_{j=i}^{6}\mathbf{Q}_{50}\cdots\mathbf{Q}_{5(i-1)}\mathbf{a}_{5i}, \quad i = 1,\ldots,6 \tag{C.4}$$

C.3   Spatial Five Degrees of Freedom Mechanisms

$$\mathbf{e}_{6i} \;=\; \mathbf{Q}_{60}\cdots\mathbf{Q}_{6(i-1)}\mathbf{e}_{60}, \quad i = 1,\ldots,6 \tag{C.5}$$

and the position vectors are expressed as follows

$$\mathbf{r}_{6i} \;=\; \sum_{j=i}^{6}\mathbf{Q}_{60}\cdots\mathbf{Q}_{6(i-1)}\mathbf{a}_{6i}, \quad i = 1,\ldots,6 \tag{C.6}$$